Endothelial Alpha Globin Controls Nitric Oxide Signaling

Thomas Collins Stevenson Keller IV
Tallahassee, Florida

B.S. Physics, Davidson College, 2014

A Dissertation presented to the Graduate Faculty
Of the University of Virginia in Candidacy for the Degree of
Doctor of Philosophy

Department of Molecular Physiology and Biological Physics

University of Virginia
August, 2019

Abstract

Accurate control of vasodilatory signals is critical to the maintenance of blood pressure in mammals. One mechanism whereby vascular endothelium can control the diameter of the vessel is through nitric oxide (NO) signaling, a small gaseous molecule that is endogenously produced in endothelium and diffuses to smooth muscle. NO synthesis is tightly regulated through endothelial NO synthase (eNOS), the main enzyme contributing to NO production. One recently-discovered regulator of NO signaling is endothelial expression of a hemoglobin, specifically alpha globin (without its beta chain partner). Alpha globin binds directly to eNOS and, through its prosthetic heme group, can scavenge NO at the source of production. Disrupting the interaction of alpha globin and eNOS is a druggable goal with implications in anti-hypertensive therapy. The work presented in this thesis is focused on understanding the signaling and molecular interactions involved in, and the physiological impacts of, endothelial alpha globin regulating of vascular NO signaling.

The research presented in chapter 2 focuses on understanding the signals that induce endothelial alpha globin expression. Forcing endothelial contact with smooth muscle in an artery is sufficient to cause alpha globin production. The production of alpha globin is needed to change the vasodilatory mechanism by decreasing the proportion of dilation signals that come from NO. In chapter 3, I show that displacing alpha globin from eNOS increases NO signaling in the resistance vasculature. Using a peptide that mimics the region of alpha globin that binds with eNOS (named HbαX), we can disrupt alpha globin/eNOS complex formation to increase perfusion and decrease systemic blood pressure. This HbαX peptide binds directly to eNOS and has therapeutic relevance for hypertensive disease states.

The research presented in chapter 4 was completed during an internship at Heinrich Heine Universität and focuses on the role of NO in protecting the intrinsic deformability of red blood cells and, thus, blood pressure regulation. Reactive oxygen species can modify the red blood cell cytoskeleton and cause an increase in rigidity, which was correlated with hypertension in humans. I show that NO acts to protect these cells from increased reactive oxygen species through increasing the red blood cell antioxidant capacity and, therefore, protects the cells from increased rigidity.

Another disease context with dysfunctional NO signaling is pulmonary hypertension, which is the focus of chapter 5. Using a model of hypoxia-induced hypertension and our HbαX peptide to increase NO availability, we hypothesized that pulmonary hypertension could be alleviated by increasing dilatory signals using the HbαX peptide. Interestingly, the chronic administration of HbαX seemed detrimental to the pulmonary tissue. We observed increased nitrosative stress that damaged lung tissue downstream of increasing NO, rather than a vasodilatory response and alleviating pulmonary hypertension. Although the predicted increase in NO was observed with HbαX, the physiological consequence was not the one predicted, thus reminding us that the total physiological context of the disease state is more complex than one regulatory interaction.

In order to further our knowledge of how alpha globin can regulate eNOS and NO signaling, an understanding of the molecular interactions determining the alpha globin/eNOS complex using recombinant proteins was pursued and described in chapter 6. After attempting docking of the two protein structures *in silico*, the experimental approach of crosslinking mass spectrometry was established to define the residues on eNOS that interact with alpha globin. Work in this area is still ongoing, but will provide valuable context for how NO is controlled in the endothelium by this protein-protein interaction.

Finally, in chapter 7, research focused on an engineered a mouse model harboring a deletion within the sequence of alpha globin that binds to eNOS is described. This deletion decreases alpha globin and eNOS association in the endothelium and increases vasodilatory NO. The increase in NO impacts blood pressure homeostasis, because although the total blood pressure was normal in the mice harboring the heterozygous deletion, the dilatory capacity of individual arteries was decreased due to decreased NO-response proteins.

Overall, this work furthers the understanding of NO signaling, the role of alpha globin in controlling NO flux, and therapeutic potential of targeted disruption of the alpha globin and eNOS interaction in the vasculature.

Dedication

Science, especially graduate work, is not a solitary pursuit. I have relied on many, many people to achieve the work that is presented in this thesis. I am writing a few down here; thank you for the tangible efforts that each of you have had in helping along this work.

I have had the privilege of working with two mentors, two lab families, two sets of experts in their respective fields; for that experience, I am grateful. In no small way have each of the Isakson and Columbus lab members helped me through experimental, analytic, personal, optimistic, sleep-deprived (among other adjectives) trials and tribulations. To Brant and Linda, a dynamic duo that motivated me, coached me, and let me explore my ideas at the bench, thank you. To Jen, Ashton, Meagan, Marissa, Jason, Tracy, Nicole, and a host of undergraduates, thank you for putting up with my shenanigans, teaching me (with my soluble protein) the biophysical properties of membranes and membrane proteins, and enduring lab meetings that included thinking about mice. To Angie, Scott, Josh, Miranda, Isola, Lauren, Leon, Alex, Claire, Abby, Henry, Lukas, Nenja, Gilson, Shu, Yang, and another host of undergraduates, thank you for keeping me caffeinated, keeping the confocal on, and allowing me to learn from each of you.

To friends outside the lab, thank you for being a necessary pressure release. Whether it was 7:00 AM bike rides in Crozet, Sunday soccer games, cookouts, breweries, or Mario Kart; the laughter that we were able to share will be with me forever.

To my parents, my sister and brother-in-law, and their beautiful daughters, thank you for always providing a warm place where I could escape the lab and wear shorts in December. Your loving support has meant the world to me, and I would not be where I am

without everything that I have learned from you. I model myself to try to be more like each of you.

To Madison, our journeys have intersected in a way that we have become attached at the hip. Your love and support means everything to me; and I am so happy to be joining our families soon. Thank you for everything you have done for me, for us, throughout our years at Davidson and in Virginia. As we ship off to our next stops, I think we will be back here. Let's enjoy the ride, together.

"Eventually, all things merge into one, and a river runs through it. The river was cut by the world's great flood and runs over rocks from the basement of time. On some of those rocks are timeless raindrops. Under the rocks are the words, and some of the words are theirs."

A River Runs Through It, N. Maclean

TABLE OF CONTENTS

List of Abbreviations

$[Ca^{2+}]$	Concentration of Calcium Ions
3-NT	3-nitrotyrosine
AH1 / AH2	Autoinhibitory region 1 / 2
AHSP	Alpha Hemoglobin Stabilizing Protein
Alpha globin	the Alpha subunit of hemoglobin
ALT	Alanine aminotransferase
AMP	Adenosine Monophosphate
AMPK	Adenosine Monophosphate-activated Protein Kinase
AngII	Angiotensin II
ANOVA	Analysis of Variance
AST	Aspartate aminotransferase
ATP	Adenosine Triphosphate
BSA	Bovine Serum Albumin
BUN	Blood urea nitrogen
CA	Carotid Artery
CaM	Calmodulin
cAMP	Cyclic Adenosine Monophosphate
Cav1	Caveolin 1
CCh	Carbachol
cGMP	Cyclic Guanosine Monophosphate
COSY	Correlation Spectroscopy
Cx40	Connexin 40
Cyb5R3	Cytochrome b5 Reductase 3

DAF-FM DA	4-amino-5 methylamino-2’,7’-difluorofluorescenin diacetate
DCF	Dichlorofluorescein
DTT	Dithiothreitol
EC	Endothelial Cell
EDC	1-Ethyl-3-(3-dimethylaminopropyl)carbodiimide
EDH	Endothelial Derived Hyperpolarization
EDTA	Ethylene Diamine Tetraacetic Acid
EET	Epoxyeicosatrienoic acid
EI	Elongation Index
EM	Electron Microscopy
eNOS	Endothelial Nitric Oxide Synthase
eNOSox	The oxygenase domain of eNOS
ESI	Electrospray Ionization
ET-1	Endothelin-1
ET1A	Endothelin-1 Antagonist
FAD	Flavin Adenine Dinucleotide
FMN	Flavin Mononucleotide
GFP	Green Fluorescent Protein
GSH	Reduced Glutathione
GSSG	Oxidized Glutathione
GST	Glutathione-S-Transferase
GTP	Guanosine Triphosphate
H&E	Hematoxylin and eosin
H_4biopterin	5, 6, 7, 8-tetrahydrobiopterin
hAoEC	Human Aortic Endothelial Cell
HbαX	Hemoglobin Alpha X, the alpha globin mimetic peptide

HSP90	Heat Shock Protein 90
IEL	Internal Elastic Lamina
IgG	Immunoglobulin G
IK_{Ca}	Intermediate Conductance Calcium-activated Potassium Channel
iNOS	Inducible Nitric Oxide Synthase
IP	Intraperitoneal
IP_3	Inositol Triphosphate
kDa	Kilodalton
K_{IR}	Inwardly-rectifying Potassium Channel
L-NAME	L-Nitroarginine Methyl Ester
LV	Left Ventricle
MA	Mesenteric Artery
MALDI	Matrix Assisted Laser Desorption Ionization
MEJ	Myoendothelial Junction
MFI	Median Fluorescence Intensity
MLCK	Myosin Light Chain Kinase
MLCP	Myosin Light Chain Phosphatase
MS	Mass Spectrometry
NADPH	Nicotinamide Adenine Dinucleotide Phosphate
NMR	Nuclear Magnetic Resonance
nNOS	Neuronal Nitric Oxide Synthase
NO	Nitric Oxide
NOESY	Nuclear Overhauser Effect Spectroscopy
NOS	Nitric Oxide Synthase
NOSIP	Nitric Oxide Synthase Interacting Protein
PAI-1	Plasminogen Activator Inhibitor-1

PAM	Photoacoustic Microscopy
PDE	Phosphodiesterase
PE	Phenylephrine
PH	Pulmonary Hypertension
PI3	Phosphoinosotide 3
PKA	Protein Kinase A
PKC	Protein Kinase C
PLA	Proximity Ligation Assay
$pp60^{Src}$	Protein kinase related to Src Family
PVDF	Polyvinylidene Fluoride
PVP	Polyvinylpyrrolidine
PYK2	Proline-rich Tyrosine Kinase 2
RBC	Red Blood Cell, an erythrocyte
ROS	Reactive Oxygen Species
RV	Right Ventricle
RVSP	Right Ventricular Systolic Pressure
SAXS	Small Angle X-ray Scattering
ScrX	Scrambled sequence of HbαX
SEM	Scanning Electron Microscopy
sGC	Soluble Guanylyl Cyclase
siRNA	Small Interfering Ribonucleic Acid
SK_{Ca}	Small Conductance Calcium-activated Potassium Channel
SMC	Smooth Muscle Cell
sO_2	Oxygen Saturation
SS	Shear Stress
tBuOOH	Tert-Butyl Hydroperoxide

TDA	Thoracodorsal Artery
TEM	Transmission Electron Microscopy
TOCSY	Total Correlation Spectroscopy
VEGF	Vascular Endothelial Growth Factor

Chapter 1: Introduction

Some sections adapted from: Xiaohong Shu, T.C.S. Keller IV, Daniela Begandt, Joshua T. Butcher, Lauren Biwer, Alexander S. Keller, Linda Columbus, Brant E. Isakson. “Endothelial nitric oxide synthase in the microcirculation.” *Cell and Molecular Life Sciences*, 72 (23), 4561-4575.

Blood pressure homeostasis and the role of nitric oxide

Accurate control of blood pressure is a primary homeostatic mechanism in mammals to maintain circulation and tissue perfusion. Without proper perfusion, organs cannot extract oxygen for metabolic function, clear waste for later filtration, or be protected by circulating immune cells that travel through the blood vasculature. The two main drivers of blood pressure are cardiac performance and vascular resistance; while other mechanisms such as fluid and electrolyte balance (*1*), blood viscosity (*2*), nervous system-derived stimuli (*3*), and hormonal regulation (*4, 5*) contribute chronic and acute effects on blood pressure, all of these physiological forces and signals feed back into the effects of the heart rate and vascular resistance to ultimately tune blood pressure homeostasis.

The circulatory system is finely tuned to maintain oxygenation and waste clearance for the function of all other organ systems. The circulatory loop is made up of the heart, the blood (a fluid mixture of plasma and all of the various cells that travel around the system), and blood vessels. The heart generates pressure that pushes the blood into all of the vessels. Although a significant part of cardiovascular disease and the research into such is centered around heart function, I will leave the heart’s role as essentially that: the pump that forces the blood through the vasculature.

In mammals, the heart provides pressure to perfuse the two loops of our circulatory system. in our two-loop system. Two atria receive venous blood that is returning to the heart, feed it into the ventricles that create the pumping force to move blood into the arteries. The systemic loop of the circulatory system is driven by the left ventricle; this is the more muscular, higher pressure side of the circulatory system, and thus the left ventricle has thick walls to generate sufficient driving force for perfusion of the brain, muscles, kidneys, and other organs (save for the lungs). The pulmonary circulatory loop is driven by the right ventricle to perfuse the lungs, which are the site of oxygen and carbon dioxide exchange. This circulatory loop is low pressure, with a normotensive pulmonary blood pressure of around 25 mmHg (compared to around 100 mmHg in the systemic circulatory loop). Thus, the right ventricle, although similar in pumping volume capacity to the left ventricle, is less muscular and has thinner walls. Each ventricle of the heart empties into large arteries capable of transporting the pumped volume of blood (the aorta receives blood from the left ventricle, and the pulmonary artery from the right ventricle) during systole, and fill again immediately during diastole.

Large conduit arteries move massive quantities of blood quickly to distant parts of the body. These large arteries branch many times, through feed arteries and to arterioles (of diameter about 100 μm). From conduit arteries to smaller arteries, there are many differences both in form and function: larger arteries are more muscularized and experience greater transmural pressure than smaller arteries. Additionally, smaller arteries are very reactive, constricting and dilating to control blood pressure and perfusion. Ultimately, the arterioles branch into capillaries, with a diameter approximately that of a single red blood cell (< 8 μm). Capillaries contact every part of the body, with no more than about 10 μm between their lumens. The decrease in vascular diameter is meaningful; oxygen and nutrient extraction, cell migration, and deposition of waste are not

instantaneous processes, and perform better when flow and shear stress in the blood are lower in the smaller vessels of the circulatory tree.

Across the differences in size of the vessel, similar cell types make up the vascular wall. From the outside of the vessel, smooth muscle cells are the actuators of constriction and dilation. These morphologically long and spindly cells wrap around the vessel lumen perpendicular to the direction of flow. They have specialized actin and myosin protein fibers to enact constriction in response to intracellular increases in [Ca^{2+}] and subsequently coordinate decreases in the lumen diameter. Endothelial cells line the lumen of the blood vessel, and thus are highly communicative in interactions with other cells. Immune cells stick and roll along endothelium in order to infiltrate tissue from the vascular lumen. Nutrients and signals coming through the blood are taken up and distributed by the endothelium. As signal integrators, endothelial cells have diverse and important roles in vascular biology.

The function of the endothelium remains mostly constant as the reactive cellular lining of the blood vessel, but some vascular beds are specialized in endothelial function. The single cell layer is remarkably diverse in form and function from large vessels to the smaller arterioles that determine blood pressure.

The endothelium of conduit vessels is tightly connected and relatively impermeable to immune cell infiltration and plasma components. This is both due to intrinsic endothelial connectivity and the speed of blood flow in the large vessels. As the volume of blood flow is constant across the vascular tree, the velocity of blood decreases with an increase in the total cross-sectional area of vascular lumen. The total area for blood flow increases from one aorta (about 4 cm^2 to millions of capillaries with an area of about 3000 cm^2); thus, the flow velocity will decrease from 20 cm/s to 0.03 cm/s. In the conduit arteries, there are relatively few, and the laminar flow is high. Functionally, this makes it harder for immune cells to attach, roll, and infiltrate sub-endothelial spaces. The vasculature of large arteries

has one endothelial layer surrounded by multiple smooth muscle layers. The multiple smooth muscle layers act to counteract the transmural pressure and give structural support to facilitate flow. In between layers of smooth muscle, there are fibrous laminal layers that are made and deposited by smooth muscle. These laminae are made up of fibrous proteins that lend structure to the vessel and support cell communication.

In direct contrast to the largest arteries, capillary (the smallest vessels, with a diameter of about 8 μm – barely big enough for one erythrocyte to pass through at a time) beds are organized to have slow blood velocity, promoting filtration and gas exchange. Organs with filtration function (kidney, liver, and spleen) have capillaries perforated with large or small fenestrae, or the barrier might be totally discontinuous with large “sinusoidal” spaces between cells. These promotes filtration functions of the endothelium and allow solutes, plasma components, and even cells to exit the blood stream.

In between the two extremes, the resistance vasculature has an endothelial layer surrounded by a medial layer of only a few cells. One to two layers of smooth muscle surround the endothelium, and a single internal elastic lamina layer separates the endothelium from smooth muscle. An anatomical hallmark of the resistance vasculature is the presence of myoendothelial junctions (MEJs). These endothelial projections through holes in the laminal layer directly contact the underlying smooth muscle. Within the MEJ, gap junctions physically couple the endothelium and smooth muscle at these points, caveolae act as a scaffold to harbor signaling proteins, and the endoplasmic reticulum extends into the MEJ to coordinate signaling for endothelial communication with smooth muscle. The interplay of endothelial and smooth muscle signals acts to control blood pressure at the level of individual vessels.

In order to appropriately perfuse all tissues, blood pressure is tightly regulated. While most arterial vessels are able to constrict and dilate to agonists *in vitro*, the arterioles are the vessels primarily responsible for determining blood pressure *in situ*. Mechanical,

chemical, and physical signals can promote constriction and dilation responses. The interplay between constriction and dilation in individual arterioles can direct blood flow to specific organs and muscle beds, as well as determines a general set point for overall blood pressure. Vascular cells have a remarkable ability to integrate diverse signals into physiological function; there are many different factors contributing to dilation and constriction signaling.

My work has primarily focused on one mechanism whereby cells in the vascular wall create vasodilatory signals to control blood pressure and tissue perfusion. A potent vasodilatory molecule, nitric oxide (NO) is produced by enzymes in the endothelium and can activate relaxation pathways in smooth muscle (*6, 7*). NO is membrane permeable and highly reactive, and thus has a short half-life *in vivo*. Omnidirectional diffusion is possible, where NO can interact with free metal centers, radical species, and some amino acids for various physiological function. Smooth muscle cells express a receptor for NO in soluble guanylyl cyclase (sGC), a heme-coordinate protein that converts guanosine triphosphate (GTP) into cyclic guanosine monophosphate (cGMP). Protein kinase G is activated by binding of GTP to its regulatory domain, and can then phosphorylate myosin light chain kinase, rendering the kinase inactive and unable to contribute to contraction signaling. cGMP is subsequently broken down by phosphodiesterase enzymes to stop the vasodilatory signaling. This signaling pathway is critical to the maintenance of blood pressure, and thus study of NO and its control informs many aspects of vascular biology.

Production of nitric oxide in the endothelium

Nitric oxide (NO) is produced by a family of enzymes called nitric oxide synthases (NOS). There are three NOS isoforms, neuronal NOS (nNOS; *NOS1*), inducible NOS (iNOS; *NOS2*), and endothelial NOS (eNOS; *NOS3*), all of which differ slightly in

physiological role and expression profile. nNOS is expressed in the neurons and skeletal muscle and produces NO as a cellular signaling molecule. iNOS is expressed in immune cells and produces NO as a precursor to cytotoxic free radicals for defense against invading bacteria. The next section focuses on eNOS, which is expressed in endothelial cells, and its role in vascular function. NO and its metabolites are found in both the macrovascular (aorta and medium arteries) and microvascular (arterioles/resistance arteries and capillaries) circulation. Endothelial-derived NO acts as a potent vasodilator through diffusion to smooth muscle cells that surround vessels and decreases leukocyte adhesion to the endothelial cells, thereby affecting immune response and inflammation. To fully understand the role of eNOS and NO in the roles of whole-body blood pressure regulation and inflammatory response, the molecular structure and regulatory modifications of eNOS that affect NO production need to be understood.

eNOS structure, co-factors, and phosphorylation

The functional form of eNOS is a homodimer (*8*) with each monomer containing an N-terminal oxygenase and C-terminal reductase domain connected by a central calmodulin (CaM) binding sequence (**Figure 1**) (*9, 10*). Several crystal structures exist of the different domains from different isoforms and organisms; additionally, reconstruction of the active form of inducible NOS has been determined via single particle cryo-electron microscopy (*11*). The eNOS dimer is stabilized by 5, 6, 7, 8-tetrahydrobiopterin (H_4biopterin) (*12*) and zinc (*13, 14*) binding to the oxygenase domain. In the human eNOS sequence, zinc binding is coordinated by cysteines 94 and 99 from each monomer and is structurally, but not enzymatically, important. H_4biopterin binds between the interface of heme and the dimer, stabilized by Van der Waals and hydrophobic interactions (*15*). In addition to

stabilizing the eNOS dimer, H_4biopterin is proposed to modulate the redox potential of the heme prosthetic group.

To start the electron transfer reaction, reduced nicotinamide adenine dinucleotide phosphate (NADPH) binds to the C-terminal reductase domain of one monomer of the eNOS dimer. Within this reductase domain, an electron flows from NADPH to other bound cofactors: flavin adenine dinucleotide (FAD), followed by flavin mononucleotide (FMN). The electron then flows to the heme on the oxygenase domain of the other eNOS monomer. The dimerized form is essential for this activity because the electron is transferred between subunits. The reduced heme then catalyzes the synthesis of NO from the substrates of L-arginine and oxygen, creating L-citrulline as a byproduct (*16*). A conformational change of the FMN binding domain is postulated such that the FMN domain "swings" from the reductase to the oxygenase domain in order to shuttle the electron between subunits.

The eNOS dimer is inactive without further modification due to two autoinhibitory regions (residues 596 – 640 (AH1) and 1165 – 1178 (AH2) (*17, 18*)) in the reductase domain that modulate the coupling between the oxygenase and reductase domains. AH1 is postulated to interact with the flexible linker between domains (residues 481 – 520) and occludes the CaM binding sequence from interacting with CaM. Only the Ca^{2+}-bound conformation of CaM binds to eNOS, thereby connecting activation of eNOS to intracellular calcium concentration ($[Ca^{2+}]_i$). AH2 regulates the interaction of the FMN and NADPH binding regions in the reductase domain; it is postulated to "lock" the FMN domain into a position optimum for electron acceptance and thus must undergo a conformational change to donate an electron to heme (*18, 19*).

The N-terminus of eNOS is proposed to be predominantly unstructured and contains three acylation sites at residues 2, 15, and 26. Glycine 2 is co-translationally myristoylated and is a requirement for membrane localization. Cysteine residues 15 and 26 are post-

translationally palmitoylated. The specific role of the palmitoylation is not clear, but stabilization of membrane association and/or sequestration into lipid domains has been proposed (*20*). DHHC21, a palmitoyl transferase that has an Asp-His-His-Cys motif, palmitoylates eNOS; its depletion affects physiological localization of eNOS, causing a subsequent decrease in NO production (*21*).

Based on these structural features, there are two ways to regulate eNOS function: modulate the dimer or modulate the coupling of electron transfer from the reductase domain to the oxygenase domain while in the dimeric conformation. Both of these modes of regulation appear to occur variously through cofactor availability (*e.g.*, a decrease in H_4biopterin due to enhanced oxidation), post-translational modifications, cellular localization, and/or protein-protein interactions.

Regulation of eNOS by protein-protein interactions

In addition to CaM, several other proteins directly bind eNOS and modulate its activity (**Table 1**). In contrast to the activating role of CaM, one of the most well characterized inhibitors of eNOS activity is caveolin-1 (Cav1). Cav1 is the main coat protein of caveolae, which are membrane microvesicles that harbor membrane-associated proteins in endothelial cells (ECs) (*22*). Within caveolae, Cav1 directly associates with eNOS near the CaM-binding sequence and sterically prevents activation by CaM (*23*), decreasing NO production. Other proteins interact with eNOS; these include heat shock protein 90 (HSP90) (*24-26*), NOS interacting protein (NOSIP) (*27, 28*), β-actin (*29, 30*), and the alpha subunit of hemoglobin (alpha globin). All of these binding partners cause eNOS translocation from the plasma membrane and activate NO production, except alpha globin. HSP90 binds to eNOS residues 310-323, which are proximal to the Cav1 binding site (*24*). Released from Cav1, HSP90 enhances CaM association and phosphorylation on

activating residue S1177 via protein kinase B (Akt) (*31*), (**Table 2**) thereby increasing NO production. NOSIP binds to the C-terminal region of the oxygenase domain (residues 366-486) (*32*) and ubiquitinylates eNOS (*28*), decreasing NO production and marking the enzyme for degradation.

β-actin-eNOS association is directly related to oxygen capacity in the microenvironment of the EC. In hyperoxemic conditions, eNOS associates with the actin cytoskeleton via direct binding with β-actin (*33, 34*). Although NO is an effective regulator of blood pressure and vascular function, increased NO bioavailiability in an O_2 rich environment often leads to detrimental reactive oxygen species (ROS) formation.

The most recently characterized inhibitory protein partner of eNOS in the microcirculation is alpha globin (*35, 36*). As discussed below, NO bioavailability is decreased by alpha globin expressed in a polarized region of the microvascular endothelial cell known as the MEJ. This localized expression of alpha globin affects the eNOS signaling domain by directly interacting with the oxygenase domain of eNOS to inhibit NO production as well as scavenging NO via the alpha globin heme group.

Post-translational modification of eNOS

Activating phosphorylation. eNOS activity can be enhanced upon phosphorylation at several residues through multiple pathways and kinases (**Table 2**). The following is a description limited to the sites in which the activation or inhibition has been identified and the structural consequences postulated for each. Additional phosphorylation sites were recently identified (e.g. T33, S53, and S836 through proteomics approaches (*37*)); however, their physiological significance has not been investigated.

Three characterized phosphorylation sites that enhance NO production are located in the autoinhibitory regions of the reductase domain (**Table 2**; S615, S633, and S1177).

The introduction of negative charge at each of these sites likely disrupts the interactions of the autoinhibitory regions (e.g. S615 and S1177) or modulates the CaM dependence of eNOS activation (e.g. S633). Various eNOS activators including bradykinin, vascular endothelial growth factor (VEGF), ATP and statins transiently promote phosphorylation at these three sites depending on which kinase phosphorylates the site (*38-45*). S615 is phosphorylated by Akt and protein kinase A (PKA) (*38*), S633 by PKA (*41, 45*) and AMP-activated kinase (AMPK) (*46*), and S1177 by numerous kinases, including Akt, PKA, AMPK, cyclic GMP-dependent protein kinase, and Ca^{2+}-CaM-dependent protein kinase II (CaM kinase II) (**Table 2**). Mutation of any one of these sites to aspartate as a phosphomimic increased NO production in cells expressing the mutant proteins (*28, 38*). In addition to these sites, Y81 is phosphorylated by Src kinase and increases NO production (*47, 48*); however, the structural mechanism of activation is unknown.

Inhibitory phosphorylation. There are three well-characterized phosphorylation sites that inhibit eNOS activity (**Table 2**; S114, T495, and Y657) with different molecular consequences due to their divergent locations in the eNOS structure. S114, located in the oxygenase domain, is phosphorylated by protein kinase C (PKC) (*49*) and AMPK (*46*). Although contradictory data exist (*50, 51*), phosphorylation at S114 is more likely to reduce eNOS activity (*49, 52*). S114 is located in an unresolved loop in the oxygenase domain crystal structure, away from the heme. Thus, phosphorylation at this site could inhibit activity by preventing interactions between the reductase and oxygenase domain rather than by modulating the redox activity of heme. Alternatively, S114 phosphorylation may modulate protein-protein interactions, as S114 phosphorylation is required for peptidyl-prolyl isomerase binding (*53*) and may promote eNOS interaction with Cav1.

T495 is located in the CaM binding sequence (**Figure 1B**, purple text) and is phosphorylated by PKC (*in vivo*) and AMPK (*in vitro*) (**Table 2)** (*54, 55*). PKC phosphorylation at this site decreases eNOS activity by reducing the affinity of CaM (*56*).

The structure of CaM bound to the eNOS recognition sequence suggests that the introduction of a negative charge at position 495 destabilizes the CaM – eNOS interaction through repulsion from CaM glutamate residues 7 and 127, although other mechanisms are possible (e.g. destabilizing the helical structure of the CaM binding sequence) (*57*).

Y657 is phosphorylated by the proline-rich tyrosine kinase 2 (PYK2) (**Table 2**) and decreases eNOS activity (*58*). Without phosphorylation, this particular residue directly interacts with FMN through pi-pi stacking (*19*). Its phosphorylation may modulate the reduction potential of FMN or the dynamics of the FMN binding domain, thereby decreasing the efficiency of electron transfer within the eNOS dimer.

Summary of eNOS regulation

Describing each regulatory element independently provides an unrealistic perspective of eNOS regulation. Phosphorylation or dephosphorylation at each of the aforementioned sites, protein-protein interactions, and the bioavailability of cofactors can occur simultaneously, and all or combinations of these events may regulate eNOS activity. For instance, AMPK phosphorylates both an activating (S1177) and inhibiting (S114) eNOS site. In addition, many stimuli influence multiple pathways that regulate eNOS activity. The well-characterized vasodilator bradykinin stimulates NO synthesis by promoting S1177 phosphorylation (*43*) and T495 dephosphorylation (*59*). Fluid shear stress signals through a cascade resulting in phosphorylation of eNOS S114 (decreasing NO production), S633 (increasing NO production), Y657 (decreasing NO production), and S1177 (increasing NO production) (*58, 60*). This complexity requires a careful and thorough understanding of the cellular system and stimuli, as well as a cumulative understanding of the regulatory processes at work.

Localization of eNOS within the microvascular endothelium

The resistance and microvasculature is the location in the vascular tree where blood pressure is determined. Understanding how arterioles control their diameter and resistance to flow requires an understanding of NO-production capabilities of the endothelium of these vessels.

Within microvascular ECs, the vast majority of eNOS is localized to plasma membrane caveolae and associated with the main coat protein of caveolae, Cav1. The targeting of eNOS to the plasma membrane (other NOS isoforms do not localize to the plasma membrane (*61*)) is an important step in its activation. A number of proteins that regulate eNOS are also targeted to caveolae (for review, see (*62*)). For example, CaM has a similar pattern of subcellular distribution.

Upon agonist stimulation of ECs, increases in $[Ca^{2+}]_i$ cause eNOS redistribution to the cytosol and dissociation with Cav1 (*63*). eNOS has no transmembrane domain; thus, post-translational modifications involving fatty acylation (described above) are necessary for targeting and anchoring eNOS to the plasmalemmal caveolae, increasing bioavailable NO (*64-67*).

The lipid composition of caveolar membrane domains is crucial for normal eNOS localization and activation. Normally, cholesterol is enriched in caveolae, and disruption or depletion of cholesterol concentrations causes redistribution of eNOS to an intracellular compartment and decreased NO production (*68*). The signaling phosphosphingolipid ceramide is also able to activate eNOS independently of calcium in cultured macrovascular endothelial cells (*69*), though this mechanism may be different in the microvasculature or *in vivo*.

In addition to localizing to caveolae and the Golgi membrane, eNOS can be localized to mitochondria, perinuclear regions, and the actin cytoskeleton, but these pools of enzyme contribute less to total NO production compared to the eNOS present in the Golgi

membrane and plasmalemmal caveolae. Active eNOS associates with the cytoplasmic *cis* face of the Golgi apparatus, as evidenced by colocalization with mannosidase (*70, 71*) and association with DHHC21. In the cardiac microvasculature, eNOS expression is higher in arterial versus venous endothelium, and this difference may be due to a greater level of Golgi association in the coronary arteries (*72*). eNOS expression has been shown to be higher in venules than arterioles, but there is still some controversy over the differences between arterial and venous expression and activity of eNOS. Wagner *et al.* hypothesized that the high eNOS activity in arterial ECs reflects a role in regulating arteriolar tone and that venular-derived NO plays a key role in local thrombosis (*73*). The differential regulation and function of eNOS in arterioles and veins is further shown by experiments where, during thrombosis, inhibition of eNOS had no effect on arterioles but induced an increase of leukocyte adhesion in venules (*74*). These results could support the idea that there are differences in eNOS function between arterioles and venules, showing the role of eNOS in regulating arteriolar vasodilation and venous inflammation.

Using NO or ROS for vasodilation

The ultimate goal in understanding production of NO or reactive nitrogen species is to contextualize the resulting physiological effects. To regulate blood pressure, NO produced in ECs relaxes adjacent SMCs, causing dilation and lowering total peripheral resistance. In the resistance arterial vasculature, eNOS is responsible for 20-50% of dilation (*62, 75-82*), with endothelium derived hyperpolarization (EDH) accounting for the rest. However, NO appears to be responsible for a higher percentage of dilation in the conduit arteries (up to 100% of the dilatory component) (*83-86*). The contribution of NO bioavailability to dilation declines as the vascular tree progresses from being predominantly a pressure reservoir in large conduit arteries to a highly regulated distribution network in the

capillaries, but cannot be simply explained by expression levels as eNOS is located throughout different vascular beds (*87*). Several mechanisms could account for the reduction in reliance on NO bioavailability for dilation in the microcirculation.

Post-translational modifications. Differential post-translational modifications of eNOS could alter eNOS function and activity in each level of the vascular tree (*88-90*). As discussed above, eNOS phosphorylation is a key regulator of eNOS activity. The hemodynamic profile within blood vessels (specifically shear stress) impacts the activity of eNOS. While reports of shear stress throughout the vascular system are variable and depend on the vascular bed, methods of measurement, and animal model, there is agreement that conduit and large arteries are sensitive to shear stress, while areas with low shear stress experience lower NO bioavailability and increased plaque development (*91-95*). Indeed, eNOS is upregulated and activated (via phosphorylation of S1177) in rabbit carotid arteries in areas of high shear stress (*96*). Further evidence, also using *in vivo* measurements in rabbits, showed significantly lower expression of eNOS in coronary arteries compared to the aorta, which correlates well with hemodynamic signaling (*97*). In porcine vasculature, large conduit arteries that experience increases in wall shear stress positively correlate with eNOS expression (*98*). In porcine coronary arteries and arterioles, eNOS expression decreases as the vessels decrease in size (*99*), although shear stress was not measured in the latter study. This observation highlights apparent distinctions between large and resistance vessels, which include eNOS expression and activation via sensitivity to shear stress. There are currently no well-defined differences in eNOS post-translational modifications from arteries to arterioles that definitively explain the decreased reliance of arterioles on NO for dilation. While some uncertainty exists, vascular beds do regulate eNOS activity through differences in post-translational modifications; these remain intriguing therapeutic targets in hypertensive pathologies.

Localization. Subcellular localization of eNOS could account for the variation in eNOS activity observed (see above) (*89, 90, 100*). Activation of the caveolar and Golgi pools of eNOS via S1177 phosphorylation occurs by two different mechanisms, with caveolae-associated eNOS being more sensitive to $[Ca^{2+}]_i$ fluxes and Golgi-associated eNOS being more sensitive to Akt phosphorylation (*71*). Subcellular localization of eNOS affects functionality, and Golgi-localized eNOS is indicated to play an important role in the S-nitrosation of proteins (*101*). Given its close proximity to calcium currents and the larger amount of NO it produces, plasma membrane-bound eNOS in caveolae has a greater effect on SMC relaxation through cGMP signaling (*71, 102*). Thus, eNOS in microvascular ECs may be preferentially located in the Golgi (for S-nitrothiols) or caveolae (for direct NO production) depending on the vessel diameter.

Scavenging. NO may be present throughout the vasculature but is scavenged, allowing for EDH to dominate the dilatory component of resistance arteries. This observation is supported by recent research identifying the alpha subunit of hemoglobin (alpha globin) in EC and noting its enrichment at MEJs (*103*). Alpha globin is a potent scavenger of NO, and in ECs, the oxidation state of its heme dictates either NO diffusion into the SMCs or irreversible NO scavenging (*36, 104*). eNOS was also found to be enriched at the MEJ and forms a macromolecular complex with alpha globin (*35, 104, 105*). When the eNOS/alpha globin complex was disrupted, the functional outcome was increased NO bioavailability and lower blood pressure in mice (*35*). Given the spatial limitations found at the MEJ, and knowing that MEJs increase in frequency from proximal to distal arteries, it is postulated that alpha globin serves as a “sink” for NO, irreversibly scavenging NO production from eNOS (*106*). Together, the subcellular localization of eNOS to the MEJ could provide an explanation for the diminished impact of NO in the vasodilation of resistance vasculature, largely due to the increased frequency of MEJs

(and alpha globin) that serve as gateways to inhibit NO bioavailability to SMC and allow for EDH to predominate in driving vasodilation.

ROS and vessel size

Differences in the levels of reactive oxygen species (ROS) and byproducts generated by NO between small resistance and large conduit arteries may be responsible for the differences in NO dilatory abilities. ROS could serve as second messengers or activators of selective channels within vascular beds (*107, 108*). Vascular cells have been shown to have different oxidant profiles across the vascular tree (*109*). For example, the cerebral circulation is abundantly supplied with superoxide and products of NADPH oxidase, more so than other vascular beds, and these compounds have strong dilating effects on the basilar and middle cerebral arteries (*109*). These effects were limited in the aorta, carotid, and mesenteric arteries; but dilation in response to acetylcholine was similar across all vessels in the same study. Other reactive species, including $ONOO^-$, superoxide ($O_2^{\bullet-}$), and H_2O_2 have shown important roles in cellular communication. $ONOO^-$, a nitric oxide-derived oxidant, is formed when superoxide and NO react (*110*), and can not only oxidize DNA, proteins, and lipids, but also interfere with important vascular function by disrupting eNOS function. Oxidation of the Zn^{2+} coordination by $ONOO^-$ inactivates eNOS by uncoupling its dimer, which leads to synthesis of $O_2^{\bullet-}$ rather than NO (*108*). In addition, $ONOO^-$ inhibits Akt and increases AMPK-dependent S1177 phosphorylation of eNOS and downstream production of $O_2^{\bullet-}$, thereby reducing the bioavailability of NO (*107*). $O_2^{\bullet-}$is a cytotoxic gaseous molecule that is quickly degraded by superoxide dismutases that turn the radical into either O_2 or H_2O_2. H_2O_2 also possess an important role in the microcirculation: H_2O_2 can act as a vasoconstrictor and regulator of blood pressure (*111*). However, the mechanisms by which elevated concentrations of H_2O_2 lead to vascular dysfunction remain unclear. It is worth noting that H_2O_2 has a dual effect on eNOS function,

separately stimulating (*112*) and inhibiting (*113*) eNOS activity (*114*). One effect of H_2O_2 is via activation of $pp60^{Src}$, resulting in eNOS phosphorylation at Y418 (via autophosphorylation) and Y215 (an SH2-domain), both of which are inhibited by antioxidants (*115*). H_2O_2 induced $pp60^{Src}$ activation stimulates eNOS activity via downstream PI3 kinase and appears to be both concentration- and time-dependent in its resulting effects; i.e., H_2O_2 stimulates activity at lower levels (*114*) but inhibits eNOS activity at higher levels (*114*).

Myoendothelial junction components as controllers of vascular function

The MEJ is situated to be uniquely effective in controlling physiological function of the vasculature. As the resistance vasculature is responsible for determining blood pressure upstream, the control of arteriole constriction and dilation sets whole body blood pressure and perfusion on a rapid scale. NO is a potent vasodilator, and the precise control of its production and availability across the vascular tree is of critical importance.

In the large arteries, NO is a dominant mechanism of vasodilation. The conduit arteries have multiple lamina layers, which add radial stiffness to the vessel. Each of these layers is thick (up to about 5 μm) and dense with fibrous matrix. With a comparatively large distance between endothelial and medial layers in these vessels, a diffusible signal like NO has an advantage over relatively localized signals ion channels. After production in the endothelium, the dilatory signal can be distributed widely and affect cells distal from ones in direct contact. The ability of NO to diffuse and affect cells in multiple medial layers is essential for action in larger vessels. Although the conduit arteries are not the classical mediators of blood pressure, diameter changes can affect global blood flow and homeostasis. An intrinsic mechanism to regulate diameter is needed to maintain arteriolar

perfusion and be able to respond quickly to challenges. The relatively short-lived effects of NO are set up to have large arteries respond quickly to blood pressure changes.

At the level of the resistance arteries, MEJs allow cell-cell contact between endothelium and smooth muscle. The physical coupling is often accompanied by gap junction protein expression in the MEJs (*116*). The physical coupling allows some signaling molecules to diffuse through the MEJ to affect smooth muscle contraction. Additionally, calcium sequestering and sensitive proteins are found in MEJs, as is eNOS and a novel regulator of NO availability, hemoglobin alpha. This domain of the endothelial cell harbors vasodilatory machinery and affects the functional dilatory capacity of the vessel.

NO signaling is still effective in the resistance vasculature, but across many observations, NO is not the dominant mechanism for dilation in the smaller arterioles. Endothelial derived hyperpolarization mechanisms have been convincingly described as playing an increasingly larger role as the size of the vessel decreases. When the endothelial cells can locally affect the smooth muscle, the mechanism of creating relaxation can be much more localized. Small and intermediate conductance calcium-activated potassium channels (SK_{Ca} and IK_{Ca}, respectively) are expressed on the basolateral membrane of endothelial cells. After increases of intracellular [Ca^{2+}], these channels can be activated (though interaction with calcium sensing protein CaM to release K^+ ions into the extracellular space. The increased Ca^{2+} in the space between endothelium and smooth muscle has been suggested to enhance the activity of the Na^+/K^+ ATPase transporter or inwardly-rectifying K^+ channels (K_{IR}) on vascular smooth muscle. Increases in extracellular K^+ hyperpolarize the smooth muscle, preventing constriction and allowing other pathways to dilate the vessel. Myoendothelial gap junctions may also play a role in the electrical coupling of the cells in the vascular wall, and could transfer some charge into the smooth muscle cell in concert with channels releasing K^+. Small molecules such as

inositol triphosphate (IP_3) and cyclic adenosine monophosphate (cAMP) have been suggested as messengers that can cross gap junctions from endothelium to smooth muscle to enact vasodilation through secondary messenger pathways.

Other mechanisms that can cause dilation, independent of NO, include lipid-based metabolites of arachidonic acid (namely, epoxyeicosatrienoic acids (EETs)) (*117*), hydrogen peroxide (*118, 119*), and prostaglandins (*120-122*), just to name a few. These mechanisms are important, but others have done a much more thorough job reviewing these than I am capable of for now.

Alpha globin's role in determining a dilatory mechanism

Why does the relative contribution of NO-based dilation decrease down the vascular tree? One correlative piece of evidence is the expression of hemoglobin alpha (hereafter, alpha globin) in the endothelium of small arteries. It was shown *in vitro* and *in vivo* that the physical connection of smooth muscle and endothelial cells induces the expression of alpha globin in vascular endothelium. Note that this is not the expression of the hemoglobin as it exists in the red blood cell, a tetramer with two alpha and two beta chains. The monomeric alpha globin chain is stabilized in endothelium by alpha hemoglobin stabilizing protein (AHSP), which is co-expressed in arterial endothelium of resistance arteries compared to large arteries. Endothelial alpha globin, bound to AHSP, has a heme group accessible to gas binding, and thus can scavenge and dioxygenate NO produced by eNOS. This is a critical control block to post-production NO availability, as sequestration of NO by the alpha globin heme can inactivate it after dioxygenation, turning it to nitrate (NO_3), an inert compound.

NO scavenging by alpha globin is helped by the close apposition of the eNOS and alpha globin proteins in the endothelium. eNOS is often sequestered by its interaction with

caveolin-1 into caveolae in the MEJ; alpha globin is predominately localized to the MEJ in endothelial cells. Additionally, work from the Isakson and Columbus labs has shown that alpha globin and eNOS are sufficient to form a protein complex *in vitro*. That alpha globin and eNOS can associate and are expressed in the same domain of endothelial cells somewhat explains the decreased role of NO signaling in resistance arteries, where alpha globin is present.

In the original study, knockdown of alpha globin using siRNA resulted in increased NO availability from cell culture and ex vivo mouse thoracodorsal artery (a model of skeletal muscle resistance arteries). Functionally, a reduced vasoconstriction response (that was rescued by the NOS inhibitor L-nitroarginine methyl ester, L-NAME) to phenylephrine was observed in *Hba*-siRNA-treated vessels, suggesting that the knockdown of alpha globin increased the available NO derived from NOS enzymes.

A ten-amino acid motif on alpha globin was noted to be especially conserved in mammals. This region, ^{35}LSFPTTKTYF^{44}, was used to disrupt immunoprecipitation of alpha globin and eNOS from overexpression systems *in vitro*. Based on the biochemical competition for eNOS binding, it was hypothesized that this peptide could be used to disrupt the alpha globin/eNOS complex *in vivo*. To accomplish this, a *tat* motif from Human Immunodeficiency Virus was added to the N terminus of the alpha globin peptide. The *tat* tag has the sequence NH_2-YGRKKRRQRRR-COOH. Although it is not completely clear how the fusion of the basic residues to proteins and other peptides allows for cell entry, the *tat* fusion has been used in multiple studies to introduce an exogenous protein into cell culture and murine models. Together, this *tat*-alpha globin peptide fusion was named HbαX. Addition of the *tat* tag did not disrupt biological activity of the alpha globin mimetic region, and enhanced cell permeability to allow for *in vivo* study.

Recent work has given some more context to this protein complex. The region identified as the eNOS-interaction motif also has some overlap with the face of alpha

globin that interacts with its stabilizing protein. Recent work has demonstrated that alpha globin interactions with AHSP and eNOS are mutually exclusive; when bound to eNOS, alpha globin is stabilized and thus does not require AHSP, and vice versa. This handoff is required because alpha globin is unstable in solution without a binding partner. Similarly, in erythrocytes (and their precursors), alpha globin is bound first by AHSP and then chaperoned until it complexes with one beta globin chain for half of its physiological tetramer (two alpha and 2 beta chains form hemoglobin as it is classically known). In endothelium, it is possible that AHSP plays a similar role: stabilizing alpha globin folding and heme insertion before delivery of alpha globin to eNOS.

Although the interaction of alpha globin and eNOS allows alpha globin to bind and scavenge the newly produced NO, the iron in the heme group must be recycled from a Fe^{3+} (methemoglobin) to Fe^{2+} state before it is able to bind more NO. A potent reductase enzyme has been demonstrated as one way that the heme in alpha globin can be recycled for future scavenging reactions. Cytochrome B5 reductase 3 (Cyb5R3) is an enzyme that uses NADH as an electron donor to reduce methemoglobin to an active, ferrous form. This is required for continued scavenging of NO by alpha globin. It is not known whether Cyb5R3 is a third mutually exclusive binding partner of alpha globin in endothelium, however it accesses the heme group for reduction, the action of Cyb5R3 is essential for continued NO scavenging. Cyb5R3 knockdown decreases blood pressure, which is consistent with depleted stores of active alpha globin.

Overall, endothelial alpha globin has been demonstrated as an important factor in the control of NO signaling in the resistance vasculature.

Possible pharmacological intervention for NO in the microcirculation

In clinical settings, the effects of NO have been known for over a century (*123*). Before the therapeutic mechanism was known, successful treatment of vascular diseases was achieved by oral doses of nitroglycerin. NO is released from organic molecules by enzymatic processing; e.g., nitroglycerin is converted to NO via xanthine oxidoreductase and mitochondrial aldehyde dehydrogenase (*124*). Other organic molecules can deliver NO in physiologic conditions, but applications are more limited because of cytotoxic effects (*125*). A classic example, sodium nitroprusside, interacts with hemoglobin to release NO and a relatively large amount of cyanide, thereby undermining its long-term therapeutic effectiveness (*126*). NO is a prime target for the treatment of hypo- or hypertension. Increased NO release yields decreased blood pressure (an effective, if short term, treatment of hypertension), while reduced NO release inhibits vasodilation, effectively increasing blood pressure to combat hypotension. Thus, control of eNOS enzymatic activity is an important tool for therapeutic regulation of blood pressure.

Pharmacological intervention to activate or inhibit eNOS represents an important component in treatment of cardiovascular disease, although one that would require tight regulation. All human NOS isoforms (including eNOS, neuronal NOS, and inducible NOS) require dimerization for efficient production of NO (*127-129*). NOS monomers first form a “loose dimer” via inter-molecular cysteine coordination to the heme group. The initial homodimer interaction are subsequently stabilized by binding BH_4 and the substrate, L-arginine (*130*). Some imidazole-containing molecules can bind competitively in the L-arginine pocket and prevent dimerization (*131, 132*). L-nitroarginine methyl ester (L-NAME) is a common reagent for in vivo inhibition of NO production because L-NAME is converted to L-nitroarginine by cellular esterases. L-nitroarginine does not undergo the oxidation reaction that converts L-arginine to L-citrulline, thus inhibiting NO production by limiting substrate/enzyme interaction. These effects are dose-dependent and can be

overcome by a sufficient saturation with L-arginine (*128*). Although commonly used as an in vitro inhibitor of eNOS, L-NAME has been used clinically as a therapy for hypotension as a result of septic shock (*133, 134*). The target of the therapy is usually iNOS, although L-NAME is a general NOS inhibitor because it is a competitive inhibitor of the normal substrate.

Recent advances in manipulating eNOS activity have come through peptide-based regulation. Small peptides (10-20 residues) that mimic the binding sequences of interaction partners can be used to disrupt activating or inhibiting interactions. One method of molecular control of eNOS is by controlling interactions with Cav1 (*135, 136*). In caveolae, eNOS is spatially localized with Cav1, facilitating direct interaction. Residues 82-101 (the scaffolding domain) of Cav1 are responsible for binding to eNOS (*137*). To further study the interaction, alanine substitution in the Cav1 peptide allowed for functional output studies of critical residues. F92 is the critical residue in Cav1 that inhibits NO production possibly by interrupting an interaction of W445 with H_4biopterin (*138*). Mutation of F92 abrogates the inhibitory activity of the Cav1 peptide. *In vivo* results show that simultaneous delivery of F92 and A92 Cav1 peptides does not abolish NO production completely – the tighter binding affinity of the A92 peptide (23 nM compared to 49 nM for the F92 peptide) competitively inhibits the modulatory interaction of Cav1 (*138, 139*).

Another inhibitory regulator of eNOS and NO-induced vasodilation is alpha globin. In the regulation of vascular tone, alpha globin acts in two ways: as a scavenger of NO in the MEJ (*36*), and as a direct inhibitor of eNOS comparable to Cav1 (*103, 135, 137*). Evidence for the direct inhibition of eNOS comes from co-immunoprecipitation of alpha globin and eNOS (*35*). In the same study, a synthetic alpha globin peptide mimicking putative binding residues of alpha globin abrogated the interaction between native alpha globin and eNOS in vivo, leading to a significant decrease in blood pressure.

Both peptide therapeutics mentioned have achieved success *in vivo* (*35, 135, 138, 139*), but no human clinical data is yet available. However, laboratory data suggest promising results for peptide-based therapy targeting eNOS.

Role of eNOS in red blood cells?

Until recently, red blood cells (RBCs) have been viewed predominantly as a site of NO consumption due to the large propensity of hemoglobin to scavenge NO (*140-143*). In this context, the possibility of NO production in RBCs was considered unlikely (*144*). However, the story may be more complex than previously assumed. NO consumption rates in RBCs are two orders of magnitude lower than cell-free hemoglobin (*143*), likely due in part to decreased interactions between RBC-bound hemoglobin and NO in the lumen (*145, 146*). Potential barriers to NO scavenging by hemoglobin on RBCs include an RBC-free zone at the periphery of the vessel lumen (where NO is produced) (*141, 142*) and RBC membranes inhibiting NO diffusion into the circulating cell (*140*).

The presence of NOS in RBCs has been reported by multiple groups with varying details. Circa 2000, studies stated that both eNOS and iNOS are present in RBCs (*147, 148*), though Kang *et al*. reported that RBC NOS isoforms were not catalytically active. Furthermore, both groups hypothesized that if functional NOS were expressed on RBCs, the observed ability of RBC hemoglobin to scavenge NO from its surroundings would be compromised by competitive binding of locally-produced NO (*148*). In contrast, more recent evidence has been presented to suggest that RBCs universally express a catalytically active eNOS on the inner leaflet of the plasma membrane and in the cytoplasm (*144, 149*). RBC eNOS may also play an important role in both routine and diseased vascular function, as its activity and impairment was found to correlate with flow-mediated vessel dilation and endothelial dysfunction, respectively (*149*). Other research

suggests that RBC eNOS contributes to circulating nitrite levels, which may play a role in blood pressure regulation (*150*).

Though subject to some controversy, RBCs may be an important source of NO in the microvasculature. Under normoxic conditions, more NO may be produced in RBCs than any other cellular compartment(*149*), and NO production by RBC eNOS could have multiple physiological functions. One hypothesis is that RBC eNOS can create an “NO shield” against scavenging by RBCs, preventing interruption of intracellular signaling (*149*). Furthermore, shear stress in hypoxic conditions has been indicated to activate RBC eNOS (*151*), which in turn could play an important role in the regulation of RBC deformability to ensure adequate perfusion and oxygen distribution in the context of hypoxic conditions (*152*). This proposed function in particular suggests the potential for importance of NO from RBC eNOS in regulation of vascular flow. Finally, a broader RBC endocrine – or “erythrocrine” – function has recently been proposed in which RBCs provide systemic NO regulation throughout the vasculature (see (*153*) for details). Thus, an emerging perspective may be that much of the NO interacting with RBCs is produced locally, and that RBCs provide a transport function involved in the localization of NO signaling.

A major remaining question is to what extent RBCs represent an *in vivo* sink for vascular NO, and how this role is altered among different physiological regions and pathological states (e.g. across a range of blood oxidation levels or other variations in blood chemistry). Even when considered simply as a sink for NO, the role of RBCs in this context could be more dynamic than initially assumed if RBC eNOS can locally provide a shielding effect against NO scavenging. The variable extent of an RBC eNOS shielding effect could conceivably modulate the impact of NO release from other sources, such as eNOS in the endothelium, by allowing a given RBC to scavenge less or more NO from its surroundings. The possibility of this phenomenon is relevant to the study of NO regulation

of local myogenic tone and inflammation. Additionally, the ability of RBCs to influence the speciation of nitrogen oxides could define the potential of these cells as major signaling players in the vasculature. The ability of RBCs to scavenge and release NO in various settings suggests that they may be capable of activating or inhibiting NO signaling pathways in response to changes in blood chemistry across the vascular tree. Because of the key role of RBCs in the microcirculation, this potentially important site of NO generation requires further investigation in the contexts of vasodilation and inflammation.

There are numerous translational avenues that can come from a deep understanding of a fundamental process in vascular physiology. Understanding vascular biology, especially of small arterioles and the way that NO signaling is affected by alpha globin, is of key importance for understanding hypertension. The molecular determinants of the interaction can inform the mechanisms of alpha globin's control of NO signaling, as well as provide targetable motifs for novel therapeutics.

Figure and Tables

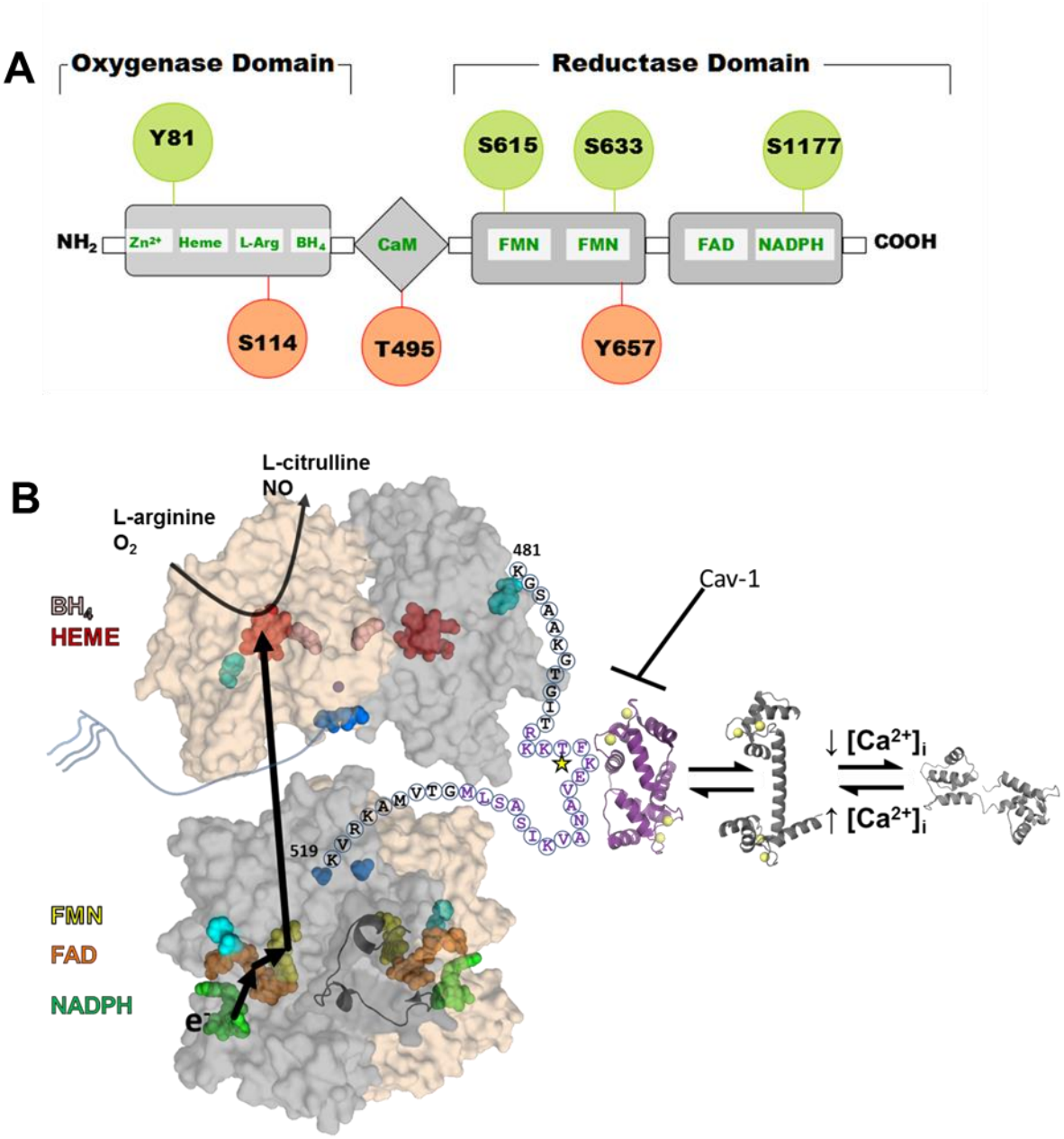

Figure 1. Structure and regulation of eNOS. (A) eNOS has oxygenase (residues 98 – 486), Calmodulin (CaM) binding (491 – 510), and reductase (756 – 1002) domains. All

three domains contain phosphorylation sites (indicated by circles) that modulate eNOS activity (red for decreased activity and green for increased activity). (B) Structural model of the full length eNOS. The crystal structure of the human oxygenase domain and a homology model of the reductase domain (using the rat nNOS reductase structure (PDBid: 1TLL) as the template) are shown in a surface representation with one subunit colored gray and the other tan. The autoinhibitory loop (residues 596 – 640) is rendered as a cartoon for one subunit. Cofactors are rendered as spheres and colored: NADPH, green; FAD, orange; FMN, yellow; heme, red; H_4biopterin, pink; and zinc, purple. The N- (blue) and C-terminal (cyan) are also rendered as spheres. The linker between the oxygenase and reductase domains is shown for one subunit with the letters indicating the primary sequence. Purple text highlights the CaM binding domain with the star indicating the T495 phosphorylation site. The structure of CaM bound to a peptide corresponding to the eNOS sequence is shown in purple, and the calcium-bound and unbound CaM structures are shown in shades of gray. This model is based on that proposed by Garcin *et al*. (*19*).

Table 1. eNOS binding partners

Protein	eNOS Binding Residues	Molecular Effect	NO Production Effect
β-Actin	326 – 333(*30*)	Hyperoxemia-dependent, stabilizes active form(*29*)	Increased
Calmodulin (CaM)	481 – 519(*57*)	Ca^{2+}-dependent, stabilizes dimer for activation, increases dissociation from membrane	Increased
Caveolin-1 (Cav1)	350 – 358 (*154*)	Disrupts CaM binding, sequesters eNOS into caveolae(*135*)	Decreased
Hemoglobin, α chain (Alphaglobin)	In oxygenase domain(*35*)	Scavenges NO, decreases activation(*103*)	Increased
Heat shock protein 90 (HSP90)	310 – 323(*24*)	Releases eNOS from Cav1(*25*), helps phosphorylation via Akt recruitment(*26*)	
NOS interacting protein (NOSIP)	366 – 486(*27*)	Traffics eNOS away from membrane, ubiquitin ligase activity(*28*)	Decreased

Table 2. eNOS phosphorylation regulation

Phosphorylation Effect	Phosphorylation Site	eNOS Domain	Protein Kinases	Phosphorylation Stimulators
Active	Y81(*47*)	Oxygenase	$pp60^{src}$	H_2O_2, shear stress
	S615(*38*)	Reductase	Akt, PKA	Bradykinin, ATP, VEGF, statins(*43*)
	S633(*41*)	Reductase	PKA	Shear stress, VEGF, bradykinin, ATP, statins(*38, 39, 43*)
	S1177(*155*)	Reductase	Akt, PKA, AMPK, PKG, CaM kinase II	Shear stress, VEGF, bradykinin, insulin, H_2O_2, estrogen, adiponectin, leptin, histamine, thrombin, ischemia, troglitazone, statins(*39, 40, 43*)
Inactive	S114(*46*)	Oxygenase	PKC, AMPK	Shear stress, HDL
	T495(*54*)	CaM Binding	PKC, AMPK	Insulin, angiotensin
	Y657(*58*)	Oxygenase	PYK2	Insulin, angiotensin, shear stress(*60*)

Chapter 2: Myoendothelial junctions, alpha globin, and tuning dilation phenotype: conduit arteries can look and act like a resistance artery

Adapted from: Shu, Xiaohong H., Claire A. Ruddiman, TC Stevenson Keller IV, Alexander S. Keller, Yang Yang, Miranda E. Good, Angela K. Best, Linda Columbus, and Brant E. Isakson. "Heterocellular Contact Can Dictate Arterial Function." *Circulation research* (2019).

Abstract

Resistance arteries and conduit arteries rely upon different relative contributions of endothelial derived hyperpolarization (EDH) versus nitric oxide (NO) to achieve dilation. Anatomically, resistance arteries contain many myoendothelial junctions (MEJs), endothelial cell (EC) projections that make contact with smooth muscle cells (SMCs). Conduit arteries have very few to no MEJs. It is unknown whether the presence of MEJs in conduit arteries is sufficient to alter vasodilatory and other heterocellular signaling.

We previously demonstrated that plasminogen activator inhibitor-1 (PAI-1) can regulate formation of MEJs. Thus, we applied pluronic gel containing PAI-1 directly to conduit arteries (carotid arteries, CAs) to determine if this could induce formation of MEJs. We found a significant increase in EC projections resembling MEJs that correlated with increased biocytin dye transfer from ECs to SMCs. Next, we used pressure myography to investigate whether these structural changes were accompanied by a functional change in vasodilatory signaling. Interestingly, PAI-1-treated CAs underwent a switch from a conduit to resistance artery vasodilatory profile via diminished NO signaling, and

increased EDH signaling in response to the endothelium-dependent agonists Ach and NS309. Following PAI-1 application, we also found a significant increase in carotid expression of endothelial alpha globin, a protein predominantly expressed in resistance arteries. Carotids from mice with PAI-1, but lacking alpha globin (*Hba1*$^{-/-}$), demonstrated that L-NAME, an inhibitor of NO signaling, was able to prevent arterial relaxation.

The presence or absence of MEJs is an important determinant for influencing heterocellular communication in the arterial wall. In particular, alpha globin expression, induced within newly formed EC projections, may influence the balance between EDH and NO-mediated vasodilation.

Introduction

Endothelial cell (EC)-mediated vasodilation of arteries can generally be achieved either through production of nitric oxide (NO) and/or via endothelial derived hyperpolarization (EDH) of smooth muscle cells. NO is produced by endothelial nitric oxide synthase (eNOS) and diffuses to smooth muscle cells (SMCs) to promote vasodilation by binding to its cytosolic receptor soluble guanylyl cyclase, which produces cyclic guanosine monophosphate (*156*). EDH refers to a signaling pathway that typically begins with the opening of small- and intermediate-conductance calcium-activated potassium channels (SK_{Ca} and IK_{Ca}) on ECs, leading to the efflux of potassium ions from smooth muscle cells (SMCs) (*157-160*). Hyperpolarization of smooth muscle due to reduced cytosolic positive charge leads to dilation. Both mechanisms of dilatory signals described above must be tightly regulated throughout the vascular tree to maintain blood pressure homeostasis. It has been established that the relative contribution of these endothelial-mediated vasodilatory mechanisms differ based on the size of the vessel; large conduit arteries such as the carotid and aorta rely on NO signaling to dilate, whereas in smaller, resistance arteries like the mesenteric arteries, EDH is an additional and important mechanism of dilation (*161*).

An anatomical difference exists in the structure of the conduit and resistance arteries that may account for the difference in functional dilation. ECs in resistance arteries have unique signaling microdomains named myoendothelial junctions (MEJs) that penetrate the fibrous internal elastic lamina (IEL) to make heterocellular contact with SMCs via gap junctions (*106, 162-165*). This direct heterocellular contact allows for electrochemical communication between ECs and SMCs to facilitate vasodilation predominantly through the EDH pathway (reviewed extensively (*82, 159, 166-168*)). In contrast, conduit arteries have a significantly reduced number of MEJs compared to resistance arteries, as well as a significantly thicker IEL (~0.5 μm in resistance arteries compared to up to 5 μm in aorta)

that allows them to handle high transmural pressures in proximity to the heart (*169-172*). Conduit arteries preferentially dilate via the NO pathway, presumably because NO is a highly diffusible signaling molecule that can cross the multiple thick IEL layers (*82, 103, 173-175*). In contrast, the expression of alpha globin in endothelial cells of resistance arteries may provide a constraint on the ability of NO to diffuse from endothelium to smooth muscle, limiting the role of NO in this setting (*103, 176, 177*).

Our lab has previously demonstrated that plasminogen activator inhibitor-1 (PAI-1) is highly enriched at the MEJ and that decreases in PAI-1 correlate with fewer MEJs. It is not known whether PAI-1 is sufficient to induce MEJ formation, and whether the induction of MEJs also induces endothelial alpha globin expression. Here, we apply recombinant PAI-1 to the carotid artery (a conduit, with low alpha globin expression and MEJ number) in live mice. These mice have transiently increased IEL holes and some endothelial projections, as well as alpha globin expression that mirrors the time scale of MEJ formation. The endothelial projections have protein signatures resembling MEJs, functional gap junction coupling between EC and SMC, and a changed vasodilatory phenotype (from primarily NO-mediated to mixed NO/EDH phenotypes). This model system has allowed us to study how arterial function is influenced by anatomical features of endothelium from different vascular beds.

Materials and Methods

Mice: All mice and procedures were approved by the University of Virginia Animal Care and Use Committee. Male C57Bl/6 (Taconic Biosciences) and Hba1$^{-/-}$ (Jackson Labs) mice were used between 10-12 weeks of age. Male mice were used in this study for consistency in comparison of results to our previous work, as well as to minimize possible variability given N-values.

Plasminogen activator inhibitor-1 (PAI-1): Lyophilized PAI-1 (500 IU, Technoclone, Vienna) powder was reconstituted by addition of 200 µl distilled water followed by gentle agitation for 5 minutes at room temperature (2.5 x 10^6 IU/L stock solution) that yields enzyme in its active form for ~12 hours or being bound to vitronectin. 40 µl/tube aliquots were stored at -70° C. At 4° C immediately prior to use, 40 µl stock solution of PAI-1 was mixed with 460 µl of sterile saline solution containing 35% F127 Pluronic Gel (Molecular Probes).

Mouse surgery: Mice were anesthetized with an intraperitoneal (i.p.) injection of a freshly made ketamine/xylazine mixture (Fort Dodge; 80 mg/kg and Vedco; 6 mg/kg, respectively). The pluronic gel/PAI-1 mixture (preparation described above) and pipettes were kept at 4° C and placed on ice just before use. The mouse was placed in the supine position, the hair of the neck area was removed with Nair lotion, and the neck skin was washed with 70% ethanol followed by iodine solution. A 10-mm incision was made on the anterior neck from the clavicle towards the chin and the skin was carefully cut open with scissors. The two lobes of thymus were carefully separated with forceps to expose the left common carotid artery (CA) lateral to the trachea. The CA was carefully separated from the vagus nerve and the tissue around the trachea. The tip of the forceps was carefully placed under the carotid, and the carotid was lifted slightly away from surrounding tissue. While holding the carotid artery (CA) away from surrounding tissues, the pluronic gel/PAI-

1 mixture (100 IU PAI-1 in 500 µl or 2 x 10^5 IU/L solution) or pluronic gel (500 µl of 35% pluronic gel) was topically applied to the outside of the left CA and solidified within one minute of application. Pluronic gel/PAI-1 mixture or pluronic gel only was kept on CAs for 1, 2, 3, 4, 5, 7, 14 or 21 days. At the end of the pluronic gel/PAI-1 or gel only incubation, mice were sacrificed using CO_2 asphyxia. A 10-15 mm incision was performed and the CA was carefully dissected using a stereomicroscope. Tissues were constantly kept moist with ice cold Krebs-HEPES containing (in mmol/L) NaCl 118.4, KCl 4.7, $MgSO_4$ 1.2, $NaHCO_3$ 4, KH_2PO_4 1.2, $CaCl_2$ 2, HEPES 10, glucose 6, and supplemented with 1% BSA. Once free of surrounding tissues and cleaned, the CA was used for a variety of experiments (see Supplemental Figure 1 for visual representation). Carotids for pressure myography were approximately 500 µm in diameter and 5 mm in length.

Visualizing holes and MEJs: Three methods were used, including: (1) fluorescent microscopic measurement of holes in the IEL, which used Alexa Fluor 633 hydrazide (Molecular Probes) to visualize the IEL, (2) endothelial denuded CA viewed with scanning electron microscopy (SEM), and (3) transmission electron microscopy (TEM) on intact CAs to visualize endothelial extensions.

Measurements of carotid artery vasoreactivity: CAs were isolated after treatment as described above, and cannulated in a pressure myograph chamber (Danish MyoTechnology, DMT) **(***76***)**.

In order to evaluate the effect of PAI-1 on the vasoreactivity of CA, where indicated, experiments were conducted in the presence or absence of selective blockers of endothelium-mediated vasodilator pathways. In order to block NO generation alone, we used the nitric oxide synthase (NOS) inhibitor L-nitro-arginine methyl ester (L-NAME, 300 µmol/L; Sigma). In order to block both NO generation and the EDH pathway, we used (1) the cyclooxygenase inhibitor indomethacin (10 µmol/L; Sigma), (2) the intermediate-conductance calcium-activated potassium channel (IK_{Ca}) blocker 1-[(2-chlorophenyl)

diphenylmethyl]-1H-pyrazole (TRAM-34, 10 µmol/L; Sigma), (3) the small-conductance calcium-activated potassium (SK_{Ca}) channel blocker apamin (300 nmol/L), and (4) L-NAME. After a 30-minute stabilization period in the circulating bath, the arteries were pre-constricted with 50 µmol/L phenylephrine (PE) followed by cumulative concentrations of Ach (10^{-9} to 10^{-4} mol/L). To activate IK_{Ca} and SK_{Ca} channels, NS309 (3 µmol/L), was added to pre-constricted CAs. All vessels were then washed with a Ca^{2+}-free Krebs-HEPES solution to obtain maximal passive diameter of the vessels. Internal diameter was measured throughout the experiments using the DMT MyoVIEW software. Vasoconstriction to PE was calculated as percent of initial diameter: %constriction = D_{PE} / $D_{initial}$ * 100, and relaxation to Ach or NS309 was calculated as a % relaxation: % relaxation = $[(D_{Ach} – D_{PE}) * 100]/(D_{max}-D_{PE})$, where D_{PE} was the diameter of the CA 10 minutes after application of 50 µmol/L PE; $D_{initial}$ was the diameter prior to the addition of PE; D_{Ach} was the diameter of the CA after application of a given dose of Ach; and D_{max} was the maximal diameter of the CA measured at the end of experiment.

Biocytin dye transfer: CAs were removed per above after experimental conditions, cannulated, and flushed with Ca^{2+}-free Krebs-HEPES buffer, followed by perfusion through with new buffer supplemented with 0.01% Tween20 + 2.68 mmol/L (1 mg/ml) biocytin for 15 minutes at room temperature. After washing the lumen and bath with Ca^{2+}-free Krebs-HEPES buffer, CAs were fixed in 4% PFA for an hour at room temperature, washed in PBS, and cut open longitudinally with the endothelium *en face*. Next, they were permeabilized in PBS containing 0.01% TritonX-100 for 30 minutes followed by an hour incubation in 1:500 streptavidin conjugated to Alexa Fluor 568 (also in PBS with 0.01% TritonX-100). CAs were imaged with an Olympus Fluoview 1000 confocal microscope.

Western blot: Blotting was performed as previously described (*178*). Briefly, CAs and third-order mesenteric arteries were isolated, homogenized in ice cold protein lysis buffer, and sonicated. Samples were mixed with Laemmli buffer and subjected to protein

electrophoresis using 4-15% Bis-Tris gels, then transferred to a polyvinylidene fluoride (PVDF) membrane. Blots were incubated with anti-alpha hemoglobin or anti-VE-cadherin primary antibodies (Abcam) overnight at 4ºC, respectively, followed by fluorescently tagged secondary antibodies (LICOR) for 1 hour at RT. They were visualized and quantitated using Licor Odyssey as previously described (N=minimum of 4 mice) **(***178***).** Data were analyzed with a one-way ANOVA test (Bonferroni post-hoc) where $p < 0.05$ was considered significant.

Statistics: For *in vivo* experiments, animals were randomly assigned groups by an independent third party. An independent researcher performed vasoreactivity or morphology and scores were re-assigned to treatment groups afterward. Power analysis was performed (α=0.05; > 20% change) to determine group sizes and study power (>0.80) using G*Power (*179, 180*). Thus, some experiments only required an N=3 while others required $N \geq 4$. One-way ANOVA followed by Tukey's multiple comparisons test or two-way ANOVA followed by Sidak's multiple comparisons test were used as necessary. For non-Gaussian distributed data (Shapiro-Wilk normality test), non-parametric statistical tests were used and indicated in the figure legend (Kruskal-Wallis test followed by Dunn's multiple comparisons test). Analysis was performed using GraphPad Prism version 7.0 for Mac OS X (GraphPad Software, La Jolla, CA) with $p < 0.05$ considered significantly different. Data are expressed as mean +/- SEM.

Results

Conduit arteries, including the carotid artery (CA), have a thick lamina layer separating the endothelium and smooth muscle, and few endothelial projections to connect the two cell types. We have previously demonstrated that PAI-1 is one regulator of myoendothelial junction (MEJ) formations (*116, 181*). We sought to determine whether exogenous PAI-1 application to a conduit artery could form functional MEJs, and what the physiological differences exist because of MEJ formation in the carotid.

To apply PAI-1 specifically, pluronic gel was used to localize recombinant, active PAI-1 to a unilateral carotid vascular bed (**Figure 1**). Initial screening for internal elastic lamina (IEL) holes occurred at 1, 2, 3, 4, 5, 7, 14, and 21 days. At these time points, the CA was excised, laid *en face*, and fixed for fluorescence imaging using the autofluorescence of the lamina layer. Days 1, 7, and 21 were illustrative of the transient nature of the holes, so work after the initial screening experiment continued using only these days. We found the maximum number of holes was observed at day 7 with PAI-1 treatment (**Figure 2A-G**). To confirm the holes observed by autofluorescence were not due to loss of fluorescence alone, the endothelium was stripped and the *en face* vessel was imaged using scanning electron microscopy (**Figure 2H-N**). Because not all IEL holes contain endothelial projections or MEJ proteins, we confirmed that the endothelium was infiltrating the IEL layer using transverse sections and transmission electron microscopy (**Figure 2O-U**). In all cases, there was a transient effect of PAI-1 treatment; the number of holes and endothelial projections increased at 7 days, but had returned to baseline values at day 21. The IEL holes induced in the CA match the mesenteric and thoracodorsal arteries in terms of hole size (**Figure 3A**), even though the IEL of the CA is much thicker (0.5 μm in resistance arteries (not shown), compared to about 3 μm in the CA (**Figure 3B**)). PAI-1 treatment did not change the thickness of the IEL (**Figure 3B**), so endothelial projections were not influenced by decreased distance between the endothelium and smooth muscle.

Although we observed increased endothelial projections, it was not known whether increased numbers of projections at day 7 would result in functional MEJs. Indeed, markers of MEJs appear to localize to the holes at day 7 (**Figure 4**). The presence of VE-cadherin in the top row shows that the endothelial monolayer is intact in these images. Connexin 40 (Cx40) is a component of gap junctions that form between endothelium and smooth muscle in the mature MEJ (*181, 182*). Some, but not all holes seen in the carotid are positive for Cx40 staining, suggesting that functional gap junction channels have formed between endothelium and smooth muscle after PAI-1 treatment and induction of holes. Additionally, alpha globin expression is normally restricted to resistance arteries where MEJs are more common than in the carotid. After 7 days of PAI-1 treatment, alpha globin expression is seen in the CA and localizes to the IEL holes (**Figure 4, third row**). The expression of these MEJ markers suggest that the endothelial projections through the IEL holes induced by PAI-1 allows protein machinery for functionally coupling endothelium and smooth muscle in a conduit artery.

Although Cx40 and alpha globin are present, we wanted to determine the extent of physical coupling by testing gap junction connectivity between EC and SMC. Biocytin is a small uncharged molecule that can pass through gap junctions and can be detected by labeling with streptavidin. Loading of the endothelium with biocytin allows for determination of the gap junction connectivity of endothelium and smooth muscle layers. In **Figure 5A**, the endothelium monolayer was loaded consistently with biocytin dye across the treatment conditions shown. At day 0, there is little connectivity between endothelium and smooth muscle, shown by little red signal (positive signal for biocytin) in the smooth muscle layer. At day 7, where IEL holes and endothelial projections are maximal, dye is transferred from the endothelium to smooth muscle. This dye transfer can be inhibited by pretreatment with α-glycyrrhetinic acid (αGA), a non-specific but effective gap junction inhibitor (*183*). Across all times and treatment conditions, dye transfer was observed

maximally at day 7 of PAI-1 treatment (**Figure 5B**). Another test of endothelial-smooth muscle functional coupling is the dilation of the vessels to the IK_{Ca} and SK_{Ca} channel activator, NS309 (3 μM, **Figure 5C**). Dilation to NS309 suggests that EDH signaling, normally low abundance in conduit arteries, is intact and active. At day 7 of PAI-1 treatment, NS309 induced a significant, endothelium-dependent, vasodilation signal. Thus, we can correlate the presence of MEJ machinery to functional coupling of the endothelium and smooth muscle that is normally restricted to resistance arteries.

EDH is the dominant vasodilatory mechanism to cholinergic stimulation in arteries with many MEJs. This is the case in resistance arteries, and is opposite to the normal behavior of conduit arteries where NO dominates signaling (and where there are few MEJs). Using our model of inducing MEJ formation in the CA, we sought to determine if the presence of MEJs is sufficient to determine the vasoreactivity profile of the artery. Using a host of pharmacological interventions, we narrowed down on the mechanism of vasodilation. L-nitroarginine methyl ester (L-NAME) is an arginine analog that inhibits NOS enzymes generally, preventing NO generation from eNOS in endothelium. Application of L-NAME to *ex vivo* cannulated and pressurized CAs largely blunts dilation to increasing doses of acetylcholine (ACh) (**Figure 6A**, Day 0, blue line). There is no additional inhibition of dilation by inhibiting other endothelial-derived vasodilation pathways (**Figure 6A**, Day 0, red line). Apamin, TRAM-34, and indomethacin were used (inhibitors of IK_{Ca} channels, SK_{Ca} channels, and cyclooxygenase enzymes, respectively) in addition to L-NAME. Only at day 7 of PAI-1 treatment was there a difference in the L-NAME alone and L-NAME + other inhibitors; L-NAME was not able to fully blunt the dilatory signals, but inhibiting all of the pathways above completely inhibited the vasodilation (**Figure 6A**). This mode of vasodilation has characteristics of conduit and resistance artery.

One of the major components of the vasodilatory control from MEJs is the expression of alpha globin. Alpha globin is able to bind to eNOS and scavenge NO, preventing dilatory

action (*35, 103, 184*). At baseline, alpha globin expression is low in the carotid artery (**Figure 7A**, Day 0). Matching the immunofluorescence above, alpha globin expression was maximal in the CA at day 7, and decreased with the decrease in MEJs by day 21. This was confirmed in CAs from Hba1$^{-/-}$ mice; a neomycin cassette in the gene for Hba1 prevents correct translation and decreases protein expression globally (**Figure 7B**). Comparing to a model of resistance artery in the mesentery (**Figure 7C**), the day 7 CA matches the alpha globin expression of that vessel most closely. However, it is unknown whether the expression of alpha globin was determining the vasoreactivity profile of the CAs treated with PAI-1 for 7 days.

The same surgery, PAI-1 application experiments, and analysis were performed on the Hba1$^{-/-}$ mice. IEL holes, endothelial projections, dye transfer, and NS309 reactivity were all increased to a similar extent as C57Bl/6 mice for the *Hba1*$^{+/+}$ and *Hba1*$^{-/-}$ mice (**Figure 8A-E**). There were no differences between *Hba1*$^{+/+}$ and *Hba1*$^{-/-}$ groups in all cases. However, differences exist in the vasoreactivity profile depending on the expression of alpha globin. In **Figure 8F**, *Hba1*$^{+/+}$ display a similar profile to the C57Bl/6 mice, in that L-NAME does not completely blunt the vasodilatory response. However, with the *Hba1*$^{-/-}$ mice, L-NAME has a much larger influence on the vasodilation. The L-NAME and “L-NAME + other inhibitors” dilation curves are much closer in the *Hba1*$^{-/-}$ genotype. This suggests that NO is still a dominant mechanism of dilation in the CA, even with increased MEJ formation. Overall, the expression of alpha globin in MEJs of resistance arteries seems to facilitate NO-independent dilation mechanisms to dominate.

Discussion

We have previously demonstrated that PAI-1 is enriched in MEJs (*185*). In this study, we further investigated the involvement of PAI-1 in MEJ formation by directly applying PAI-1 to the CAs of mice via pluronic F-127 gel, a useful medium that can deliver high concentrations of PAI-1 to carotid arteries while avoiding adverse systemic effects. The local increase in PAI-1 at the CA resulted in major phenotypic shifts in structure and function to make this conduit artery resemble a resistance artery. For example, CAs normally have very few holes in the IEL, nor EC projections (i.e., MEJs) through those holes; however, following 7 days of PAI-1 treatment, both of these anatomical phenomena developed. In addition, indications of direct heterocellular coupling between endothelium and smooth muscle were also apparent. This included Cx40 expression in the newly formed IEL holes, blocked biocytin transfer with gap junction inhibition via α-GA, and NS309 dilation. However, direct evidence of heterocellular contact via electrical coupling (e.g.,(*160, 186*)) could not be demonstrated. Regardless, the significant upregulation of IEL holes, endothelial projections, and functional heterocellular coupling represents an important anatomical and functional shift in a conduit artery.

It is unclear why the IEL holes are temporary, but it could represent either an unresolved inflammatory response or degradation of the exogenously applied PAI-1; this will require elaboration in future studies. However, this temporal loss of the IEL holes formed following PAI-1 treatment speaks to the dynamic nature of IEL holes/MEJs and the potential necessity of a constant stimulus to maintain the ability to form MEJs, especially in resistance arteries. Here we report not only an increase in IEL holes but also the formation of endothelial projections. Although this manuscript does not address the proportion of IEL holes that contain MEJ markers, the significant upregulation of endothelial projections is itself an important anatomic change. Since exogenous application of PAI-1 alone induces formation of IEL holes and MEJ-like projections within

the carotid, this represents an important advancement in our understanding of the development of these critical vascular signaling microdomains. The spatial distribution of PAI-1 across the vascular wall may be one such avenue to explore; with PAI-1's local translation and enrichment at MEJs (*187*), it is possible each MEJ signaling domain may be capable of regulating its own formation.

Functionally, the induction of endothelial projections (i.e., MEJs) in the carotid was able to introduce a larger contribution of EDH into the vasodilatory component of these conduit arteries. Pressure myography experiments revealed relaxation via the IK_{Ca}/SK_{Ca}-channel activator NS309 only in PAI-1-treated CAs at 7 days post treatment. In addition, L-NAME, an inhibitor of NO production, was unable to prevent vasodilation via the ACh pathway in PAI-1-treated carotids. These pressure myography results indicate a switch from primarily NO-based signaling, normally characteristic of conduit arteries, to a predominantly EDH-based mechanism, which is suggestive of resistance arteries. The correlation of this switch in dilatory mechanism alongside increased MEJ formation mimics the anatomical and functional observations of resistance vessels, thereby implicating MEJs as a potentially critical endothelial signaling microdomain that determines the dominant dilatory pathway of arteries.

Interestingly, increased alpha globin expression was also detected in CAs following PAI-1 treatment. Alpha globin expression is normally limited to resistance arteries, but not conduit arteries **(***35***).** Alpha globin has been shown to complex with eNOS to regulate NO-signaling in the resistance vasculature (*176, 177*). Its expression at the MEJ may act to finely control vasodilation by limiting the diffusion of eNOS-derived NO to the SMC (*35*). Contact between ECs and SMCs is required for the expression of alpha globin in ECs (*103, 188*), and in the newly formed EC projections that resulted from PAI-1 treatment, alpha globin expression is significantly increased which correlated with limited dilatory effect of NO (**Figures 7 and 8**). However, in mice with a disrupted alpha globin gene

product (due to the insertion of a neomycin cassette into exon 2 of the Hba1 gene), the dependence on NO signaling is not lost: relaxation is almost completely blunted with L-NAME alone (as in an untreated CA), with little additive effect from EDH inhibitors (**Figure 8**). Within the vasculature, cell-cell interactions induce protein expression to influence cellular function (*103, 188-191*) and our results embody this motif: alpha globin expression is induced upon heterocellular contact (EC-SMC coupling) and alters cellular/organ function (mechanism of arterial relaxation). This data also fits well with previous work demonstrating alpha globin's regulation of eNOS (*176, 177*) and suggests that alpha globin expression is important for EDH based signaling to predominate. Indeed, disruption of the alpha globin/eNOS interaction via a mimetic peptide leads to increased NO signaling in resistance arteries (*35, 177*). Based on this and the data we show here, alpha globin at newly formed endothelial projections in PAI-1-treated carotids likely participates in the switch to EDH-based relaxation through limiting the effects of NO-based vasodilation. It is also possible that the PAI-1 enzyme may be simultaneously acting on eNOS to reduce NO-availability, enhancing the inhibitory effect to ensure EDH predominates. The interaction between PAI-1 and eNOS may be an interesting avenue to explore in future studies.

Since the major anatomical differences between a conduit and resistance artery are the IEL and points of heterocellular contact via MEJs, our finding that the induction of EC projections (i.e., MEJs) can switch a conduit artery's dilatory mechanism from NO-dominated to likely EDH-dominated demonstrates a match between form and function. Our data suggests that MEJs with alpha globin are an important signaling microdomain, and could be the reason why EDH predominates in resistance arteries.

Figures

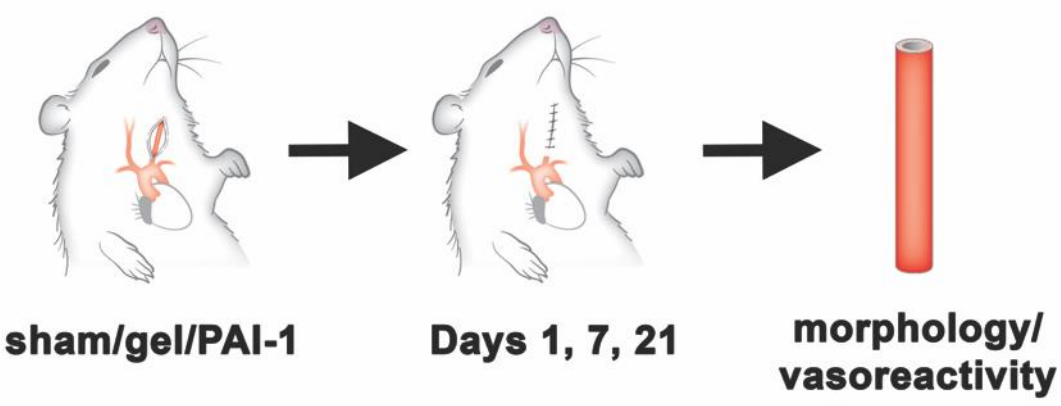

Figure 1. Model of pluronic gel/PAI-1 application to one carotid artery. A 10-mm incision was made on the anterior neck, and the carotid was carefully separated from the vagus nerve and other surrounding tissues. Pluronic gel was added to surround the artery, and the site closed with interrupted sutures. The mouse was able to recover, and experiments occurred at 1, 7, and 21 days after initial surgery to assay the vessel for morphology and reactivity.

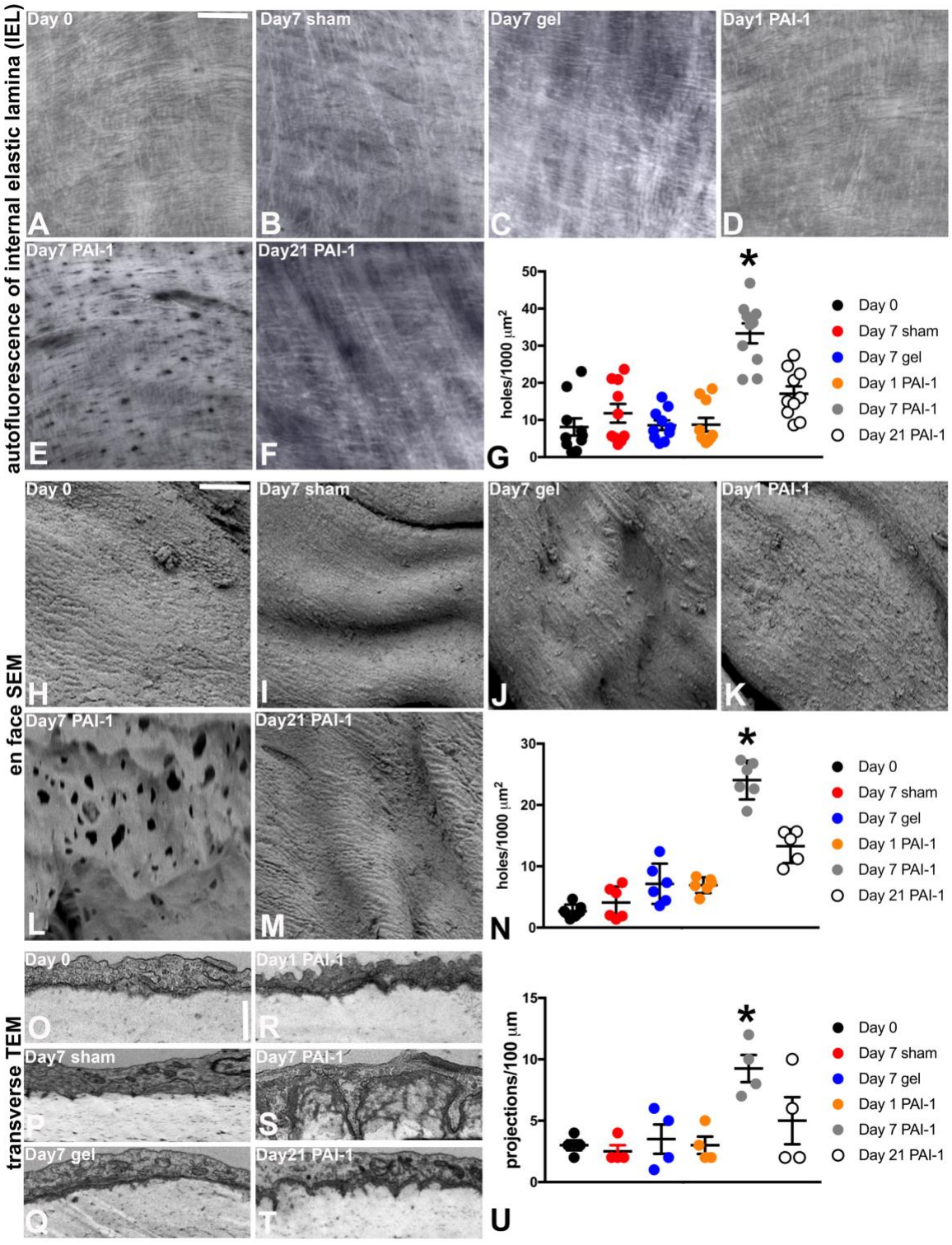
autofluorescence of internal elastic lamina (IEL)
Day 0
Day7 sham
Day7 gel
Day1 PAI-1
A
B
C
D
Day7 PAI-1
Day21 PAI-1
E
F
holes/1000 μm²
G
Day 0
Day 7 sham
Day 7 gel
Day 1 PAI-1
Day 7 PAI-1
Day 21 PAI-1
en face SEM
H
I
J
K
L
M
N
transverse TEM
O
R
P
S
Q
T
projections/100 μm
U

Figure 2. Formation of holes and cellular extensions into the internal elastic lamina of carotids after PAI-1 application. A-F, Representative confocal images of the IEL from CA *en face* preparations at 0, 7, and 21 days following PAI-1 treatment and from sham control. The number of holes per 1000 μm^2 is quantified in **G**. Scale bar in A is 20 μm and representative for A-F. In **H-M**, SEM images of the IEL from CA *en face* preparations at 0, 7, and 21 days following PAI-1 treatment and from sham control, with quantification of holes per 1000 μm^2 in **N**. Scale bar in H is 2 μm and representative for H-M. In **O-T**, TEM images on transverse sections at 0, 7, and 21 days following PAI-1 treatment and the sham controls, with number of projections per 100 linear µm quantified in **U**. In all cases, each dot on graphs in G, N, and U indicates the average of 3 random fields of view from 1 mouse. Scale bar in O is 1 µm and representative for O-T. In each graph, N=4 mice per experimental time point; *=$p<0.05$.

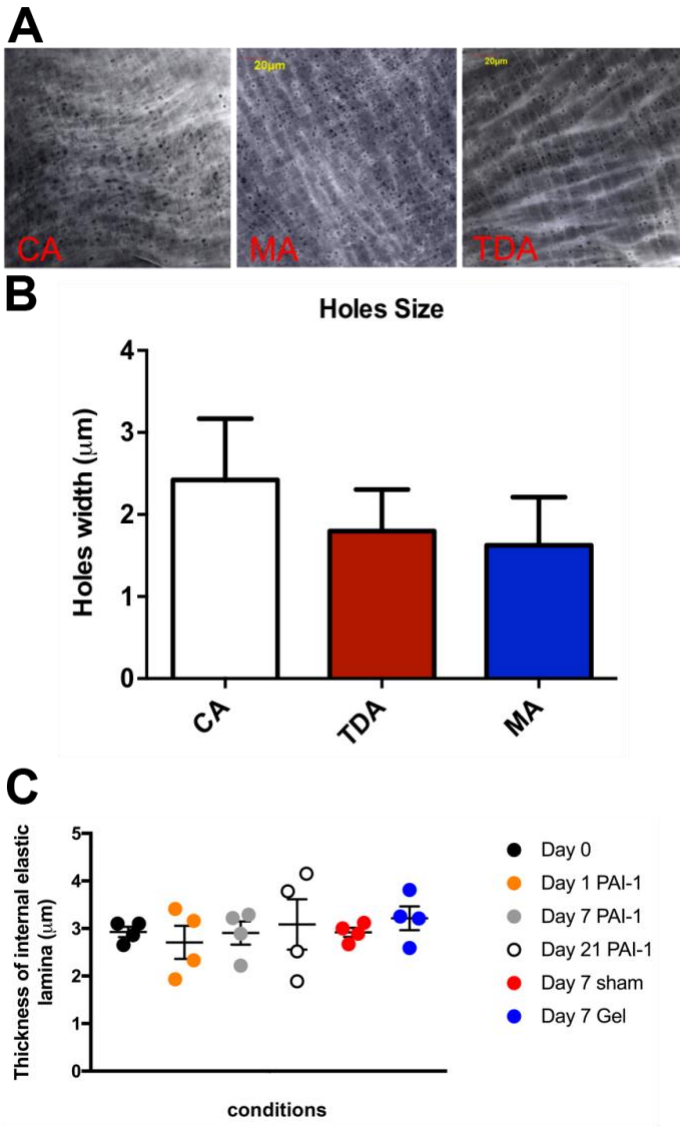

Figure 3. PAI-1 induced hole size is similar to resistance arteries and independent of IEL thickness in the CA. A IEL holes visualized via autofluorescence of the laminal layer. Representative images from the carotid artery (CA), a third-order mesenteric artery (MA), and thoracodorsal artery (TDA). Scale bars represent 20 μm in each case. **B** Average hole diameter is not different across the three vascular beds. **C** The thickness of

the IEL is unchanged by PAI-1, pluronic gel, or sham surgeries across days 0 to day 21. Thickness was measured by confocal Z depth of the autofluorescence layer.

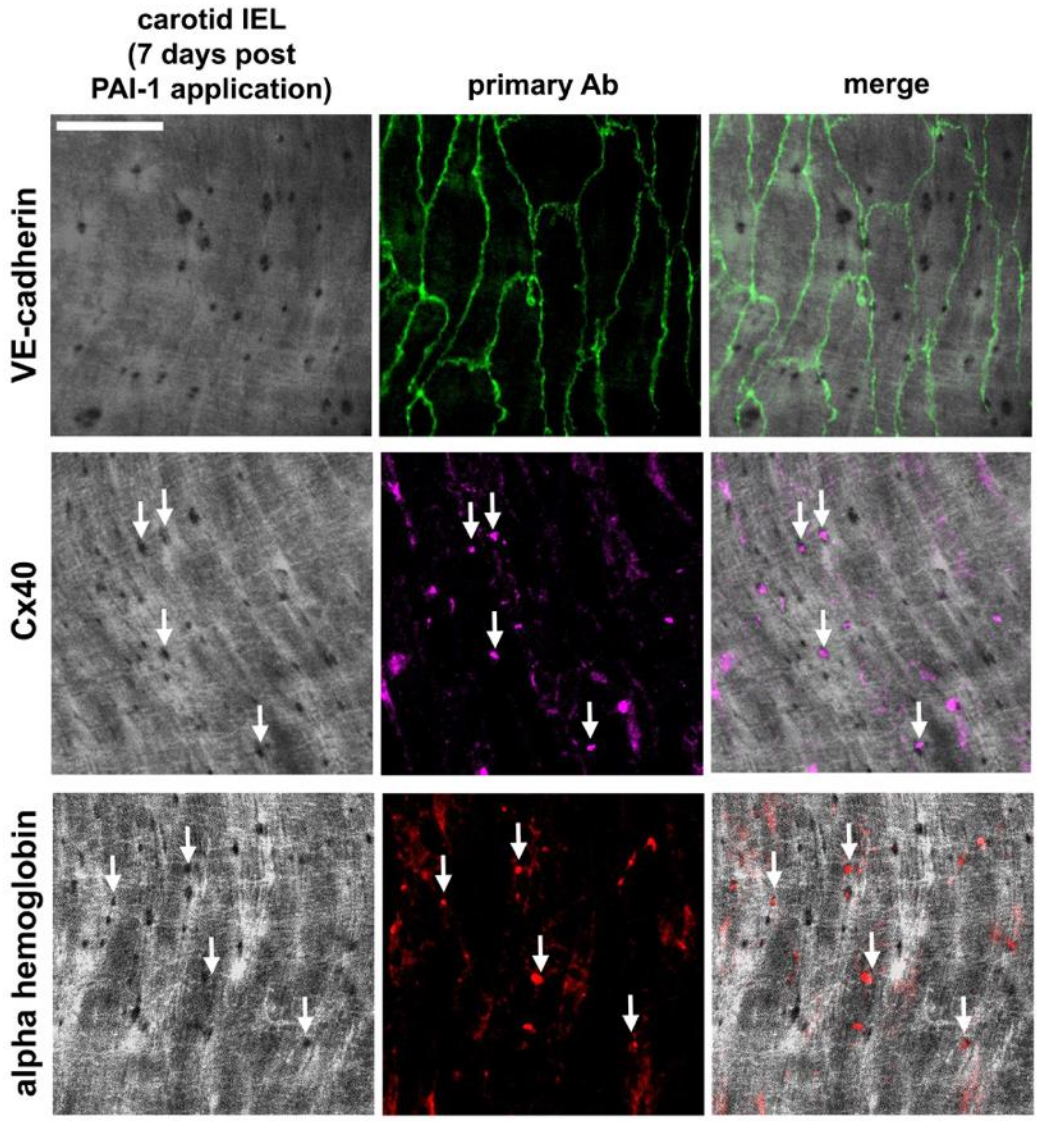

Figure 4. MEJ markers Cx40 and alpha globin are observed in the holes of the CA after PAI-1 application. Top row VE-cadherin marks the border of the endothelial cells in an *en* face preparation of the CA after PAI-1 application. **Middle row** Cx40 (magenta) is observed in the holes of the IEL from the CA (arrows mark the same IEL holes across the three images. **Bottom row** alpha globin localizes to IEL holes, in a similar pattern to Cx40. Arrows mark the same location in all images of the row. Scale bar in upper left is 20 μm and is representative for all images.

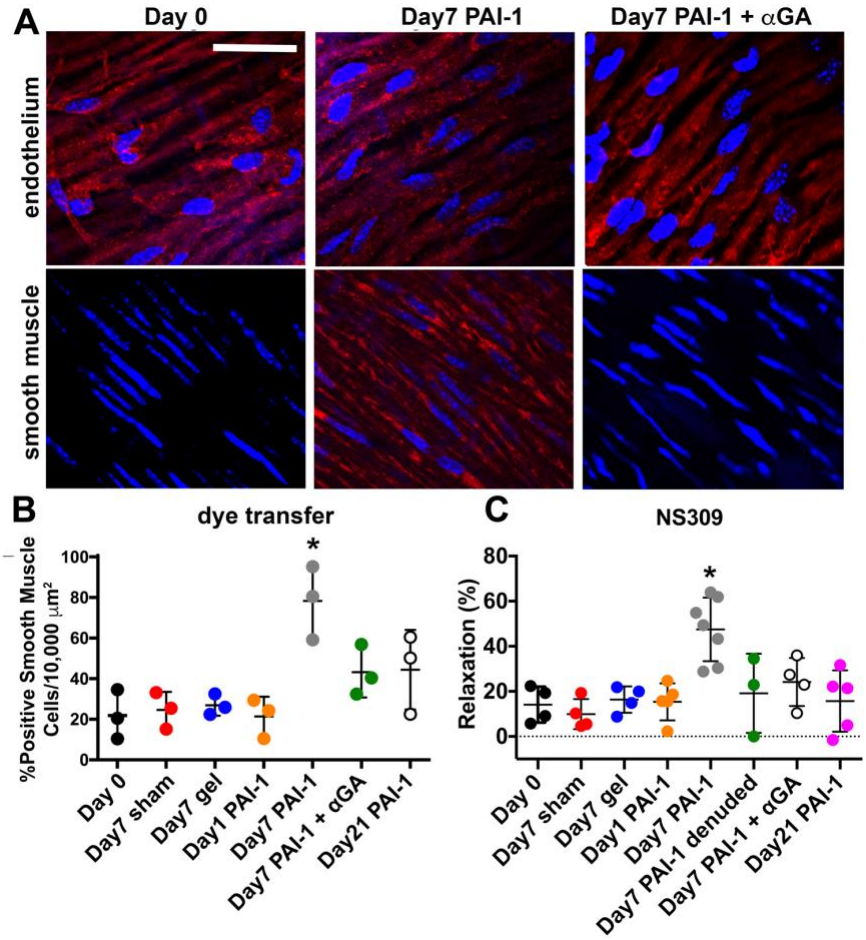

Figure 5. Endothelium and smooth muscle cells of the carotid are functionally coupled after PAI-1 application. A Representative images of biocytin highlighted with streptavidin conjugated Alexa 568 fluorophore (red); nuclei in blue (DAPI). The XY-plane of endothelium is shown in the top row and smooth muscle in the one below. Note the addition of α-GA blocked biocytin transfer to smooth muscle in carotids treated with PAI-1 for 7 days. Scale bar is 20 μm. A Kruskal-Wallis test followed by Dunn's multiple comparisons test was used to establish significance. **B** Percent streptavidin-positive smooth muscle cells per 10,000 μm^2 after loading of endothelium with biocytin. In **C**, carotids were stimulated with 3 μmol/L NS309 and relaxation was measured. Each dot on

graphs in B and C indicates the average of 3 random fields of view from 1 mouse, minimum N=3 mice per experimental condition. Note the addition of α-GA, and denuding endothelium, prevented relaxation of carotids treated with PAI-1 for 7 days. In each graph, *=$p<0.05$.

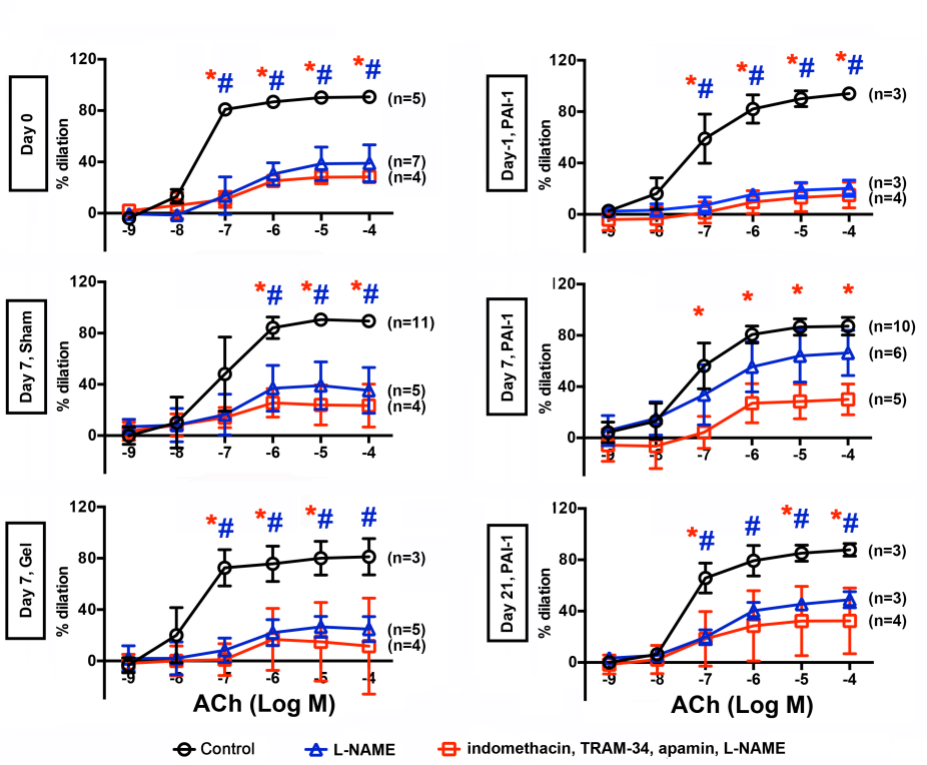

Figure 6. When myoendothelial junctions are present in carotids, acetylcholine-induced relaxation is no longer predominately reliant on nitric oxide. Dose response curves to ACh; black circles are untreated control carotids, blue triangles are carotids treated with L-NAME, and red squares are carotids treated with L-NAME plus the inhibitors TRAM-34, indomethacin, and apamin. N values indicate the number of carotids. In all experiments, a minimum of N=3 mice were used per time point per experimental condition. *=p<0.05 indicates control compared to L-NAME, TRAM-34, indomethacin, and apamin; #=p<0.05 indicates control compared to L-NAME.

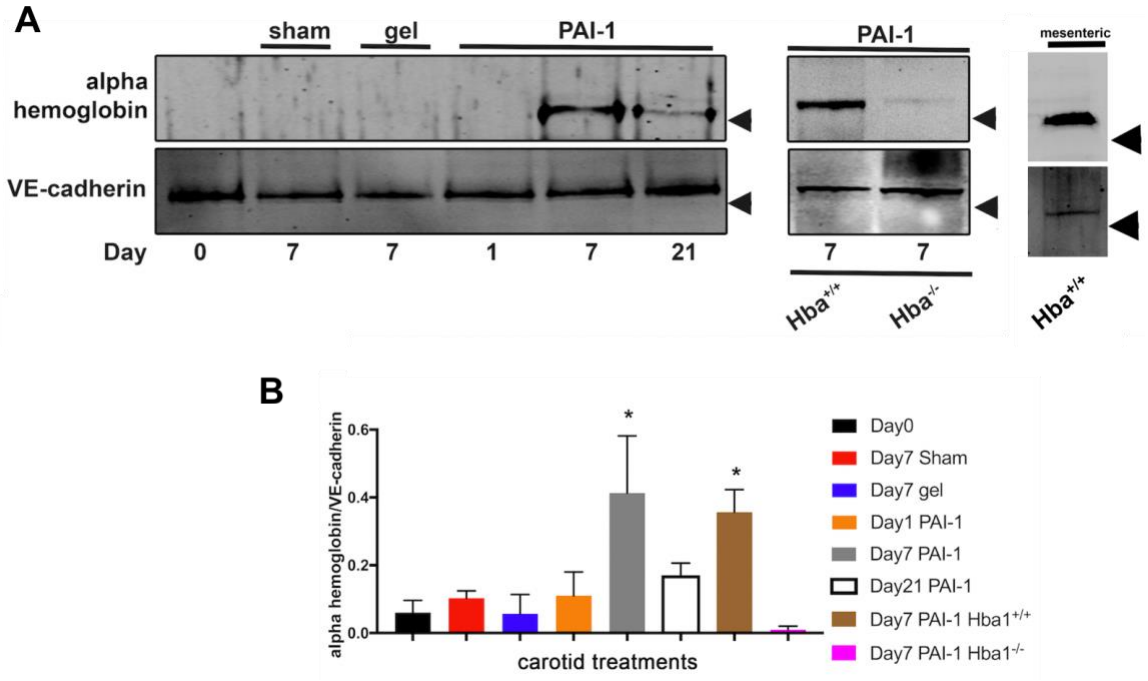

Figure 7. Expression of alpha globin in carotid arteries after PAI-1 application. In **A,** Western blot for alpha globin from carotids, with VE-cadherin used as loading control for endothelium. In the second panel, expression of alpha globin at 7 days post-PAI-1 application is shown in samples from $Hba1^{+/+}$ and $Hba1^{-/-}$ mice. Compare the alpha globin expression at day 7 with alpha globin expression in the mesenteric artery (third panel). Arrows indicate 10 kDa for alpha globin, and 100 kDa for VE-cadherin. **B** Quantification of alpha globin expression from the carotid artery lanes shown in A. Note the significant increase in alpha globin 7 days after PAI-1 treatment that decreases by day 21, matching hole and endothelial projection prevalence.

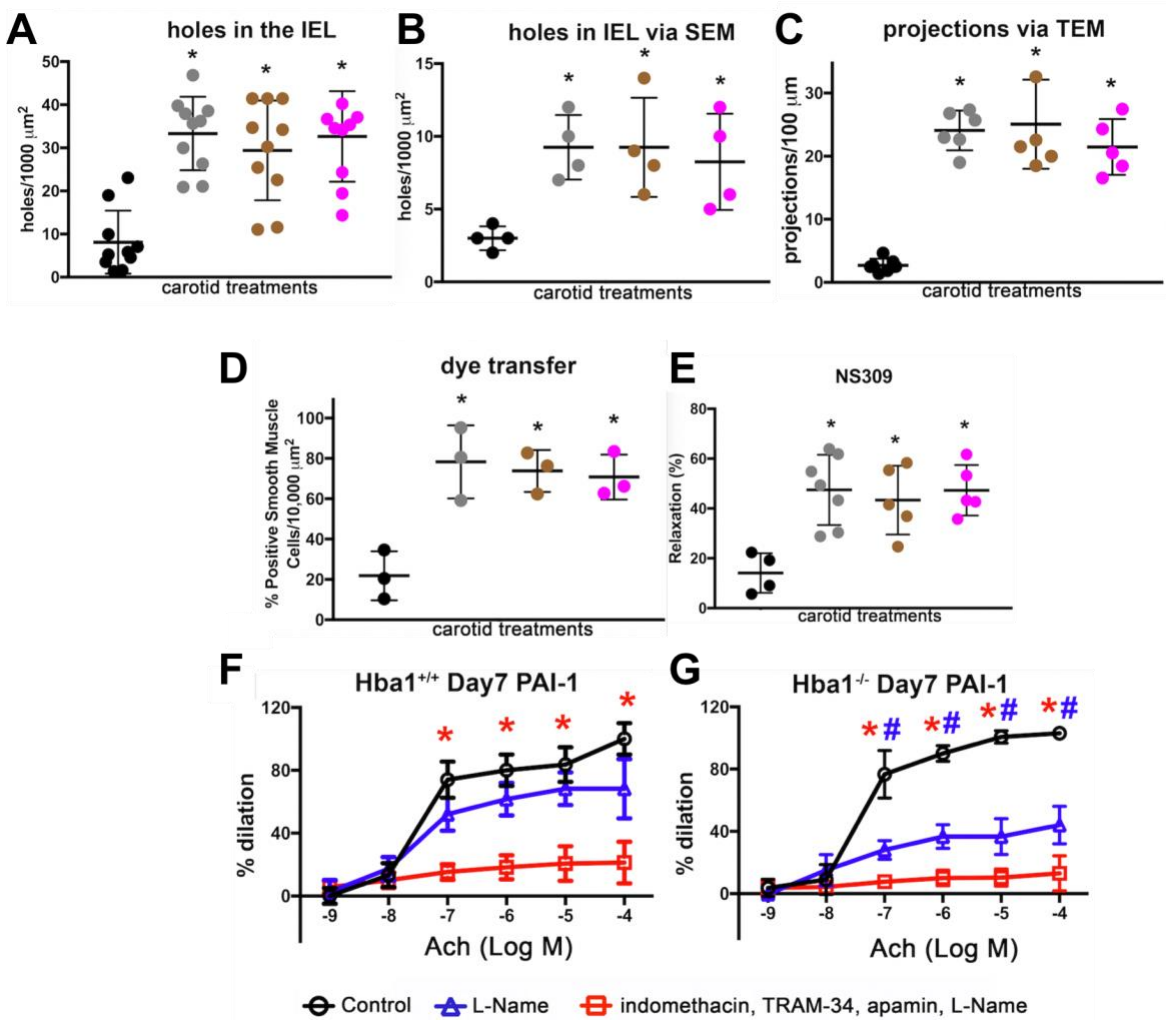

Figure 8. Induction of alpha globin expression within heterocellular contacts regulates nitric oxide diffusion, but not myoendothelial junction formation. In **A** and **B**, the number of holes in the IEL were assessed via fluorescent microscopy (A) and SEM (B). In **C**, endothelial projections down into the IEL were assessed the same way as in Figure 1. Coupling of endothelium and smooth muscle was experimentally determined using biocytin dye transfer (**D**) and relaxation to NS309 (**E**). In A-E, colors indicate identical time points; black is day 0 after PAI-1 on a C57Bl/6 mouse, grey is day 7 after PAI-1 on a C57Bl/6 mouse, brown is day 7 after PAI-1 on a $Hba^{+/+}$ mouse, and pink is day 7 after PAI-

1 on a $Hba^{-/-}$ mouse. In **F** and **G**, CAs were collected from $Hba^{+/+}$ (**F**) or $HBA1^{-/-}$ (**G**) mice 7 days after PAI-1 application, cannulated, pressurized, and tested in the presence of L-NAME or L-NAME with the inhibitors, indomethacin, TRAM-34, and apamin. Loss of alpha globin had no effect on the number of holes in the IEL, cellular extensions, dye transfer, or NS309 induced relaxation (IK_{Ca}/SK_{Ca}), indicating MEJs were still capable of forming (**B-E**). However, data in **F** and **G** demonstrate the mechanism of endothelial vasodilation was altered without alpha globin present. In all cases, each dot on graphs in A-E indicates the average of 3 random fields of view from 1 mouse. In F-G, each dot represents 1 mouse. In each graph, * and # = $p<0.05$. In B-G, * indicates control compared to respective carotid treatment. In H and I, * indicates control compared to inhibitors L-NAME, TRAM-34, indomethacin, and apamin; # indicates control compared to L-NAME.

Appendix

Contributions from authors:

X Shu and CA Ruddiman performed experiments, especially *en face* imaging and vasoreactivity. ME Good, Y Yang, and AS Keller performed vasoreactivity and other experiments as needed. X Shu and TCS Keller were responsible for carotid/PAI-1 surgeries. AK Best supervised mouse colony management, L Columbus and BE Isakson supervised project.

TCS Keller amended figures and manuscript text for this version of the manuscript is his Ph.D. dissertation.

Chapter 3: Modulating Arterial Hemodynamics through disruption of the alpha globin / eNOS macromolecular complex

Adapted from: Keller IV, TC Stevenson, Joshua T. Butcher, Gilson Brás Broseghini-Filho, Corina Marziano, Leon J. DeLalio, Stephen Rogers, Bo Ning, Jennifer N. Martin, Sylvia Chechova, Maya Cabot, Xiaohong Shu, Angela K. Best, Miranda E. Good, Alessandra Simao Padilha, Michael Purdy, Mark Yeager, Shayn M. Peirce, Song Hu, Allan Doctor, Eugene Barrett, Thu H. Le, Linda Columbus, and Brant E. Isakson. "Modulating vascular hemodynamics with an alpha globin mimetic peptide (HbαX)." *Hypertension* 68, no. 6 (2016): 1494-1503.

Abstract

The ability of hemoglobin to scavenge the potent vasodilator nitric oxide in the blood has been well established as a mechanism of vascular tone homeostasis. In endothelial cells, the alpha chain of hemoglobin (hereafter, alpha globin) and endothelial nitric oxide synthase form a macromolecular complex, providing a sink for nitric oxide directly adjacent to the production source. We have developed an alpha globin mimetic peptide (named HbαX) that displaces endogenous alpha globin and increases bioavailable nitric oxide for vasodilation. Here we show that, *in vivo*, HbαX administration acutely increases capillary oxygenation and blood flow in arterioles and produces a sustained decrease in systolic blood pressure in normal and angiotensin II-induced hypertensive states. HbαX acts with high specificity and affinity to endothelial nitric oxide synthase, without toxicity to liver, kidney, and no effect on p50 of O2 binding in red blood cells. In human vasculature, HbαX

blunts vasoconstrictive response to cumulative doses of phenylephrine, a potent constricting agent. By binding to endothelial nitric oxide synthase and displacing endogenous alpha globin, HbαX modulates important metrics of vascular function, increasing vasodilation and flow in the resistance vasculature.

Introduction

Endothelial nitric oxide synthase (NOS3, eNOS) production of nitric oxide (NO) is a critical step in homeostatic regulation of vascular tone and function (*7, 173*). NO is a potent vasodilatory gas, activating soluble guanylyl cyclase in smooth muscle cells to prevent constriction and decrease resistance in vessels from the aorta to arterioles. Intracellularly, eNOS is localized at a subcellular structure unique to the vasculature called the myoendothelial junction (MEJ), where endothelial cells project through the inner elastic lamina to directly contact the surround smooth muscle cells (*192*). Localization of eNOS in the MEJ places signal generation (NO production) directly adjacent to the site of action (smooth muscle cells). Critically, many positive and negative regulators of eNOS are sequestered in the MEJ, including calmodulin and caveolin-1, respectively (*135, 138, 139, 154, 193*).

Previously, we published a new paradigm for regulation of NO signaling: expression of the alpha subunit of hemoglobin (alpha globin) in endothelial cells is critical for NO scavenging effects in resistance vasculature (*35, 103*). In the vasculature, alpha globin is preferentially expressed in MEJs where it can bind directly to eNOS (*103*). The formation of a macromolecular complex with alpha globin and eNOS was verified by immunoprecipitation, proximity ligation assay, and immunofluorescence microscopy in both murine arteries and a vascular cell co-culture system (*35, 103*). Since alpha globin is a potent scavenger of NO, we hypothesized that the binding of alpha globin to eNOS was critical for efficient scavenging. To disrupt the macromolecular complex, and thus increase NO availability, we designed a peptide mimicking a species-conserved sequence in alpha globin (*35*). This peptide, termed HbαX, was shown *in vivo* and *in vitro* to have vasodilatory properties. The physiological response (blunted vasoconstriction in response to phenylephrine (PE), a norepinephrine analog) to HbαX is similar to alpha globin depletion (via siRNA knockdown) from endothelium of *ex vivo* murine arterioles (*103*). The

decreased constriction is sensitive to an eNOS inhibitor, L-nitroarginine methyl ester (L-NAME), implicating eNOS/NO as the major vasodilator in the absence of alpha globin. Without alpha globin, NO is not efficiently scavenged, increasing diffusion to smooth muscle cells and activation of dilatory pathways.

However, the pharmacologic properties of HbαX, its effect on blood flow, and its possible therapeutic effect in long-term hypertension treatment in humans is still not known. In this study, we measure hemodynamics including flow rate and oxygen saturation in murine resistance vasculature in response to HbαX administration, and show that the mechanism of action (binding of HbαX to eNOS to disrupt complex formation) produces a sustained decrease in blood pressure with little toxicity. Importantly, we demonstrate that this mechanism is translatable to human microvasculature.

Materials and Methods

Murine and Human Subjects Declaration

All mouse procedures were performed in accordance with the University of Virginia's Institutional Animal Care and Use Committee. Human studies were approved by a University of Virginia Institutional Review Board and conformed to the principles of the Declaration of Helsinki and U.S. Federal Regulations.

Photoacoustic Microscopy

An established multi-parametric photoacoustic microscopy (PAM) system (*194, 195*) was utilized to acquire oxygen saturation of hemoglobin (sO_2) and blood flow speed at the microscopic level in vivo. SKH1-Hr^{hr}- hairless mice were used in this study (n=3). Throughout the experiment, mice were anesthetized with 1.5% vaporized isoflurane, and body temperature was maintained using a heating pad. The ear to be imaged was gently pressed against the base of a water tank heated to 37°C. A bolus (20 mg/kg) of HbαX was administered intraperitoneally without moving the mouse. A 1 mm × 2 mm field of view was imaged prior to the injection and at 5, 60, and 120 minutes post-injection (see **Supplementary Figure 1**). Quantification of the sO_2 and flow in the arteriole and venule of the mice was performed as described previously (*195*).

Blood pressure

Radiotelemetry blood pressure measurement and Angiotensin II (AngII) osmotic mini-pump insertion (Alzet, model #2006) were performed as described (*35, 196*). Briefly, the pumps were loaded with AngII with a constant infusion rate of 1000 ng/kg/min, and a 6-week maximum life span as noted by the manufacturer. Injections of saline or peptides (5 mg/kg) were performed every other day between 16:00-19:00 via IP. Control peptide was a scrambled sequence of HbαX, (FPYFSTKLTT) (*35*).

Monitoring of bone marrow, liver and kidney toxicities

Submandibular punctures were performed every 15 days and approximately 200 uL of blood was obtained for measurement of liver and kidney function by the University of Virginia blood pathology lab.

Lucigenin Assay for measuring superoxide production in tissues

Measurement of tissue superoxide level was performed as previously described(*197*). Briefly, approximately 5 mg of tissue was added to oxygenated KREBS-HEPES buffer (KREBS-HENSELEIT buffer (Sigma, K3753) plus 25 mmol/L $NaHCO_3$, 20 mmol/L Sodium HEPES, 2.5 mmol/L $CaCl_2$, pH= 7.2-7.4) and incubated at 37°C for 30 minutes. Oxygenated buffer and lucigenin reagent (N,N′-Dimethyl-9,9′-biacridinium dinitrate, Sigma, M8010) were added to the wells of a microplate for final lucigenin concentration of 5 µmol/L in the well. After baseline readings, tissue samples were added to wells and luminescence values were recorded. Tissue was then dried at 60-70°C overnight. Values are reported as counts/mg dry tissue.

Co-immunoprecipitation of eNOS and HbαX peptide

A monolayer of human aortic endothelial cells (hAoECs) was lysed in non-reducing RIPA buffer and incubated at 4°C with excess biotin-HbαX for 2 hours. Rabbit anti-eNOS antibody was added and incubation proceeded at 4°C overnight. 20 µL of Sheep-anti-rabbit Dynabeads was added the next day and allowed to incubate on ice for 2 hours. The Dynabeads were washed with buffer and split for gel samples. The first fraction was diluted with non-reducing running buffer and added directly to gel lanes. The other fraction was subjected to elution in low-pH conditions without reducing agents before non-reducing running buffer was added. Samples were run on a Tris-glycine gel kept on ice using a constant current of 20 mA to prevent significant heating, and transferred to a PVDF membrane. The membrane was blocked with TBS/3%BSA before addition of rabbit anti-eNOS primary antibody. Fluorescent detection was achieved with anti-rabbit 700nm (eNOS) and avidin 800nm (biotin) on a Licor Odyssey Imager.

Red blood cell oxygen

Measurement of red blood cell oxygenation was performed as described previously (*198*). Blood was collected from n=3 healthy human volunteers and each sample was tested in each treatment condition.

Recombinant protein expression and purification

Protocol for eNOS protein isolation adapted from Fischmann *et al*. (*15*).

Briefly, *E. coli* (strain UT5600 (*199*)) were transformed with a pGEX-2T vector coding for eNOS residues 66-492 (Uniprot: P29474). 500 mL GC media (20 g/L casein hydrolysate*, 5 g/L potassium phosphate (pH = 7)*, 10% v/v glycerol*, 4 mmol/L $MgSO_4$*, 100 ug/mL ampicillin, 60 ug/mL levulinic acid, 5 µmol/L hemin (dissolved in DMSO), * denotes autoclaved reagent) was prepared in 2L baffled-bottom flasks and inoculated with 10mL overnight cultures of bacteria containing the pGEX plasmid (above) and set to shake at 37^{o}C and 225 rpm. At OD_{600} = 0.8, flasks were induced with 1mM IPTG and the temperature was reduced to 25^{o}C. After 14 hours, bacteria were harvested from media by centrifugation at 500 x g and pellets were frozen for >24 hours at -20^{o}C.

Frozen pellets were resuspended in lysis buffer (25 mmol/L Tris-HCl pH 7.4, 200 mmol/L NaCl, 4 mmol/L DTT, 1 mmol/L EDTA, 10 µmol/L H_4biopterin, and one Roche Protease Inhibitor Cocktail tablet) and homogenized with a Microfluidics M-110L compressed air microfluidizer. Lysate was centrifuged at 18000 x g to remove cell debris, and supernatant was incubated with glutathione agarose (Peirce Scientific) equilibrated with purification buffer (25 mmol/L Tris-HCl pH 7.4, 200 mmol/L NaCl, 4 mmol/L DTT, 1 µmol/L H_4biopterin) at 4^{o}C for 30 minutes. After washing, Thrombin protease (Sigma) was added to the resin, and the cleavage reaction was incubated nutating at 25^{o}C for >12 hours.

Eluant from the thrombin cleavage reaction was passed over benzamidine agarose equilibrated with purification buffer to remove the protease. The solution containing eNOS

was concentrated with a 30,000 MWCO centrifuge filter (Millipore) and was run over a size exclusion column for further purification.

Fluorescence polarization

FITC-labeled HbαX was dissolved in a small amount of water and diluted to 5 nmol/L in 5 mL of the above purification buffer. Recombinant eNOS is titrated into the wells of a 96-well plate from a maximum of 1 μmol/L.

In 700 μL, eNOS is diluted to 1 μmol/L in purification buffer containing 5 nmol/L HbαX peptide. In an opaque 96-well plate, 100 μL of 5 nmol/L HbαX solution was pipetted into wells 2-11 in triplicate rows. In the first well of the three rows, 200 μL of 1 μmol/L eNOS/5 nmol/L HbαX solution was added to the empty well. 100 μL of well 1 was serially diluted into wells 2-12 and the reaction was incubated at room temperature for 30 minutes. Fluorescence polarization was measured using a SpectraMaxM5 fluorescent plate reader using a top read configuration. Excitation of FITC fluorophore used 495 nm light, and emission was read at 519 nm. The data was normalized to highest polarization point and fit with a ligand depleted model (*200*). For competition experiment, **Figure 4B**, the only change is in HbαX concentrations: the 5 nmol/L total ligand stays constant, but in the solution, 2.5 nmol/L is fluorescently labeled and 2.5 nmol/L is unlabeled. In **Figure 4C**, 5nmol/L labeled HbαX was used as the dilution buffer for serial dilution of 1 μmol/L unlabeled HbαX.

Far Western blotting

Far Western blotting followed the protocol of Wu, Li, and Chen (*201*). However, our biotin-HbαX peptide was incubated directly on the membrane (in lieu of a target protein antibody) in combination with an anti-eNOS primary antibody. Secondary antibodies were used as described above for detection.

Human ex vivo vasoreactivity

Under IRB-HSR Study 17194, human volunteers with hypertension (elevated blood pressure above 140 mm Hg systolic) had an approximate 40 mm x 20 mm biopsy of adipose tissue removed from the abdomen, which was immediately placed in ice-cold KREBS buffer, and arterioles dissected manually within 30 minutes of removal. The arterioles (approximately 50-90 μm) were cannulated, pressurized, and subject to phenylephrine cumulative dose-response curves as extensively described by us (*35, 202, 203*).

Statistical Analyses

All results are presented as mean ± SEM. Statistical analysis was performed by one-way ANOVA unless otherwise noted. p-values < 0.05 were considered significant and are denoted by *.

Results

An alpha globin mimetic peptide increases flow in resistance arteries

Previously (*35*) we have shown that HbαX blunts vascular constriction to PE and decreases murine mean arterial pressure acutely. However, we were unable to determine if the peptide had a corresponding effect on blood flow. Using photoacoustic microscopy (PAM), we investigated hemoglobin concentration oxygen saturation (sO_2), and blood flow (**Figure 1**) in the ear microvascular bed of SKH1 hairless mice. The abnormal strain and imaging location was used so that high-resolution images and precision measurement of these hemodynamic parameters in individual vessel segments could be obtained. Although there is an increase in sO_2 in the venule after HbαX injection, we could not detect a change in arteriole sO_2. However, as a result of HbαX injection, we could detect increased blood flow in both arteriole and venule.

An alpha globin mimetic peptide can sustain low blood pressure

Although the summed acute effects of an alpha globin mimetic appear to indicate a possible effect to lower blood pressure, its long-term effect on blood pressure in a chronic model of hypertension had not been determined. For this reason, we measured blood pressure over time when mice were injected every other day with 5 mg/kg HbαX. During baseline condition, (**Figure 2A**), mice were normotensive, but injections of HbαX decreased blood pressure after two days. This shows that HbαX has an effect in non-pathological situations. During AngII-induced hypertension, the blood pressure lowering effects of HbαX are more pronounced. The mice had AngII-induced hypertension for ten days prior to injection of HbαX. As shown in **Figure 2B**, chronic AngII administration resulted in hypertension, with increase systolic blood pressure from a baseline of 110 mmHg to ~170 mmHg. Injection of HbαX resulted in a significant decrease of systolic blood pressure by ~30 mmHg. It has been proposed that prolonged AngII exposure can cause superoxide ($O_2^{\bullet-}$) production via eNOS dimer uncoupling, thus contributing to

hypertension by causing endothelial dysfunction (*204*). In a separate group of mice, AngII was delivered via osmotic mini-pumps at 1000 ng/kg/min and HbαX or saline was injected as described above. Since Ang II induces superoxide generation in the kidney and vasculature, kidney and mesenteric tissues were obtained to determine superoxide levels using a lucigenin based chemiluminescence assay Indeed, superoxide generation was increased in both kidney (**Figure 2C**) and mesenteric tissues (**Figure 2D**) with AngII administration compared to sham. HbαX attenuated superoxide generation in the mesenteric circulation, but not in whole kidney tissues.

To test toxicity of an alpha globin peptide over such a sustained period of time, mouse blood was drawn every 15 days during the control blood pressure measurements in **Figure 2A** and several blood-based organ function parameters were measured. The level of hemoglobin (**Figure 3A**) and number of white blood cells (**Figure 3B**) were unchanged, suggesting that HbαX had no effect on bone marrow function. Next, we determined kidney and liver parameters and found no difference in blood urea nitrogen (BUN) (**Figure 3C**), serum creatinine (**Figure 3F**), alanine and aspartate aminotransferase enzymatic activity (ALT, **Figure 3D**, and AST, **Figure 3E**) between HbαX and control treated groups. The sum of these results demonstrates that the HbαX peptide itself is a potent modulator of long-term blood pressure and has no detectable kidney or liver toxicities in the 60-day period during which the peptide was administered.

An alpha globin mimetic peptide and eNOS have strong affinity

Because eNOS requires homodimerization for full activity, the ability of the peptide to bind eNOS dimers was assayed with non-denaturing gel electrophoresis. In a monolayer of cultured human aortic endothelial cells (hAoECs), the majority of eNOS exists as a dimeric species (**Figure 4A, Left, lane 1**). Incubating a biotin-tagged HbαX peptide allowed for immunodetection of the peptide with a streptavidin-conjugated antibody, as seen in **Figure 4A, middle**. The colocalization of the eNOS dimer and biotin bands

(**Figure 4A, right**) shows that eNOS and HbαX are able to form a complex when eNOS is in its active form. In order to quantify HbαX/eNOS association, we show that the peptide also binds to eNOS in vitro using recombinant protein. **Figure 4B** shows the binding of HbαX to the oxygenase domain of eNOS (residues 64 – 492). Serial dilution of the larger protein eNOS (~50 kDa) from 1 μmol/L with a constant background of 5 nmol/L FITC-labeled HbαX (~1.5 kDa) allows us to look at the binding affinity using fluorescence polarization measurement on a microplate reader. A ligand depleted model was used to fit the data points to calculate a K_D (*200*) (red dashed line, **Figure 4B** and **4C**). To confirm the binding affinity of 7 ± 2 nmol/L, the same assay was run with 2.5 nmol/L labeled and 2.5 nmol/L unlabeled HbαX. The competition for binding site is theoretically observed as a doubling of the binding affinity because only half of the ligand is observable using the wavelength for FITC fluorophore emission, and is seen experimentally as an increase to K_D = 13 ± 5 nmol/L (**Figure 4C**). As a control, HbαX self-oligomerization was tested by serially diluting unlabeled HbαX from 1 μmol/L in a solution containing 5 nmol/L FITC-labeled HbαX. The lack of a hyperbolic curve in **Figure 4D** shows that there are no observable effects of peptide oligomerization in the sample.

Another test of the specificity of HbαX for eNOS is to determine if there are possible effects on the other component of the endothelial NO regulatory system, hemoglobin. Because HbαX is distributed through the circulation, we investigated the effects of the peptide on hemoglobin in red blood cells (RBCs) to confirm that there is no disruption of O_2 carrying ability. To show that HbαX was not inducing hypoxia and initiating a vasodilatory signaling cascade upstream of eNOS, we checked the partial pressure of oxygen needed for 50% saturation of hemoglobin. Using freshly isolated human blood, the addition of HbαX or a control peptide did not significantly change the oxygen p50 of hemoglobin in RBCs (**Figure 5A**). To verify the effect of HbαX in endothelium, bovine hemoglobin was serially diluted in a constant 5 nmol/L FITC-HbαX solution and

fluorescence polarization was measured. The lack of a hyperbolic curve in **Figure 5B** shows that there is no binding of HbαX to hemoglobin in vitro. Taken together, these results show that HbαX is predominantly binding to eNOS, and we propose that this binding is resulting in increased NO bioavailability due to reduced scavenging by alpha globin.

Effects of the alpha globin mimetic peptide in human arterioles

Finally, to demonstrate the translational potential of HbαX, we tested the peptide *in vitro* (using recombinant human eNOS, described above) and *ex vivo* (measuring vasoreactivity of human arterioles excised from adipose biopsy samples). **Figure 6A** shows a Far Western blot of eNOS using HbαX as a probe. Briefly, purified recombinant human eNOS was run in a non-denaturing, low temperature polyacrylamide gel and transferred to a PVDF membrane for blotting with biotin-HbαX and anti-eNOS antibodies. Fluorescent secondary antibodies show the overlap of eNOS and biotin bands, indicating that HbαX is able to bind to human eNOS. To confirm that disruption of the alpha globin/eNOS complex is relevant to human physiology, we assayed the distribution of alpha globin in the human vasculature. As previously demonstrated in mice, alpha globin is observed in the biopsied human arterioles, but not beta globin (**Figure 6B**). Finally, the effect of peptide administration was assayed via vasoreactivity of human arterioles excised from adipose biopsies obtained from patients with hypertension (see **Table 1**). The arterioles excised from these patients were responsive to the vasoconstricting agent phenylephrine (PE). However, when HbαX is incubated with the arteriole (5 nmol/L), the PE dose response is significantly blunted. This is identical to the observed effect in peptide-treated C57BL/6 mice (*35*), which was restored with a NOS inhibitor. This data provides initial evidence that HbαX may alter human peripheral resistance. When summed with the murine data above, the evidence supports a potential therapeutic value of HbαX in hypertension.

Discussion

Here, we report hemodynamic changes in mice and humans after injection of the alpha globin mimetic peptide HbαX. We hypothesize that HbαX acts as a vasodilator by displacing alpha globin from eNOS and disrupting its ability to scavenge NO at the source.

The result of increased NO levels by inhibiting scavenging can be seen using PAM in **Figure 1**. Using the dual optical absorbance wavelengths of oxy- and deoxyhemoglobin, total hemoglobin concentration and sO_2 is measured in live tissue (*195*). Oxygen saturation of hemoglobin in the vessels is described in **Figure 1**. A difference exists in the sO_2 of arteries and veins at baseline, as expected. Upon injection of the HbαX peptide, arterial sO_2 is unchanged (red trace) and venous sO_2 increases (blue trace) after 60 minutes. The vessel-type dependent response is consistent with physiological response to increased blood flow. Arterial oxygenation is not changed because HbαX does not change hemoglobin oxygenation dynamics as shown in **Figure 5**. Venous oxygenation increases due to total increases in oxygen concentration in the tissue, so that low-O_2 induced diffusion is decreased in capillary beds. This is the result of increased blood flow in the tissues, as seen in **Figure 1**. Administration of HbαX increased flow in both arterioles and venules after 60 minutes. The result of higher flow is increased O_2 distribution in the tissue surrounding capillary beds. Although the effects were only studied in ear tissue, similar effects are expected across all resistance vasculature. Additionally, NO does not provide a majority of the vasodilatory signals in resistance vasculature under normal physiology, but with relative overproduction, the impact is likely increased.

Injections every other day were enough to decrease systolic pressure in mice at baseline and mice made hypertensive by constant infusion of AngII. Even without elevated blood pressure, the administration of HbαX decreased systolic pressure by approximately 5 mmHg (**Figure 2A**). This shows that increasing NO has an effect in non-pathological contexts because there is constant regulation of NO availability by alpha globin, and that

disrupting the macromolecular context permits increased NO signaling in smooth muscle cells. In an AngII model of hypertension, administration of HbαX resulted in a ~30 mmHg decrease in blood pressure compared to saline and control peptide treatment that was constant until the end of pump lifetime (red line, **Figure 2B**). AngII has been shown to increase damaging superoxide radical formation in the tissues due to activation of NADH and NADPH oxidase through its type 1 receptor (*205, 206*). In order to address whether the large decrease in blood pressure in HbαX treated-treated mice in AngII-hypertension is in part due to a reduction in superoxide levels, lucigenin was used to assay tissue production of $O_2^{\bullet-}$ in the kidney (a major target organ of AngII) and the resistance mesenteric vessels. In whole kidney tissues, AngII-induced superoxide generation was not attenuated by HbαX injection. This could be explained by lack of sensitivity of the assay due to the presence of many other cell types, including epithelial cells that do not express eNOS; thus, any effect of HbαX on eNOS would be difficult to detect when whole renal tissue is assessed. However, there was lower superoxide levels in the mesenteric tissue after treatment with HbαX. This could be due to a scavenging effect of superoxide by NO, forming peroxynitrite and other nitroxide species (*207*). Increased NO availability by disruption of alpha globin/eNOS binding could lead to slightly lower superoxide levels in the resistance vasculature. Although the damage of free oxygen radicals produced by Ang II-activated oxidases is not completely mitigated by this mechanism, some radical scavenging is likely beneficial to endothelial function. Although the decrease in blood pressure with HbαX did not return to 110 mmHg as seen in the basal condition, a decrease in systolic blood pressure of 30 mmHg is clinically significant and desirable in treatment. Other mechanisms of hypertension, including aldosterone dis-regulation or increased sympathetic drive, may also be sensitive to increases in NO production because the constrictive signaling pathways are distinct from those involved in NO action. The interplay

of increased dilatory signals among the constrictive signals might be enough to shift the balance towards lower overall blood pressure.

Because HbαX was administered as a peptide injection, the toxicity readouts are important before considering human treatments. There are no detectable effects on liver or kidney function when the peptide is injected for up to 60 days. Because HbαX is a peptide chain, the breakdown products (amino acids) should be relatively inert, and cleared intracellularly or from blood using endogenous protein breakdown machinery. Critically, the injection of the mimetic peptide did not increase white blood cell count, indicating no inflammatory response to the peptide (**Figure 3B**). Because the sequence is found in endogenous hemoglobin, it is unlikely that antibodies would be developed against the sequence. Measures of liver and kidney function (assayed by urea, ALT, AST, and plasma creatinine levels, **Figure 3 C-F**) showed no difference between saline, control peptide, or HbαX treated mice, illustrating no detectable toxicity and its potential as a novel therapeutic agent in the treatment of hypertension by increasing NO availability in endothelial cells.

To confirm the proposed mechanism of HbαX on the disruption of the alpha globin/eNOS complex (*35*), we assayed the binding of HbαX and eNOS *in vitro*. In cultured ECs, HbαX immunoprecipitates with dimeric eNOS protein (**Figure 4A**), showing that eNOS can remain in its active oligomeric state when the peptide is bound. An active eNOS enzyme is critical for increased NO availability with HbαX treatment, as the peptide works to disrupt the formation of an alpha globin/eNOS macromolecular complex. Our model suggests the alpha globin mimetic peptide HbαX competes with the full alpha globin chain for a binding pocket on the oxygenase domain of eNOS, and previous work has shown fluorescently labeled HbαX colocalized with alpha globin in the MEJ, where a functional pool of eNOS is located in ECs (*35, 103, 192*). These results suggest proximity of the functional parts, but do not directly show binding. We use FP assays to prove that HbαX

binds to eNOS and determine the binding affinity. In our experiment, we determined that HbαX and eNOS bind with low nanomolar affinity (**Figure 4B**). As validation of this result, half of the fluorescently labeled HbαX in the ligand buffer was replaced with unlabeled HbαX. This competition experiment effectively doubles the observed binding affinity because only labeled peptide (now at half the concentration) is able to be measured and is competing for the same number of binding sites. Roughly, a doubling of the binding affinity is observed in this mode (**Figure 4C**). This is not an affect attributable to HbαX oligomerization, because there is no observable binding curve from data in **Figure 4D**.

There is considerable evidence that NO can also be modulated by RBCs as well as the endothelium. It has been elegantly demonstrated that NO production in erythrocytes can occur either by nitrite conversion or by eNOS in the RBCs (*208-213*). It is possible that free NO availability in the circulating cells is regulated by a similar mechanism as in ECs due to the vast amounts of hemoglobin present directly adjacent to a membrane-bound NOS enzyme. Overproduction of NO in RBCs might lead to higher levels of methemoglobin within the cells and negatively affect the O_2 carrying capacity of the red blood cells. A reduced O_2 capacity for RBCs might trigger a hypoxic response leading to the observed vasodilation *in vivo*. To determine if HbαX application could increase NO production and higher p50 values for isolated RBCs, freshly isolated human blood was incubated with concentrations of HbαX much higher (30 μmol/L, **Figure 5**) than would be encountered with therapeutic administration. Even with this level, there was no effect on the p50 of RBC hemoglobin in intact RBCs. With this result, we believe that the effects on RBC eNOS are not the major contributor to the vasodilatory response seen in our system. However, the systems for NO bioavailablity in RBCs may be inherently different in terms of a signaling mechanism, or the peptide may not have been able to penetrate the membrane of the RBC.

The translational capacity of HbαX to disrupt the alpha globin/eNOS complex to increase NO production is shown in **Figure 6**. HbαX is able to bind to the oxygenase domain of eNOS, and this interaction is physiologically relevant in human vasculature. The expression of alpha globin in arteriole ECs (but not in the aortic root) shows that disruption of the alpha globin/eNOS interaction predominantly occurs in resistance vasculature, where blood pressure is controlled. The effect of HbαX can be observed *ex vivo* on individual arterioles using pressure myography. After incubation with HbαX, blunted vasoconstriction to PE is observed in arterioles excised from humans with hypertension (**Table 1**). Thus, in the context of systemic high blood pressure, increasing local NO signaling in the resistance vasculature might provide therapeutic benefit. This result provides a base for novel treatments of hypertension by increasing endogenous NO production.

There are further questions raised by these results. Our previous work has used an eNOS inhibitor, L-nitroarginine methyl ester (L-NAME), to show that blunted response to PE is a NO-dependent phenomenon (*35, 103*). A lack of human volunteers for biopsy prevented tests of L-NAME sensitivity in human arterioles, a limitation of using human samples in research. The dynamics of the alpha globin/eNOS interaction is also of importance. The binding affinity, k_{on}, and k_{off} rates for the full alpha globin chain binding to eNOS are yet to be determined and will provide evidence for a model of static or transient interaction in the scavenging of NO by alpha globin. Having a model of the alpha globin/eNOS interaction that includes dynamics will be useful in further modification of the HbαX peptide for better pharmacokinetics.

In conclusion, this study provides evidence for modulation of blood flow and decreasing blood pressure using an alpha globin mimetic peptide to prevent NO scavenging. The peptide, HbαX, disrupts an alpha globin/eNOS macromolecular complex by binding to eNOS and increases blood flow and oxygen saturation *in vivo*. HbαX does

not appear to affect bone marrow, liver or kidney function. The target specificity of the peptide prevents negative interactions with endogenous hemoglobin, and enhances NO signaling, leading to vasodilatory effects to lower blood pressure.

Figures

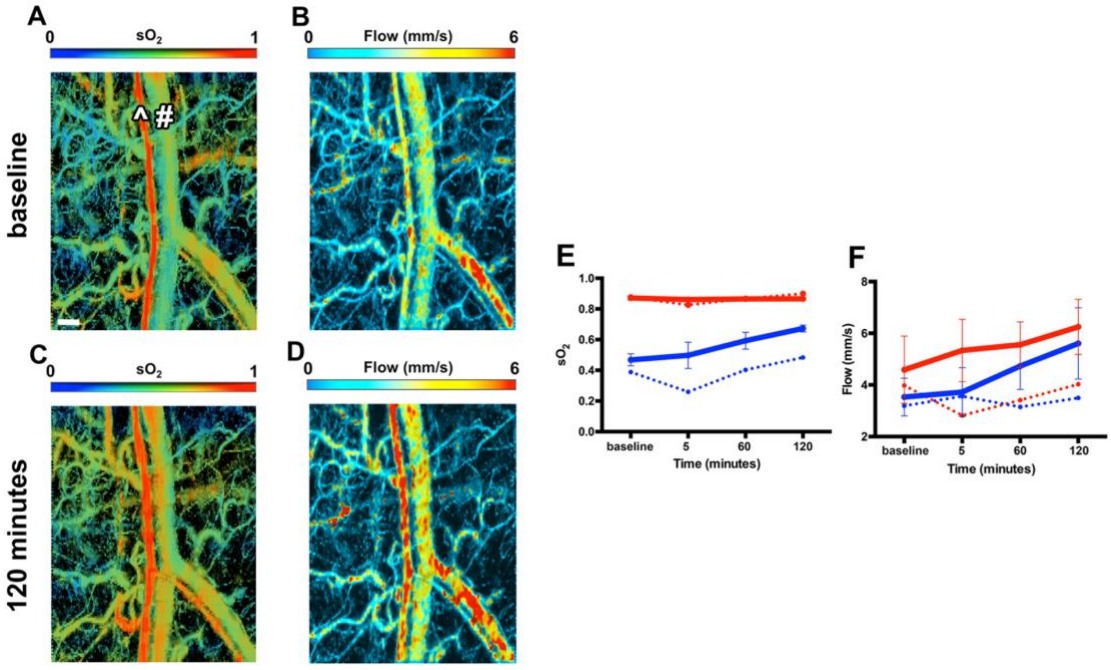

Figure 1: Acute increased O_2 saturation and blood flow in microvasculature with single injection of HbαX in vivo. A-D Photoacoustic microscopy images of O_2 saturation (sO_2) and blood flow from microvasculature of murine ear at baseline in **A** and **B** and 120 minutes post HbαX injection in **C** and **D**. All images are from the same portion of the ear. The ^ symbol denotes an arteriole and # denotes a venule. Qualitatively, sO_2 increases after HbαX injection shown by warmer colors in the regions of capillary beds. Linear velocity of the blood is increased in both arterioles and venules with red coloring denoting regions of highest flow. Quantification of sO_2 and average flow velocity from mice receiving HbαX injection (solid lines, n=3) and saline injection (dotted lines, n=3) are shown in **E** and **F**; red denotes arteriolar value, blue denotes venular. Scale bar in A is 100 μm.

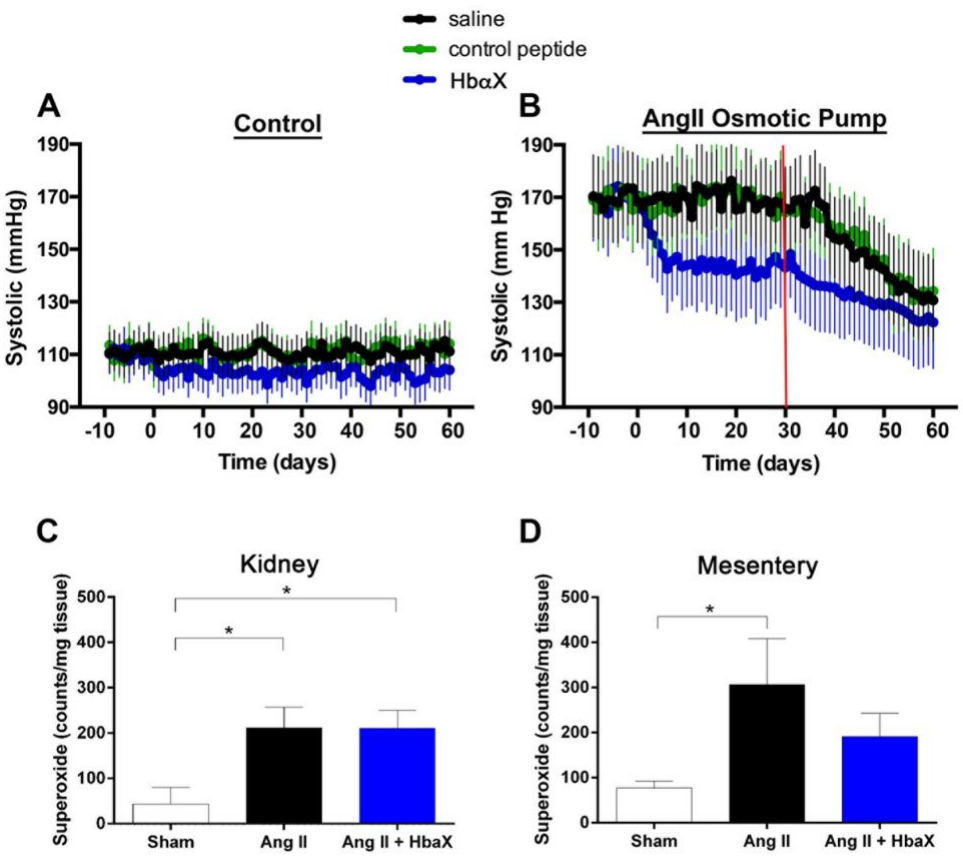

Figure 2: Sustained decrease in systolic blood pressure with HbαX: Either normotensive mice (**A**: N=4) or mice with osmotic pumps loaded with AngII (**B**: N=4) were injected every other day starting at day 0 with saline (black), a scrambled control peptide (green; 5 mg/kg) or HbαX (blue; 5 mg/kg) and systolic blood pressure via radiotelemetery was obtained daily. A baseline was measured for 10 days prior to the start of injections. Red line in B denotes approximate end of AngII infusion due osmotic pump lifetime. Superoxide production from kidney **C** and mesenteric **D** tissues was assayed from mice with AngII pumps and HbαX injections (n=3) or saline injections (n=3), or receiving sham surgery (n=4).

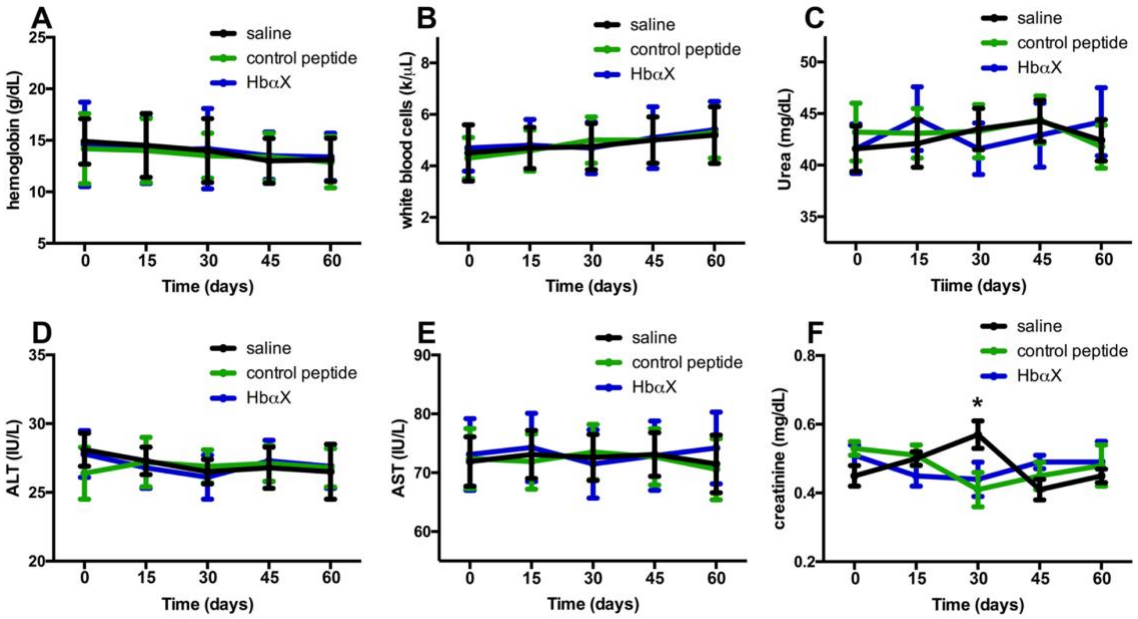

Figure 3: Prolonged injection of the alpha globin mimetic peptide does not lead to murine toxicity. Approximately 200 μL of blood was drawn via submandibular puncture every 15 days, starting prior to the first injections on day 0 of saline (black), control peptide (green) or HbαX (blue). The blood was subject to blood pathology laboratories at the University of Virginia to test for basic parameters that could indicate toxicity. These include a change in levels of hemoglobin **A**, white blood cells in aggregate **B**, urea **C**, ALT **D**, AST **E**, and creatinine **F**. Although some variability was observed, there was little significant difference using two-way ANOVA and an alpha level of $p < 0.05$. N=3 mice per condition.

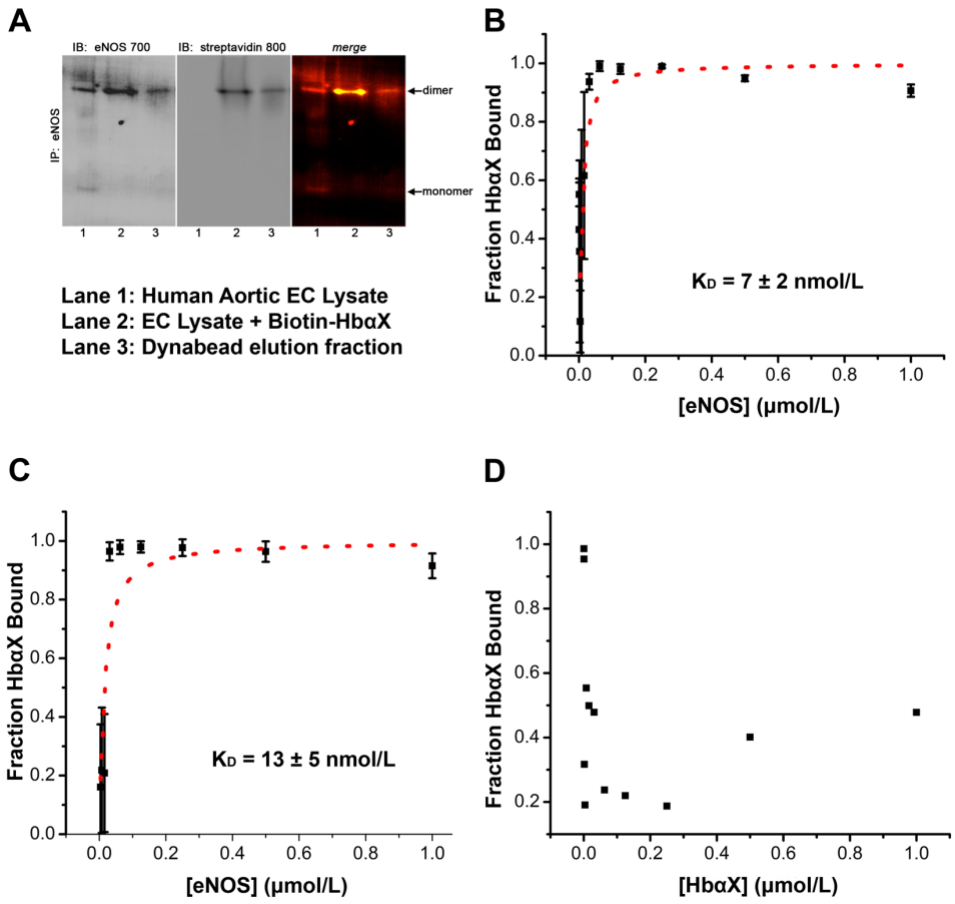

Figure 4: An alpha globin mimetic peptide and eNOS dimers bind with high affinity. **A,** Co-immunoprecipitation of eNOS and biotin-labeled HbαX from hAoECs shows that HbαX binds to the dimeric form of eNOS. Non-denaturing IP and electrophoresis conditions were used to preserve the conformational state of eNOS. Lane 1 shows EC lysate as a control for eNOS species. Lane 2 is from beads incubated with EC Lysate and biotin-conjugated HbαX peptide. Lane 3 is sample eluted from dynabeads with low pH. **B,** Fluorescence polarization assays show nanomolar binding affinity between fluorescein isothiocyanate (FITC) – labeled HbαX and the oxygenase domain of eNOS. The concentration of FITC-HbαX is 5 nmol/L in (B). The total concentration of peptide in **C**, was held constant, but only half (2.5 nmol/L) was fluorescently tagged. This effectively will double the observed binding affinity because of the 1:1 competition for binding site. **D,**

shows no curve because no binding was observed between HbαX peptides. The concentration of labeled peptide was held constant (5 nmol/L) and was used to serially dilute unlabeled HbαX. In **B-D**, the points represent mean and bars indicate standard deviation, samples were run in triplicate in one experimental preparation.

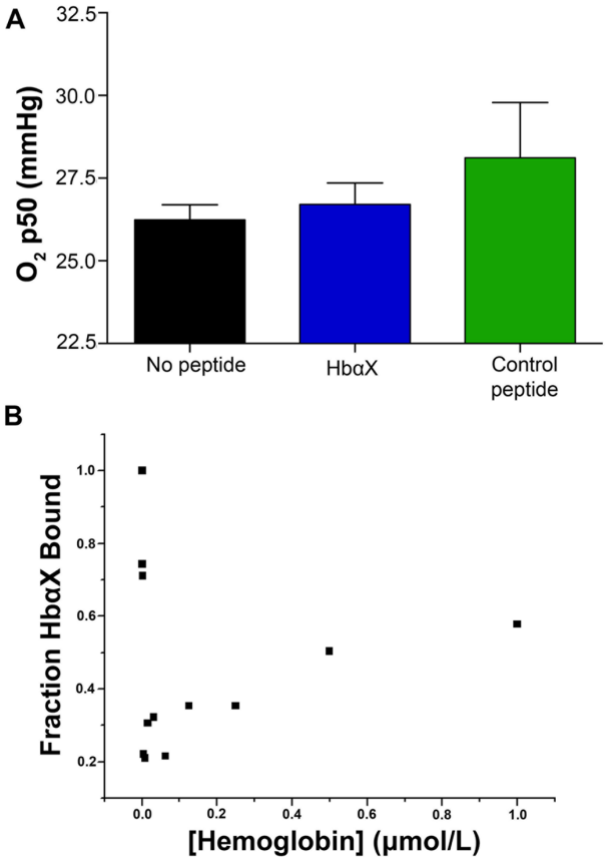

Figure 5: An alpha globin mimetic peptide does not alter the O_2 binding parameters of hemoglobin. A, The oxygen p50 of whole human blood was measured and was found not to be altered by incubation for 5 minutes with HbαX (blue) or a scrambled control peptide (green) (n=3 experiments for each condition). **B,** Fluorescence polarization of 5 nmol/L FITC-labeled HbαX incubated with bovine hemoglobin shows no concentration-dependent binding of the molecules due to the lack of a hyperbolic shape.

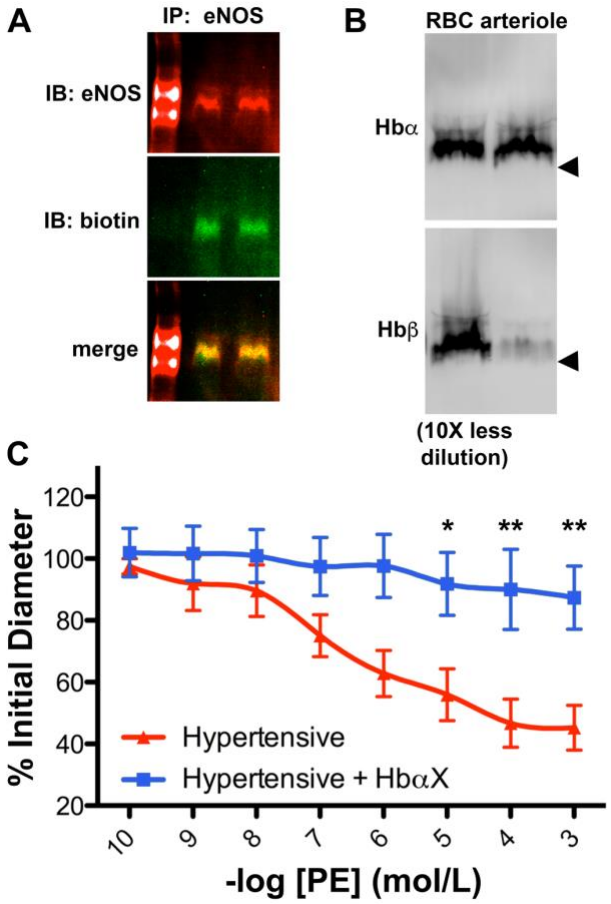

Figure 6: An alpha globin mimetic peptide significantly reduces hyperconstriction in arterioles from human patients with hypertension. A, Far-Western blotting for recombinant human eNOS oxygenase domain on a non-denaturing gel using anti-eNOS and biotin-HbαX probes and corresponding secondary antibodies for fluorescent detection. Left lane serves as a molecular weight marker, but it is not used to estimate molecular weight due to the non-denaturing condition of the gel. The samples were run in duplicate. **B,** Western blot of the expression of alpha globin without its beta globin partner is confirmed in human arterioles, and a 10-fold dilution of RBC samples is used as a positive control for alpha and beta globin chains. Arrowheads indicate 10 kDa. **C,** Resistance arterioles (approximately 100 μm in diameter) isolated from human adipose tissue biopsies were cannulated and subject to phenylephrine cumulative dose-response

curves in the absence (black) or presence (blue) of 5 μmol/L HbαX. (n=4). * indicates $p<0.05$, ** indicates $p<0.01$ using two-way ANOVA and a Bonferroni post-test.

Table 1: Metrics of hypertensive human subjects for *ex vivo* vascular reactivity. Data collected as part of the UVA IRB-HSR Study 17194.

4 Male		
0 Female	**Average**	**SEM**
Age	**47.75**	**4.23**
BMI	**36.75**	**5.24**
Systolic	**144.5**	**5.67**
Diastolic	**84.75**	**1.96**

Appendix

Author contributions:

PAM experiments were conducted by BN, CM, SMP, and SH. Telemetry experiments were performed by JTB, GBBF, with assistance from TCSK. Superoxide generation was assayed by GBBF and TCSK with guidance from SC and TH Le. Blood collection was performed by JTB. Protein purification and binding experiments were performed primarily by TCSK, with help and guidance from JNM, MC, MP, MY, and LC. Oxygen affinity was performed at Wash. U (St. Louis) by SR and AD. Western blotting was performed by TCSK and LJD. Vasoreactivity was performed by JTB, MG, and BEI, with human samples collected with help from EB. Angela K. Best managed the animal colony, animal and human protocols, and experimental equipment. All authors provided experimental guidance, edited and approved the final manuscript. TCSK compiled figures, wrote and edited the manuscript with guidance from LC and BEI.

Chapter 4: Nitric oxide preserves red blood cell deformability under conditions of oxidative stress

Adapted from: Lukas Diederich, Tatsiana Suvorava, Roberto Sansone, TC Stevenson Keller IV, Frederik Barbarino, Thomas R. Sutton, Christian M. Kramer, Wiebke Lückstädt, Brant E Isakson, Holger Gohlke, Martin Feelisch, Malte Kelm, Miriam M Cortese-Krott. "On the effects of reactive oxygen species and nitric oxide on red blood cell deformability." *Frontiers in physiology* 9 (2018).

Abstract

The main physiological function of red blood cells (RBCs) is defined by their mechanoelastic properties and deformability, which allow them to dynamically adapt to changes in blood flow and squeeze through capillaries smaller than their own diameter. Decreased RBC deformability was found in several disease states associated with oxidative stress and endothelial dysfunction / impaired nitric oxide (NO) bioavailability like hypertension. Both oxidants and NO, whether exogenously applied or endogenously produced have been shown to affect RBC deformability *ex vivo*, but the mechanisms underpinning these effects are unknown. The aim of this study was to analyze the effects of changes in redox state, oxidative stress, and NO on RBC deformability. In a cohort study of age-matched healthy and hypertensive participants, we found that RBC levels of reactive oxygen species were increased, levels of NO were unchanged, and RBC deformability was decreased in RBCs from hypertensive patients. To study the effects of oxidants on redox state and RBC deformability, RBCs were treated with increasing concentrations of t-butyl hydroperoxide (tBuOOH). We found that high concentrations of tBuOOH (≥ 1mM) decreased the reduced/oxidized glutathione ratio (GSH/GSSG), quantified by liquid chromatography mass spectrometry. These pro-oxidative changes

were associated with decreases in RBC deformability as assessed by ektacytometry and increased blood bulk viscosity measured in a low shear viscosimeter. Accordingly, RBCs from Nrf2 knockout mice, a strain genetically deficient in a number of antioxidant enzymes, were more susceptible to tBuOOH-induced impairment in RBC deformability compared to WT mice. To study the role of NO in RBC deformability, we treated RBC suspensions from human volunteers with NO donors and nitrosothiols and analyzed deformability of RBCs from mice lacking endothelial NO synthase (eNOS). We found that NO donors induced S-nitrosation of the cytoskeletal protein spectrin, but did not affect human RBC deformability or bulk blood viscosity; moreover, under unstressed conditions RBCs from eNOS KO mice showed fully preserved RBC deformability compared to WT. Pre-treatment of human RBCs with nitrosothiols did protect from tBuOOH-mediated loss of deformability. Taken together, these findings suggest that NO does not affect RBC deformability *per se*, but preserves RBC deformability in conditions of oxidative stress.

Introduction

There is accumulating evidence that red blood cells (RBCs), beside their function as transporters of respiratory gases and regulators of systemic acid/base equilibria, may also exert non-canonical functions, including systemic redox buffering and regulation, as well as control of NO metabolism (*214*). In fact, RBCs were shown to scavenge, transport, and produce NO, both under hypoxic and normoxic conditions, and to carry an endothelial NO synthase (eNOS) and its downstream signaling molecules/pathway including a soluble guanylate cyclase (*212, 215, 216*).

The biochemical, biophysical and mechanical properties of RBCs, as well as their structural characteristics, are optimized for their effective functioning. RBCs carry very high (supersaturated) concentration of hemoglobin (equivalent to 10 mM heme), which is kept in the reduced Fe^{2+}/oxygen binding state by a battery of antioxidant enzymes (*214*). The very peculiar cytoskeleton, which is mainly composed by hexagonal units of spectrin, confers stability, flexibility and elasticity; moreover, the distribution and biophysical characteristics of the protein confers RBC their typical biconcave “donut like” shape. RBC shape and deformability properties allow the cells to dynamically adapt to changes in hydrodynamic forces along the vascular tree, as well as to squeeze through capillaries smaller than their own diameter at rest (*214*).

RBC deformability was found to be decreased in several disease states associated with oxidative stress and endothelial dysfunction and/or impaired nitric oxide (NO) bioavailability, like hypertension and diabetes (*217-219*). A linear relationship between deformability and RBC oxidative stress has been found in studies involving sickle cell disease patients (*220*). In disease states ROS-mediated damage of RBC membrane components is thought to contribute to erythrocyte rigidity and membrane fragility, which results in intravascular hemolysis and release hemoglobin into the plasma (*214*).

However, the biological chemistry and biochemistry of the processes controlling physiological RBC deformability, and the underlying signaling pathways are unknown.

There is compelling evidence that treatment with thiol-reactive molecules like diamide or oxidants like peroxides strongly impairs RBC deformability (*221, 222*), as well as change the shape of RBCs (*223, 224*), suggesting an important role of intracellular redox status in control of RBC deformability and structural characteristics. In contrast, both exogenously applied NO donors or NO produced endogenously by eNOS within RBCs were shown to improve RBC deformability (*225-227*), and that S-nitrosation of intracellular proteins like hemoglobin (*226*) or spectrin (*228*) and/or activation of sGC (*225*) were proposed to be involved in these effects. However, these findings are not without controversy. Recent studies have shown that treatment of human RBCs with NO donor DEA/NO, NOS substrate (L-arginine) and sodium nitroprusside did not improve deformability of RBCs (*229, 230*). Similarly, NOS inhibition or inhibition of sGC in RBCs did not affect their deformability significantly (*215*).

The aim of this study was to analyze the effects of changes in redox state and NO metabolism on RBC deformability in healthy state and under conditions of altered redox state. To accomplish this, deformability was measured in healthy RBCs and in RBCs of hypertensive patients as well as in mouse models of impaired resilience to oxidative stressors and decreased NO bioavailability. We found that changes in intracellular redox state occurring in disease or provoked by treatment with oxidants decrease RBC deformability and blood viscosity. Although treatment with NO donors did not significantly affect RBC deformability *per se*, it rescued RBC from adverse changes induced by oxidants. Preserving the antioxidant capacity of RBCs is therefore of fundamental importance not only to avoid hemolysis but also to maintain RBC deformable in response to hydrodynamic forces.

Materials and Methods

Materials and stock solutions

If not indicated otherwise, all chemicals were purchased by Sigma Aldrich (XX, Germany) and were of the highest quality available. MilliQ quality water was used to prepare all home-made solutions (Millipore), HBSS+ was purchased by Invitrogen. Working solutions of *tert*-butylhydroperoxide (t-BuOOH) (#458139, Sigma) were prepared by diluting 1M stock in HBSS. stock solutions of DEA/NO (50 mM) (#D5431, Sigma Aldrich) were prepared in 10 mM NaOH and kept on ice until use. Stock solutions of CysNO were prepared as described (*231*) Briefly 200 mM stock solution of nitrite (#1.065.490.100, VWR) and L-cysteine hydrochloride (#C8277, Sigma Aldrich) were mixed in equal part in acidic conditions.

Human study and collection of human blood

For ex vivo analyses young (20-40 years old), healthy volunteers were recruited and enrolled only after giving written consent to participate before enrollment (ClinicalTrials.gov Identifier: NCT02272530). To analyze the effects of hypertension on RBC function, study participants (40-60 years old) were recruited from the outpatient clinic of the Department of Cardiology, Pneumology and Angiology, Düsseldorf University Hospital. The study was approved by the ethics committee of the Heinrich-Heine-University of Düsseldorf, and registered in the coordination center for clinical trials of HHU (KKS, registration ID 201307443). Both studies were conducted in accordance with the Declaration of Helsinki.

Collection of blood from Nrf2 KO, eNOS KO and WT mice

All mouse experiments were approved by the LANUV (State Agency for Nature, Environment and Consumer Protection) and conducted in agreement with the German ‘Tierschutzgesetz’ and the ‘Guide for the Care and Use of Laboratory Animals’ of the US National Research Council. The mouse strains used in this study were wildtype C75BL/J

(Janvier, France), Nrf2 knockout (KO) (BRC No. 01390); kindly provided by Rinken (Koyadai, Tsukuba, Ibaraki, Japan) and eNOS KO (*232*). Mouse whole blood was drawn in anesthetized mice by cardiac puncture using heparin as anticoagulant. Whole blood was immediately used for experiments as described below.

Determination of intracellular ROS by loading with DCF and flow cytometry

For determination of ROS in RBCs, blood was collected from the antecubital vein of human donors into tubes containing heparin (5000 I.U.) kept on ice and processed within 2 hours. Blood was diluted 1:500 with ice cold Dulbecco's PBS to reach a final RBC concentration of approximately $4x10^5$ RBC/µL and divided into 1 ml aliquots. Aliquots were treated either with 20 µM diclorofluoresceine diacetate (#D-399, DCF-DA, Invitrogen) to assess ROS, or with 20 µM Thiol Tracker (TT, #10095, Invitrogen) to assess free thiols or 10 µM DAF-FM (#23844, Invitrogen) to assess NO levels for 30 minutes, washed and analyzed in a FACS BD FACSCanto II flow cytometer (BD Bioscience) as described (*231*).

Red blood cell isolation

Human whole blood anticoagulated with heparin was transferred into a 20-mL syringe without plunger with a cap within a Falcon tube and centrifugated at 800 x *g* for 10 minutes at 4 °C. Plasma and buffy coat were aspirated and RBCs were eluted from the Syringe by removing the syringe's cap. The remaining RBC pellet was washed three times with Hank's balanced salt solution with Ca^{2+} ($HBSS^{+}$) (#14025050, Invitrogen) by centrifugation at 300 x *g*. 10 minutes, 4°C. RBC pellets were kept on ice or equilibrated in in pre-warmed HBSS+ at 37°C at a cell concentration 40% hematocrit (Ht) on a rolling plate until used for experiments as indicated below.

Determination of GSH and GSSG by liquid chromatography mass spectrometry

Washed human RBC suspension at 40% Ht were incubated for 10 min at 37°C with increasing concentration of tBuOOH (as indicated in the figure legend), and then centrifuged at 300 x *g* for 5 minutes at 4°C, put on ice and used immediately for GSH and

GSSH determination. Washed RBC pellets from Nrf2 KO mice, eNOS KO mice or WT mice were stored at -80°C. A defined volume (100 µL) of RBC pellet was lysed and protein precipitated in a solution of 5% sulfosalicylic acid (SSA) (#S7422, Sigma Aldrich) and 10 mM N-ethylmaleimide (NEM) (#E3876, Sigma Aldrich) in double distilled water (ratio 1:5). After addition of the internal standard (2mM glutathione ethylester, #G1404, Sigma Aldrich), cell lysis was completed in an ultrasonic bath for 20 seconds. Afterwards samples were centrifuged for 10 minutes, 10,000 x *g* and at 4 °C. Cell pellets were washed once with the same volume buffer used before, centrifuged with the configurations used in the last step and both supernatants merged. To separate analytes, a gradient elution on a Zorbax Eclipse Plus C18 RRHD 2.1x50mm 1.8 micron (Agilent) was chosen with 0.1% formic acid in double distilled water (A) and acetonitrile (B) (0-2 min: 99 % A, 1 % B; 2-7 min: 99 % A, 1 % B → 1 % A, 99% B; 7-12 min: 1 % A, 99 % B; 12-12.1 min: 1 % A, 99 % B → 99% A, 1 % B, 12.1-16 min 99 % A, 1 % B) on a 1290 Infinity UPLC system (Agilent) and analyzed in an Agilent 6550 iFunnel Accurate-Mass Quadrupole Time-of-Flight Mass Spectrometer (Q-TOF MS). Ionization source was set to positive mode with the configurations: gas temperature 220 °C, drying gas 12 L/min, nebulizer 35 psig, sheath gas temperature 330 °C, sheath gas flow 11 L/min, Vcapillary 2500 V, nozzle voltage 1000 V, fragmentor 30 V). Data were analyzed using an Agilent MassHunter Workstation Software (Agilent).

Effects of tBuOOH on RBC deformability and bulk blood viscosity

To analyze the effects of tBuOOH on both shear induced elongation and bulk blood viscosity, whole blood was split into 1 mL aliquots and blood samples were incubated by addition of 100 µL tBuOOH working solutions to reach the concentrations corresponding to 3 mM, 5 mM and 7mM tBuOOH or 200 µM CysNO. Incubation time was carried out for 10 minutes at 37 °C, followed by measurements of deformability and viscosity under the same experimental conditions.

To examine the effects of tBuOOH on RBC from Nrf2 KO mice as compared to WT mice, RBC pellets were diluted at 25% in HBSS+, and treated for 10 min with tBuOOH at RT. Treatment was stopped by centrifugation (800 g, 4°C, 10 minutes).

To test the effects of NO donors according to previous literature RBCs RBC suspensions in HBSS buffer (see § 2.5) at 0.016% Hct were treated with DEA/NO (0-200 µM) and incubated for 10 minutes at 37 °C. Treatment was stopped by centrifugation (800 g, 4°C, 10 minutes), and after removing the supernatant the cell pellet was kept on ice (for max 10-15 min) until ektacytometry measurement.

To determine the effects of nitrosothiols, RBC suspensions in HBSS+ at 25% Ht were treated with CysNO as indicated for 10 minutes at 37°C. To stop treatment samples were centrifuged (800 g, 5 minute, 4°C) In a further series of experiments, samples were treated with CysNO as indicated for 10 minutes at 37°C, washed 2 times with 4 volumes of HBSS buffer by centrifugation for 5 minutes at 800 g at 4 °C, and then treated with 3 mM tBuOOH, as indicated, for 10 minutes at 37°C. Treatment was stopped by centrifugation (800 g, 4°C, 10 minutes), and after removing the supernatant the cell pellet was kept on ice (for max 10-15 min) until ektacytometry measurement.

Determination of shear-induced elongation of RBCs by ektacytometry

For determination of shear-induced elongation of RBCs, 25 µL of whole blood or RBC pellet (as indicated in the figure legends) were added to 5 mL pre-warmed (37°C) high viscosity PVP solution (#QRR30901, RR Mechatronics) to yield a cell suspension behaving closely to a Newtonian liquid. Using the laser optical rotational red cell analyzer (Lorrca, RR Mechatronics) the deformability index (EI) was measured at a range of different shear stresses (0.30-50 Pa*s), as indicated. For *Lineweaver-Burke* transformation, the reciprocal values for the deformability index were plotted against the reciprocal values of the respective shear stress. After linear regression maximal

deformability (EI_{max}) and half maximal shear stress ($SS_{1/2max}$) were calculated as described previously. (*233*).

Determination of whole blood bulk viscosity by low share viscosimetry

Whole blood viscosity measurement were measured at 37°C for a range of different shear rates (0.5-150 1/s) in 1 ml sample volume using the LS300 viscometer (proRheo, Althengstett, Germany) as described (*234*).

Detection of spectrin nitrosation by biotin switch assay

RBC suspensions were prepared by diluting. 500 µL of washed RBCs in phosphate buffered saline PBS (137 mM NaCL, 2.7 mM KCl, 10 mM Na_2HPO_4, 1.8 mM KH_2PO_4, pH = 7.4) containing DTPA (10^{-6} M) and incubated with 50 mM CysNO for 30 minutes at room temperature. CysNO was removed using Pall Nanosep 10kDA MWCO spin columns (#Z722073, Sigma Aldrich). RBC were re-suspended in lysing buffer with protease inhibitors (150 mM NH_4Cl, cOmplete ULTRA Tablets (#5892953001, Roche), in H_2O). After protein determination by Lowry (#5000116, DC Protein Assay, München, Bio-Rad), The biotin switch assay was carried out according to manufacturer's protocol using a concentration of 0.8 mg/ml protein (S-Nitrosylated Protein Detection Kit, #10006518, Ann Arbor, Cayman). Afterwards samples were loaded onto a 7% Nupage Novex Tris/Acetate precast gel and western blot was performed as described elsewhere (REF). Membranes were incubated with a primary mouse anti-spectrin antibody (Dilution) (#3396, Sigma Aldrich) at 4°C overnight, followed by parallel assessment of spectrin and biotin signals on the same nitrocellulose membrane using anti-mouse Cy3-coupled antibodies (A10521,Thermo Fisher) and strepdavidin- coupled to the Cy5 fluorophore (#438316 Thermo-Fisher).

*Statistic*s

All data were analyzed by using GraphPad Prism PC software version 6.01 (Graph Pad, USA), and are expressed as mean ± S.E.M. of n individual samples as stated in

Results and Figure Legends. Statistical comparisons between groups were performed one-way or two-was ANOVA as required by experimental setting followed by an appropriate multiple comparison post-hoc test (Tukey's or Dunnet's) or T-Test as indicated. Comparison of data form hypertensive subjects with aged-matched controls was carried out by non-parametric Mann-Whitney testing. $P<0.05$ was considered statistically significant.

Results

RBCs from hypertensive patients have decreased deformability and increased intracellular ROS levels

Hypertension is a pathological condition associated to endothelial dysfunction and impaired RBC deformability (*235*), and a link between oxidative stress/NO deficiency in RBCs and loss of deformability was proposed (*214, 236*) but never investigated in detail. As observed before (*235*) we found that RBCs from patients with hypertension showed significantly decreased shear-induced elongation as assessed by ektacytometry in a LORRCA. Elongation index (EI) was decreased at discrete low shear rates (1.73 Pa: healthy mean = 0.2753, hypertension mean = 0.2568, **Figure 1A**) while no difference was detectable at a higher shear stress. The data were analyzed using the Lineweaver-Burk transformation (*233*) by plotting the reciprocal values for EI against reciprocal shear stress ($r^2_{hypertension}$ = 0.91, $r^2_{healthy}$ = 0.83), and we found that $SS_{1/2max}$ and EI_{max} were not significantly different in hypertensive subjects as compared to aged matched controls. To detect reactive oxygen species in human RBCs, RBCs were loaded with the DCF probe, and intracellular fluorescence was assessed as median fluorescence intensity as compared to unloaded cells (MFI) by flow cytometry. We found a significant increase of intracellular levels of ROS (as assessed by analyzing the intracellular fluorescence of DCF) in RBCs from hypertensive patients as compared to aged matched controls (Figure 1 B). To detect levels of free total (high molecular weight and low molecular weight) thiols, we loaded RBCs with Thiol Tracker®, which reacts with “free” reduced intracellular thiols. We found no difference in free thiol levels in RBCs of patients with hypertension as compared to aged matched controls. Likewise, the levels of NO metabolites in RBCs measured by intracellular DAF fluorescence (*216, 231*) as well as intracellular nitrite and nitrate concentrations were similar in both study groups. Taken together, these data show

that RBCs from hypertensive patients have decreased EI at low shear stresses and increased intracellular ROS while intracellular NO levels were preserved.

Tert-butylhydroperoxide decreases redox reserve and impairs red blood cell deformability and whole blood viscosity

Next, we aimed to analyze the effects of oxidative challenge and changes in intracellular redox state on RBC deformability. To analyze intracellular redox changes in RBCs following treatment with tBuOOH, we measured intracellular levels of reduced glutathione ("free GSH"), the levels of oxidized glutathione (GSSG) and their ratio (GSH/GSSG), which is indicative of the RBC anti-oxidative capacity. Treatment with tBuOOH with concentrations of more than 1 mM significantly decreased free GSH levels in RBCs in a concentration-dependent fashion, while GSSG levels simultaneously increased (**Figure 2A**). The ratio of GSH and GSSG stayed stable at the low concentrations of tBuOOH starting to drop with a t-BuOOH concentration of 10^{-4} M (Figure 2B), as a result of depletion of reduced GSH and increase of GSSG at high tBuOOH concentrations (**Figure 2A and B**).

To evaluate whether the redox changes induced by tBuOOH influence RBC deformability, we analyzed both shear-induced elongation by using a LORCA, as well as changes in "bulk" blood viscosity by using a low shear viscosimeter; both measurements were carried out under comparable conditions. tBuOOH in concentrations less than 3 mM did not affect any of the parameters of RBC deformability while significantly impaired EI at discrete shear stresses in concentrations starting from 3 mM (**Figure 2C**). However, transformation of the data using Lineweaver Burk equation resulted in values for E_{imax} and $SS_{1/2max}$ not significantly different from control, however at high concentrations linearity of the Lineweaver-Burk relationship was lost. Assessments of bulk blood viscosity by low shear viscosimetry revealed that tBuOOH in concentrations of 7 mM significantly increased blood viscosity (**Figure 2D**). Plotting values of EI and whole blood viscosity

assessed at the same shear rates demonstrated that tBuOOH-induced decrease of deformability in a concentration dependent fashion, which corresponded to a simultaneous increase in bulk viscosity (**Figure 2E**). These data suggest that tBuOOH induced changes in intracellular viscosity and elasticity of the cytoskeleton of single cells as well as the overall rheological properties of RBCs in blood.

Effects of tBuOOH on RBC deformability in Nrf2 knockout mice

To test whether the relationship between intracellular redox status in RBCs and RBC deformability could be found in a in vivo model of oxidative stress, we analyzed RBC deformability of Nrf2 KO mice. The transcription factor Nrf2 controls the expression of phase II antioxidant enzymes. and Nrf2 KO mice were shown to have increased susceptibility (decreased resilience) to oxidative challenge (*237*), as well as decreased levels of GSH in heart and aortic tissue (*238*). Unexpectedly, at baseline we did not observe any significant difference in intracellular concentrations of free GSH, but we found instead a compensatory decrease in GSSG, accompanied by an in GSH/GSSG ratio (**Figure 3A**). Moreover, we did not observe any differences in deformability of RBCs at baseline (**Figure 3C**) between Nrf2 KO and WT mice. In contrast, treatment of RBCs from Nrf2 KO mice with 50 or 100 µM tBuOOH induced a significant impairment of erythrocyte deformability in RBCs from Nrf2 KO mice at both low and high ranges of shear stress, and significantly decreased EI_{max} as compared to WT (**Figure 3C and D**). These findings suggest that the compensatory increase in GSH/GSSG ratio in RBCs from Nrf2 KO is not enough to protect RBCs from oxidant-induced impairment of RBC deformability as compared to WT RBCs.

Red blood cell deformability is not affected by endogenously produced or exogenously applied NO

Both endogenous and exogenous applied NO were described to affect RBC deformability, assessed ex vivo as RBC filterability (*212*), or by ektacytometry (*225*).

These data were recently challenged by two independent groups showing no effects of SNP (*229*) or NO donors or NOS inhibitors on RBC deformability determined by ektacytometry (*230*). To analyze the effect of NO on RBC deformability RBCs were exposed to increasing concentrations of the NO donor DEA/NO (**Figure 4A**). In our setting incubation of RBCs with DEA/NO did not significantly influence deformability indexes over a whole range of shear stresses. Lineweaver-Burk transformation of the data followed by calculation of EI_{max} (**Figure 4B**) and $SS_{1/2}$max (**Figure 4C**) resulted in values not significantly different from control conditions. Only treatment with a high concentration of DEA/NO of 200 µM significantly decreased RBC deformability (**Figure 4B**). These data indicate that exposure of RBCs to exogenous NO does not influence RBC deformability in a beneficial manner.

To examine the effects of endogenous produced NO in RBCs, we compared RBC deformability of global eNOS knockout mice with RBC deformability of wild type mice (**Figure 4C**) and found that genetic deficiency for eNOS had no effect on RBCs deformability. This was evidenced by completely identical deformability curves measured in WT and eNOS KO at discrete shear stresses and the calculated values for EI_{max} and $SS_{1/2max}$ after Lineweaver-Burk transformation (**Figure 4D**). Likewise, the levels of GSH or GSSG or their ratios were not different between both strains (**Table 1**). Thus, RBC deformability is not directly affected by endogenously produced NO by eNOS or exogenously applied NO.

Treatment with nitrosothiols leads to nitrosation of cytoskeletal protein and rescue from tBuOOOH-mediated damage.

There is evidence of a role of nitrosation of critical thiols of the cytoskeletal protein spectrin in regulation of RBC deformability (*227*). To study whether S-nitrosation reactions impact RBC deformability we incubated RBCs with the nitrosothiol CysNO. We found that CysNO increased S-nitrosation of the cytoskeletal protein spectrin, as determined by biotin

switch assay and western blotting (**Figure 5A**). However, similar to what we observed with the NO donor DEA/NO, treatment with CysNO did not affect EI, EI_{max} and $SS_{1/2max}$ nor bulk viscosity in CysNO-treated RBCs compared to untreated cells (**Figure 5B, C**)

To analyze the effect of CysNO on tBuOOH-induced impairment of RBCs deformability, we pre-incubated RBCs with CysNO, washed them, and treated with tBuOOH. The deformability curves showed that pre-treatment with CysNO at concentrations of 0.001 mM and 1 mM significantly improved RBC deformability (**Figure 5B**). These effects were especially profound with increased shear stresses as demonstrated by increases in EI (**Figure 5D**, E_{imax} and $SS_{1/2max}$ showed no significant differences).

Taken together, treatment of RBCs with high concentrations of nitrosothiols leads to nitrosation of the cytoskeletal protein spectrin but did not affect RBC deformability, as assessed by shear-dependent elongation and bulk viscosity measurements. Although no effects of NO donors or nitrosothiols were observed on RBC deformability as measured by two independent techniques, nitrosothiols protected RBCs against tBuOOH-mediated loss of RBC deformability.

Discussion

In this work, we investigated how changes in intracellular redox state of RBCs, NO and nitrosation reactions may affect RBC deformability. We found that 1.) in hypertensive patients decreased RBC deformability was accompanied by an increase in intracellular ROS levels, with unchanged intracellular NO levels; 2) changes of intracellular redox state provoked by treatment with oxidants impaired RBC deformability and blood viscosity; 3) although treatment with NO donors and nitrosothiols did not significantly affect RBC deformability per se, it rescued RBCs from adverse changes induced by oxidants. Taken together, these findings suggest that NO itself does not acutely affect RBC deformability,

but may contribute to protection of critical thiols from oxidation preserving RBC deformability.

Relationship between intracellular redox state and mechanical properties of RBCs

There is a large amount of literature describing the effects of oxidants, alkylating agents, Ca^{2+}/Ca^{2+} ionophore, NO donors and nitrosothiols, as well as NOS inhibitors, and the sGC inhibitor ODQ on RBC deformability (*221, 222, 225, 229, 239*). However, especially in the case of NO donors and inhibitors of the sGC pathway, these effects were not found by other laboratories (*229, 230*), including ours (*215*), and as also shown here by using eNOS KO mice. Speaking in general terms, RBC deformability is defined as the ability of RBCs to change their shape in response to external hydrodynamic forces, which are exerted on the cells. Intrinsic determinants of RBC deformability are 1.) the geometry of the cells (relationship between surface area and cellular volume); 2.) intracellular viscosity and 3.) the elastic properties of the membrane/ membrane viscosity.

RBC deformability measurements have been carried out by analyzing stress-strain relationships; *i.e.* by applying a deforming force (on the whole cell or on a small portion of the membrane) and analyzing the resulting deformation of the cells by direct microscopic observation or indirect estimations, like analyzing changes in light diffraction pattern during ellipsoidal deformation (ektacytometry) or changes in bulk viscosity. Under these conditions, the overall deformation of RBCs depends on both intrinsic properties of the RBC (geometry, intracellular viscosity, membrane elasticity) as well as the extracellular bulk viscosity, which is in turn dependent on cell concentration, plasma /medium viscosity, hydrodynamic forces, cell aggregation, and cell-cell interactions) (*240*). Thus, depending on the forces applied and the experimental setup, each system induces changes in shape that are more or less influenced by changes in cell geometry, intracellular viscosity or extracellular medium composition in a different way. This is particularly relevant if the biological chemistry and biochemistry of changes in RBC deformability by oxidants or NO

metabolites are investigated in a complex system like the RBCs (and may help to explain some of the discrepancies as discussed in detail below)

In our study RBC deformability was measured in shear flow as changes in cell elongation in diluted cell suspensions in high viscous PVP medium (by LORRCA) or as changes in bulk viscosity in RBC suspensions at (physiological) hematocrit in response to a range of shear rates. In the LORRCA measurements, the deforming force (τ) is dependent on both component shear rate (γ) and medium viscosity (η_o) is expressed a "bulk shear stress" and expressed in Pa.

$$\tau = \gamma \times \eta o \quad [1]$$

In the LORRCA the high viscous medium is the PVP solution (η_o) and the degree of deformation is mainly determined by the RBC viscosity parameter (η_i and η_m) in relation to viscosity of the suspension medium; parameters like cell geometry, or cell adhesion play a minor or non-existent role. In the viscosimeter, LS300, where measurements were carried out in whole blood, the blood itself behaves like a highly-concentrated cell suspension analogous to a highly viscous medium. Here intracellular viscosity and membrane elastic properties, but also cell volume and the cell-cell interactions, affect shear-induced deformation. This is very important aspect to consider for interpretation of the results presented in the present work and the work of others before analyzing the effects of chemical and biochemical treatments on RBC deformability. Intracellular viscosity (η_i) is mainly dependent on the concentration and physicochemical properties of hemoglobin (*241, 242*), which in clinical settings defined as MCHC (mean corpuscular hemoglobin concentration). In healthy humans, MCHC is 32 g/dl and η_i is 7 mPa*s (without elastic behavior); the intracellular viscosity increases with MCHC in a nonlinear fashion and it is almost quadrupled at MCHC = 40 g/dl (*242*). Membrane viscosity η_m depends on elasticity of the spectrin cytoskeleton and its interactions with hemoglobin (which increases under oxidative conditions as well as transmembrane proteins/ the lipid bilayer)

(*243, 244*). Therefore, changes in RBC deformability as assessed by LORRCA (or similar methods measuring stress-induced elongation) are likely to occur because of changes of structure/integrity of hemoglobin or of the cytoskeletal proteins (*222, 245, 246*), as a consequence of an oxidative challenge.

Here we found that only tBuOOH, which decreased intracellular free GSH/GSSG ratio, significantly affected shear induced-elongation and bulk blood viscosity (**Figure 2**). Lower concentrations did not exert any effects, indicating that changes in RBC deformability are related to intracellular oxidative stress damage. This agrees with previous results demonstrating that high millimolar concentrations of tBuOOH induce hemoglobin oxidation, changes in viscosity of hemoglobin solutions, membrane lipid peroxidation (*222, 247*), as well as oxidative modifications of cytoskeletal proteins (including crosslinking) (*222*). Interestingly, oxidants are also known to promote crosslinking of hemoglobin to cytoskeletal proteins (*244*), probably further contributing to impairment of RBC deformability.

Of interest, we found that Nrf2 KO RBCs show decreased antioxidant resistance indicated by an increased susceptibility to tBuOOH-induced impairment of RBC deformability. In fact, the effects of tBuOOH on the elongation curves of Nrf2 KO RBCs were significant at lower tBuOOH concentrations compared to WT RBCs. Additionally, decreased GSSG concentration and GSH/GSSG ratio we observed in RBCs from Nrf2 KO mice, but the concentration of reduced GSH was not different as compared to RBCs from WT controls. Accordingly, the total free thiol levels (comprising low molecular weight and high molecular weight thiols) assessed by derivatization with a fluorescent Thiol Tracker was similar in both groups. Therefore, in Nrf2 KO mice RBCs (differently from other organ compartments) are able to compensate for redox dysregulation at baseline, however are more susceptible to oxidant challenge-induced impairment of RBC deformability.

An important observation here is that very high (non-physiological) concentrations of tBuOOH were needed to affect intracellular redox state and RBC deformability impressively demonstrating high antioxidant capacity of RBCs and their resilience to oxidant damage. Although the concentrations applied were high, we did not observe significant hemolysis in our samples. According to previous studies, much higher concentrations of peroxide (H_2O_2 or tBuOOH) were needed to induce hemolysis (*247*) further emphasising the very high antioxidant capacity of RBCs. This peculiarly high redox buffer capacity of RBCs is likely due to the need of keeping hemoglobin in a reduced-Fe^{2+}, oxygen-binding form. Interestingly, the major source of ROS in RBCs thought to be Hb itself through the autoxidation reaction of Hb (*214*). Moreover, redox dysregulation, *e.g.* due to genetic deficiency of enzymes providing redox equivalents (like GAPDH) or antioxidant/detoxifying enzymes (like GPx), is correlated to increased membrane fragility and intravascular hemolysis and hemolytic anemia (*214*). Taken together, these results demonstrate that healthy changes in intracellular redox reserve of RBC may profoundly affect their intrinsic flexibility long before the loss of membrane integrity and hemolysis occur. Changes in ROS levels as well as EI in RBC from hypertensive patients may reflect redox modifications of intracellular proteins (hemoglobin, spectrin), which should be investigated in future studies.

Protective effects of treatment with nitrosothiols on RBC deformability.

The effects of NO on RBC deformability were attributed to the ability of NO donors (*225, 226*) or endogenously produced NO by eNOS (*227*) to induce nitrosation reactions of intracellular proteins, including hemoglobin (*226*) and the cytoskeletal protein spectrin (*227*). Here we found that neither treatment with NO donors nor nitrosothiols affected RBC deformability and blood viscosity under the conditions applied in this study. These data are in contrast with previous published results (*227, 233*), but are supported by recent findings of from two independent groups showing no effects of different NO donors on

deformability of human RBCs (*229, 230*) as assessed by microfluidic ektacytometric technique (*229*), or by osmotic gradient ektacytometry (*230*). In both papers, SNP showed a protective effect on RBC deformability in response to Ca^{2+}- stress induced by treatment with Ca^{2+}/Ca^{2+} ionophore. Importantly we here provide evidence that RBC deformability is fully preserved in RBCs from eNOS KO mice as compared to WT mice; accordingly, treatment with the NOS inhibitor ETU *in vitro* or *in vivo* did not affect RBC deformability in wild type mice. In previous publications we and others have shown that NOS-inhibition changed human RBC filterability (*212, 236*), which is dependent on both RBC deformability and aggregability (*248*). In chicken RBCs, treatment with a NOS inhibitor decreased RBC deformability and RBC velocity in the microcirculatory system of the chorioallantoic membrane (*249*). However, chicken RBCs are nucleated and their eNOS-dependent effects might be different from the effects in mammalian non-nucleated RBCs. Although we cannot exclude that sample preparation and handling might have been different between the laboratories describing NO-dependent changes of RBC deformability and those who showed no changes including ours, we could not find any methodological difference, which may explain these discrepancies.

Nitrosation of critical thiols was suggested as one of the possible molecular mechanism underlying the NO-dependent changes of RBC deformability. Nitrosation of cytoskeletal protein spectrin was proposed to be involved in the control of RBC deformability assessed by LORRCA (*227*). Likewise, in another study (*226*), treatment with NO donors was suggested as a way to “load” RBC with nitroso-species, including s-nitrosohemoglobin (i.e. NO bound to Cys93 in the beta chain of hemoglobin), increase RBC deformability (again assessed by LORRCA) and thus may improve oxygen delivery to the tissues. We have also found that treatment with high concentrations of the nitrosothiol CysNO induced intracellular nitrosation of the cytoskeletal protein spectrin (as shown before(*227*)), however treatment with only CysNO did not affect RBC deformability

or blood viscosity. Instead, we observed that pre-treatment with CysNO protected the cells against tBuOOH-induced impairment of RBC deformability.

Taking into consideration the well-known effects of oxidants and thiol reactive molecules like NEM and glutaraldehyde on RBC deformability (*221, 250*), it is tempting to speculate that nitrosation of critical thiols by CysNO may protect intracellular proteins from oxidation and /or cross-linking reactions. Interestingly, it was proposed that nitrosylation of hemoglobin (i.e. formation of a NO-Hb complex centered on the heme iron) may protect against toxicity of tBuOOH in the K562 erythroid cell line, as assessed by EPR (*251*); the authors of this work proposed that nitrosyl-heme complex is likely to be more difficult to be oxidized by tBuOOH. Formation of methemoglobin (*247*) was also proposed to protect RBCs from tBuOOH-induced oxidative degradation of hemoglobin and lipid peroxidation. Another possibility is that treatment of RBCs with nitrosating agents loads RBCs with both high molecular weight and low molecular weight nitroso-species, which may be more prone to reaction with tBuOOH, allowing a more efficient detoxification of the oxidant. It is important to point out that the current experimental data do not allow us to explain the chemical biology and the molecular mechanisms underpinning the effects of oxidants and the protective effects of nitrosothiols on shear-induced elongation and therefore these considerations should be seen as speculative.

Summary and Conclusion

Although RBCs were considered for a long time as simple bags carrying hemoglobin and allowing gas exchange in accordance to the demand of the tissues, and thereby regulating acid/base equilibria, significant evidence exists that their function is far more complex than that. In this study, by using eNOS KO mice that neither eNOS-dependent NO formation nor NO donors affect RBC-deformability *per se*; instead, NO in RBCs may contribute to preserve their resilience to intracellular oxidative modifications and loss of flexibility. More insights on the chemical, biochemical and biophysical interactions

regulating the mechanical properties of RBCs (which include intracellular viscosity largely dependent on Hb, elasticity and plasticity of the cytoskeletal network regulated by protein-protein interactions and the fluidity of the membrane) will shed light on the molecular mechanism of these effects. These future studies should include both, experimental observation of *ex vivo* and *in vivo* behavior of RBCs, as well as computer-aided multiscale modelling of RBCs (from atomistic levels of proteins to rheological behavior in flow conditions along the vascular tree), accompanied by studies analyzing the role of redox changes in tissue perfusion.

Figures and Tables

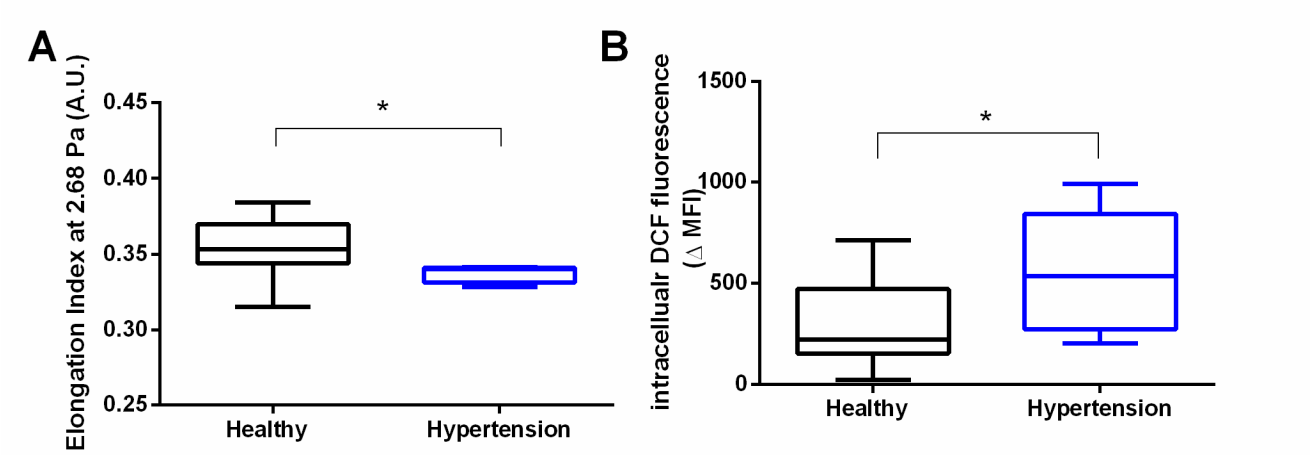

Figure 1: RBCs from patients with hypertension have decreased RBC deformability and increased ROS levels. A Decreased elongation Index (EI) measured in RBCs of hypertensive (n=4) and healthy (n = 9) participants at a shear rate of 2.68 Pa. **B** RBCs of hypertensive participants (n = 9) have increased intracellular dichlorofluorescein (DCF) values as compared to healthy controls (n = 11) (MFI, mean fluorescence intensity; ΔMFI = MFI loaded RBCs – MFI unloaded RBCs). Comparison *Mann-Whitney test, $p < 0.05$. All ektacytometric measurements were performed in whole blood diluted in PVP solution and measured in a range of shear stress from 0.3 – 10 Pa.

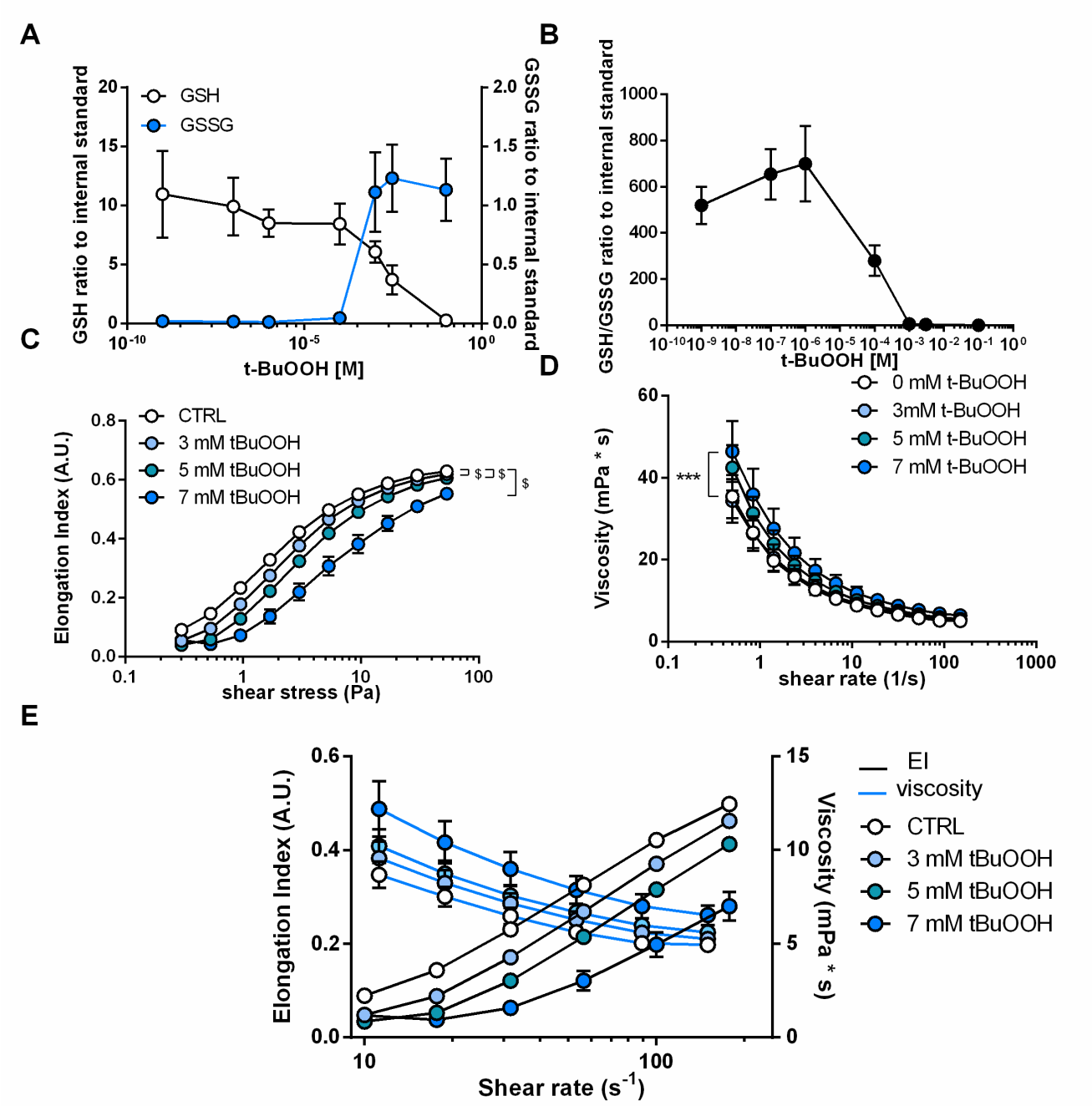

Figure 2. Changes in intracellular redox state by treatment with tBuOOH decrease RBC deformability and increase blood viscosity in a concentration dependent fashion. A Intracellular GSH/GSSG levels relative to internal standard treatment of RBCs with different concentrations of tBuOOH (0 M, 10^{-9} M, 10^{-7} M, 10^{-6} M, 10^{-4} M, 10^{-3} M, $3x10^{-3}$ M, 10^{-1} M). Reduced GSH levels decreased with a simultaneous increase of GSSG the

oxidized form (n = 5). **B** Ratio of reduced GSH and GSSG calculated from the values in (A). **C** Deformability index (EI) against shear stress curves for increasing concentrations of tBuOOH (3 -7 mM,) showing impaired RBC deformability (n = 6). $ denotes statistically significant for 3 mM tBuOOH for shear rates of 0.3 -9.48 Pa, 5 and 7 mM for all shear rates. **D** Increased viscosity over a range of different shear rates with increasing concentrations of tBuOOH (n = 6). *** denotes p = 0.0004 for 5 mM between shear rates of 0.5 and 3.98 s^{-1} and 7 mM for shear rates between 0.5 and 11.22 s^{-1}. **E** Comparison of changes in viscosity and EI at matching shear rates show inverse relationship between the two parameters (STAT). Statistics: (A) – (B) Friedman test and Dunn's multiple comparison tests. (C) – (D) 2-way ANOVA and Dunnett's multiple comparisons test.

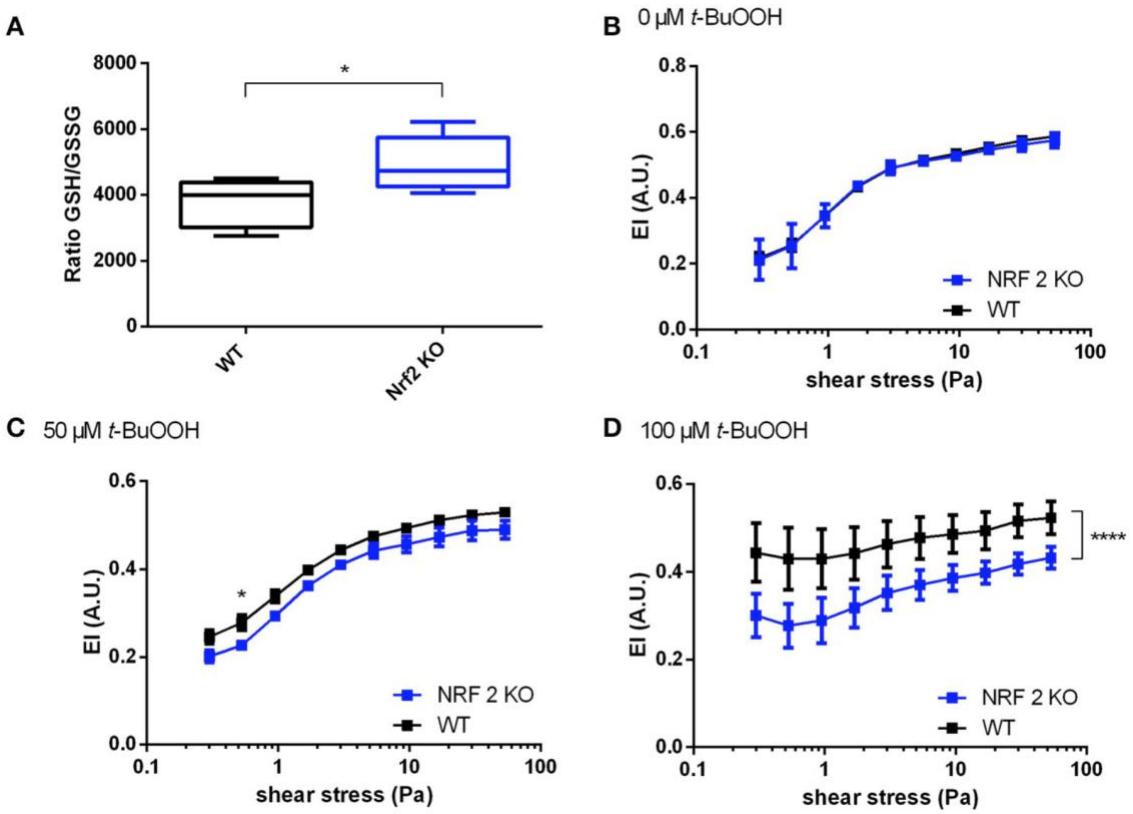

Figure 3. Increased susceptibility of Nrf2 KO RBC to tBuOOH-induced impairment of deformability. A The ratio of GSH/GSSG in Nrf2 KO is increased compared to WT mice (n=5), * denotes $p<0.05$. **B** No difference exists between deformability curves in WT mice and Nrf2 KO mice as determined by ektacytometry (n=6, $p = 0.44$). **C** RBCs from Nrf2 KO mice show a significant decrease of EI values after treatment with 50 µM tBuOOH (n=6, * denotes $p < 0.05$). **D** EI is different over the whole range of shear values for Nrf2 KO RBCs treated with 100 µM tBuOOH as compared to wild type controls (n=6, **** denotes $p < 0.0001$). Comparisons were made with Student's t-test (A), and 2-way ANOVA with Sidak's correction (B-D).

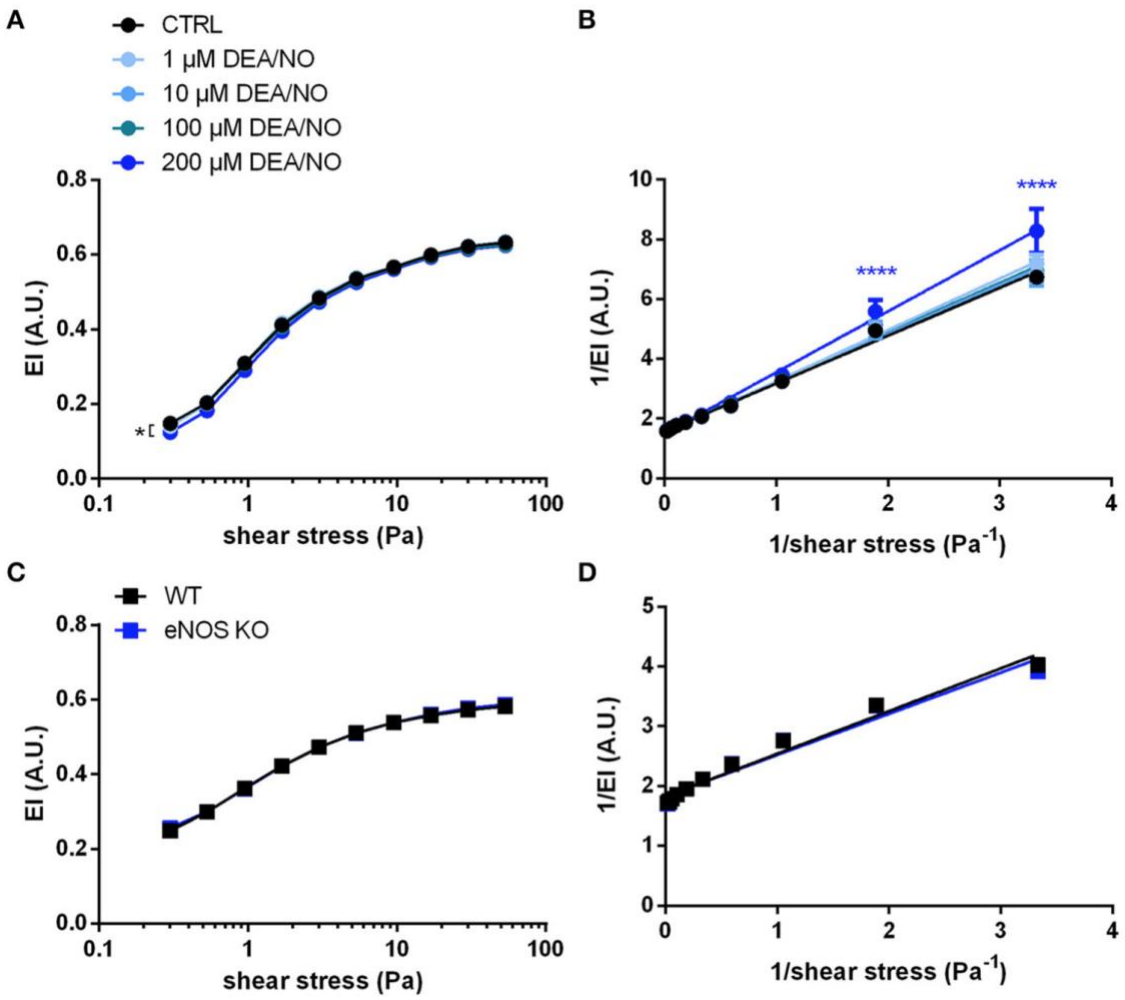

Figure 4. Nitric oxide does not influence RBC deformability measured by ektacytometry. A Treatment with the NO donor DEA/NO did not affect EI; the highest concentration (200 μM DEA/NO) significantly decreased RBC deformability between the shear stress ranges of 0.3-5.3 Pa and 30-53.33 Pa. (n=6, * denotes $p < 0.05$ for the ranges stated). **B** The Lineweaver-Burk transformation resulted in curves that are not different except at low shear stress values for 200 μM DEA/NO. **** denotes $p < 0.0001$. **C** Deformability curves of RBCs isolated from eNOS KO mice do not differ from that of WT mice. (n=6, $p = 0.47$). **D** Lineweaver-Burk transformation of eNOS KO and WT curves show no difference between groups. ($p = 0.60$). All comparisons made with 2-way ANOVA and Dunnett's correction.

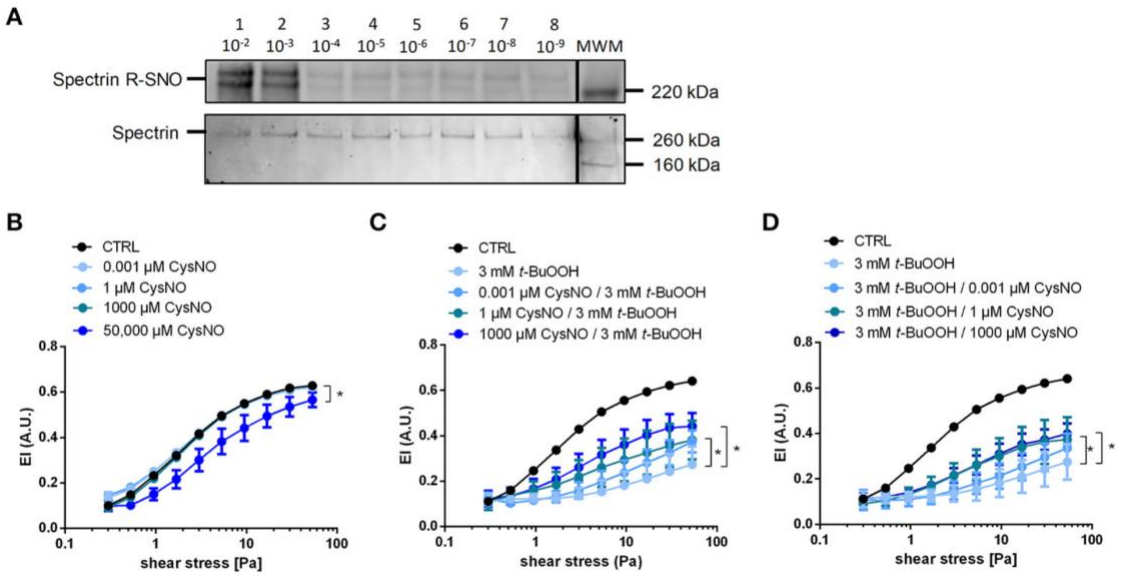

Figure 5. Treatment with CysNO leads to S-nitrosation of spectrin and protect RBCs from tBuOOH-induced impairment of RBC deformability. A S-nitrosation of spectrin following treatment of RBC suspension with 10-9 to 10-2 M CysNO for 30 minutes as assessed by biotin switch (upper image). Total spectrin, on the same membrane determined by Western blot. Each lane is labeled with the treatment concentration of CysNO. Lane MW marker is cropped into this gel image. **B** Increasing concentrations of CysNO did not affect RBC deformability, except at the highest concentration (50,000 µM CysNO). * denotes $p < 0.05$ for shear stresses from 0.53 to 53.33 Pa. **C** Pre-incubation of RBCs with different concentrations of nitrosating agent CysNO significantly rescued RBC deformability after treatment with 3 mM tBuOOH. (n=5, * denotes difference from 3 mM tBUOOH, with $p < 0.05$ for 1 µM CysNO and 1000 µM CysNO in the shear stress range 5.33 to 53.33 Pa). **D** Post-incubation of RBCs with different concentrations of nitrosating agent CysNO significantly rescued RBC deformability after treatment with 3 mM tBuOOH. (n = 5, * denotes difference from 3 mM tBUOOH alone, with $p < 0.05$ for 1 µM CysNO and 1000 µM CysNO in the shear stress range 5.33 to 53.33 Pa). Comparisons made with 2-way ANOVA and Dunnet's correction.

Table 1 – Glutathione content and redox state in RBC from eNOS KO, Nrf2 KO and WT mice

	eNOS KO	Nrf2 KO	WT
GSH	$3.76*10^6 \pm 0.26*10^6$	$3.77*10^6 \pm 0.14*10^6$	$3.93*10^6 \pm 0.23*10^6$
GSSG	946.0±161.3	781.5±68.6	1058±46.4
Total GSH	$3.76*10^6 \pm 0.26*10^6$	$3.77*10^6 \pm 0.14*10^6$	$3.94*10^6 \pm 0.23*10^6$
GSH/GSSG	3974,63	4821,5	3718,34

Appendix

LD, RS, TCSK, FB, CMK, and WL were responsible for planning and executing experiments. TCSK planned, performed, and analyzed viscosity and elongation experiments. BEI, HG, MF, MK, and MMCK supervised experiments and manuscript preparation. LD, TS, and TCSK wrote the manuscript, and all authors were involved in critical feedback and editing.

Chapter 5: Increasing nitric oxide signaling in pulmonary hypertension: a viable treatment option?

Abstract

Endothelial dysfunction, especially dysregulation of nitric oxide (NO) signaling, plays a significant role in the development of pulmonary hypertension. The lack of vasodilatory signaling though decreased NO synthase enzyme levels and overall NO availability leads to increased pulmonary blood pressure and hypertrophic cardiac right ventricular remodeling. We have developed a peptide that decreases the interaction of alpha globin and eNOS in endothelium, and leads to increased vasodilatory signaling in the systemic circulation. Here, using a model of pulmonary hypertension induced by hypoxia and SU5416, we tested whether increasing NO signaling via our alpha globin mimetic peptide, HbαX, would decrease pulmonary blood pressure and relieve increases in afterload on the right ventricle. We show that increased NO via disruption of the alpha globin/eNOS complex has a detrimental effect on right ventricular systolic pressure, right ventricular hypertrophy, and has no benefit on fibrous tissue load in the lung. This is in contrast to *ex vivo* application of the peptide to isolated pulmonary arterioles, where dilation to cholinergic stimulation was increased after peptide treatment. In fact, tissue levels of the oxidative/nitrosative stress marker 3-nitrotyrosine (a product of protein tyrosine residues and the oxidant peroxynitrite) were significantly increased in peptide-treated animals. These results demonstrate the criticality of balancing vasodilation and oxidative stress in the long-term treatment of pulmonary hypertension. Future therapeutic strategies should take these findings into account, either by an antioxidant co-treatment or through alternative pathways to vasodilation.

Introduction

Endothelial dysfunction, especially decreased vasodilatory nitric oxide (NO) signaling, leads to cardiovascular complications and underlies many cardiac causes of death. In the lungs, endothelial dysfunction can lead to pulmonary hypertension (PH) and significant cardiovascular consequences. Specifically, loss of sufficient vasodilatory signaling leads to increased pulmonary arterial pressure which increases afterload on the right ventricle (RV), causing RV hypertrophy to compensate for decreased lung perfusion. Mortality rates increase following RV hypertrophy and diagnosis of PH, with an average survival time of 2.8 years (*252*). It has been observed that patients diagnosed with PH have decreased abundance of one enzyme responsible for NO production, endothelial nitric oxide synthase (eNOS), in the pulmonary vasculature (*253*). This might contribute to pulmonary hypertension due to decreased NO availability.

Inhaled NO is currently used as a therapeutic for PH. As a potent vasodilatory molecule, delivery of NO targeted to the pulmonary vasculature can provide acute relief of elevated pulmonary blood pressure. However, the effects of inhaled NO are short acting, and treatment with inhaled NO can cause a phenomenon known as rebound hypertension when removed. Additionally, chronic administration is challenging to accomplish because supraphysiological levels of NO in inhalation can be lethal and need to be accurately controlled. Thus, a tolerable, sustained elevation of endogenous NO signaling might be desirable as a treatment PH.

NO is produced in endothelium primarily through an enzymatic reaction: eNOS metabolizes L-arginine into NO and L-citrulline (*254*). This process is tightly regulated through substrate availability, cofactor binding, post-translational modification of eNOS and other protein-protein interactions. A recently discovered regulator of NO availability, and thus vasodilation, is the expression of the alpha chain of hemoglobin (hereafter, alpha globin) in the endothelium of small arteries (*35, 103*). Critically, alpha globin is able to bind

directly to eNOS; this direct interaction helps alpha globin scavenge NO and prevent vasodilation. A small 10-residue motif on alpha globin determines eNOS binding. We developed a peptide that contains this motif (called HbαX) and competes with full length alpha globin for eNOS, thereby disrupting alpha globin/eNOS complex formation. In the systemic vasculature, disrupting the alpha globin binding to eNOS allows for increased NO availability and decreased mean arterial pressure (*184*). Displacement of alpha globin reduces its ability to scavenge NO. This mechanism correlates with the observation that PH is rare in patients with alpha thalassemia, where genomic loss of one or both alpha globin alleles prevents expression of alpha globin (*255*). Without expression of alpha globin in the pulmonary endothelium, there would be no scavenging reaction as described by Straub *et al*. (*35*).

As pulmonary arteries contain the same machinery for alpha globin scavenging of NO, a similar effect of decreased pressure after HbαX administration (see (*184*)) might be expected in models of PH. Indeed, application of the HbαX peptide to *ex vivo* pulmonary arterioles increases the dilatory effects of NOS stimulation through muscarinic receptors (*256*). In order to assess sustained NO availability as a therapeutic avenue for PH, we used the HbαX peptide to disrupt the alpha globin/eNOS complex *in vivo* using a murine model of PH. Overall, this work will establish the relevancy of increasing NO availability through decreased alpha globin-dependent scavenging as a treatment for PH.

Methods

Hypoxia/SU5416 model of pulmonary hypertension

The induction of pulmonary hypertension was based on the work of Ciuclan *et al*. (*257*), and is depicted in **Figure 1**. Briefly, experimental mice were kept in hypoxic environment (10% O_2) for three weeks. At timepoints of day 1, 7, and 21, mice were injected with SU5416 to induce further PH development. Mice were monitored and housed in compliance with animal protocols from the University of Virginia and Emory University. All experimental protocols were approved by the IACUC of each university.

Animals

Male C57Bl/6 mice, from Jackson Labs (Bar Harbor, Maine) between 10 and 15 weeks of age were used for all experiments.

Administration of ET1A and peptides as PH therapies

Throughout the experiment, the endothelin antagonist ambrisentan was administered in the drinking water. Ambrisentan was administered at 100 mg/kg for three weeks.

For peptide administration, HbαX and ScrX were used. HbαX is the ten-residue motif that has been shown to disrupt alpha globin and eNOS binding (*35, 184*). The sequence of the HbαX peptide as it is used in these experiments is YGRKKRRQRRRLSFPTTKTYF. The beginning 11 residues are a *tat* motif derived from HIV that allow the target peptide to enter cells, and the remaining 10 residues mimic the alpha globin complex that binds to eNOS. The ScrX peptide is a sequence scrambled control of the LSFPTTKTYF region with the same *tat* tag. In each case, peptides are dissolved in sterile PBS and injected intraperitoneally every other day at two doses, 10 and 20 mg/kg, as noted below.

Right Ventricular Systolic Pressure (RVSP) measurement

Catheterization of the pulmonary artery with a pressure transducer gave a measure of the right ventricular systolic pressure (RVSP). This was done via methods previously published by the Sutliff Laboratory (*258*). This work was performed at Emory University.

RV/LV+S measurement

The Fulton Index (mass of right ventricle compared to left ventricle and septum) was used as a measure of right ventricular hypertrophy. The right ventricle was carefully separated from the septum wall and the tissues were dried in a 60°C oven overnight before weighing.

Immunohistochemistry

Lungs were harvested after RVSP measurement, perfused with PBS to clear blood, and fixed in formalin overnight at 4°C. Formalin-fixed tissues were embedded into paraffin blocks and sectioned at 8 μm for staining. For macro-histological analysis, sections were stained with hematoxylin and eosin (H&E) and Masson's Trichrome, with help from the UVA Research Histology Core.

Nitrotyrosine (rabbit anti-3-nitrotyrosine, abcam #42789) was used to mark nitrosative stress within the intact tissue. At room temperature, tissue sections were treated with Histoclear (3x5 min) to remove paraffin, rehydrated with an ethanol gradient 100% / 100% / 95% / 95% / 70% for 3 minutes each, and immersed in distilled water for 20 minutes. Slides were then microwaved with a citrate-based antigen retrieval solution for 2 min x 4, with a 2-minute break between each microwaving step. After the final microwaving step, the heated slides and solution were left in the microwave to incubate for a further 30 minutes. Next, fresh PBS replaced the antigen retrieval solution and was incubated on the benchtop for approximately 5 minutes. Sections were circled with a hydrophobic marker to minimize blocking and antibody solution used. Blocking solution was made of 9.0 mL of PBS, 500 μL of serum from the secondary antibody animal, 25 μL of Triton X-100, and 500 μL of gelatin from cold water fish skin. The same solution was used for antibody dilution. Abcam rabbit anti-nitrotyrosine (ab42789) was used at a 1:250 dilution, incubation with primary antibody was overnight at 4°C. After 3 washes in PBS, the secondary antibody (donkey anti-rabbit AlexaFluor 647) was diluted in the blocking/antibody solution

and incubated on the slides in the dark for 1 hour at room temperature. Slides were mounted with Prolong Gold Anti-fade Mounting Media with DAPI, covered with a coverslip, and sealed with nail polish before imaging on a Olympus Fluoview 1000 confocal microscope. Fluoview software controlled image acquisition. Images were taken with a 20x/0.85 NA lens.

Immunohistochemistry and immunofluorescence quantification

To quantify fibrotic area, the “Colour Threshold” plugin on FIJI (available from G. Landini at http://www.mecourse.com/landinig/software/software.html). Cutoff values and macro code is available in the appendix of this manuscript. Total fibrous area was divided by total stained area as a normalization parameter. Total fluorescence in the nitrotyrosine channel was used as signal and normalized to average intensity of the DAPI fluorescence.

Results

Induction of pulmonary hypertension (PH) in this mouse model was accomplished using a low oxygen (hypoxia, 10% O_2) environment, as well as three injections of the drug SU5416 (once weekly) (**Figure 1**). This model is considered a “gold standard” in rodent models of PH because it closely mimics the human indications of disease, including plexiform lesion formation. In response to the induction of PH, the groups in the hypoxia/SU5416 treatment had increased hematocrit. This was unchanged across therapy or control treatment groups after three weeks of hypoxia treatment (**Figure 2**). Increased hematocrit following hypoxia has been observed in other studies and may serve as a compensatory mechanism by increasing oxygen carrying capacity of the circulating blood. However, the resulting increase in blood viscosity might also contribute to RV hypertrophy (*259*).

Three weeks of hypoxia and SU5416 caused an increase in pulmonary pressure from a mean of 24 mmHg in normoxia (room air, no SU5416) to 35.4 mmHg in the hypoxia/SU5416 group, indicative of PH development (**Figure 3A**). PH mice were then treated with HbαX to determine if decreased NO scavenging could ameliorate elevated pulmonary pressure. For a positive control and comparison to a current standard of care, an endothelin-1 antagonist (ambrisentan, ET1A) was administered contemporaneously with hypoxia introduction. For a negative control, animals were treated with a scrambled peptide (ScrX). In all PH treatment groups, right ventricular systolic pressure (RVSP) was increased compared to control, untreated animals (normoxic, no SU5416). Scrambled and HbαX treated groups were not statistically different from untreated hypoxia animals. HbαX and ScrX-treated animals had a RVSP that was higher, and statistically different from the ET1A-treated animals; additionally, ET1A was not different from control. There was also no difference observed between the ScrX- and HbαX-treated groups, although the mean of 20mg/kg HbαX was increased compared to ScrX (**Figure 3A**). The heart rate among

the animals did not change across the hypoxia or drug treatments, indicating that the changes in RVSP were not due to cardiac function (**Figure 3B**), but from the pulmonary vascular effects induced via our model system.

As a result of the increased pulmonary pressure, the right ventricle was remodeled. An increased RV mass, compared to the tissue mass of the left ventricle and septum (LV+S), indicates hypertrophic remodeling (commonly scored with the Fulton Index). Increased afterload on the right ventricle contributes to the detrimental remodeling, which could eventually lead to right heart failure. In our groups, the Fulton Index for each of the hypoxia/SU5416 groups was increased compared to normoxic baseline, consistent with expected PH murine model (**Figure 3D**). Again, there was no difference in right heart hypertrophy when comparing between peptide treatments and no treatment in hypoxia. However, as expected, the ET1A treatment resulted in decreased Fulton Index values compared to hypoxia/SU5416 peptide treatments, yet was still elevated (and statistically different) from baseline, demonstrating the need for improved therapeutics. Overall, HbαX treatment did not have a beneficial effect on the parameters of PH measured in this model.

While we did not observe reduced RVSP following HbαX treatment, we were curious if elevated eNOS activity could improve other aspects of PH etiology. Previously, it has been reported that NOS enzymes can prevent deposition of fibrous tissues and plaques in a variety of tissues (*260-263*). Thus, we hypothesized that HbαX administration might ameliorate the lung fibrosis characteristic of PH via increased NO signaling. To determine fibrotic area from tissue slices, quantitative immunohistochemistry was used (**Figure 4A, B**). Masson's trichrome stain, where fibrous places of tissue appear bright blue, was used to determine a mask for area quantification (μm^2). Using standard light microscopy images, a color deconvolution method was used to assign specific RGB values for each pixel in order to differentiate between fibrous and cellular tissue. The code generated for this plugin in ImageJ is included in the supplemental materials for this chapter. No

differences were observed in the fibrotic area from any of the treatment groups (**Figure 4B**).

To this point, it was unclear whether the HbαX peptide was increasing NO signaling in the pulmonary vasculature. To indirectly assay the ability of HbαX to increase NO signaling in the lung, antibodies were used to detect the protein modification 3-nitrotyrosine (3-NT), which forms on modifiable protein residues after NO reacts with the superoxide anion to make peroxynitrite (**Figure 4C**). The HbαX-treated lung had increased 3-NT signal intensity compared to ScrX-treated lung, suggesting increased NO availability (**Figure 4D**). As the nitrated tyrosine is generally considered a deleterious protein modification, this led us to consider potential negative effects of increased NO signaling in the hypoxic lung vasculature. For instance, dysfunctional 3-NT modified proteins might negate the expected therapeutic benefit of increasing NO in the lung vasculature. Overall, our data suggests that treatment of pulmonary hypertension with this alpha globin mimetic peptide does not seem to be a viable paradigm and alternative approaches should be considered.

Discussion

PH is a destructive disease with poor prognoses, and limited available treatment options (for review, see (*264*)). Currently, a few classes of therapies are used to treat PH: inhaled NO and NO donors, endothelin-1 antagonism, synthetic prostacyclins, phosphodiesterase inhibitors, and soluble guanylyl cyclase stimulators or activators.

Inhaled NO and NO donors have use as a therapy for PH, although application and other effects limit their use to acute treatments. Inhaled NO requires careful monitoring, as it can be cytotoxic at high concentrations (*265, 266*). Generally, therapy sessions are needed a few times a day for less than an hour at a time, and any therapeutic effect is withdrawn with stopping NO inhalation. Slight improvements in the pharmacokinetics of NO inhalation can be achieved by nebulized nitrite or NO donors (*267, 268*). These therapies are effective for about an hour, due to the slower release of NO from reactions with nitrite reductases or release of NO from donors (*269*). There are no documented uses of NO donors for long-term PH therapy, so it is unknown whether continued use NO donors would have similar effects on hemodynamic parameters as in this study.

However, since NO is a potent systemic vasodilator, promoting endogenous NO bioavailability may be a more viable option since it circumvents the harmful cytotoxic side effects of exogenous NO administration. In order to do this, we use a mimetic peptide (HbαX) to competitively bind eNOS and prevent alpha globin binding, which scavenges NO to prevent its participation in vasodilation signaling. Thus, we sought to investigate increased NO availability via HbαX administration as a possible treatment for pulmonary vascular hyperconstriction *in vivo* based on our previous *ex vivo* studies (*256*).

In our PH model, mice were subjected to hypoxia (10% O_2 cf. ~20% O_2 in room air) and three injections of SU5416 (a VEGFR inhibitor) to induce a PH pathology similar to human conditions (*257*). This model mirrors human development of PH more closely than hypoxia alone, as the increases in RVSP, RV/LV+S mass, and vessel muscularization are

greater with SU5416 injections. This model is widely used for PH studies (161 citations as of May 3, 2019) and thus provides a solid context for our strategy of increasing NO availability as a therapeutic.

To test the effects of increasing NO signaling on PH development, we used our alpha globin mimetic peptide to disrupt binding of the NO-scavenging alpha globin protein and endothelial nitric oxide synthase. We have seen in the systemic circulatory loop that this peptide is able to increase vasodilation and decrease blood pressure, both in WT mice and in a model of angiotensin II-induced hypertension (*184*). This effect has been translated to *ex vivo* pulmonary vessels (*256*). In hypoxia-treated mouse pulmonary arteries, application of HbαX restores vasodilatory capacity. In fact, arteries of human patients with PH (WHO groups I and III, with or without a concurrent diagnosis of systemic sclerosis) had increased alpha globin in PA lysates (*270*). This suggests that disruption of the alpha globin/eNOS complex is a viable path forward for increasing NO signaling and ameliorating elevated pulmonary blood pressure.

In our model (**Figure 1**), we have induced increased right ventricular systolic pressure via a hypoxic environment and injection of SU5416. This increased pressure in the pulmonary circulatory loop feeds back onto the heart and causes a compensatory right ventricular hypertrophy. Increased RVSP can be ameliorated in our model using ambrisentan, an endothelin-1 antagonist. However, increasing NO signaling via HbαX has no effect on RVSP (means of 34.7 and 37.6 mmHg for 10 and 20 mg/kg HbαX cf. 35.4 mmHg for PH control condition). Although not statistically different, the high dose of HbαX seems to be worse than the low dose, as well (**Figure 3A**).

Increased NO availability was observed indirectly through a downstream product, 3-nitrotyrosine, in the HbαX-treated animals compared to scrambled controls (**Figure 4**). This result is both a blessing and a curse for these studies: increased NO was the goal of the peptide treatment, yet the expected therapeutic benefit was not observed since RVSP

remained elevated. This is likely due to the modification of proteins by products downstream of NO availability; these modifications can cause functional dysregulation at the protein level (*271*). Peroxynitrite (chemical formula $ONOO^-$) is a potent protein modifying chemical, and can be formed from NO reacting with the superoxide radical $O_2^{\bullet}$, forming $ONOO^-$. Solvent-exposed cysteine, methionine, and tryptophan residues can be directly modified by peroxynitrite, while tyrosine is likely modified after formation of other nitrating species downstream of peroxynitrite itself (*271*).

The formation of peroxynitrite relies on the reaction of NO and superoxide. Superoxide is known to be increased in conditions of PH (*272, 273*). In our model, we increase NO availability via application of our alpha globin mimetic peptide. Thus, the reaction of these two gaseous signaling molecules might create unwanted peroxynitrite, damaging proteins and lung tissue *in vivo*. This is in contrast to expected results from extension of Alvarez's work in *ex vivo* pulmonary arterioles (*256*). While *ex vivo* NO is able to dilate smooth muscle in isolated pulmonary arterioles, the tissue milieu complicates this process. With hypoxia, alveolar macrophages have been identified as a possible source of superoxide and other reactive oxygen species that can damage tissues (*270, 274, 275*). In the context of elevated superoxide, increased NO generated from eNOS would thereby increase peroxynitrite, protein modification, and tissue damage.

In vivo, superoxide dismutase (SOD) neutralizes superoxide to either molecular oxygen (O_2) or hydrogen peroxide (H_2O_2, which can then be metabolized by catalase). SOD has been used therapeutically, either through direct application of a soluble SOD isoform or through gene transfer, to alleviate elevated pulmonary blood pressure in rodent and newborn lamb models (including a model of persistent pulmonary hypertension of the newborn) (*276, 277*). In the case of the newborn lambs, inhaled NO was used in combination with recombinant SOD, and SOD enhanced the vasodilatory effect of NO inhalation as a therapy. This suggests that limiting peroxynitrite-induced protein

modifications contributes to the intended therapeutic benefit of increased NO signaling. The model of superoxide scavenging potentially bioactive NO has been noted before, although generally in the context of inhaled NO and not increasing endogenous eNOS-derived NO signaling. This could be further explored in our studies, using a combined therapy of HbαX and application of active SOD or a gene therapy/viral introduction of SOD isoforms. Although the combination therapy may prove difficult to achieve, it could alleviate the nitrosative stress that is observed with the HbαX peptide alone.

There is still a need for development of new therapeutic strategies in the treatment of PH. Of course, other signaling axes have been investigated as targets, but have yet to achieve benefit without harmful side effects. For example, antagonism of the endothelin-1 (ET-1) receptor decreases constriction signals, and treatment of via ET-1 antagonists is effective, but not without significant disadvantage (*278*). An FDA drug approved for PH treatment, sitaxentan, is no longer prescribed due to liver toxicity in patients. Ambrisentan is still used clinically, but might have teratogenic side effects, so is not recommended in all cases.

In addition, synthetic prostacyclins or prostacyclin analogs are used to mimic the vasodilatory action of molecules produced by cyclooxygenase enzymes in the endothelium. Like inhaled NO, this class of drugs is ultimately effective, but has a narrow pharmacokinetic window (half-life for three different formulations rage from six minutes to four hours) (*279*). Routes of administration of this drug are limited to inhalation (with a special nebulizing inhaler) or continuous intravenous or subcutaneous infusion. Because of the complicated dosage profile, synthetic prostacyclins are not an ideal therapeutic for PH treatment.

Phosphodiesterase (PDE) inhibitors are used to increase the effectiveness of endogenous NO signaling. By preventing the breakdown of the soluble guanylyl cyclase (sGC) product cyclic guanosine monophosphate (cGMP), PDE inhibitors prolong the

signaling effect of NO dilatory stimuli. These drugs are generally tolerated well, although can be ineffective if endothelial dysfunction has disrupted normal NO-sGC-cGMP signaling (*264*). In one recent study, a combination therapy of an approved ET-1 antagonist and PDE inhibition was more effective at preventing adverse events than either monotherapy (*278*). By working to decrease constriction (ET-1 antagonism) and boosting dilatory signals (PDE inhibition), this combination therapy seems to be a future way forward for PH treatment.

The final, most recently developed, class of drugs for PH treatment are sGC stimulators and activators (*280*). These molecules work on smooth muscle sGC to increase cGMP generation and dilation of the pulmonary vasculature. Importantly, sGC activators are designed to work without NO stimulation, on oxidized (inactive) forms of sGC (*281-283*). These molecules are especially relevant in inflammatory states of PH, where inactive sGC predominates and is unable to respond to vasodilatory NO signals. Future work with these compounds is increasing selectivity of the effect to the pulmonary vasculature, either through formulation or administration, but initial studies show much promise in effective treatment of PH.

Overall, there are increasingly effective strategies for the treatment of PH, although chronic elevation of NO in the hypoxic lung may not be an effective treatment for PH in the long term. However, future studies could combine this with SOD to investigate if preventing the harmful peroxynitrite-driven protein modifications allows for therapeutic NO signaling to dominate.

Figures

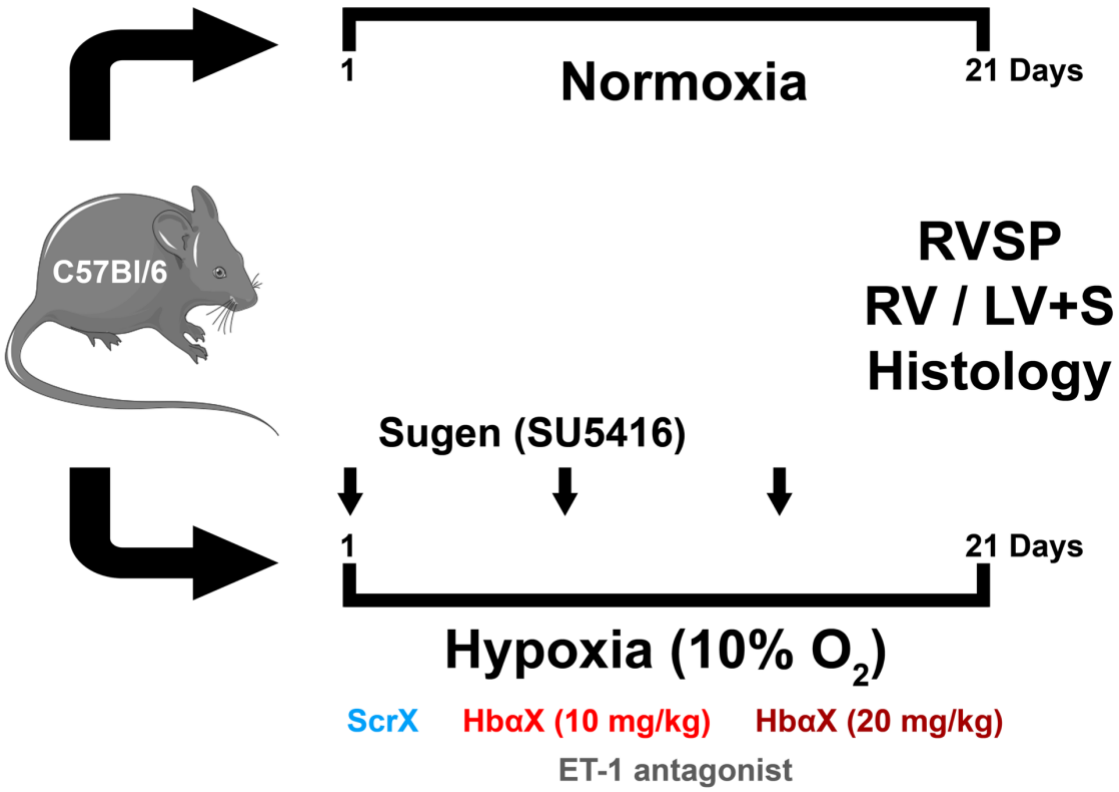

Figure 1. A hypoxia/SU5416 model is used to test therapeutic strategies after the induction of PH. Male, 10 to 15-week old C57Bl/6 mice from Jackson Labs were used in this study. To induce hypertension, mice were kept in 10% O_2 for 21 days, with three injections of SU5416 at days 1, 7, and 14. Additionally, a peptide mimicking the eNOS binding region of alpha globin (called HbαX) was injected intraperitoneally every other day at two doses, 10 or 20 mg/kg. A sequence scrambled control (ScrX) was injected on the same days at a dose of 20 mg/kg. To compare to a standard of care, an endothelin-1 antagonist (ET1A, ambrisentan) was administered in the drinking water at 100 mg/kg. At the end of 21 days, right ventricular systolic pressure (RVSP) was measured, the heart and lungs were harvested for measures of the RV/LV+S ratio and morphological and histological experiments.

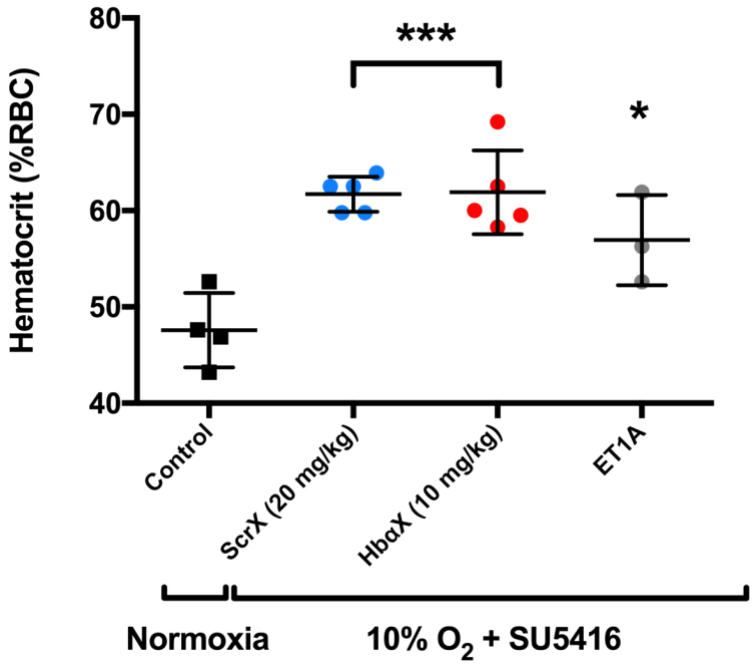

Figure 2. Hypoxia induced elevations in hematocrit were observed in treatment groups. Decreased oxygen and SU5416 injections increased the hematocrit in representative groups of the experimental model. * denotes $p < 0.05$ compared to normoxia control; *** denotes $p < 0.0005$ compared to normoxia control.

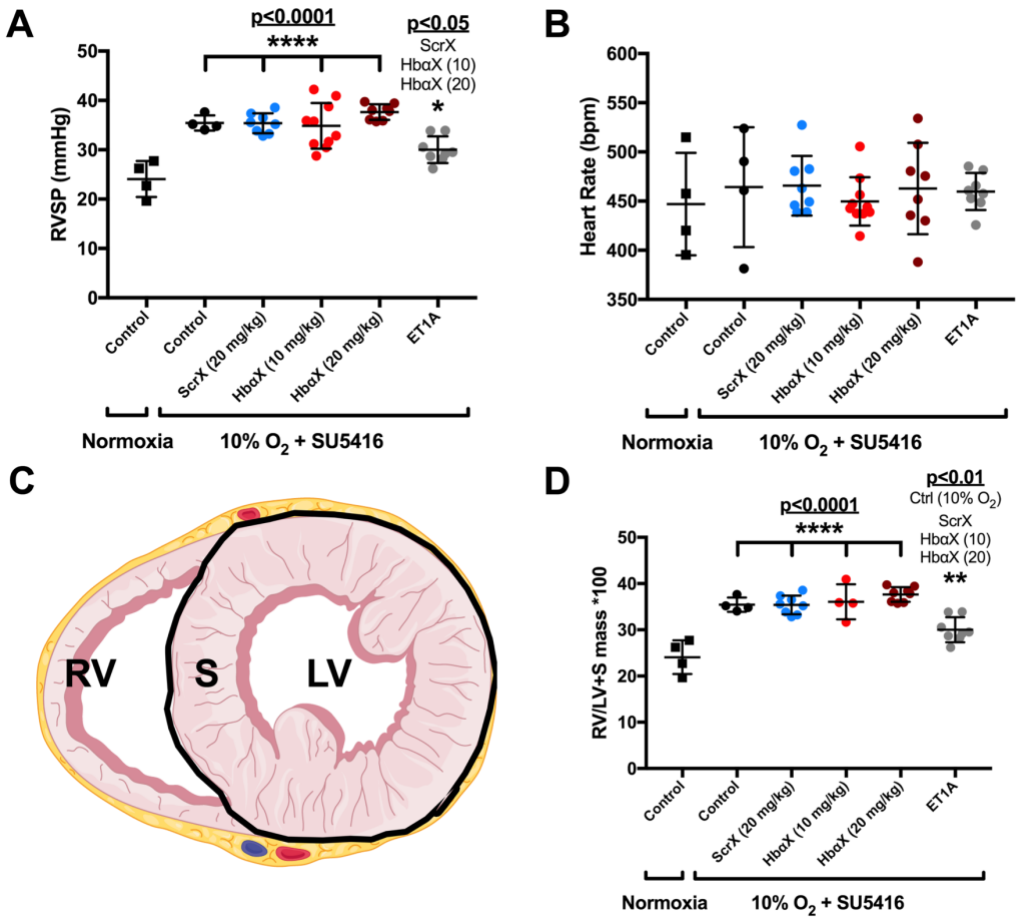

Figure 3. HbαX treatment does not alleviate PH, and performs worse than an ET1A standard of care. **A**, Right ventricular systolic pressure (RVSP) is measured via catheterization of jugular vein. Peptide treatments (ScrX, HbαX) do not decrease RVSP. ET1A treatment is still elevated compared to normoxia control, but is different from the peptide treatments. Asterisk denotes comparison to normoxia control, with the p value above. Differences to other groups are listed above the comparison with the corresponding p-value. **B**, Heart rate, measured concurrently with RVSP, did not change among groups. **C**, Diagram of the sections of the heart used for the Fulton Index, or mass of the RV normalized to LV and septum. **D**, Quantification of the Fulton Index as a percentage. Peptide treatments were not changed from hypoxia/SU5416 control. The ET1A was elevated compared to normoxia control, but was decreased ($p < 0.01$)

compared to all other hypoxia groups. Comparisons were made with a One-way ANOVA with Tukey correction. Individual points represent measurement from 1 animal.

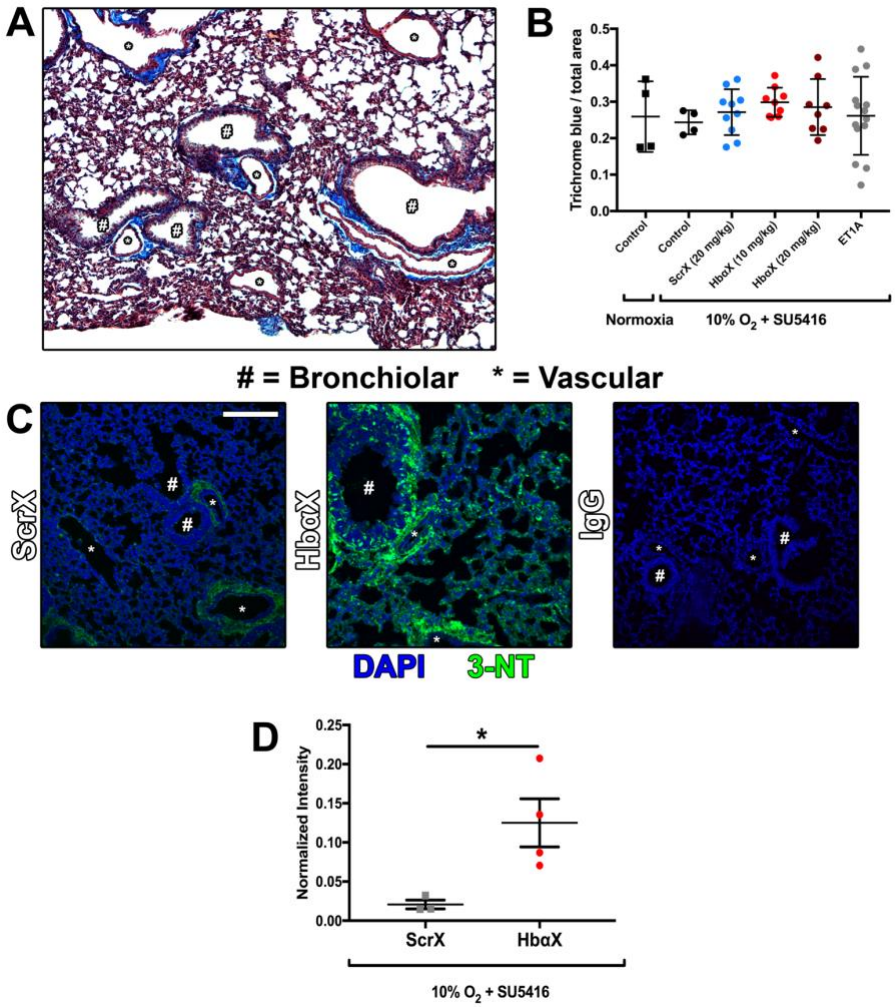

Figure 4. Fibrotic area was unchanged, but nitrosative stress damage was increased in HbαX treatment groups. A, example of Masson's Trichrome stain of pulmonary tissue. Fibrous tissue, especially perivascular and peribronchiolar, is stained in blue. # denotes bronchiole lumen, * denotes vascular lumen. **B**, total fibrous area from each mouse is normalized against total stained area in the image as in A. Each point represents average area normalization from at least 4 fields of view from one mouse. **C**, Staining for nitrotyrosine (3-NT) as a marker of NO production and nitrosative stress. DAPI (blue) stains nuclei, and 3-NT is colored green. # denotes bronchiole lumen, * denotes vascular lumen. Rabbit IgG was used as a staining control. **D**, Quantification of 3-NT

staining in ScrX and HbαX treatment groups. 3-NT was significantly increased in HbαX treated compared to ScrX treated (* denotes $p < 0.05$ via Student's t-test).

Appendix

Macros for FIJI/ImageJ:

Quantifying total stained area from IHC

Named “Trichrome_total.ijm”

```
run("8-bit");
setAutoThreshold("Default");
//run("Threshold...");
setAutoThreshold("Default");
//setThreshold(0, 130);
setOption("BlackBackground", false);
run("Convert to Mask");
run("Create Selection");
run("Measure");
```

Quantifying total fibrous stained area in view, by selecting the region of the image with “Hue” values between 100 and 170

Named “Trichrome_blue.ijm”

```
run("Threshold Colour");
// Threshold Colour v1.16------
// Autogenerated macro, single images only!
// G. Landini 8/May/2015.
//
min=newArray(3);
max=newArray(3);
filter=newArray(3);
a=getTitle();
run("HSB Stack");
run("Convert Stack to Images");
selectWindow("Hue");
```

```
rename("0");
selectWindow("Saturation");
rename("1");
selectWindow("Brightness");
rename("2");
//Hue values are seen here
min[0]=100;
max[0]=170;
filter[0]="pass";
min[1]=0;
max[1]=255;
filter[1]="pass";
min[2]=0;
max[2]=255;
filter[2]="pass";
for (i=0;i<3;i++){
  selectWindow(""+i);
  setThreshold(min[i], max[i]);
  run("Convert to Mask");
  if (filter[i]=="stop")  run("Invert");
}
imageCalculator("AND create", "0","1");
imageCalculator("AND create", "Result of 0","2");
for (i=0;i<3;i++){
  selectWindow(""+i);
  close();
}
selectWindow("Result of 0");
close();
selectWindow("Result of Result of 0");
rename(a);
// Threshold Colour ------------
run("8-bit");
setAutoThreshold("Default");
//run("Threshold...");
```

```
//setThreshold(0,200);
setOption("BlackBackground", false);
run("Convert to Mask");
run("Create Selection");
run("Measure");
```

Chapter 6: Efforts to determine the molecular architecture of the alpha globin/eNOS complex

Abstract

Nitric oxide (NO) signaling is a key regulator of blood pressure homeostasis, inducing vasodilation and reducing peripheral resistance. We have shown that inhibiting the alpha globin/endothelial nitric oxide synthase (eNOS) interaction is a target for increasing NO availability, leading to blood vessel dilation. A small, ten-residue peptide mimicking an alpha globin sequence competes for eNOS binding with the full-length alpha globin, disrupting complex formation through direct binding to eNOS. Continued development of therapeutic small molecules targeting this critical protein-protein interaction will be aided by a structural model of the binding interface of alpha globin and eNOS. Additionally, a molecular model of the interaction informs the mechanism of NO signaling inhibition by alpha globin.

Computational modeling was attempted with rigid protein structures, yielding no consensus interaction motif on eNOS. A model of the HbαX peptide generated by NMR-based restraints was next attempted to improve modeling, but proline isomerization in the peptide prevented accurate modeling. Empirical determination of interaction domain has been undertaken using crosslinking mass spectrometry. Recombinant eNOS oxygenase domain and the alpha globin mimetic peptide were crosslinked covalently and proteolyzed with multiple proteases. High resolution electrospray ionization-MS is used to determine the modified residues to reconstruct the interaction computationally. Using recombinant full-length alpha globin, we can validate results from the peptide/eNOS interaction and understand the molecular determinants of this protein-protein interaction. Overall, the

molecular understanding of this complex could lead to future therapeutics to increase NO signaling for hypertensive pathologies.

Introduction

Nitric oxide (NO) is a gaseous vasodilatory signaling molecule that is produced in the endothelium and diffuses to the smooth muscle to activate intracellular receptors and cause smooth muscle relaxation (*7, 173*). The enzymatic source of NO in the vascular wall is endothelial nitric oxide synthase (eNOS), an oxido-reductase enzyme that converts arginine to NO and citrulline (*254*). Our groups have shown previously that one critical regulator of NO availability in the endothelium is the alpha subunit of hemoglobin (hereafter, alpha globin), as it forms a complex with eNOS and prevents diffusion of NO by binding the gas with a prosthetic heme group (*35, 103*). NO can either be sequestered by the heme group or alpha globin can dioxygenate NO (forming nitrate, NO_3^-), rendering it inactive.

The motif of alpha globin that interacts with eNOS was elucidated previously (*35*), but the complementary region or sequence of eNOS has not been characterized. I have demonstrated that a small peptide mimicking the alpha globin binding motif (called HbαX) binds to the oxygenase domain of eNOS (*184*), but a more specific interaction is needed to fully characterize the protein complex.

We know that eNOS exists physiologically as a dimer, and that interaction of the reductase domain and the oxygenase domain is required for production of NO (*11, 254*). Additionally, many other proteins, cofactors, and post-translational modifications regulate the ability of eNOS to produce NO. How alpha globin regulates NO availability in the context of the myriad factors controlling eNOS activity is not known, but can provide understanding for how the signal integration and fine-tuning of dilation is achieved through this protein-protein interaction.

In our efforts to characterize this protein complex, we have undertaken broad techniques to observe the interaction domain specifically. I have specifically used HbαX as a proxy for full-length alpha globin in the studies of binding. Other groups have

attempted crystallization of the HbαX/eNOS oxygenase domain (eNOSox) complex (*Yeager group, UVA, unpublished*), but the resultant crystals showed no electron density for the HbαX peptide to assign the interaction domain. I began this study with a docking attempt using the GRAMM-X webserver (*284*). With inconclusive results from the docking of rigid crystal structures, I wanted to create a model of the HbαX peptide to use in docking with less rigid restraints. Solution NMR was the best technique to observe any secondary structure in the HbαX peptide. Proline isomerization introduced ambiguity in the results from NMR, and thus, a peptide structure could not be determined empirically. I have since undertaken a crosslinking mass spectrometry approach to identify the interacting residues on eNOS through covalent modification of the eNOS residues. Using restraints that are generated from mass spectrometry, a complex can be constructed. Increased confidence in the complex orientation can be achieved through other methods with full-length alpha globin, like small angle x-ray scattering or single particle cryo-electron microscopy.

Materials and Methods

Protein-protein docking via computational modeling

Computational docking was accomplished using the Vakser Lab GRAMM-X webserver (http://vakser.compbio.ku.edu/resources/gramm/grammx/). Models used were PDBid 3NOS for eNOS, and 1Z8U (chain B) for alpha globin. 30 models were generated with the potential ligand interaction residues restrained to the HbαX peptide, residues 35-44 in the alpha globin gene sequence. Models were roughly sorted based on location of the alpha globin and scored generically as possible binding conformations.

Nuclear Magnetic Resonance (NMR) spectroscopy

Nuclear Magnetic Resonance spectroscopy was performed at the University of Virginia Biomolecular NMR facility. Spectrometers were Bruker AVANCE operating at 600 and 800 MHz equipped with Bruker 5mm TXI cryoprobes and recorded at 313K. Spectra were processed with NMRPipe/NMRDraw and assignments were made with CARA and NMRFAM-SPARKY. Pulse programs used were optimized for water suppression and mixing time. For ^{13}C-^{1}H Heteronuclear Single Quantum Coherence spectroscopy, the pulse program ‘hsqcedetgpsisp’ was used; for Nuclear Overhauser Effect Spectroscopy spectra, the pulse program ‘noesygpphw5’ was used; for total correlation spectroscopy spectra, the pulse program ‘dipsi2esgpph’ was used; for double quantum filtered correlation spectroscopy spectra, the pulse program ‘cosydfesgpph’ was used. All pulse programs are available as standard packages in the Bruker pulse program catalog. DSS (4,4-dimethyl-4-silapentane-1-sulfonic acid) was used as an internal standard for chemical shift referencing.

Growth and purification of eNOSox

Purification of eNOSox was as described in (*184*). A detailed protocol is expounded in the appendix of this dissertation. Briefly, affinity purification using a glutathione-*S*-transferase fusion tag allowed for rough purification of eNOSox. The GST tag was cleaved off, and eNOSox was further purified using size exclusion chromatography to greater than 95% purity. Samples were kept in buffer with reducing agent at 4ºC until use, but no longer than 72 hours after final size exclusion column.

Gel electrophoresis and western blotting

eNOSox samples were run on a 4-12% gradient Tris/glycine polyacrylamide gel for electrophoresis. When required, the proteins in the gel were transferred to a nitrocellulose membrane for western blotting. The anti-eNOSox antibody was from antibodies-online, catalog #1889187; the anti-tat antibody is from abcam, catalog #ab63957. Both antibodies were used at 1:1500 dilution. Blocking solution was Licor Odyssey Blocking solution, and this was used for antibody dilution also.

Crosslinking reaction, gel band excision, protease digestion, and MALDI-MS

1-Ethyl-3-(3-dimethylaminopropyl)carbodiimide (EDC) crosslinking was performed according to the ThermoFisher general protocol. Gel band excision and protease digestion were based on Shevchenko *et al*. (*285*). MALDI-MS was performed according to UVA Mass spectrometry core guidelines. A specific protocol for all steps is included in the appendix of this dissertation.

Computational Small Angle X-ray Scattering simulation

SAXS modeling was based on three GRAMM-X-generated models (and one model of eNOS alone) that have different profiles for radius of gyration. These models were uploaded into the AquaSAXS webserver for solvation and scattering calculations to generate the scattering intensity.

Results

Determining the conformation of the alpha globin/eNOS complex allows us to understand how alpha globin can control NO availability. I have undertaken a multi-faceted approach to understand how these two proteins form a binding complex in order to gain insight into the mechanism of a novel role for alpha globin as a modulator of systemic blood pressure.

Multiple structures of alpha globin and eNOS have been solved by x-ray crystallography (I have primarily used PDB ID 1Z8U (*286*) for alpha globin and 3NOS (*287*) for eNOSox). 3NOS is a high-resolution structure of the eNOSox dimer with arginine substrate, a heme group in the active site, and dimerization cofactors tetrahydrobiopterin and zinc ion. 1Z8U was used as the model of alpha globin because it has alpha globin bound to its stabilizing protein, which is the form of alpha globin found in vascular endothelium. Although these structures are rigid, packed into a suitable crystal lattice, their structures may allow for computational construction of the protein complex based on complementary folding. Using the rigid protein structures and a modified Lennard-Jones potential, a step function is generated which minimizes the energy potential based on low-resolution reconstructions of the structure (*284, 288, 289*). After initial energy minimization calculations (taking into account Van der Waals potentials, especially), each low-resolution complex is scored by the number (out of about 4000 initial models) that cluster within about 5 Å of that structure. From there, predictions that are likely to be incorrect based on potentials, rules from other structures, etc. are removed and the set of predictions is again filtered to a number specified by the user (*284*). Overall, the prediction algorithm performs well, and has been used in numerous studies to predict protein complexes (greater than 500 citations on June 1, 2019).

Generating the models was an initial step in determining whether a consensus motif on eNOS for alpha globin binding was easily determined by computational docking. Using

the GRAMM-X server, I defined one interaction motif on alpha globin as the HbαX peptide sequence (*35*), amino acids 35-44 in the *HBA1* gene. For alpha globin's interaction with eNOS, we have shown previously that HbαX interacts with the oxygenase domain directly through immunoprecipitation and fluorescence polarization binding studies (*184*). In the models in **Figure 1**, alpha globin is shown in blue, with the HbαX region highlighted in red in each of the models. Thus, we used the full eNOS oxygenase domain as the interaction partner for alpha globin. Physiologically, eNOS is active and stable through dimerization of the oxygenase domain (*11*); therefore the dimeric eNOSox in 3NOS (*287*) was used for the GRAMM-X study. In **Figure 1**, dimeric eNOSox is shown in gray, with each of the monomers in a different shade. Overall, each of the models is in the same view in the figure, with only alpha globin changing location between images. Some models do not have alpha globin interacting with eNOS through the HbαX motif, and can thus be excluded. Other models are inconclusive based on lack of information for eNOS specific activation by the reductase domain (*11*). There seems to be no consensus motif where alpha globin consistently interacts with eNOSox; thus, alternative approaches are needed to determine where on eNOSox the HbαX peptide and full length alpha globin bind.

To more accurately represent the HbαX peptide (which we know binds with high affinity to eNOSox (*184*)) in computational models, I wanted to determine the structure of the HbαX peptide *de novo* without the constraining properties of the rest of the alpha globin protein. This peptide is about 2 kDa, which is below a lower limit of feasibility for structure determination by circular dichroism spectroscopy (while maintaining any flexibility that would exist in solution). Also, there is no assurance of secondary structure, so circular dichroism spectroscopy was not an effective method to determine any structural features of the peptide. Because the peptide is soluble to approximately millimolar concentrations in solution, I turned to solution nuclear magnetic resonance (NMR) spectroscopy as a method of determining the conformation of the peptide for unbiased docking studies.

Using the full tat-HbαX peptide (sequence show in **Figure 2A**), I was able to obtain homonuclear ^{1}H-^{1}H and heteronuclear ^{15}N-^{1}H correlation spectra used in routine peptide structure determination at natural abundance from a peptide concentration of 750 μM. Homonuclear experiments, such as total correlation spectroscopy (TOCSY), could be obtained on a 600 MHz magnet, although spectra were higher quality and required less experiment time for well-resolved peaks using an 800 MHz magnet equipped with a cryoprobe. The tat- HbαX TOCSY spectrum and "fingerprint" regions for methyl ^{1}H-^{1}H and amide ^{1}H-^{1}H correlations shown in **Figure 2B-D** was obtained with the 800 MHz spectrometer using a mixing time of 220 ms. This was the optimal mixing time for this peptide, as it allowed for magnetization transfer to reach protons on residue sidechains that a shorter mixing time (175 ms) did not (while avoiding excessive spin diffusion away from the sidechains). As a result, many spin systems were identified from the TOCSY spectrum, and I could begin assignment of the residues.

In general, amino acids can be identified by the specific combination of spins (NMR spectrum peaks) in each spin system. Distinct chemical shifts are seen for each of the magnetic nuclei that make up the amino acid, and these chemical shifts are also affected by the chemical bonds that each atom is involved in. For example, hydrogen (commonly referred to as a proton, or ^{1}H, in NMR terminology) is magnetically active and very abundant. When two ^{1}H are bound to one oxygen atom (to form water, H_2O), the chemical shift of the hydrogen atoms is approximately 4.8 parts per million (ppm). The same atom, when bound to a nitrogen (as an amide proton on a protein backbone), can have a chemical shift that ranges from about 8-8.5 ppm. The peaks that interact in a single spin system give clues to the identity of the amino acid, specifically through the number of peaks in a spin system, and the location of unique atoms (like the proton bound to the gamma carbon in the side chain of threonine). NMR has been used for the determination of protein structure due to the ability to identify specific amino acids in proteins (*290*).

However, in the spectra of the tat-HbαX peptide, there was an unexpected increase in the total number of anticipated spin systems in the NH-finger print region (from about 8 to 8.5 ppm chemical shift values). From the peptide sequence, we expect 20 spin systems to appear in this region (the proline in the sequence has a distinct peptide bond that does not share the same chemical characteristics, so does not have an NH shift in this region). Some of the arginine residues experience a similar magnetic environment, so they may not have fully distinct chemical shifts; I observed 21 spin systems in the NH-NH region of the TOCSY spectrum. Further, in identifying the amino acid identity of spin systems, I was initially confused in the assignment of threonine peaks (zoomed regions shown in **Figure 2C** and **2D**). Although there are only three threonine residues in the protein sequence, five spin systems that had characteristic threonine resonances (of the protons bound to the alpha, beta, or gamma carbon: Hα, Hβ, and Hγ, respectively) were observed (Hγ in orange, **Figure 2C**, and Hα with Hβ in cyan, **Figure 2D**). The threonines are labeled with X, Y, Z, A and B to denote separate spin systems, although they are not necessarily in sequential order from the peptide sequence. Overall, this result complicated the assignment of spin systems and sequential assignment because the spin systems were not unique in assignment to the peptide sequence residues.

Initially, the extra threonine spin systems were confusing in their origin. One possible explanation is that the threonines neighboring the proline were experiencing different magnetic environments when the proline was undergoing isomerization. The isomerization would create two distinct conformations of the HbαX peptide. The different magnetic environment would change the chemical shifts of the threonines, resulting in multiple spin systems that arise from the same residue. Additional experiments were needed to determine that the lone proline in the peptide sequence was undergoing isomerization reactions to generate two conformations of the HbαX peptide. In a heteronuclear single quantum coherence experiment, using natural abundance ^{13}C in the

peptide, I was able to assign the proline Hδ resonances. Initially, with a high signal threshold, only one proline Hδ pair was visible. However, with a lower threshold value, a second proline pair appeared in the same region (**Figure 2E**). With only one proline in the amino acid sequence, we hypothesized that this proline was undergoing isomerization and causing two conformations in the full HbαX peptide chain. The magnetic environment was similarly affected by the change in proline, and caused major and minor peaks in the threonine spin systems in our experiments.

Because two conformations of the HbαX peptide would not double the amount of computational docking models to generate and verify, this approach of computational modeling based on empirical determination of the HbαX peptide structure was more complicated than originally planned. Thus, we elected to table peptide structure determination in favor of a crosslinking mass spectrometry approach to determine peptide, and alpha globin, binding to eNOS.

In order to determine the region of eNOSox that interacts with alpha globin by mass spectrometry, purified components must be crosslinked and digested into suitable fragments for identification of peptides. The covalent linking of functional groups can readily be accomplished with chemical crosslinkers with reactivity to amine and carboxy groups, which are present on the amine tail at the end of the peptide and the side chain of the common amino acid lysine (amine), or the side chains of glutamate and aspartate, or the end of the tat-HbαX peptide chain (carboxy). After crosslinking, the products can be separated by size on a polyacrylamide gel matrix, excised, and digested in-gel by proteases. The resulting peptides can be identified using electrospray ionization (ESI) mass spectrometry, where modified residues would result in a different peptide mass-to-charge (m/z) ratio from unmodified counterparts. A general workflow is shown in **Figure 3A**, and I have used this workflow recently to begin to determine where on eNOS the HbαX peptide binds. Starting with the HbαX peptide is reasonable due to its high affinity

for eNOSox (*184*). Also, the tat-HbαX peptide has three total lysines and one terminal amine to use as targets for the EDC crosslinker. Because it is soluble in aqueous buffers, it can easily be mixed with eNOSox for crosslinking reactions. The tat fusion tag is able to be detected through antibody-based techniques, and thus efficiency of crosslinking can be assayed. Initial experiments with the HbαX peptide can be expanded to use the full length alpha globin protein for confirmation of the discovered binding site.

To crosslink the HbαX peptide and eNOSox, I used eNOSox purified from *E. coli* lysates. Recombinant protein purification from *E. coli* is advantageous for rapid, low-cost, large-scale production (milligram quantities of purified protein are possible) compared to eukaryotic cell culture. However, many of the endogenous pathways for post-translational modification (in the case of eNOS: myristoylation, palmitoylation, phosphorylation) are absent from bacterial cell culture. Overall, the quantities of protein from bacterial cell culture are preferred for these experiments, although the determined binding site on eNOS will be confirmed with eukaryotic protein purification. A glutathione S-transferase (GST) fusion tag appended to the N-terminus of eNOSox allowed for affinity-based purification on a glutathione-conjugated agarose column. After incubating lysate from *E. coli* transformed with the GST-eNOSox construct with the glutathione agarose, other components of the lysate could be washed away while eNOSox remained bound to agarose beads. After cleavage of the GST fusion tag and size exclusion chromatography, eNOSox purified to > 95% was obtained. The eNOSox construct that I have used has a molecular weight of 48.6 kDa, and when heated and in reducing conditions (as in a polyacrylamide gel), runs at that molecular weight (see **Figure 3B**, “eNOSox monomer”). However, in physiological form, eNOSox is primarily dimerized with the help of Zn^{2+} coordination and tetrahydrobiopterin incorporation (*254*). After crosslinking, the relevant dimer state of eNOSox is covalently linked and stable against heat and reducing conditions (**Figure 3B**, “- HbαX” lane). This dimer is approximately 100 kDa in size, which

is close to the expected molecular weight from two monomers. The intermolecular, eNOSox-to-eNOSox crosslinks are stable under reducing conditions and heat (**Figure 3B**). Addition of the HbαX peptide in these same conditions did not disrupt the eNOSox dimer (**Figure 3B**, "+ HbαX" lane). Also, reducing conditions and heat were not able to disrupt the eNOSox/HbαX crosslinking reaction. Using immunoblotting, I probed for eNOSox (red signal in "-heat" and "+heat" lanes) and the tat moiety (green signal in the lanes; the merged image shown has the colocalization of the signals in yellow). Boiling the gel samples for 10 minutes in reducing conditions neither broke the eNOSox-eNOSox crosslinks (as demonstrated by the molecular weight of the sample) nor diminished tat-HbαX signal in the +heat sample. The crosslinker was stable across reducing and denaturing conditions, thus we wanted to probe for crosslink-modified peptides seen in protease-digested samples.

To isolate relevant samples for protease digestion and peptide identification, I used an in-gel digestion technique. My own version was based on the protocol published by Shevchenko *et al*. (*285*). This protocol was originally designed for identification of proteins from two-dimensional gel electrophoresis, where individual proteins separated by size and isoelectric point could be specifically excised, digested, and identified by sequences via mass spectrometry. I used a similar approach to isolate only the dimer band of the eNOSox crosslinking products. Because this is the physiological form of eNOS, I wanted to probe the interaction of HbαX and eNOSox as it might exist *in vivo*. After carefully excising the eNOS dimer band, it was destained, washed, dried, and prepared for rehydration with protease-containing buffer.

So far, two proteases have been used to digest the crosslinked eNOSox sample: trypsin and Asp-N (**Figure 4A**). Trypsin has been used in many mass spectrometry studies; it has multiple cleavage sites and generates many peptides that can be identified by mass spectrometry methods. Trypsin cleaves peptide bonds immediately after arginine

and lysine residues, which are abundant in protein sequences. Asp-N is less widely-used in general, due to its specificity in only cleaving immediately N-terminal of aspartate residues. Together, these proteases provide mostly orthogonal cleavage sites that can be used to narrow in on specific regions of eNOS that are modified by HbαX. Trypsin has many cleavage sites in the tat-HbαX peptide itself, with only a few residues of the alpha globin-mimicking region that are unaffected by trypsin proteolysis. eNOSox also has many cleavage sites. In a 40-residue region taken from amino acids 160 to 200 in eNOSox, there are 7 cleavage sites for trypsin, with the longest peptide possible (assuming no missed cleavages) being 9 residues (**Figure 4A**, blue arrows). In contrast, Asp-N cleaves much more sparsely, with only 2 cleavages in the same region, and a long peptide of greater than 35 residues being possible with Asp-N reaction (**Figure 4A**, pink arrows). Additionally, there are no aspartate residues in the tat-HbαX peptide, so any modifications in eNOSox should be from the entire HbαX peptide; thus, the cleavage pattern of eNOSox with and without HbαX crosslinking could contain eNOSox peptides modified by the full-length tat-HbαX (which has a molecular weight of about 2 kDa). Using these two proteases allows for peptide fractionation that can identify large regions and obtain sequence data from more specific modification of residues on eNOSox that are interacting with HbaX

Overall, we expect 128 peptides from trypsin cleavage and 28 cleavages from Asp-N in the eNOSox sequence (based on minimum length of 5, with maximum 2 missed cleavages). We have observed about 100 peptide products from trypsin cleavage, yielding about 80% coverage of the eNOSox sequence. From Asp-N cleavage, sample quality issues precluded identification of many peptides from eNOSox. These experiments will need to be repeated to identify and characterize the crosslinked residues from eNOSox that are interacting with HbαX. In **Figure 4B**, a full cleavage pattern obtained from eNOSox with (red trace) or without HbαX (black trace) is shown after trypsin proteolysis. Each of the peaks shown on this mass spectrum, obtained from a matrix-assisted laser desorption

ionization (MALDI) mass spectrometer, represents one peptide generated from eNOSox proteolysis. Although this is a relatively low-resolution method, the good dispersion of peptides shows that efficient cleavage was achieved with trypsin. Within the spectrum, most of the proteolysis products are similar from the +/- HbαX reaction, but this is expected due to the size difference of eNOSox and HbαX; each eNOSox monomer is 48.6 kDa, while the HbαX peptide is only 2 kDa. The products were similar through many parts of the spectrum, but some differences existed in regions highlighted in **Figure 4C** and **4D**. Arrowheads point to m/z species that are unique to eNOSox alone or eNOSox + HbαX reactions; black signifies a peak that is present in eNOSox + EDC alone, while red denotes a peak only seen in eNOSox + HbαX + EDC.

Due to the lower number of cleavage sites for Asp-N, fewer peptides were observed in the total spectrum (data not shown). However, peptides in the range of 1000 to 5000 Da were observed; from these reactions, many of the peptides that were observed in eNOSox + EDC were absent in the eNOSox + HbαX + EDC reaction (black arrowheads). Although these peptides are observed, they have not been characterized with sequence information yet. Ongoing ESI mass spectrometry experiments are being used to determine the site on eNOSox that is modified by the crosslinking to HbαX.

Discussion

In order to determine the conformation of the alpha globin/eNOS complex, I have tested a few biophysical methods to have empirical evidence for the site of interaction. Previous work on this complex from the Yeager group at the University of Virginia (especially M. Cabot and M. Purdy) focused on X-ray crystallography to determine the binding region of the HbαX on eNOSox. eNOSox has been crystallized beautifully and to high resolution, with and without substrates or other cofactors, and this was accomplished by the Yeager group. However, with either peptide soaking or co-crystallization efforts, an electron density for HbαX was not observed for any eNOSox crystallization conditions. Despite its wide use, crystallization as a technique is notoriously finicky, and in this case, was not suitable for determining where on eNOSox alpha globin was binding.

This is where I started my work on this project. We knew that alpha globin and eNOS were interacting, that a peptide mimicking ten residues on alpha globin could compete for eNOS binding with full length alpha globin, but did not have evidence for a region on eNOS that was the interaction site. I showed that one region of alpha globin, a peptide termed HbαX, could bind directly to eNOSox that I produce in *E. coli* (*184*). With inspiration from other studies, my first thought was to use docking studies to determine where on eNOSox the HbαX peptide was interacting. Starting with the full length alpha globin protein, I used the GRAMM-X webserver (*284, 288*), as our groups had done previously to determine a site on alpha globin that could interact with eNOS (*35*), to find a consensus sequence on eNOSox where alpha globin binds (**Figure 1**).

Many of the models seem to cluster around the C-terminal end of the oxygenase domain, although the oxygenase domain is less than half of the full length eNOS sequence, so some models from **Figure 1** could interfere with the reductase domain orientation of the full eNOS protein. Although the structure of full length inducible NOS (a closely related NOS isoform) has been solved (*11*), the density of eNOS solved by electron

microscopy was not of high enough resolution to allow for docking of known crystal structures into the reconstruction. Knowing where the reductase domain of the NOS isoform interacts with the oxygenase domain could narrow the restraints for the docking algorithm; however, at this point, the possibilities are too broad for appropriate hypothesis testing based on the docking results.

Without a consensus binding motif from the protein-protein interaction server, I wanted to narrow the constraints on the alpha globin - eNOSox interaction by having an empirical model of the HbαX peptide to use as a docking candidate. Solution NMR provides a reasonable technique for determining structure and conformation of small proteins and peptides *de novo*. The small size and high solubility of the HbαX peptide (about 2 kDa) makes it ideal for solution NMR; the peptide tumbles rapidly in solution to give an isotropic orientation with favorable spin relaxation properties, and sufficient amount of magnetically-active isotopes can be achieved for heteronuclear experiments. In a homonuclear ^{1}H-^{1}H TOCSY experiment, the peaks for individual spin systems were well-resolved, and some spin systems could be assigned as specific amino acids (**Figure 2B**). Other spectra (not shown) were taken and used for attempted assignment of TOCSY peaks to the tat- HbαX amino acid sequence. A ^{1}H-^{1}H correlation spectroscopy (COSY) experiment uses pulses that select for amide proton and Cα proton couplings, which is an essential for unambiguous resonance assignments. COSY experiments are specifically designed for protons that are coupled through less than three bonds (as are the protons on the amide and alpha carbon). The physical, through-bond coupling of these protons gives rise to cross (or off-diagonal) peaks in the spectrum. Generally, amino acid identities cannot be identified from COSY spectra alone, as the chemical shifts of the Cα resonances are similar across amino acid species. This is one reason why a TOCSY experiment is needed for spin system assignment – the magnetization transfer is longer in TOCSY experiments and allows visualization of proton couplings across the amino acid sidechain. Although the

TOCSY experiment provides details about spin system identity, it does not give information about sequence *per se*.

Generally, combination of a COSY or TOCSY experiment with a ^{1}H-^{1}H nuclear Overhauser effect spectroscopy (NOESY) experiment allows for sequential assignment of residues in the peptide chain. NOE couplings are distinct from COSY or TOCSY couplings because they are through-space instead of through-bond. This not only provides information about sequential residues, but also intramolecular couplings of protons that are close in space. Tertiary protein structure relies on NOE restraints generated from integration of NOESY peaks. Distances within the peptide bond are on average: $(C=O)_j$–$(C\alpha)_j$ = 1.53 Å; $(C\alpha)_j$-$(NH)_j$ = 1.47 Å; $(NH)_j$-$(C=O)_{j+1}$ = 1.32 Å (j denotes a residue at random position within the polypeptide chain; j+1 is the subsequent, and j-1 would be the residue immediately previous). The distance limit of NOE signal enhancements is about 4-5 Å, which allows for $(NH)_j$ coupling to $(C\alpha)_{j+1}$ or $(C\alpha)_{j-1}$. The sequential coupling should introduce an unambiguous path through the peptide chain, as the strips of an individual spin system in the NOESY spectrum will have resonances between neighboring spin systems. This is commonly used in solving protein structures via solution NMR (*290, 291*).

The process of sequential assignment was complicated in the HbαX peptide by the proline isomerization. Because the threonines nearby the proline were sensitive to the isomerization, there were five threonine spin systems observed in the TOCSY spectrum (**Figure 2B**, **2C**, and **2D**). The proline isomer introduced ambiguity in the threonine spin systems and thus complicated sequential assignment. Additionally, with two conformations of the HbαX peptide, there was no definitive experiment that would eliminate one as a binding partner for eNOSox. Determining the conformation of HbαX that binds to eNOSox *in silico* is at best, tedious, and at worst, inconclusive.

For this reason, solution NMR as a method of conformational reconstruction of the alpha globin or HbαX/eNOSox complex was abandoned in favor of empirical interaction

observed by crosslinking mass spectrometry. To this point, I have only worked with eNOSox and the HbαX peptide, although another advantage of this technique is that it can readily be expanded to the full-length alpha globin protein. Currently, the tat tag on the HbαX peptide is antibody-targetable and allows for immunoblotting as confirmation of crosslinking (**Figure 3C**). One issue that I have yet to solve fully is the relative instability of alpha globin in solution when not bound by alpha hemoglobin stabilizing protein (AHSP) or bound to a partner like beta globin (*292*). I have generated a Green Fluorescent Protein (GFP)-fusion alpha globin (and with help from others, have improved upon that original design), that should keep alpha globin soluble for binding. I will need to confirm that the GFP-alpha globin binds to eNOSox sufficiently, using immunoprecipitation, and surface plasmon resonance or biolayer interferometry experiments, before continuing the crosslinking efforts with alpha globin. The binding of alpha globin to eNOS should stabilize the alpha globin in solution sufficiently to allow for crosslinking before mass spectrometry. Lechauve *et al*. have shown that the binding of alpha globin to AHSP is exclusive of its binding to eNOS (*292*); thus, alpha globin bound to eNOS is a relatively stable interaction that we should be able capture with crosslinking and analyze with mass spectrometry methods.

For the eNOSox and HbαX interaction, two major species are seen in the crosslinking reaction. eNOS dimerizes via the oxygenase domain (*11*); thus, the recombinant eNOSox is expected to dimerize in solution. We observe a major species at approximately 100 kDa, equal to the molecular weight expected from dimeric eNOSox. In the gel shown in Figure 3B, there is a minor species at 48 kDa in both the + and – HbαX lanes. The crosslinking of HbαX to eNOSox does not disturb dimerization; thus, we might expect that binding of alpha globin does not perturb eNOSox dimerization. This is important because dimerization is critical for production of NO by eNOS. Electrons are shuttled from the first chain's reductase domain through cofactors to the second chain's active site, so if HbαX

(and probably alpha globin) do not disrupt dimerization, that process may still occur. This result needs to be confirmed with the full length alpha globin protein.

I have primarily used EDC as a crosslinking reagent in these experiments. EDC is a zero-length carboxy to primary amine reactive molecule and can link the HbαX peptide to complementary residues on eNOSox. The zero-length reaction of EDC allows for reactions that are specific to the interacting residues, and importantly, avoids HbαX-HbαX crosslinking. Using another crosslinker, bisulfosuccinimidyl suberate (an amine-amine crosslinker with an 8-atom spacer), I saw significant laddering of the HbαX peptide and little HbαX/eNOSox crosslinking. I have not used that crosslinker for further studies because of the peptide laddering, which prevents HbαX-eNOSox interaction by depleting available HbαX. Reagents with longer spacers might prove useful for full-length alpha globin/eNOSox crosslinking, but have been less worthwhile in current studies.

Using multiple proteases with distinct cleavage patterns allows for complementary data collection for reconstructing the HbαX/eNOSox complex after proteolysis. Trypsin is a protease commonly used in mass spectrometry workflows, as it has specific cleavage sites on the peptide bond immediately following arginine and lysine residues. These two residues make up 11.4% of the residues in eNOSox, and thus provide sufficiently small proteolysis products for analysis. Digestion of the eNOSox species by trypsin and subsequent analysis on the ESI-MS showed that >80% of eNOSox was covered by products from trypsin proteolysis. This is a good initial result for identifying peptides modified by crosslinking. However, one significant disadvantage of using trypsin proteolysis is the number of cleavage sites in the tat-HbαX peptide itself. The tat region has only three peptide bonds (out of eleven) that are not targets for trypsin proteolysis; therefore, the cleavage products may be not identified as such once crosslinked to the eNOSox peptides. Using an orthogonal protease allows for differential peptide products to facilitate identification of the crosslinked residues. I have used Asp-N protease for this

reason. Asp-N cleaves peptide bonds specifically only before aspartate residues; there are 0 aspartates in the tat-HbαX sequence and 25 in the eNOSox sequence. The resulting cleavages are generally in different bonds, although some overlap exists between individual sites of trypsin and Asp-N (**Figure 4A**), and the resulting peptides are not of the same length. Additionally, because there are no cleavage sites for Asp-N in the tat-HbαX, any crosslinking reaction should modify one (or more) eNOSox peptides with the full HbαX peptide sequence and molecular weight. In the MALDI-MS experiment, there are multiple eNOSox+ EDC m/z species that do not have corresponding peaks in the eNOSox + HbαX + EDC spectrum (**Figure 4D**). Full analysis of the Asp-N cleavage reaction after crosslinking has been started, but not completed, as of this writing.

Overall, the mass spectrometry results will be critical in identifying interacting residues within the alpha globin/eNOS binding site. To aid in the reconstruction of the full complex, I have considered other physical methods for determining orientation. To get a general sense of the orientation of alpha globin relative to eNOS, I have thought about using small angle x-ray scattering as a technique to determine the relative orientation of alpha globin monomers to eNOSox dimer. I have based three “states” that have different overall orientation of the complex on three models from the GRAMM-X server predictions (**Figure 5A**, **5B**, and **5C**). Using these states, I generated a theoretical SAXS scattering profile based on solvation calculations and x-ray scattering predictions provided by the AquaSAXS web server (*293*). The overall scattering profile of these states is shown, and differences exist especially between eNOSox alone (model not shown) and any of the three states (**Figure 5D**). Some differences exist in the middle values of q, although it is unclear how different these states would appear in noisier, less-ideal, datasets. Additionally, the size of the HbαX peptide would preclude use of this SAXS method for empirical determination of the orientation – the small peptide would likely not affect the scattering profile enough to be observed in this experiment.

Another avenue to explore for determining the orientation of the complex is combining restraints from crosslinking mass spectrometry with data on complex orientation via electron microscopy (EM). Some tools and workflows already exist for combination of these complementary datasets for determining a high-resolution model of the complete protein structure (*294-296*). Overall, the functionality of the crosslinking MS combined with EM makes for an attractive approach to determine the structure of protein complexes. Although there are challenges in sample preparation for EM, the foundations of combining empirical interaction data with the powerful molecular reconstruction of protein complexes by single particle cryo-EM is viable, and something that I have considered as a future direction for this project.

Determining the molecular architecture of the alpha globin/eNOS complex is an important goal for understanding the mechanism of alpha globin inhibiting NO availability. The binding site of alpha globin on eNOS is unknown, and understanding how these two proteins interact can inform pharmaceutic development as well as advancing our understanding of vascular biology.

Figures

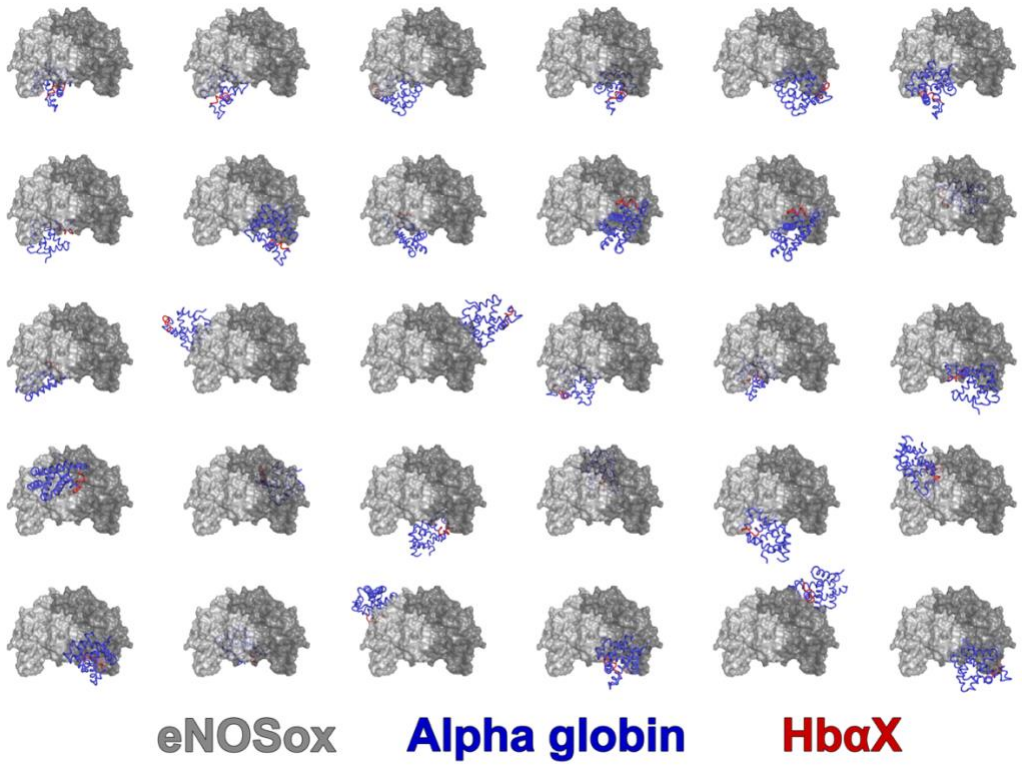

Figure 1: *In silico* modeling of the alpha globin/eNOS interaction domain did not yield a consensus binding motif on eNOS. The GRAMM-X protein-protein docking web server (http://vakser.compbio.ku.edu/resources/gramm/grammx/) was used (input PDBids: 1Z8U.A for alpha globin, 3NOS for eNOS) to generate 30 states of alpha globin/eNOS interaction using the HbαX motif as a constraint for interaction. All 30 models are shown, with the dimeric eNOS oxygenase domain in gray surface (each monomer in a different shade), alpha globin in blue cartoon, and HbαX highlighted in red. There was no clear interaction that was more likely than others from these models.

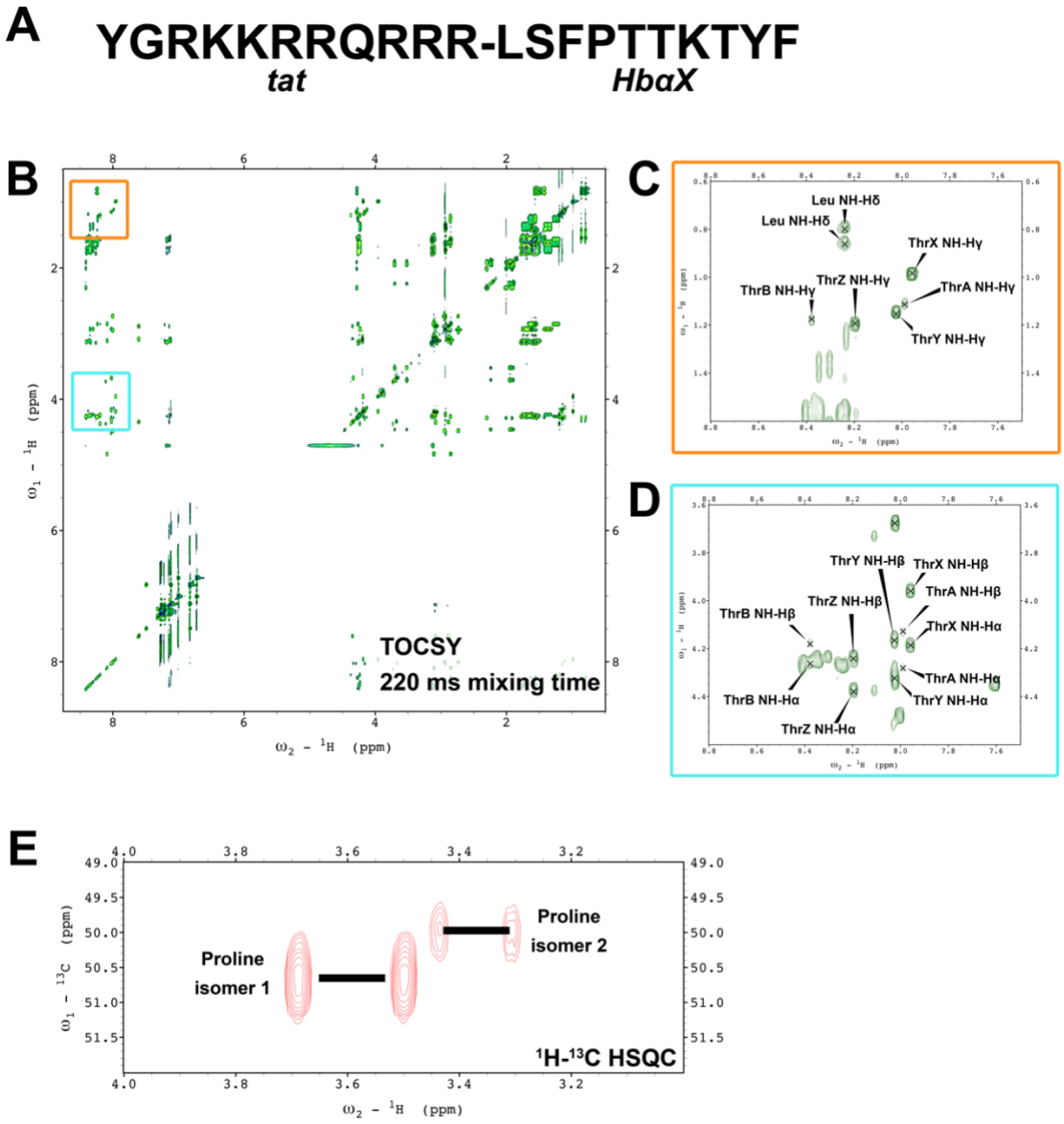

Figure 2: Proline isomerization allows the HbαX peptide to adopt multiple conformations in solution. In **A,** the sequence of the tat-HbαX peptide contains three threonines and one proline residue. The space between the tat and HbαX sequences is only for representation – the peptide chain is continuous through the sequence. **B,** a total correlation spectroscopy (TOCSY) experiment with a 220 ms mixing time generated the

spectrum shown. There is good resolution in the amide region (~8 – 8.5 ppm), with clear spin systems evident for most amino acids. Zoomed regions are seen in C and D corresponding to the color outlined in B. **C,** a zoom in the region of the Hγ region of the threonine spin systems shows five peaks when three are expected. Five threonine systems are also seen in the characteristic threonine Hα/Hβ region in **D**. Threonine spin systems are labeled X, Y, Z, A, and B, though these do not correlate with sequence information. **E,** from a ^{1}H-^{13}C heteronuclear single quantum coherence spectrum (HSQC), the two populations of proline in cis or trans are shown with two sets of Hβ peaks. The proline isomerization might give rise to the extra threonine systems seen in B-D.

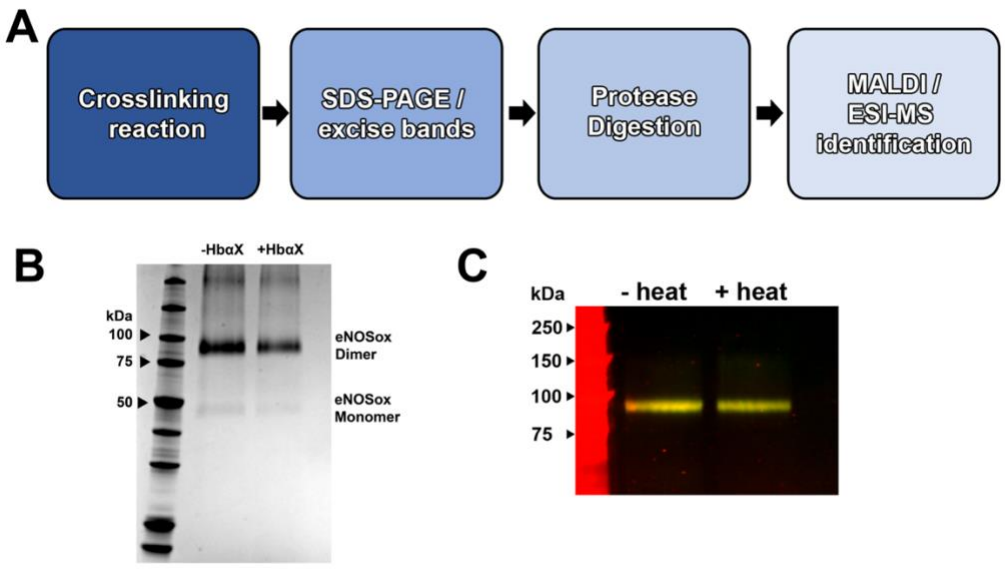

Figure 3: Crosslinking reaction does not affect eNOS dimer formation and is resistant to heat denaturation. In **A,** a workflow for the crosslinking/mass spectrometry experiments that follow. First, purified eNOS and HbαX are incubated with EDC, a zero-length carboxy-to-amine covalent linker, to crosslink the two components together. Then, the crosslinked products are isolated from SDS-PAGE gels, washed, and digested with protease while remaining in the gel matrix. This allows for isolation of correct-sized products. Confirmation of protease cleavage can be accomplished with matrix-assisted laser desorption ionization (MALDI) mass spectrometry, and specific peptides can be identified with electrospray ionization (ESI) mass spectrometry. In **B,** crosslinked products run on a polyacrylamide gel and stained with Coomassie blue show a dominant species corresponding to dimeric eNOSox (monomer weight is approximately 48 kDa). The addition of HbαX (right lane) does not inhibit dimer formation. The eNOSox dimer band is excised for in-gel digestion and MS experiments. In **C,** the eNOS/HbαX peptide crosslinking is heat-resistant, demonstrating a stable complex. The left lane is the

molecular weight marker. eNOSox was probed in red, and the tat sequence of the HbαX peptide in green; the merge of the two signals in the image is shown in yellow. Boiling the sample for 10 minutes in reducing conditions did not break the complex of eNOS and HbαX, showing stability of the eNOS/HbαX crosslinking reaction.

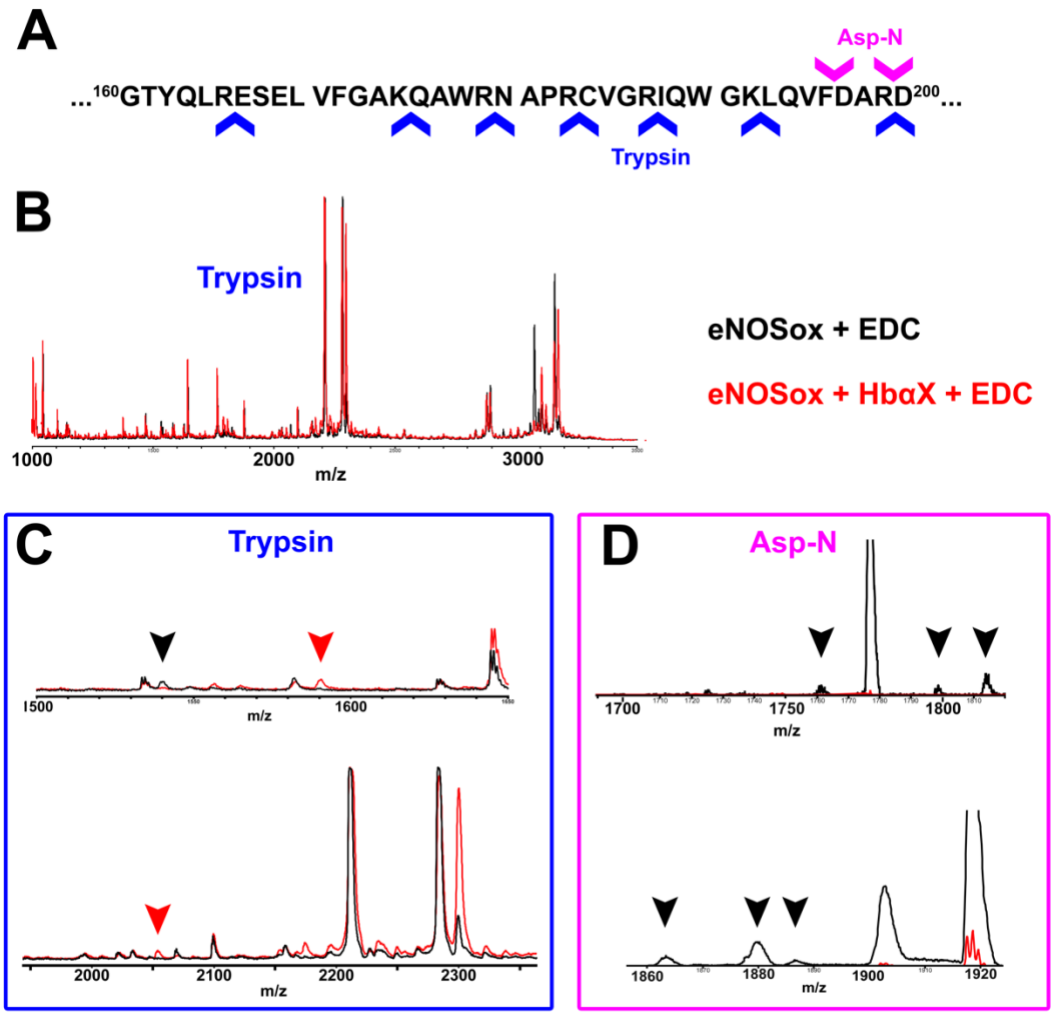

Figure 4: HbαX crosslinking gives differential cleavage fraction after protease digestion. A, an example of a sequence from eNOSox (residues 160 to 200) with protease sites marked with arrows. Trypsin, a common MS-compatible protease, has cleavage sites in this region marked by blue arrows (bottom). Asp-N cleaves before aspartate residues in the sequence, these sites are marked by magenta arrows (top). Differential cleavages are possible with these orthogonal proteases. **B,** a MALDI spectrum of m/z ratio from 1000 to 3500 shows that major peaks are similar in the eNOSox alone

(black trace) or eNOSox and HbαX crosslinked reaction (red trace). Because eNOSox is much bigger than HbαX (48 kDa vs. 2 kDa), the majority of peaks from both reactions will be from eNOSox, yielding similar overall spectra. In **C,** zoomed regions of the full spectrum show differences in tryptic digest of the eNOSox and eNOSox + HbαX reactions. Similar results are seen for the Asp-N cleavage reaction in **D,** where some Asp-N cleavage sites are not visible in + HbαX condition. In C and D, black arrows indicate m/z peaks not seen when HbαX is present, and red arrows denote peaks that only appear in the + HbαX crosslinked reaction.

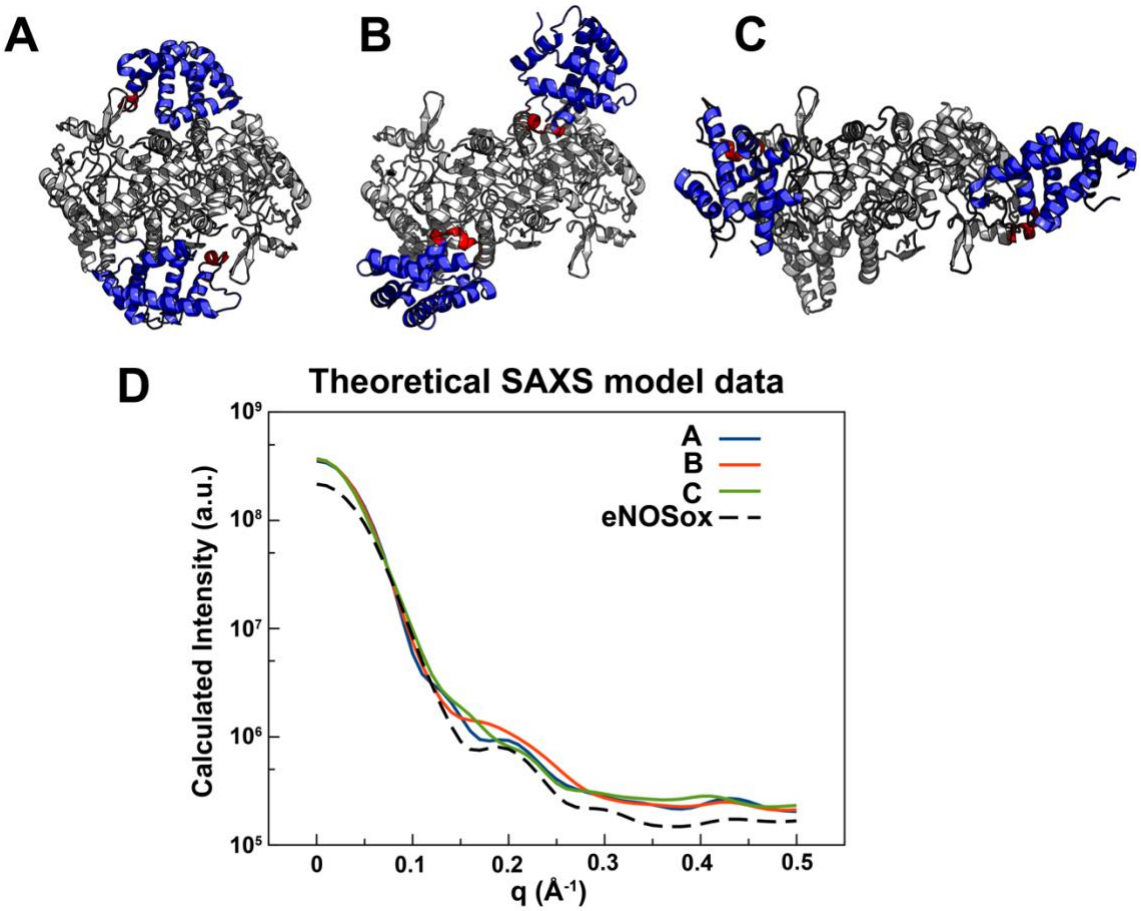

Figure 5: An (theoretical) orthogonal approach to determining the conformation of the alpha globin/eNOSox complex. Three models (chosen from models in Figure 1) were amended for a stoichiometric ratio of alpha globin and eNOSox (shown in **A-C,** eNOS in gray, alpha globin in blue, HbαX sequence in red). These examples were chosen for different radii of gyration, as extremes and intermediates of the models seen in the GRAMM-X docking models. Using a theoretical solvation and scattering server, SAXS curves were generated for the three models, and plotted together in **D** (state 1 in blue, state 2 in red, state 3 in green). Additionally, a curve for eNOSox, without alpha globin, was generated and plotted (black dashed line). The biggest difference in the curves

appears at intermediate q values (between 0.15 and 0.3). This could be an effective way to gain low-resolution structural information about the protein complex to combine with crosslinking MS experiments.

Appendix

Contributions:

TCS Keller, BE Isakson, and L Columbus developed the manuscript and experiments for this work. NK Swope contributed expertise to NMR experiments, and TA Caldwell, J Hinkle, J Shabanowitz, and D Hunt contributed to the mass spectrometry results.

Chapter 7: A unique amino acid motif on alpha globin demonstrates its critical role in vascular hemodynamics

With contributions from: Gilson Brás Broseghini-Filho, Joshua T. Butcher, Henry R. Askew Page, Christophe Lechauve, Rachel B. Weaver, Leon J. DeLalio, Poonam Sharma, Kwangseok Hong, Wenhao Xu, Mitchell J Weiss, Miriam M. Cortese-Krott, Alessandra Simão Padilha, Linda Columbus, Hans Ackerman, Swapnil Sonkusare, and Brant E. Isakson.

Abstract

Alpha globin is known to regulates nitric oxide (NO) bioavailability by forming a complex endothelial nitric oxide synthase (eNOS). Using *in silico* prediction methods, we identified an amino acid motif in alpha globin (^{36}SFPT^{39}) that is critical for eNOS binding. This prediction was confirmed using *in vitro* fluorescence polarization with recombinant protein. To assess the importance of this motif *in vivo*, we used CRISPR/Cas9 genome editing to delete amino acids 36-39 from the mouse *Hba1* gene. Whole genome sequencing confirmed targeting of the mutation to *Hba1* and demonstrated a lack of off-target mutations in *Hba2*. We found that homozygous *Hba1*$^{\Delta 36\text{-}39/\Delta 36\text{-}39}$ mice were not viable (0 mice born from 3 different heterozygous pairs; 8 litters). Interestingly, *Hba1*$^{WT/\Delta 36\text{-}39}$ animals showed no measureable differences in alpha globin protein expression in red blood cells or resistance arteries. Third-order mesenteric arteries from these mice had unaltered cholinergic– and hyperpolarization–induced vasodilation. However, there was a significant increase in NO release following stimulation with muscarinic agonists, which

was balanced by significant decreases in vascular smooth muscle mediators sGC and cGMP. Moreover, *Hba1*$^{WT/\Delta 36\text{-}39}$ mice had unchanged blood pressure but significantly increased heart rates, suggesting changes in peripheral resistance compensated by cardiac factors. These results demonstrate an important interaction between alpha globin/eNOS, mediated through the ^{36}SFPT^{39} motif, in regulating non-red blood cell based hemodynamics.

Introduction

Nitric oxide (NO) is a biologically active molecule that potently stimulates relaxation of smooth muscle cells in the vascular wall. The effects of these hemodynamic changes directly influence vascular resistance and blood pressure (*173, 297, 298*). Bioactive NO is synthesized in the endothelium by endothelial nitric oxide synthase (NOS3, eNOS), and diffuses across the plasma membranes to activate smooth muscle cell soluble guanylyl cyclase receptors (sGC) (through a sGC heme cofactor). This, in turn, elevates cyclic guanosine monophosphate (cGMP) levels which are secondary messengers for vasodilation cascades (*299, 300*).

The localization of eNOS within endothelial cells supports its function. In endothelium, eNOS can be localized within myoendothelial junctions (MEJs), which are endothelial projections through the internal elastic lamina that contact surrounding smooth muscle cells (*301*). MEJs serve as a nexus for localized heterocellular communication within the vascular wall.

Also at that site are several modulators of eNOS activity (*139, 154, 193*), including caveolin-1, calmodulin (*302*), and alpha globin. This alpha globin subunit directly binds to eNOS and modulates NO availability (*303, 304*). Previously, we have shown that a peptide mimicking a 10-residue motif of alpha globin disrupts the interaction of alpha globin and eNOS, increases NO signaling, dilates small arteries and lowers blood pressure (*184, 303*).

Although we have previously targeted the alpha globin/eNOS binding motif pharmacologically (*35, 184*), we now show that genetic disruption of the same alpha globin/eNOS binding motif, *in vivo,* recapitulates increased NO signaling and causes changes in vascular phenotypes involved in blood pressure homeostasis. To this end, we used CRISPR/Cas9 gene editing to delete amino acids 36-39 of *Hba1* in the C57Bl/6 mouse. The specific deletion of nucleotides 32,283,934 – 45 (AGC TTC CCC ACC) in

exon 2 of *Hba1* (corresponding to the beginning of the predicted eNOS binding sequence in alpha globin) provides a novel murine model for exploring the physiological role of alpha globin in regulating vascular hemodynamics *in vivo*.

Methods

Fluorescence polarization

Fluorescently labeled peptides were synthesized by Anaspec. The fluorescence polarization was performed as described previously by us.(*184*) Briefly, the oxygenase domain of eNOS was incubated with a peptide composed of the alpha globin binding sequence (LSFPTTKTYF) or the same peptide lacking Hba1 amino acids 36-39 (sequence: LTKTYF) to assess binding affinity.

Animals

All mice were male, 10-16 weeks of age at time of experimentation. Mice were cared for under the provisions of the University of Virginia Animal Care and Use Committee and followed the National Institute of Health guidelines for the care and use of laboratory animals.

Generation of CRISPR/Cas9 constructs

HBA-a1 (NC_000077.6) targeting site for guide RNAs were identified using the online Zifit targeter software version 4.2 (http://zifit.partners.org).(*305, 306*) The sgRNA target site 5'- GGAAAGTAGGTCTTGGTGGT -3' and its recommended 22 nucleotide long oligos(oligo 1: 5'- TAGGAAAGTAGGTCTTGGTGGT -3'; oligo 2: 5'- AAACACCACCAAGACCTACTTT -3') were chosen from Zifit output. Oligo1 and oligo 2 were annealed and cloned at BsaI site in DR274 vector (http://www.addgene.org/crispr/jounglab/crisprzebrafish/) followed by transformation in chemically competent XL-1 Blue cells. Antibiotic resistant positive clones were checked by sequencing with M13 primers. Positive PDR274 clones were digested with Dra1 restriction enzyme (New England Bioscience) and used as a template for in vitro transcription using MEGAshortscript T7 Transcription Kit (Life Technologies). sgRNAs were DNAse treated and purified using the MEGAclear Kit (Ambion P/N AM1908). Purity and concentration were measured using a NanoDrop spectrophotometer

Production of Cas9 nuclease mRNA utilized the pMLM313 expression vector (Addgene plasmid #42251), which harbors the T7 promoter site upstream of the translational start site, and a nuclear localization signal at the carboxy-terminal. The pMLM313 plasmid was linearized using Pme1 restriction enzyme (New England Bioscience), separated by agarose gel, and gel extracted (Clontech Nucleospin Extract II Kit Cat# 636972). The linearized and purified pMLM313 fragment was used as template for In vitro transcription of Cas9 mRNA with mMESSAGE mMACHINE T7 ULTRA kit (Life Technologies)(*307, 308*). Following transcription, Cas9 mRNA underwent poly-A tailing reactions and DNase I treatment according to manufacturer's instructions. The concentration was determined using NanoDrop.

Microinjection

Pronuclei of one-cell stage embryos were collected from superovulated donor females (B6/SJL strain) and microinjected with CRISPR/Cas9 constructs using micromanipulators and injection needles (World Precision Instruments, filament #1B100-6). Injected embryos were implanted into pseudopregnant recipient females according to NIH guidelines. 2-week-old pups born to recipient females were screened by PCR using Hba1 gene specific primers and sequenced for the presence of CRISPR/Cas9 induced mutation. The Hba1-gen-FP primers were: forward, 5’- ATATGGACCTGGCACTCGCT -3’ and reverse, 5’-GTCCCAGCGCATACCTTGAA -3’.

Whole Genome Sequencing

Whole Genome sequencing was performed by GeneWiz (South Plainfield, NJ) using contiguous amplicon sequencing on Illumina MiSeq instrument in a 2x300bp paired-end configuration. DNA library preparation without fragmentation, multiplexing, sequencing, unique sequence identification, and relative abundance calculations were performed in house at GeneWiz.

Blood cell measurements

Isolated mouse blood was analyzed by the St. Jude's Children's Hospital Blood Pathology Labs as previously described by us (*184*).

MALDI-MS identification of mutant hemoglobin

Alpha globin was immunoprecipitated from mouse red blood cell pellets after mechanical lysis. Briefly, whole blood was centrifuged and washed three times at 500 x g for five minutes at 4ºC. The erythrocyte pellet was resuspended in hypotonic solution and vortexed to lyse red cells. After a five-minute centrifugation at 10,000 x g, the supernatant was transferred to a fresh tube, and anti-alpha globin antibody was added at 1:250 v/v. The antibody was incubated with lysate for approximately 16 hours at 4ºC with gentle nutation. The antibody-alpha globin complex was then isolated using magnetic beads. Alpha globin was eluted from the antibody with a low pH solution (250 mM glycine, pH = 2.0), and diluted with acetonitrile for matrix-assisted laser desorption ionization mass spectrometry on a Bruker MicroFlex MALDI-TOF instrument, using 3,5-dimethoxy-4-hydroxycinnamic acid (sinnapinic acid) as a matrix.

Detection of globin precipitates from RBCs

Analysis of globin precipitates from erythrocyte was performed as described.(*309-313*) Briefly, washed RBCs were lysed and pellets washed extensively in ice-cold 0.05X PBS. Membrane lipids were extracted with 56 mM sodium borate, pH 8.0 with 0.1% Tween-20 at 4ºC. Precipitated globins were dissolved in 8M urea, 10% acetic acid, 10% b-mercaptoethanol, and 0.04% pyronin, fractionated by triton-acetic acid-urea (TAU) gel electrophoresis and stained with Coomassie blue.

Immunofluorescence

Thoracodorsal arteries were excised, cleared of blood, and fixed overnight in 4% paraformaldehyde. After washing with ethanol, vessels were embedded in agarose and then paraffin blocks, and sectioned at 5 µm. Paraffin was removed by Histoclear, and sections were rehydrated through a 100%/95%/70% ethanol/water gradient before

antigen retrieval in a citrate solution. PBS blocking solution (including 0.25% Triton X-100, 0.5% bovine serum albumin, and 5% donkey serum) was used to block sections and as primary and secondary diluent. Primary antibodies were rabbit anti-hemoglobin alpha (abcam, #102758, 1:250 dilution) and mouse anti-eNOS (BD Bioscience, #610296, 1:500 dilution). Secondary antibodies used were donkey anti-rabbit (Alexa 647, Life Technologies A-31571) and donkey anti-mouse (Alexa 594, Life Technologies A-21207). Stained sections were mounted with DAPI and imaged using an Olympus FV1000 confocal microscope with Olympus Fluoview software using DAPI, and Alexa 488 (to visualize autofluorescence of the elastic lamina), 594, and 647 channels for fluorescence detection.

Proximity Ligation Assay

Proximity ligation assays (PLA) were performed as described by us (*103*). Sections (as in “Immunofluorescence”) were stained with the same primary antibodies at the same concentrations. DUOLINK® PLA probes, ligase, and polymerase were all used according to manufacturer’s instructions. Sections were mounted with DAPI, and imaged with DAPI, Alexa 488, and Texas Red (for the PLA fluorophore) channels. Images of two sections per animal (with genotype blinded) were quantified by tracing the outline of the IEL in ImageJ and dividing number of punctae by total perimeter of elastic lamina.

Blood pressure

Radiotelemetry was used to monitor blood pressure and heart rate responses in conscious animals, as previously described by us (*184*).

Vasoreactivity

Cumulative dose-response curves on pressurized and cannulated third-order mesenteric arterioles (90-140 μm in diameter) were used throughout the studies as previously described by us (*184*).

Immunoblots

Third order mesenteric arteries were isolated and snap frozen before immunoblotting. Samples were homogenized in ice cold lysis buffer containing 50 mM Tris-HCl, 150 mM NaCl, 5 mM EDTA, 1% deoxycholate, 1% NP-40 in phosphate buffered saline and pH adjusted to 7.4. Samples were sonicated and subjected to protein electrophoresis using 4-12% Bis-Tris gels (Invitrogen) and transferred to nitrocellulose. Blots were incubated with primary antibodies overnight at 4ºC followed by washing. Protein was detected using Licor secondary antibodies, visualized and quantitated using Licor Odyssey as previously described

cGMP assay

Isolated arteries were treated before stimulation with the phosphodiesterase inhibitor 3-isobutyl-1-methylxanthine (IBMX; 0.5 mM) and 100 μM L-Nitro-Arginine Methyl Ester (L-NAME). Following PE stimulation (50 μM), samples were isolated and lysed in buffer provided in the cGMP XP® Assay kit (Cell Signaling) and the procedure was performed according to manufacturer instructions. A standard curve of known cGMP concentrations was used to determine the cGMP concentrations in the experimental samples. Results were then normalized to protein concentration.

Nitric Oxide imaging

Arterioles were surgically opened and pinned down on a Sylgard block in en face preparation. NO levels were assessed using DAF-FM DA (4-amino-5 methylamino-2',7'-difluorofluorescenin diacetate, 5 μM) prepared in HEPES PSS with 0.02% pluronic acid.(*314*) DAF-FM DA binds to NO and forms a fluorescent triazole compound. *En face* MAs were pre-treated with carbachol (CCh, muscarinic receptor agonist, 10 μM) in Hepes-PSS for 5 minutes at 30˚C. Arteries were then incubated with DAF-FM containing CCh for 20 minutes at 30˚C in the dark. DAF-FM fluorescence was imaged using Andor Revolution WD (with Borealis) spinning-disk confocal imaging system (Andor Technology, Belfast,

UK) comprised of an upright Nikon microscope with a water dipping objective (60X, numerical aperture (NA) 1.0) and an electron multiplying CCD camera. Images were obtained along the z-axis at a slice size of 0.05 microns from the top of the endothelial cells to the bottom of the smooth muscle cells using an excitation wavelength of 488 nm and emitted fluorescence was captured with a 525/36-nm band-pass filter. DAF-FM fluorescence was analyzed using custom-designed SparkAn software by Dr. Adrian D. Bonev (University of Vermont, Burlington, VT USA). An outline was drawn around each endothelial or smooth muscle cell to obtain the arbitrary fluorescence intensity of that cell. The background fluorescence was then subtracted from the recorded fluorescence. The fluorescence from all the cells in a field of view was averaged to obtain single fluorescence number for that field. Relative changes in DAF-FM fluorescence were obtained by dividing the fluorescence in the treatment group by that in the control group. Each field of view was considered as n=1, and several fields of view from at least three arteries from at least three mice from each group were included in the final analysis.

Statistics

Data were analyzed using Prism 7 software (GraphPad Software Inc.) and displayed in mean ± SEM. Two-tailed, unpaired Student's *t* tests or 1-way ANOVA followed by Kruskal-Wallkis multiple comparisons post hoc tests were used where appropriate. Two-way ANOVA followed by Sidak's multiple comparisons post hoc tests were used for pressure myography experiments. $p < 0.05$ was considered to be statistically significant, and is denoted by a single asterisk.

Results

A comparison between the alpha globin/AHSP binding complex and the alpha globin/eNOS interaction motif (called HbαX) reveals unique binding regions between alpha globin and each binding partner (**Figure 1A**) (PDBid: 1Z8U (*315*), 3NOS (*287*)). Using fluorescence polarization, we first tested if deletion of amino acids within the HbαX binding region was sufficient to disrupt interactions with eNOS (**Figure 1B**). The targeted residues (SFPT, residue numbers 36-39 in the alpha globin sequence) were selected due to the presence of reactive hydroxyl groups which have been proposed as a major determinant of the alpha globin/eNOS interaction (*35*). As shown in **Figure 1B**, an alpha globin mimetic peptide lacking amino acids ^{36}SFPT^{39} results in a dramatic decrease in interaction with eNOS (Kd = 16.8 nM for full peptide FASFPTTKTYF, compared with data that cannot be fit because of lack of a saturatable binding curve from the FATKTYF peptide). Next, to determine the functional consequences of this deletion *in vivo*, we used CRISPR/Cas9 to generate a mouse model lacking amino acids 36-39 through the deletion of nucleotides 32,283,934-32,283,945 (AGC TTC CCC ACC) in exon 2 of *Hba1* (**Figure 1C**). Amplicon sequencing using *Hba1* gene specific primers confirmed the presence of the 12-nucleotide deletion. These results are depicted by the presence of double peaks in the electropherogram signal produced during sequencing of heterozygous mice (**Figure 1D**). To determine if the mice expressed the mutant Hba1 protein, we used mass spectrometry to detect the mutant. Because the change in molecular weight (about 400 Da) is too small to visualize on a western blot, that is not a feasible method of detecting the Δ36-39 mutant protein. Due to the global mutation, the blood will contain the alpha globin with deletion, thus we used erythrocyte lysate to pull down alpha globin and determine the molecular weight with mass spectrometry. Blood from mutant mice contained a protein species that was 400 Da less than the major peak observed in WT

mice (**Figure 1E**). Thus, we reasoned that the *Hba1*$^{\Delta 36\text{-}39}$ protein is being expressed and translated in our mutant animals.

Whole genome sequencing was performed to validate the specificity of the CRISPR/Cas9 deletion for *Hba1*. We report here that *Hba1*, and not *Hba2*, was targeted for deletion (**Figure 2**; **Table 1**). The mice that were created from the 12-nucleotide deletion are heterozygous *Hba1*$^{WT/\Delta 36\text{-}39}$.

Out of 8 litters from 3 different *Hba1*$^{WT/\Delta 36\text{-}39}$ breeding pairs, there were no homozygous *Hba1*$^{\Delta 36\text{-}39/\Delta 36\text{-}39}$ born (**Table 2**). For this reason, we investigated E12 pups from pregnant females. We found *Hba1* $^{\Delta 36\text{-}39/\Delta 36\text{-}39}$ mice were deceased in utero, with decreases in length, dilated major vessels, and thinned myocardium (**Figure 3A** and **3B**). Additionally, the *Hba1* $^{\Delta 36\text{-}39/\Delta 36\text{-}39}$ mice had increased markers of oxidative and nitrosative stress. Increased staining with 3-nitrotyrosine indicates pathological increases in NO and superoxide, forming peroxynitrite that can damage tissue proteins non-specifically (**Figure 3C**). The increased in 3-nitrotyrosine in the *Hba1* $^{\Delta 36\text{-}39/\Delta 36\text{-}39}$ mice could be from dysregulation of NO scavenging by vascular alpha globin in development (**Figure 3D**). These observations suggest that amino acids 36-39 of alpha globin are essential for normal development and loss of this sequence is incompatible with life. The rest of the manuscript will focus on phenotypic differences between *Hba1*$^{WT/WT}$ and *Hba1* $^{WT/\Delta 36\text{-}39}$ mice, as both survived to adulthood.

To examine the functional consequences of loss of amino acids 36-39 in adult mice, we carried out a hematological and vascular characterization of the viable *Hba1*$^{WT/\Delta 36\text{-}39}$ heterozygote mice. We did not observe any hematological phenotype of the *Hba1*$^{WT/\Delta 36\text{-}39}$ deletion. Specifically, blood count parameters from the *Hba1*$^{WT/\Delta 36\text{-}39}$ mice show no difference from *Hba1*$^{WT/WT}$ mice (**Figure 4**) in total counts of white blood cells (WBC), reticulocytes (as a percentage), or number of red blood cells was not different between *Hba1*$^{WT/WT}$ and *Hba1*$^{WT/\Delta 36\text{-}39}$ mice (**Figure 4A-C**). In the red blood cells, we observed no

difference in total hemoglobin concentration, mean corpuscular hemoglobin, or mean corpuscular volume (MCV) between genotypes (**Figure 4D-F**). Additionally, soluble and insoluble fractions of hemoglobin from isolated red blood cells were not different between *Hba1*$^{WT/\Delta 36\text{-}39}$ and *Hba1*$^{WT/WT}$ mice, showing that there was normal hemoglobin tetramerization in the erythrocytes of all tested genotypes. This is distinct from reductions in the insoluble hemoglobin fractions from a mouse model of β thalassemia, which was used as a control and presents free alpha globin (unstable without a beta globin interaction partner) from isolated red blood cells (**Figure 4G**). In a blood smear stained with cresyl blue, red blood cells maintained normal morphology, and there was no increase in hemoglobin precipitation or reticulocytes in whole blood (**Figure 4H and 4I**).

Since there was no evident effect of the 4-amino acid deletion within alpha globin on hematopoiesis or circulating mature RBCs, we next tested for differences in endothelial alpha globin function. In thoracodorsal arteries, alpha globin and eNOS have been shown to uniquely co-localize in the endothelium (*103*). No observable differences in expression of either protein could be detected between *Hba1*$^{WT/\Delta 36\text{-}39}$ or *Hba1*$^{WT/WT}$ mice (**Figure 5A, 5B, 5D,** and **5E**). However, using a proximity ligation assay that only generates fluorescent signal when target proteins are close in apposition (< 40 nm) (**Figure 5C** and **5F**), we observed a significant decrease in endothelium fluorescence in *Hba1*$^{WT/\Delta 36\text{-}39}$ mice, but not control mice (**Figure 5J**). These results confirm our *in vitro* findings and suggest in *Hba1*$^{WT/\Delta 36\text{-}39}$ mice there is reduced alpha globin/eNOS interaction.

Due to significant reductions in alpha globin/eNOS complex formation within the endothelium, we tested whether the deletion of the 4 amino acids in the eNOS binding motif of alpha globin would lead to increased vasodilation due to enhanced NO availability. Third-order mesenteric arteries (MAs) from *Hba1*$^{WT/\Delta 36\text{-}39}$ and *Hba1*$^{WT/WT}$ mice were loaded with DAF-FM reagent to visualize NO detection (**Figure 6A**). In both *Hba1*$^{WT/\Delta 36\text{-}39}$ and *Hba1*$^{WT/WT}$ mice, basal NO generation in these MAs was similarly low. In control animals,

stimulation of muscarinic receptors with the agonist carbachol (CCh, 10 μM) did not induce NO generation, as expected (*316-319*). In dramatic contrast, MAs from *Hba1*$^{WT/\Delta 36\text{-}39}$ mice had a significant increase in detectable NO-dependent fluorescence (**Figure 6B**). Based on our previous published work and data herein, we anticipated that preventing alpha globin/eNOS complex formation would allow for enhanced NO production(*184*). That only agonist-induced NO availability was increased demonstrates a role for alpha globin/eNOS complex formation as a final regulator of dilatory signaling in these resistance arteries.

To determine if enhanced endothelial NO production subsequently influenced vascular wall dynamics, we performed pressure myography on intact MAs. To our surprise, vasodilation responses to increasing doses of CCh were identical for *Hba1*$^{WT/\Delta 36\text{-}39}$ and *Hba1*$^{WT/WT}$; even when increased NO availability, after production from eNOS, was inhibited using L-NAME (**Figure 7A** and **7B**). There was also no measureable differences in endothelial cell and smooth muscle cell coupling, which was assessed by vasodilation to the IK/SK-channel agonist NS309 (**Figure 7C**). In contrast, we observed decreased dilatory ability in the *Hba1*$^{WT/\Delta 36\text{-}39}$ mice when vessels were treated with the endothelium-independent vasodilator sodium nitroprusside (SNP, **Figure 7D**). Thus, although the endothelium from *Hba1*$^{WT/\Delta 36\text{-}39}$ mice have enhanced agonist-induced NO availability, the *Hba1*$^{WT/\Delta 36\text{-}39}$ smooth muscle cells did not respond to endogenous or exogenous increased NO levels, perhaps due to compensatory decreased dilatory signaling effects.

To determine the possible mechanism for decreased vasodilatory capacity in the *Hba1*$^{WT/\Delta 36\text{-}39}$ mice, we assayed vasodilation mediator proteins from isolated third order mesenteric arteries using immunoblot. In line with significantly decreased functional responses to SNP, the *Hba1*$^{WT/\Delta 36\text{-}39}$ mice also had significantly reduced sGC (β) expression as compared to controls (**Figure 8A**). No other protein examined – including eNOS, alpha globin (Hbα), myosin light chain phosphatase or kinase (MLCP or MLCK) – were altered (**Figure 8A**). Thus, we examined the tissue levels of cGMP in *Hba1*$^{WT/\Delta 36\text{-}39}$

and found them to be significantly reduced (**Figure 8B**)**,** consistent with decreased expression of sGC (β) protein. The sum of these results suggests that resistance arteries of *Hba1*$^{WT/\Delta 36\text{-}39}$ mice have enhanced NO production and NO bioavailability, but maintain homeostasis by down regulating sGC, the primary target of NO in smooth muscle.

Alterations in vascular reactivity typically result in alterations in blood pressure homeostasis. Using radiotelemetry we measured 24-hour blood pressure in conscious *Hba1*$^{WT/\Delta 36\text{-}39}$ mice. We found a trend towards lower mean arterial pressure in *Hba1*$^{WT/\Delta 36\text{-}39}$ mice (albeit not significant; **Figure 9A**). However, we also measured a significantly increased heart rate from *Hba1*$^{WT/\Delta 36\text{-}39}$ mice, a clear compensatory indicator of decreased total peripheral resistance (**Figure 9B**). In sum, the *Hba1*$^{WT/\Delta 36\text{-}39}$ mice had increased release of NO, decreased SNP responses, lower sGC levels and cGMP production, but increased heart rates. In balance, unchanged vasodilation responses and slightly reduced blood pressure (although not significant), suggests a compensatory mechanism for dealing with excessive NO release due to decreased alpha globin/eNOS interaction in the endothelium.

Discussion

The interaction between alpha globin and eNOS is characterized as late-stage regulation of NO bioavailability in the vascular wall. This means that NO production is tightly regulated even after it is synthesized, which is distinct to other regulatory factors such as activating/inhibitory post-translational modifications of eNOS. In this capacity, alpha globin provides a final checkpoint, a fine-tuning mechanism, for NO availability by scavenging generated NO in spatially relevant cell compartments, such as the MEJ (*35, 103*). Disrupting the alpha globin/eNOS complex removes this final check on NO availability, thus increasing the amount NO bioavailable and activation of vasodilatory pathways in underlying smooth muscle (*303*).

There are two gene loci that code for alpha globin in human and murine genomes. We utilized CRISPR/Cas9-engineered genome editing to target residues ^{36}SFPT^{39} in the *Hba1* gene (*Hba1*$^{\Delta 36\text{-}39}$) to specifically delete critical residues predicted to support alpha globin/eNOS complex formation (**Figure 1** and **Figure 5**), while leaving the rest of the protein functionally intact. As a result of our gene mutation we observed a loss of amino acids 36-39 in only the *Hba-a1* gene that is incompatible with life in homozygous offspring. Homozygote *Hba1*$^{\Delta 36\text{-}39/\Delta 36\text{-}39}$ mice died *in utero* (0 *Hba1*$^{\Delta 36\text{-}39/\Delta 36\text{-}39}$ pups born from 8 litters from 3 breeding pairs, **Table 2**) with morphologic evidence of dilated cardiomyopathy and vasculopathy. The eccentric dilation of the developing myocardium is often associated with low-resistance states and anemia (*320-322*). Signals such as decreased crown to rump length, dilated major vessels, and non-compaction of the myocardium in the *Hba1*$^{\Delta 36\text{-}39/\Delta 36\text{-}39}$ mouse are similar to observations in the most severe manifestation of human alpha thalassemias: hemoglobin Barts and hydrops fetalis syndromes, caused by homozygosity of the --SEA Deletion in Southeast Asia (*323-326*). There are also observations that eNOS and NO can affect the chronotropic and contractile nature of cardiac myocytes (*327-329*), but the effects of alpha globin/eNOS coupling on developing cardiac tissues have not yet

been explored. Others have noted that NO levels require fine balance in developing embryos, as both a lack – or overabundance – of NO are detrimental to the development of fetal mice (*330-332*). In this case, the increased availability of NO caused retardation of total and tissue-specific development before E12 (**Figure 3**). Previous studies have also focused on NO inhibiting implantation of embryos, although that does not seem to be the case in this *Hba1*$^{\Delta 36\text{-}39/\Delta 36\text{-}39}$ strain, as pups were seen as late as E12 (*330*). As well as a possible anemia phenotype, the effects of homozygous *Hba1* $^{\Delta 36\text{-}39/\Delta 36\text{-}39}$ could be due to dysregulation of fetal blood flow. As NO is a potent controller of placental vasodilation, increased availability might prevent proper control of arterial perfusion and prevent efficient nutrient exchange (*333, 334*). Dysregulation of blood flow within the developing fetus would have a similar effect, where perfusion to the embryo is not maintained for supporting developing organs and tissues. This necessary control of NO balance is likely lost without the final check on its production by eNOS in the developing tissues, leading to embryonic lethality in our *Hba1*$^{\Delta 36\text{-}39/\Delta 36\text{-}39}$ mice.

Mice heterozygous for the deletion (*Hba1*$^{WT/\Delta 36\text{-}39}$) were viable, however. These mice had normal blood parameters for hemoglobin concentration and red blood cell size, and number of reticulocytes was not increased suggesting that the erythrocytes in the heterozygous *Hba1*$^{WT/\Delta 36\text{-}39}$ animals have normal half-life and turnover (**Figure 4**). The hemoglobin tetramer in isolated red blood cells did not have evidence of free alpha globin, as would be expected with decreased alpha/beta globin binding (*323, 335*). Although we cannot rule out an effect of the mutation in red blood cell function based on these phenotypic observations, it seems that *Hba1*$^{WT/\Delta 36\text{-}39}$ display a phenotype consistent with effects of alpha globin mutations in the vascular endothelium more so than in the blood. This could be due to genetic redundancy of the alpha globin gene in murine, human, and other mammalian genomes. The presence of two identical protein sequences could also

be evidence for cell-type specificity in expression between the *Hba1* and *Hba2* genes that cannot be resolved by immuno-dependent techniques.

The effects of *Hba1* mutations on non-erythroid cells has not yet been characterized, thus we sought to investigate changes in vascular wall where NO is a potent regulator of hemodynamics. We observe a reduced ability of alpha globin/eNOS complex formation in *Hba1*$^{WT/\Delta 36\text{-}39}$ mice, specifically localized to endothelial cells of small arteries (**Figure 5**). Intact vessels dissected from heterozygote mice exhibited enhanced NO production after stimulation with the muscarinic agonist CCh; however, the *ex vivo* vasodilatory response to CCh were unchanged in *Hba1*$^{WT/\Delta 36\text{-}39}$ compared to controls (**Figures 6 and 7**). Additionally, a decreased vasodilation response to an endothelium-independent dilator SNP points towards insensitivity to vasodilation due to compensation from increased NO levels. We found this was due to a downregulation of smooth muscle cell sGC subunit β (**Figure 8**) in response to an increased NO release when the formation of the alpha globin/eNOS complex is disrupted. That increased NO availability decreases sGC expression has been noted previously (*336, 337*). This is in contrast to pathologies linked to decreased NO availability, which is described for pulmonary hypertensive pathologies (often associated with reduced NO levels in the lung vasculature) where stark increases in smooth muscle sGC have been observed (*338, 339*). In our study, the decreased protein level of sGC (β) in the vasculature explains the lack of a vasodilation responses to the endothelium-independent vasodilator SNP. In support of this vascular phenotype is the dilation observed in large vessels in the developing *Hba1*$^{\Delta 36\text{-}39/\Delta 36\text{-}39}$ fetus (**Figure 3**).

Interestingly, the *Hba1*$^{WT/\Delta 36\text{-}39}$ mice showed a slight (but not statistically significant) decrease in blood pressure compared to *Hba1*$^{WT/WT}$ mice (**Figure 9**). It was expected that increased NO availability would lead to decreased mean arterial blood pressure, as reductions in peripheral resistance directly influence blood pressure levels. However, due to the complex and vital nature of blood pressure homeostasis, this dynamic system can

be maintained in real-time by regional, humoral, and neuronal factors to preserve hemodynamics and promote tissue oxygenation. In α^{+}thalassemic human adolescents, a similar blood pressure phenotype was observed wherein humans with the most common alpha hemoglobin deletion variant did not have reduced blood pressure compared to non-thalassemic humans (*340*). In that study, hematological effects were evident, as expected in thalassemia, but systolic and diastolic blood pressures were unchanged. This study did not measure heart rate in combination with 24-hour blood pressure, thus, it is plausible that unmeasured vascular changes are masked by compensatory cardiac output increases (*340*). We observe compensation for a possible decrease in peripheral resistance via increased heart rate in our animal model (**Figure 9B**). In sum, our *Hba1*$^{WT/\Delta 36\text{-}39}$ mouse model could provide direction for study in compensatory mechanisms in future human studies.

The importance of alpha globin for sustaining life is highlighted not only by its genetic redundancy and complicated protein regulation, but also by the challenge of manipulating protein function to identify novel tissue level functions. In this study, we developed an innovative alpha globin mouse model using CRISPR/Cas9 genome editing whereby we can distinguish the effects of circulating and vascular wall alpha globin function. Due to the limitations of our model, we acknowledge that an endothelial cell– or erythroid–specific deletion would be ideal, but would depend on either a complicated, inducible CRISPR/Cas9 system, or gene replacement scheme due to redundancy in alpha globin genes. Instead, our approach of deleting four key amino acids predicted to bind eNOS has provided an interesting avenue to study the alpha globin/eNOS complex. Because we do not observe severe blood phenotypes, we believe that the effects on vasodilatory signaling and increased heart rate observed in our investigation are due to a predominant vascular role for alpha globin in controlling tissue level NO bioavailability. This model allows for a nuanced strategy to not only investigate the unknown dynamics regulating alpha

globin/eNOS interactions and its downstream functional effects on vascular hemodynamics and blood pressure, but also the essential developmental role for alpha globin in the developing fetus.

Figures and Tables

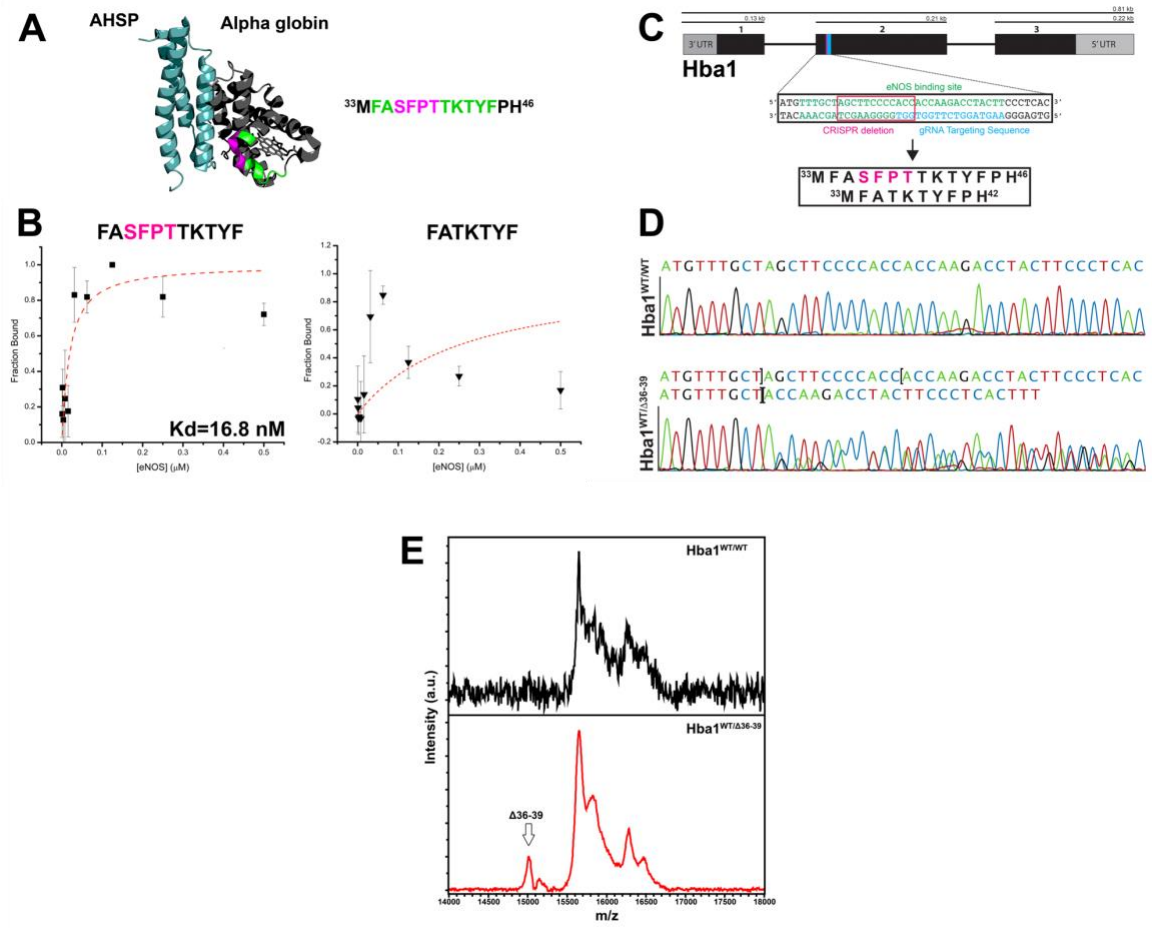

Figure 1: CRISPR/Cas9 targeted deletion of *Hba1* eNOS binding domain. A *In silico* analysis of known interactions between AHSP (teal) and alpha globin (grey) highlighting eNOS binding domain (green) and CRISPR/Cas9 deletion site (pink) (adapted from PDBid: 1Z8U). Current model of interaction suggests a trading of alpha globin between AHSP and eNOS in endothelium due to the poor solubility of alpha globin as a monomer (*292*). **B** Fluorescence polarization assay demonstrates strong binding between previously identified *Hba1* sequence and eNOS (i.e., the HbαX peptide) (*35*), but no discernable binding between the CRISPR/Cas9-mutated *Hba1* amino acid sequence and

eNOS. **C** *Hba1* (Hba-a1) gene map showing the sgRNA targeting sequence of eNOS binding domain and resultant deletion of amino acids 36-39 (12 nucleotide deletion). **D** Representative electropherogram of *Hba1*$^{WT/WT}$ and *Hba1*$^{WT/\Delta 36\text{-}39}$ sequencing. The 12-nucleotide deletion (denoted by brackets) results in detection of double sequencing peaks in heterozygous mice. **E**, Matrix-assisted laser desorption ionization (MALDI) mass spectrometry of alpha globin immunoprecipitated from whole blood (Hba1$^{WT/WT}$, black, and Hba1$^{WT/\Delta 36\text{-}39}$, red) shows a m/z species that is decreased by about 400 Da in the Hba1$^{WT/\Delta 36\text{-}39}$ mouse (the approximate weight of the SFPT deletion) (red trace, white arrow). This product was immunoprecipitated from whole blood because of the abundance of hemoglobin; since the deletion is not cell-type specific, the mutant protein would be expressed wherever Hba1 is expressed. This peak shows production of the Δ36-39 mutant alpha globin in these mice, but should not be used for quantifying relative production of the mutant protein.

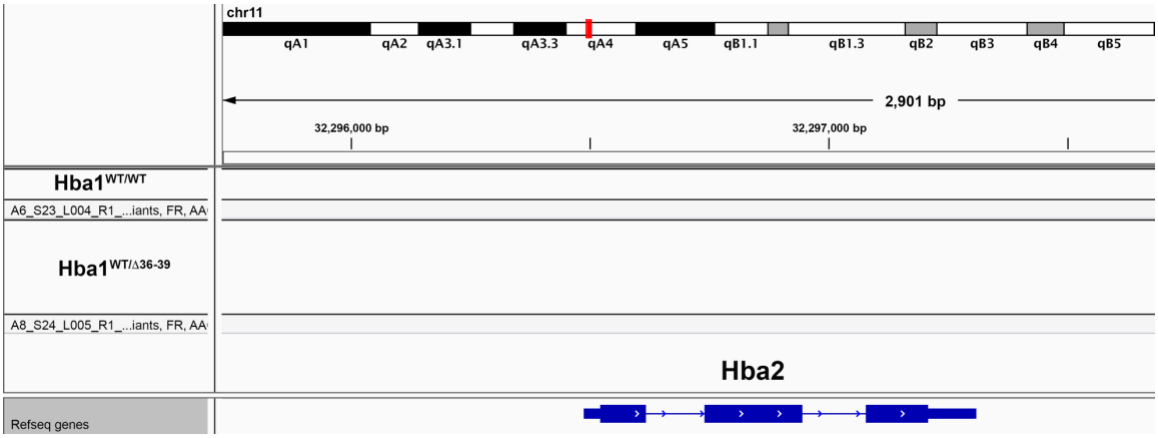

Figure 2: Whole genome sequencing of the Hba1WT/Δ36-39 mouse reveals deletion does not correspond to Hba2 gene. Nucleotide mapping of *Hba2* reveals no differences between *Hba1*$^{WT/WT}$ and *Hba1*$^{WT/\Delta 36\text{-}39}$.

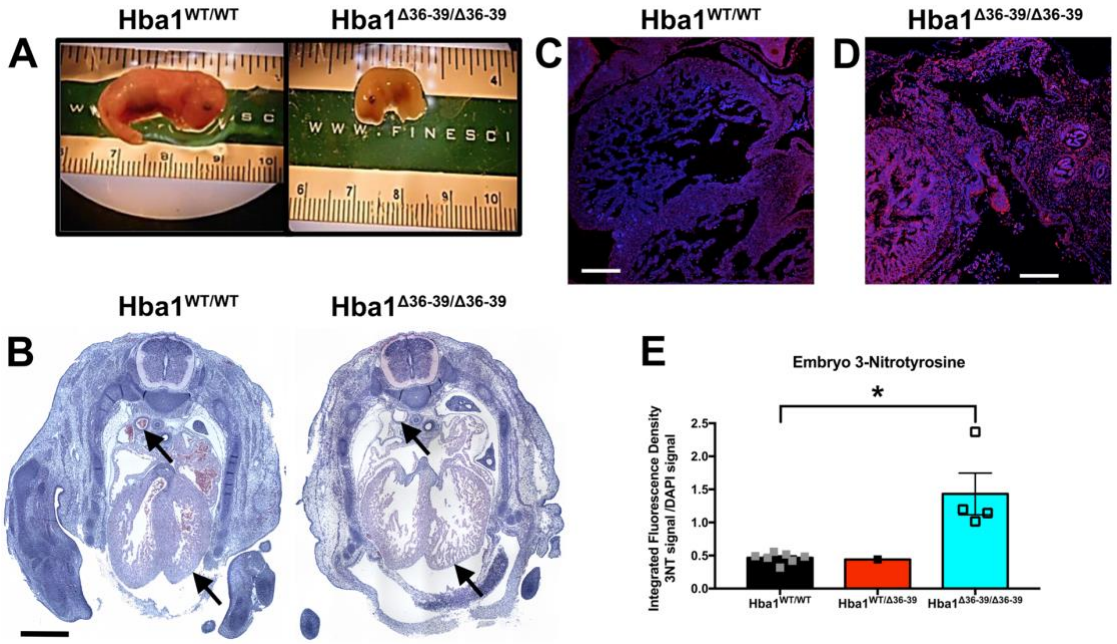

Figure 3: Hba1$^{\Delta 36\text{-}39/\Delta 36\text{-}39}$ deletion is embryonic lethal. A E12 pups immediately after removal from pregnant female. Measurement on bottom ruler is in cm. **B** Transverse sections of E12 *Hba1*$^{WT/WT}$ and *Hba1*$^{\Delta 36\text{-}39/\Delta 36\text{-}39}$ pups were sectioned at 7 μm and stained with hematoxylin and eosin. Arrows indicate dilated aorta and vena cava (top in each image) and myocardium of ventricles (bottom in each image). Non-compaction of cardiac muscle is seen in the homozygous mutant, but not in the WT control mouse. Scale bar is 1 cm. **C, D** Images of nitrotyrosine staining (red) with cell nuclei shown in blue. Images were from transverse sections of E12 embryos. Scale bar is 200 μm. **E** Quantification of nitrotyrosine signal in images from each genotype. Each point represents one animal, with greater than three images taken per animal. * denotes $p < 0.05$ between *Hba1*$^{WT/WT}$ and *Hba1*$^{\Delta 36\text{-}39/\Delta 36\text{-}39}$ pups.

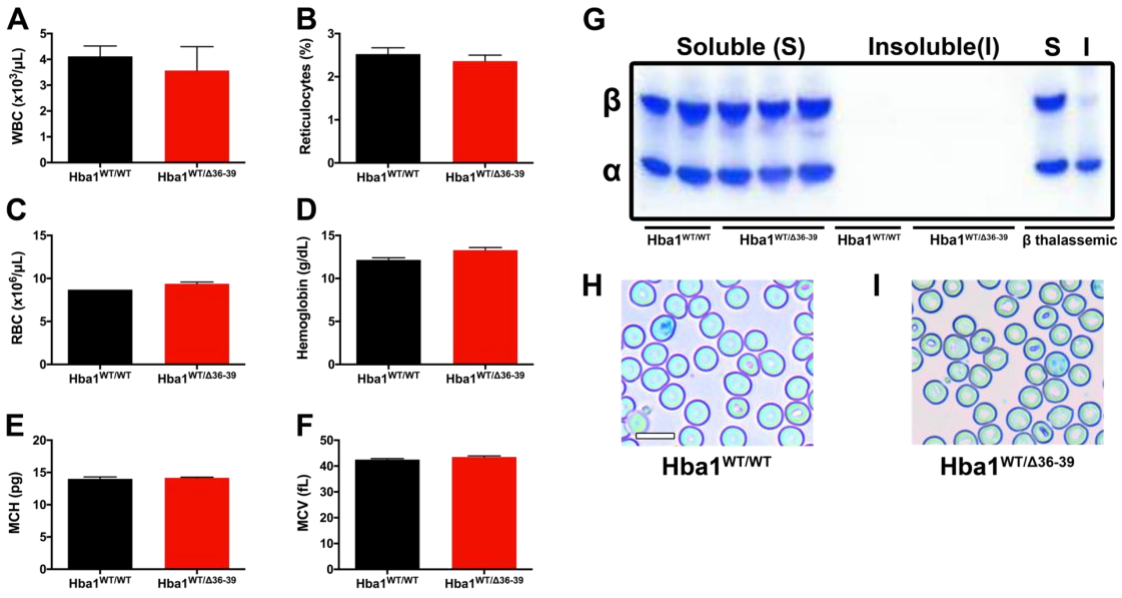

Figure 4: Hematological characterization of *Hba1*$^{WT/\Delta 36\text{-}39}$ mice show no changes in blood phenotype. Whole blood from cardiac puncture was analyzed for **A** total white blood cells (WBC), **B** reticulocytes (as a percentage of total cells) and **C** total red blood cells (RBC) (N=2). From isolated red blood cells, **D** hemoglobin, **E** mean corpuscular hemoglobin (MCH), and **F** mean corpuscular volume (MCV) were measured. No differences were observed between *Hba1*$^{WT/WT}$ and *Hba1*$^{WT/\Delta 36\text{-}39}$ genotypes. **G** From isolated red blood cells, the soluble and insoluble fractions of hemoglobin were analyzed with TAU gel electrophoresis. Alpha and beta globin were observed in the soluble fraction, with no protein in the pelleted insoluble fraction. This is compared to a beta thalassemic mouse, where alpha and beta globin are present in the soluble fraction (S), but there is alpha globin in the pellet/insoluble fraction (I) due to disrupted tetramer formation. **H, I** Representative images from Cresyl blue staining of blood smear. There is no increase in reticulocytes, hemoglobin precipitation within the red cell, or morphological deformity in the Hba1$^{WT/\Delta 36\text{-}39}$ blood. Scale bar in **H** is 10 μm.

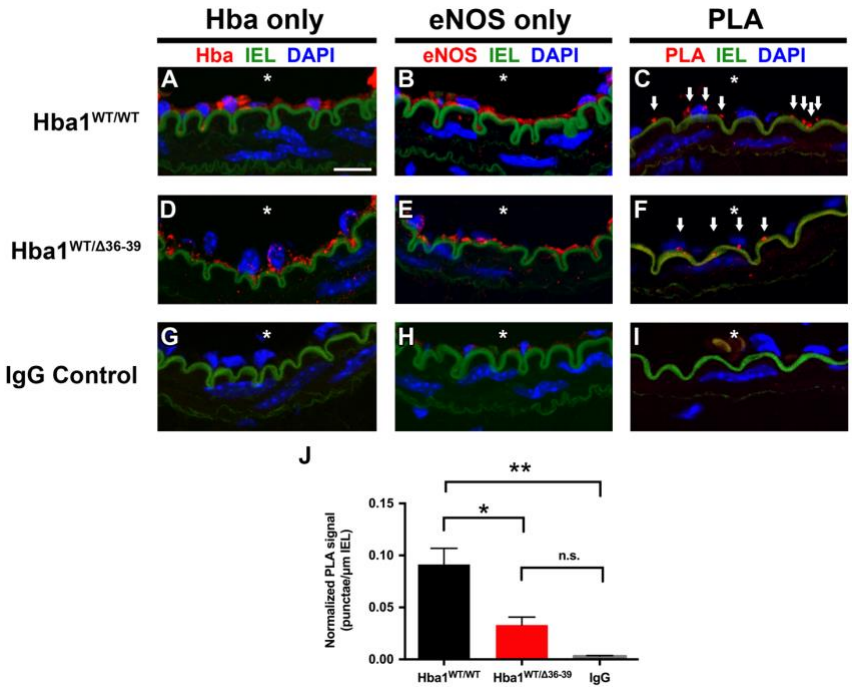

Figure 5: *Hba1*$^{WT/\Delta 36\text{-}39}$ mice have decreased alpha globin/eNOS complex formation in the endothelium of resistance arteries. Expression of total hemoglobin (**A, D,** red) and eNOS (**B, E,** red) are unchanged between the *Hba1*$^{WT/WT}$ and *Hba1*$^{WT/\Delta 36\text{-}39}$ genotypes (primary antibody controls are shown in **G** and **H** for single antibody staining, and I for the antibody combination). In all images, nuclei are labeled with DAPI and the internal elastic lamina (IEL) Proximity ligation assay (PLA) punctae (red, and marked with white arrows) are seen where alpha globin and eNOS are <40 nm apart (**C, F**). In **J**, Punctae were quantified as incidents per linear μm of IEL as determined by Image J analysis. Images were taken on an Olympus Fluoview 1000 confocal microscope with a 60X objective. Scale bar in A signifies 10 μm, and in A-I, asterisk denotes the lumen of the artery. In J only, * indicates $p<0.05$, and ** indicates $p<0.01$ compared to *Hba1*$^{WT/WT}$.

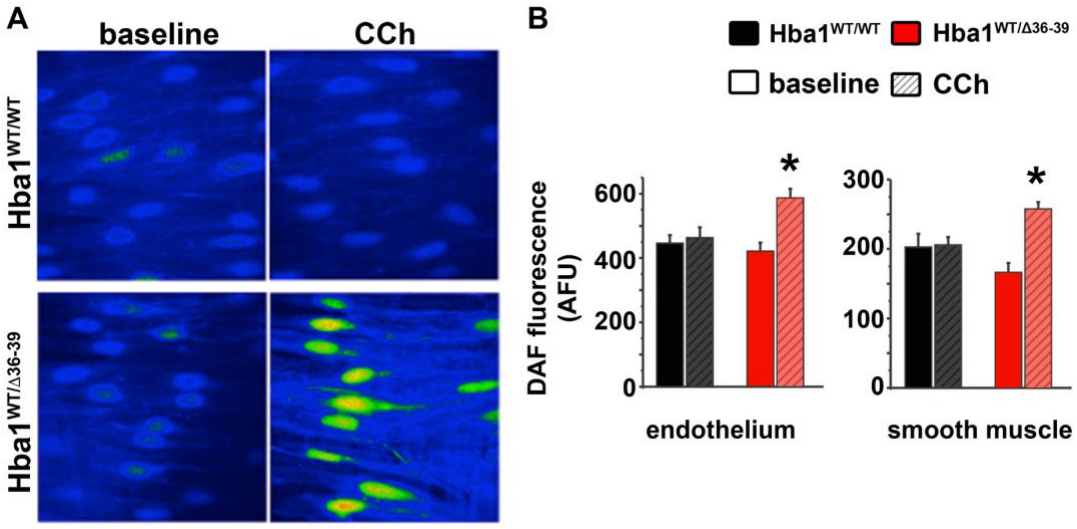

Figure 6: Nitric oxide release is significantly increased in endothelium of resistance arteries from *Hba1*$^{WT/\Delta 36-39}$ mice. (A) *En face* imaging of third order mesenteric arterioles loaded with DAF were subject to 10 μM CCh stimulation and **(B)** the data quantified in the optical slices of endothelium or smooth muscle. Black bars represent *Hba1*$^{WT/}$WT mice, and red bars denote the *Hba1*$^{WT/\Delta 36-39}$ genotype. Bars without diagonal lines are baseline, and with lines denote after CCh stimulation. N≥4 mice for all measurements. In all graphs, * indicates $p<0.05$ compared to *Hba1*$^{WT/WT}$ + CCh.

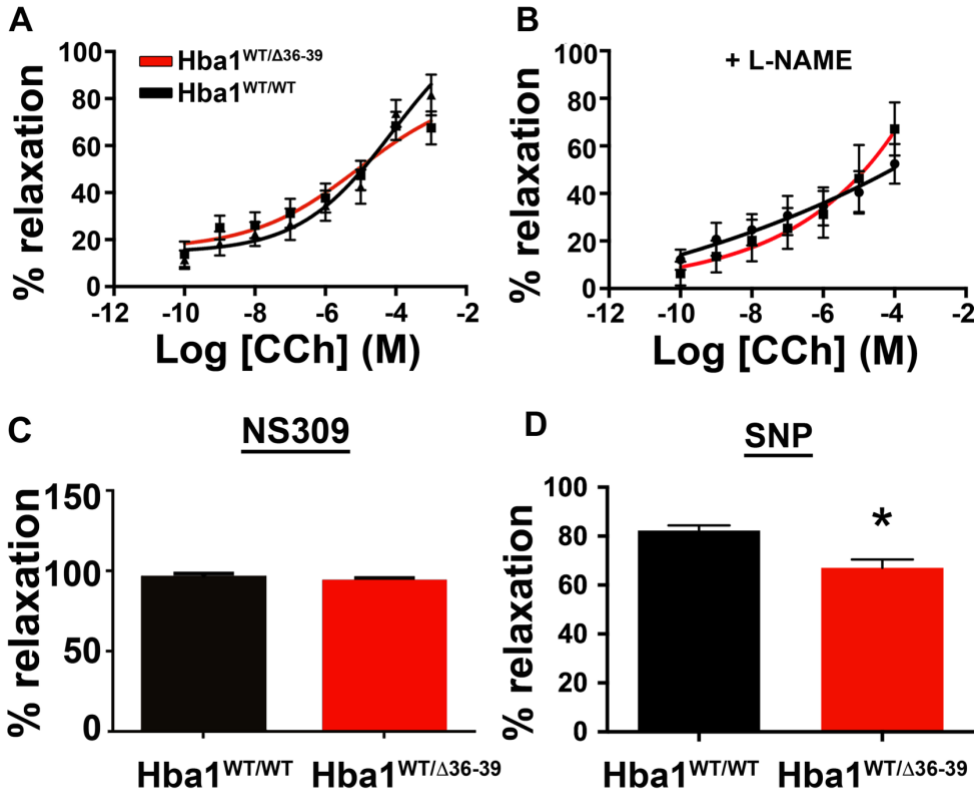

Figure 7: Endothelium-independent, but not endothelium-dependent, dilation is impaired in *Hba1*$^{WT/\Delta 36\text{-}39}$ mice. (A) A dose response to CCh was performed with third order mesenteric arterioles pre-constricted with 1 μM phenylephrine. No differences were observed at baseline or **(B)** under conditions of NOS inhibition (arterioles were incubated with L-NAME for 30 minutes prior to CCh dose). **(C)** 1 μM NS309 was applied to cannulated and pressurized third order mesenteric arterioles also pre-constricted with 1 μM phenylephrine and the response within 10 minutes compared to arterioles. No difference is observed in relaxation was observed between genotypes. **(D)** *Hba1*$^{WT/\Delta 36\text{-}39}$ show decreased dilation to 1 mM sodium nitroprusside (SNP, an endothelium-independent NO donor) compared to *Hba1*$^{WT/WT}$ controls. * indicates $p<0.05$ compared to *Hba1*$^{WT/WT}$.

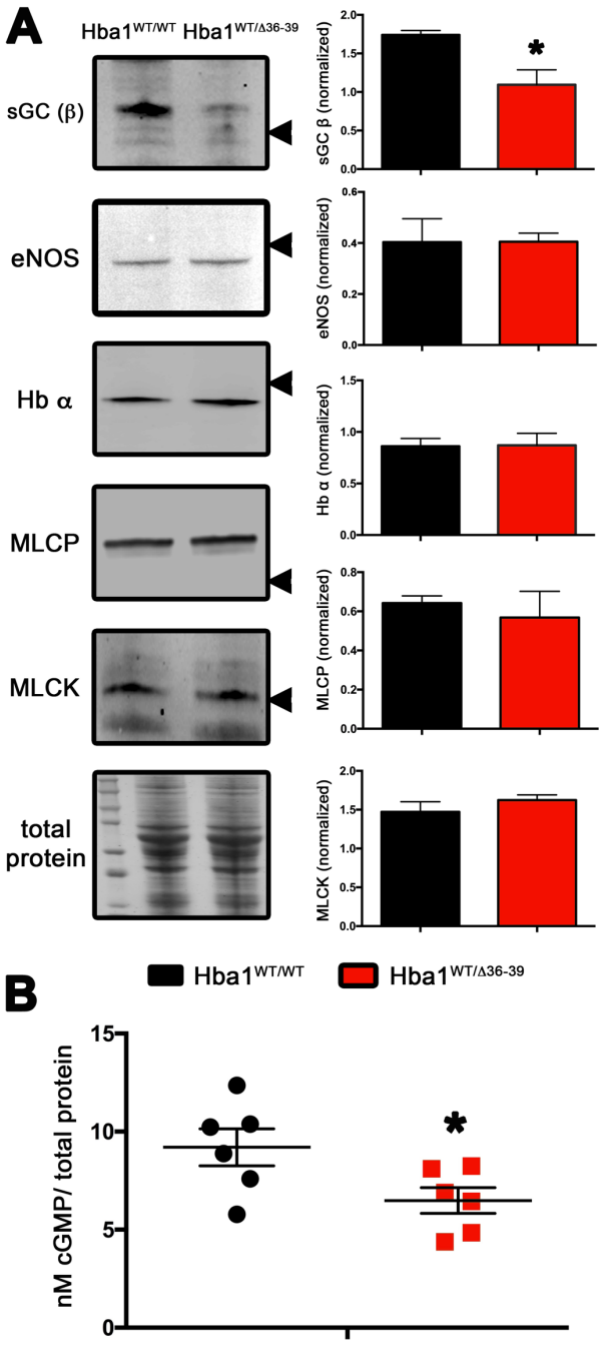

Figure 8: *Hba1*$^{WT/\Delta 36\text{-}39}$ have significantly decreased soluble guanylate cyclase and cGMP. (A) Western blots of third-order mesenteric arterioles from n=3 mice (1 blot per animal) were probed with antibodies against sGC (β), eNOS, alpha globin (Hb α),

MLCP, and MLCK, and quantified against total protein in the well. There is a significant decrease in sGC (β) in *Hba1*$^{WT/\Delta 36\text{-}39}$ mice, while other components of the dilation pathway are unchanged. Arrows to the right of the blots mark location of molecular weight markers (50 kDa for sGC, 150 kDa for eNOS, 20 kDa for Hbα, 37 kDa for MLCP, and 200 kDa for MLCK. Blots were normalized to total protein signal in the lane as a loading control). **(B)** The production of cGMP was measured in third-order mesenteric arterioles in n=6 mice. *Hba1*$^{WT/\Delta 36\text{-}39}$ mice are able to produce less cGMP than the *Hba1*$^{WT/WT}$ controls. In all graphs, * indicates $p < 0.05$ compared to *Hba1*$^{WT/WT}$.

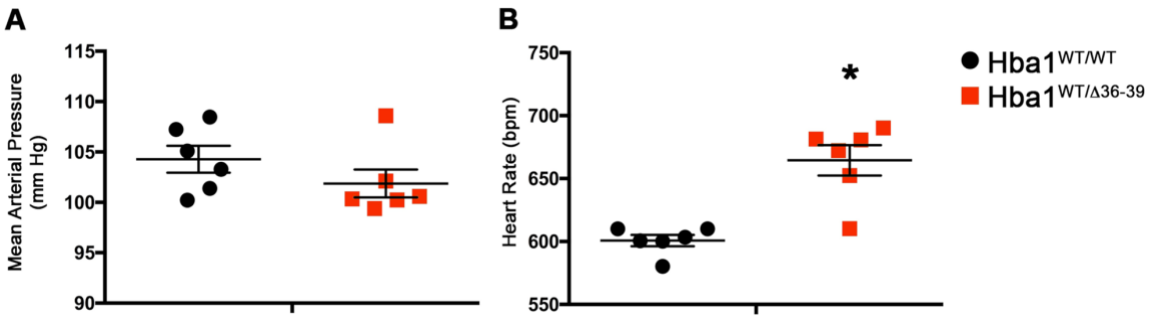

Figure 9: *Hba1*$^{WT/\Delta 36\text{-}39}$ have lower blood pressure and significantly increased heart rates. Radiotelemetery blood pressure measurements from n=6 *Hba1*$^{WT/WT}$ and n=6 *Hba1*$^{WT/\Delta 36\text{-}39}$ mice demonstrate no change in **(A)** mean arterial pressure (24-hour average over 7 days). However, **(B)** the heart rate for *Hba1*$^{WT/\Delta 36\text{-}39}$ mice is significantly increased compared to the *Hba1*$^{WT/WT}$ mice. * indicates $p < 0.05$ compared to *Hba1*$^{WT/WT}$.

Table 1: Whole genome sequencing confirmation of *Hba1* selective deletion.

Hba-a1	Region	Type	Length	Count	Coverage	Freq
Hba1$^{WT/WT}$	32283934.. 32283945	n/a	-	-	-	-
Hba1$^{WT/\Delta 36\text{-}39}$	32283934.. 32283945	Deletion	AGCTTCCCCACC	7	12	58.33333

Table 2: Lack of *Hba1*$^{\Delta 36\text{-}39/\Delta 36\text{-}39}$ in multiple *Hba1*$^{WT/\Delta 36\text{-}39}$ crosses.

Pair	M Genotype	F Genotype	litters	*Hba1*$^{WT/WT}$	*Hba1*$^{WT/\Delta 36\text{-}39}$	*Hba1*$^{\Delta 36\text{-}39/\Delta 36\text{-}39}$
1	*Hba1*$^{WT/\Delta 36\text{-}39}$	*Hba1*$^{WT/\Delta 36\text{-}39}$	2	2	10	0
2	*Hba1*$^{WT/\Delta 36\text{-}39}$	*Hba1*$^{WT/\Delta 36\text{-}39}$	3	3	15	0
3	*Hba1*$^{WT/\Delta 36\text{-}39}$	*Hba1*$^{WT/\Delta 36\text{-}39}$	3	3	16	0
TOTAL			**8**	**8**	**41**	**0**

Appendix

Author contributions: TCSK was primarily responsible for planning and executing experiments (including molecular characterization of the mutant alpha globin; blood, tissue, and embryo isolation; immunofluorescence; and western blotting) and writing the manuscript. The mouse line was developed by JTB, RBW, LC, and BEI, with experimental expertise from PS and WX. GBBF and HRAP contributed significant experimental help with vasoreactivity experiments, cGMP assays, and blood pressure measurements. CL and LJD contributed to blood and genomic characterization of the mouse, respectively, and LJD performed blood pressure telemeter implantation. KH and SS were invaluable for NO imaging and vasoreactivity expertise. MMCK, ASP, LC, HA, SS, and BEI were all critical for manuscript planning and experimental guidance.

Chapter 8: Discussion and Future Directions

Discussion

Through all of this work, I have attempted to understand alpha globin as a master regulator of NO signaling. That alpha globin and NO are intrinsically linked in vascular signaling is shown in a few ways here, but we are still understanding how endothelial alpha globin plays its part in fine-tuning the signals that come from the already exquisitely-regulated endothelial NOS.

My thesis work has focused on deeply understanding how one specialized protein-protein interaction affects a much larger homeostatic mechanism. In the context of general cell biology, alpha globin and eNOS do not cast an especially large shadow; neither are transcription factors, nor extracellular sensors, nor ion channels, but that, to me, is one of the interesting features of this work. Endothelial NOS requires so many different steps to be activated and produce NO, and that the whole concert of molecules and signals that fall into place are thwarted by one last brake to diffusion through one protein-protein interaction is truly a phenomenon to study, wrestle with, and appreciate. It takes understanding of the mechanisms from molecular interaction to control of tissue perfusion to fully grasp the complexity of these biological questions.

Here, I have attempted to do that. I have had the opportunity to work with both *E. coli* and *M. musculus*, was involved in work with retinal tissue from the icefish *C. gunnari*, have thought many times about cardiovascular dynamics of extinct species like sauropods *B. lentus* (*341*), and even played with some immunofluorescence of an artery from *G. Camelopardalis* (**Figure 1**). One of my favorite aspects of cardiovascular science is that it allows us to think about so many different aspects of science, because the principles that we study reach far and wide across the evolutionary and physiological spectrum.

I wanted to understand how endothelial alpha globin can regulate vascular reactivity, blood pressure control, and homeostasis through its interaction with the eNOS enzyme.

First, we need to understand what role alpha globin plays in relationship to eNOS in vascular endothelium. Previous work from our group has implicated alpha globin as a binding partner of eNOS in endothelium, and the presence of alpha globin is critical for the control of NO flux from endothelium (*35, 103*). Notably, the expression of alpha globin is limited to the resistance arteries, the small-diameter vessels that dilate and contract to regulate blood pressure, tissue oxygenation, and waste clearance. The expression of alpha globin is observed primarily in the myoendothelial junction (MEJ), a subdomain of endothelium that reaches through the internal elastic lamina to directly contact smooth muscle. The prevalence of MEJs is increased in the resistance vasculature relative to larger conduit arteries; the expression of alpha globin in the arterial vasculature follows the same pattern. Along with these observations, the functional performance of the vessels is changed with MEJ/alpha globin presence. Conduit arteries rely heavily on NO signaling, whereas other, non-NO mechanisms of endothelial-dependent dilation dominate signaling in resistance arteries. One general hypothesis is that alpha globin is responsible for the switch away from NO-dominated dilation in the decreasing size of the arterial vasculature.

This coordination of alpha globin expression and MEJ prevalence has been shown by us and others, but one major question remained as to whether the presence of MEJs could induce alpha globin expression *per se*. To test this, we used an observation from Heberlein *et al*. that plasminogen activator inhibitor -1 (PAI-1) is upregulated specifically in MEJs (*342*). As PAI-1 is involved in fibrous tissue maintenance, its presence in the MEJ as it pokes through the lamina layer might be to prevent remodeling of the matrix and detachment of the endothelium from the smooth muscle. In our study, we locally applied PAI-1 to the carotid artery, a conduit artery with large flow and diameter. Normally, the

carotid artery is devoid of MEJs and has low alpha globin expression. Transiently, the application of PAI-1 to the carotid artery induced holes in the internal elastic lamina, and endothelial projections through those holes. The maximum number of holes and projections occurred at 7 days after application, but the effect of PAI-1 was completely abolished by 21 days. At the time of maximal effect on lamina holes and endothelial projection, there was a significant upregulation of alpha globin expression in the carotid artery as well. Functionally, the expression of alpha globin changed the vasodilatory phenotype of the vessel. Along with the increased alpha globin, PAI-1-treated carotid arteries did not have dilation that was completely blunted by the NOS inhibitor, L-NAME. Only when other endothelium-dependent dilation mechanisms were inhibited did the carotid artery match the untreated control. Critically, this observation was absent in Hba1$^{-/-}$ mice; without alpha globin expression, the dilation of the PAI-1-treated vessel was still completely NO-dependent, even with increased MEJ formation. This study demonstrates that alpha globin is critical in the determining the dilatory phenotype of different vascular beds. Understanding the role of alpha globin in vasodilation is a key component of developing therapies to address pathologic cases of dysregulated blood pressure.

Straub *et al*. first demonstrated the expression of alpha globin in the vascular endothelium in 2012 (*103*). This discovery was followed shortly thereafter by defining the binding motif of alpha globin; ten residues ^{35}LSFPTTKTYF^{44} are sufficient to compete with full-length alpha globin for eNOS interaction (*35*). Immunoprecipitation of alpha globin via eNOS pulldown was decreased in the presence of an exogenous peptide with those residues. This sequence was named HbαX, and has been used extensively in my studies and the previous chapters of this document. HbαX, with the addition of an N-terminal HIV-derived tat sequence, is cell permeable and vasoactive. *Ex vivo* myography of resistance vessels showed an increased dilatory phenotype after cholinergic stimulation,

demonstrating that decreasing alpha globin and eNOS interaction in vascular endothelium potentiates increased dilatory signaling. This effect is inhibited by incubation of the NOS inhibitor L-NAME, demonstrating that HbαX acts to increase dilation in arterioles by increasing NOS-derived signaling. In addition to the *ex vivo* effects, intraperitoneal injection of the tat-HbαX peptide acutely decreased mean arterial blood pressure in a mouse model, showing therapeutic potential of HbαX as an antihypertensive therapy.

Further experiments for the efficacy of the tat-HbαX peptide were published in Keller *et al*. (2016) (*184*). Injections of the peptide into mice showed increased tissue oxygenation in capillary beds, and increased linear velocity of blood in the arterial circulation. Combined with the acute decrease in blood pressure from previous studies, we can postulate that this increase in flow and oxygenation is due to increased vascular diameter (reducing resistance to flow). Increased vasodilation, leading to decreased blood pressure, was also seen in long-term blood pressure studies where injection of tat-HbαX (but not a scrambled control) decreased systolic blood pressure but about 5 mmHg at baseline, and about 30 mmHg when the mice were made hypertensive by angiotensin II infusion. We showed that the peptide does not induce kidney or liver toxicity, which is key for therapeutic relevance. Additionally, HbαX does not affect alpha/beta globin tetramer function, as the O_2 p_{50} was not affected in isolated red blood cells after incubation of HbαX, showing that effects on circulating oxygen carriers are minimal.

Another result from this manuscript is that the HbαX peptide binds directly to eNOSox. Previous work using full-length eNOS from HEK cell transfections did not establish whether alpha globin was binding to the reductase or the oxygenase domain of eNOS (*35*). While the reductase domain is responsible for the shuttling of electrons via flavin nucleotide cofactors, the oxygenase domain contains the enzymatic active site. We hypothesize that alpha globin can act as a NO scavenger after production, and thus optimal positioning of alpha globin would be near the active site in the oxygenase domain.

Indeed, HbαX binding directly to the eNOS oxygenase domain was observed via far western blotting and fluorescence polarization binding experiments. A high affinity interaction of the HbαX peptide and eNOSox disrupts the alpha globin/eNOS complex and increases NO availability, as was demonstrated in long-term blood pressure studies from mice. This mechanism of action is conserved through human vessels, as we showed a blunted constriction to the constrictor phenylephrine in HbαX-treated vessels isolated from hypertensive human biopsies. Overall, this extends results on the vasoactive mechanism of disrupting the alpha globin/eNOS complex *in vivo*.

One project that broadened my view of vascular physiology in general occurred as a collaboration with Miriam Cortese-Krott's group at Heinrich Heine Universität in Düsseldorf. I have spent so much time thinking about the vascular resistance to flow, but one of the other critical determinants of Pouseille's law:

$$Flow = \frac{\pi * P * r^4}{8 * \eta * l}$$

where **flow** through the tube is related to **P** (the pressure difference at beginning and end of tube), **r** (the radius of the tube), **η** (the viscosity of the medium that is flowing), and ***l*** (the length of the tube)

is the viscosity of the medium that is flowing. There are many components of blood that flows through the vessels, but the most abundant in number and volume is the erythrocyte, or red blood cell. These cells are the hemoglobin-tetramer-carrying cells that circulate to deliver O_2 and take CO_2 back to the lungs for exhalation. Erythrocytes normally make up about 50% of the volume of blood (although there are some fluctuations in this between

sexes, disease states, and other cases). These erythrocytes are in constant contact with one another, with other cells, or with plasma proteins as they flow through the circulatory loop. The circulation has vessels of many different sizes, from large diameter conduit arteries like the aorta to the tiniest capillaries in between muscle fibers. Erythrocytes must be able to undergo these large changes in stress, from huge pressures to squeezing through a capillary. The elasticity and deformability of these cells contributes to the viscosity of blood: when erythrocytes cannot deform to traverse capillaries, the force of blood and plasma that are backed up behind the cell cause increased afterload pressure on the heart.

How do the erythrocytes maintain their ability to deform? It was shown in hypertensive disease states with endothelial dysfunction or decreased NO signaling that erythrocytes are more rigid and less deformable. The sensitivity of the red cell is especially affected by thiol modifying molecules, suggesting that intracellular cysteines (whether in proteins or antioxidants like glutathione) may play an important role in maintaining erythrocyte deformability. When we began our work, there was conflicting evidence saying whether NO would improve deformability of isolated red cells or have no effect. To unravel these lines of evidence, we began with red cells isolated from hypertensive humans.

In our experimental setup, we used a dilute suspension of freshly isolated erythrocytes in polyvinylpyrroline, a high viscosity medium that will transmit shear forces from a rotating dowel to red cells. The deformability of the individual red cells is measured by laser diffraction, and a curve of deformability can be plotted from different shear stresses. Cells isolated from hypertensive patients had decreased deformability overall, and this was correlated with increased oxidative stress. Similar decreases in deformability were achieved by treatment of the red cells with a peroxide to overwhelm the intrinsic redox balance of the red cell. The sum of individual cells being less deformable was consistent in increases in whole blood viscosity, which was significantly increased wither peroxide

treatment to mimic oxidative stress. Interestingly, we saw no result of increased cell deformability with incubation of the red cell with an NO donor alone. Only when cells were oxidative-ly stressed with the peroxide did an NO donor provide any relief (both pre- and post-treatment with the NO donor preserved deformability compared to peroxide treatment alone). This also translated to decreased whole blood viscosity, which is beneficial to maintaining flow and regulation of blood pressure. We established that the erythrocyte cytoskeletal protein spectrin can be modified by NO on its cysteine thiols (a modification termed nitrosation), and that protection from oxidative damage to deformability correlates with increased spectrin nitrosation.

A physiologic source of NO is needed for erythrocytes to maintain deformability *in vivo*. There are a few possible mechanisms that could each provide NO for erythrocyte use, although it is probable that no single mechanism is totally responsible. First, endothelial-derived NO can diffuse into the lumen of the vessel to act on circulating erythrocytes. Indeed, the presence of erythrocytes in the bloodstream is a large sink for NO due to the amount of intracellular hemoglobin in the erythrocyte. This NO could be sequestered by hemoglobin (through reversible binding to the heme group) and released as needed to modify erythrocyte cytoskeletal proteins. A second source for NO is intrinsic enzymatic production of NO via a NOS isoform in erythrocytes (*208*). This erythrocyte NOS-produced NO likely would undergo the same fate as endothelial-produced NO. A third source of NO to maintain deformability is the nitrite reductase activity of erythrocytic hemoglobin (*209*). Work from Gladwin and others have established globin proteins as non-enzymatic sources of NO through the reduction of inorganic nitrite in low-oxygen environments. The decrease pO_2 in the arterio-venous transition primes the heme group of erythrocytic alpha and beta globin for reduction of nitrite and release of NO. This is a significant source of NO that could buffer oxidative stress and protect against decreases in deformability.

Preservation of erythrocyte deformability plays a role in maintenance of blood pressure. Although I had primarily been focused on vascular sources and effects of NO signaling, this foray into blood cell signaling was a significant part of my development as a physiologist. Describing the interactions between cells that cause changes in whole blood viscosity, and relating that result back to blood pressure physiology, gave me a wider context to consider the totality of signals that are integrated in maintaining the cardiovascular system as a whole.

Another interesting broad physiological story from my thesis work is the integration of NO and dilatory signals in the disease context of pulmonary hypertension (PH). Knowing that the HbαX peptide has such drastic effect on systemic blood pressure, especially in hypertensive contexts, would increasing NO via disruption of alpha globin and eNOS binding perform as a therapy for PH?

Using a hypoxia and SU5416 model of inducing PH, we injected mice with HbαX peptide, a scrambled control peptide, or administered an approved therapeutic in an endothelin-1 antagonist. In these animals, we measured right ventricular systolic pressure as a readout of pulmonary pressure status. The systolic pressure of normotensive mice is around 25 mmHg; the mice exposed to hypoxia and SU5416 developed pressures of almost 40 mmHg. This pressure overload in disease progression leads to right ventricle remodeling and eventual heart failure.

In our experiments, mice developed PH after exposure to hypoxia and SU5416. Treatment with the endothelin-1 antagonist decreased pulmonary blood pressure and led to less severe right ventricle remodeling. Our HbαX peptide injections caused pulmonary pressure to remain elevated, and higher doses of HbαX peptide led to increased pulmonary blood pressure. Ventricle remodeling was not alleviated by peptide treatment. We first thought to check that the HbαX peptide was working as intended, and increasing

NO signaling in the pulmonary vasculature. To assay NO formation, we used a downstream product of NO, 3-nitrotyrosine. Nitrotyrosine was increased in HbαX-treated animals, demonstrating increased NO availability; however, nitrotyrosine is formed from the reaction of peroxynitrite (ONOO-) with protein tyrosine residues. Peroxynitrite formation is itself a marker of oxidative stress. We determined that the increased nitrotyrosine signal in the lung tissue, although a marker of peptide action via increased NO, was a deleterious oxidative stress reaction that prevents proper function of lung tissue. Overall, chronically increasing NO signaling in a hypoxic lung may lead to more tissue damage than beneficial effect from any dilatory signaling.

This was another example of considering the entire physiological context for a particular result. Previous work from the Straub group had demonstrated that pulmonary vessels respond to HbαX treatment with increased dilation (*256*). Although we show that increasing NO by disrupting the alpha globin/eNOS complex is not beneficial to treatment of pulmonary hypertension, the results are not at odds. *Ex vivo*, the increased NO signaling does exactly what is expected: increased vasodilation is observed. However, with the milieu of signals, oxidants, and other factors in the hypoxia model, the increased NO signaling generates nitrosative stress signals and prevents tissues from functioning normally. The same signal, in two contexts, must be interpreted individually for the results to comprehend the combined results.

Although HbαX by itself does not appear to be a viable therapeutic candidate for PH in this model, there might be some contexts that are worth revisiting. Co-administration of HbαX and a superoxide dismutase enzyme (whether by inhalation or gene therapy) could improve the outcomes of the increased NO signaling by decreasing peroxynitrite formation from reaction of NO and the superoxide anion. Additionally, increasing NO in a model of hypoxia-induced PH was demonstrated to be deleterious, but other models that cause PH might benefit from increased NO.

We have done a considerable amount of work based on the interaction of alpha globin and eNOS through knowing where on alpha globin the two proteins interact. This allowed us to make a peptide mimicking that sequence for pharmacological disruption of the protein complex. The HbαX peptide has been an invaluable tool for describing the effects displacing alpha globin from eNOS in disease contexts and for endothelial biology in general. However, we have not known the eNOS motif that alpha globin is interacting with. This is critical information for determining how alpha globin controls NO flux from eNOS.

My main hypothesis has been that alpha globin is able to bind to active eNOS (specifically the oxygenase domain, shown in (*184*)) and prevent NO diffusion after enzymatic production. Other possibilities include steric hindrance of electron shuttling from the reductase domain to the oxygenase domain, or scavenging of the active site electron needed for arginine utilization. These hypotheses can be explored with a complete model of the alpha globin/eNOS complex, which has not yet been elucidated.

To determine the interaction motif for alpha globin on eNOS, and thus determine the orientation of the protein complex, I began with docking of the rigid structures of the two proteins *in silico*. This strategy has advantages, namely that it can quickly generate models that can be tested through mutagenesis or other means. Our search with alpha globin and eNOS did not yield any consensus motifs on eNOSox that could readily be identified as probable alpha globin binding residues. To refine the search, I wanted to determine the structure and interacting residues of the alpha globin mimetic peptide, HbαX, that binds to eNOSox with high affinity. Solution NMR was the most tractable technique for determining any relevant structural features of HbαX that could interact with eNOSox. Unexpectedly, the lone proline in the HbαX sequence undergoes isomerization in solution, thus complicating the attempt of modeling the peptide empirically for docking with eNOSox. I have considered that although the proline isomerization thwarted my

efforts to model the peptide in solution, the two conformations of the peptide might enhance the binding of HbαX and eNOSox. The high affinity interaction of HbαX and eNOSox could be partly resultant of the less populated proline isomer. This proline is normally in trans in the full alpha globin protein, but when less restrained in the HbαX peptide, could bind strongly with eNOSox due to the cis isomer. Unfortunately, I am unaware of any method to “lock” the proline in either cis or trans, especially in a linear peptide form. Other methods are needed for unambiguous data on the interaction.

To this end, I have pursued crosslinking mass spectrometry as a method to observe and characterize HbαX and eNOSox interaction. The ultimate goal of this method is to reconstruct a model of the full length alpha globin interaction with eNOSox; using the HbαX peptide as a proxy allows for more rapid experimentation at this stage. I have developed my own protocol for the crosslinking and protease digestion of eNOSox and HbαX, and low-resolution mass spectrometry has identified differential peptide products that can be characterized by electrospray ionization mass spectrometry. The use of orthogonal proteases (trypsin and Asp-N) allows for confirmation of mass spectrometry results within the same experiment; using the different pieces that come from the digestion, a confirmed eNOSox interaction motif can be identified and a full model of the alpha globin/eNOS complex can be determined.

Powerful techniques to visualize the complex experimentally could supplement the data from mass spectrometry. Confirmation of the orientation of the complex by general shape and ellipticity could be accomplished by small angle x-ray scattering. Others have published workflows that combine density maps from cryo electron microscopy with restraints on protein orientation from interacting residues via crosslinking mass spectrometry. Both are reasonable extensions from this work that will greatly enhance confidence in the modeling of the protein complex. Obtaining a high-resolution model of

this complex will contribute to a mechanistic understanding of the role of alpha globin in controlling NO flux in the endothelium, which has great therapeutic implications.

Finally, I have focused efforts on non-therapeutic angles to examine the physiological implications of disrupting the alpha globin/eNOS complex in endothelium. We generated, using CRISPR/Cas9 gene editing technology, a global deletion of four residues from the eNOS-interacting region of the *Hba1* gene. Although this was neither an inducible nor a cell-type specific deletion, we have learned much about development and vascular biology from this mouse model. This Δ36-39 deletion was difficult to bear at first, but I have come to appreciate the power of the deletion within the interaction domain.

The deletion of the ^{36}SFPT^{39} from the HbαX peptide location effectively disrupts the ability of alpha globin to interact with eNOS. I showed this with fluorescence polarization binding experiments; the deletion peptide shows no discernible binding to eNOSox where the full peptide maintains high affinity for eNOSox. Expression of the mutant protein was observed in the blood of adult heterozygous *Hba1*$^{WT/\Delta 36\text{-}39}$ mice, which allowed us to characterize the effects of genetic disruption of the alpha globin/eNOS complex in endothelium.

Interestingly, we could not perform this study on homozygous *Hba1*$^{\Delta 36\text{-}39/\Delta 36\text{-}39}$ deletion animals, because there were no homozygous pups born. These pups were formed in utero, but seem to experience developmental abnormalities by embryonic day 12 that were lethal before birth. We examined E12 pups from a heterozygous parent cross in order to observe any developmental issues, and discovered stunted growth, a dilated cardiomyopathy, and distended vessels in the embryo. Additionally, the pups were highly positive for the nitrosative stress signal 3-nitrotyrosine. I believe that endothelial alpha globin may be important for development of the vascular network, and may help to detoxify excessive NO signaling during development. These hypotheses were outside the scope

of characterizing the vascular phenotype of the *Hba1*$^{WT/\Delta 36\text{-}39}$ mouse model, but could be an interesting future direction to pursue.

In the heterozygous adult mice, we did not observe any hematologic differences from a WT littermate control, allowing us to focus on characterizing vascular differences between the mice. We saw decreased alpha globin and eNOS interaction in the *Hba1*$^{WT/\Delta 36\text{-}39}$ mouse through proximity ligation assay, an immunofluorescence technique that demonstrates close apposition of the target proteins. Using a fluorescent indicator of NO generation, we demonstrated that the decreased interaction translates to increased NO availability after cholinergic stimulation. Although we observed increased NO generation in resistance arteries, the same arteries did not display major vasodilatory changes compared to control; the only difference in the dilatory phenotype was a decrease in the vasodilatory capacity to an NO donor in sodium nitroprusside. The decreased dilation to the NO donor prompted us to look at vasodilatory protein machinery: there were no changes in alpha globin, eNOS or myosin kinase and phosphatase expression, but a significant downregulation of the NO receptor in vascular smooth muscle, soluble guanylyl cyclase (sGC). This compensatory downregulation of sGC decreases vasodilatory signal transduction through cGMP and prevents dilation to the excess of NO generated in the *Hba1*$^{WT/\Delta 36\text{-}39}$ mouse. Translationally, decreased dilatory capacity may be a homeostatic response to maintain blood pressure; there was no difference in mean blood pressure in the deletion model, although heart rate was slightly elevated (suggesting lower overall peripheral vascular resistance).

One interesting aspect of this study is that we were able to decrease interaction of alpha globin and eNOS without complete deletion of either protein. The expression of the mutant protein allowed us to dissect the effects of alpha globin/eNOS interaction without disturbing other roles for alpha globin in the endothelium. Another Isakson Lab colleague has some interesting data on the action of endothelial alpha globin as a nitrite reductase.

Endothelial alpha globin has the reaction ability to convert nitrite into vasoactive NO (*211, 343, 344*), and the close position of alpha globin in the endothelium limits the diffusion distance for the NO to travel, potentiating the vasodilatory effect of nitrite reduction (which has been extensively described as an erythrocyte process). In the *Hba1*$^{WT/\Delta 36\text{-}39}$ model, we have uncoupled alpha globin from eNOS while presumably maintaining the ability of alpha globin to act as a nitrite reductase. This, combined with a model of alpha globin knockout from endothelial cells (*Cdh5*-Cre^{ERT2} *Hba1*$^{fl/fl}$, active in the Isakson Lab) allows us to dissect the distinct roles of alpha globin: as an NO scavenger through its interaction with eNOS, and as a NO generator through intrinsic nitrite reduction activity. Additionally, the *Hba1*$^{WT/\Delta 36\text{-}39}$ mutation might have contributed to the embryonic lethality of this model by virtue of not being a complete gene knockout. Because this is a “loss of function” mutation instead of a gene knockout, I have hypothesized that the checkpoints for compensation of the missing protein are tricked by the small deletion that does not affect expression or heme incorporation. This allows the expression of the mutant globin, which leads to subsequent pathological increases in NO in the developing pup.

This work could be improved in the future with an inducible knockout of these residues from the eNOS binding region of alpha globin. Although technically difficult, this could be established with a knockout/knock-in strategy. In the adult mouse, a knockout of alpha globin (the endothelial *Hba1* knockout described above) could be combined with an inducible knock-in gene via *Rosa26*-driven gene expression of the mutant protein after recombination. This could allow homozygous *Hba1*$^{\Delta 36\text{-}39/\Delta 36\text{-}39}$ mice to be generated in adulthood, with normal developmental phenotypes to overcome the embryonic lethality described in our model.

Overall, this study was an interesting way to access the genetic disruption of the alpha globin eNOS complex. We may have uncovered a developmental role for endothelial

alpha globin, and have solidified the scavenging of NO as an important mechanism for maintenance of vascular homeostasis.

Combined, these stories are my contribution to comprehending the role of alpha globin in the endothelium. We still have much to learn, some of which is described below; however, some questions remain unknown and un-asked. Alpha globin and eNOS have major implications in the regulation of blood pressure by the resistance vasculature, but is just a small piece of the field of vascular biology. I hope to know more in the future.

Future Directions

The work that has been done so far has demonstrated that NO scavenging by alpha globin controls blood pressure and is targetable by peptide therapy to increase NO signaling and decrease pressure. Future work in this area could include a more complete description of the states of eNOS that interact with alpha globin, a re-imagination of the effects of NO on pulmonary diseases, and exploring other NOS/globin couplings in other tissues.

Assaying the states of eNOS that determine alpha globin interaction

My work on the alpha globin/eNOS complex has been centered on the oxygenase domain of eNOS: this is the site where alpha globin interacts (*184*), and houses the active site of the enzyme. Determining the alpha globin binding site on the eNOS oxygenase domain is the first step to understanding how alpha globin fits into the total, complex, regulation of the full-length eNOS enzyme. The recombinant production of eNOSox does not capture phosphorylation states (activating or inactivating) of the full eNOS protein (*254*). Additionally, the interaction of the reductase and oxygenase domains in the activated enzyme might preclude alpha globin binding (or vice versa) (*11*). At this point, we have not assayed the states of eNOS that contribute to or prevent alpha globin binding.

Some of the phosphorylation states, especially in the oxygenase domain, could be engineered through mutagenesis for study. Phosphorylation of serine 114 is an inactivating phosphorylation (*345*) that could be mimicked by substitution of an aspartate residue at that position. Phosphomimicry of tyrosine (as in the activating phosphorylation of tyrosine 81 (*47*)) is more difficult to achieve; substitution of aspartate or glutamate does not preserve the structure of the amino acid as it does for serine or threonine residues.

Current strategies include incorporation of unnatural amino acids, which could be accessible with recombinant protein synthesis (*346*). The results of HbαX or alpha globin binding with eNOS in either of these cases will add to our understanding of the determinants of the alpha globin/eNOS interaction.

In order to assay the interaction of the reductase domain with the eNOSox and alpha globin, single particle cryo-electron microscopy (EM) might be required to visualize the entire protein complex. EM has been used to determine a model of the full-length inducible NOS enzyme (*11*). In that study, eNOS structure has been observed with and without calmodulin bound, although an atomic reconstruction using crystal structures was not shown. With significant optimization, the binding of alpha globin and full length should be observable by EM, as the complex is large enough to be observable. The total complex might show that alpha globin prevents reductase/oxygenase domain coupling, thereby decreasing new NO generation while maintaining optimal position for scavenging NO from the active site. Overall, the full reconstruction of the complex is something that should be pursued to understand the nature of alpha globin as the regulator of NO availability.

Pulmonary disruption of alpha globin for therapy

Although the disruption of the alpha globin/eNOS complex via HbαX was deleterious in our model of hypoxia-induced pulmonary hypertension, there could be other disease models where increased NO could be beneficial. Disease models with increased cell-free hemoglobin could benefit from heme “inactivation” by methemoglobin formation. Additionally, HbαX could find therapeutic value in cystic fibrosis treatment through increasing NO to counteract development of pulmonary fibrosis.

Sickle cell disease (SCD) is a genetic polymorphism that replaces glutamate in the sixth residue of the beta chain of hemoglobin with valine. This residue substitution has

extreme effects on quaternary structure of hemoglobin: in hypoxic conditions, the normal tetramers transiently polymerize into long chains of hemoglobin with many subunits linked end-to-end (*347*). These long chains cause abnormal red blood cell morphology by forcing the circulating cells to become long and sickled instead of being biconcave discs. Repeated cycles of sickling stress RBC membranes, leading to lysis and the depletion of RBCs from circulation, known as hemolytic anemia. Importantly, release of extreme amounts of cell-free hemoglobin into circulation severely disrupts gaseous signaling in the blood (*348, 349*).

The risk of pulmonary hypertension (PH) is significant when presented with SCD. Up to 1 in 25 patients with SCD will develop PAH, which can be fatal (when untreated, median survival time of patients with PAH is 2.8 years) (*252*). This is likely due to the presence of cell-free hemoglobin in the pulmonary circulation: deoxygenated blood returning to the lungs will have a higher prevalence of sickled cells and thus hemolysis. Free hemoglobin is a dangerous molecule in the blood due to its ROS-formation and subsequent tissue damage (*349*). The clearance mechanism for cell free hemoglobin is macrophage endocytic removal from the blood via binding to haptoglobin (*350*). This pathway becomes saturated in a hemolytic state, as production of haptoglobin cannot keep pace with RBC lysis, which leads to depletion of haptoglobin and excess hemoglobin in the blood (*347*). The deposition of free hemoglobin on the lung endothelium will disrupt normal NO signaling, causing vasoconstriction in the pulmonary arterioles.

Current treatment (NO inhalation(*351*)) is a dual therapeutic: 1) gaseous NO directly dilates pulmonary vasculature to acutely treat hypertensive crisis and 2) transformation of deposited deoxyhemoglobin to methemoglobin prevents further NO binding without heme recycling. The absence of significant quantities of extracellular CYB5R3 prevents return of the heme iron to a gas-binding redox state. Thus, NO inhalation is an effective treatment for PAH, but its effects are acute because of ongoing hemolysis in the circulation rapidly

produces new deoxyhemoglobin to scavenge NO. An HbαX-induced increase in endothelial NO release would increase conversion of extracellular hemoglobin from a deoxyhemoglobin state to methemoglobin, thereby decreasing NO scavenging potential. Increased NO release should have little effect on RBC-contained hemoglobin due to the effects of soluble CYB5R3 in RBCs that will reduce the heme iron once NO bound. Increasing the proportion of cell-free hemoglobin in the methemoglobin state will decrease the total NO scavenging potential and should increase NO signaling between endothelium and smooth muscle, alleviating some effects of PH in this disease state.

Recently, NO has undergone clinical trial as supplemental treatment for symptoms of cystic fibrosis (CF) (NIH Clinical Trial # NCT02498535, data collection was projected to end May 1, 2019). This is in response to observations that NO is decreased in the exhalations of patients with CF (*352, 353*). Additionally, before the discovery of the NO signaling pathway, L-arginine was used as a treatment for CF (*354*). Inhaled L-arginine was observed to have mucolytic and antibacterial effects, as well as improving overall pulmonary function. In the same way, our HbαX peptide could be beneficial in treatment of CF. The Phase II clinical trial mentioned above uses inhaled NO as a therapeutic; however, the administration parameters are burdensome. Patients undergo 3 -5 sessions per day at 30 minutes each to inhale NO at 160 ppm. This could potentially be helped with chronic increases of NO availability by decreasing endogenous scavenging by endothelial alpha globin. The titration of NO increases would need to be tightly controlled to avoid pathologic pulmonary tissue damage as was seen in our hypoxia/SU5416 model of PH.

Other globin/NOS interactions

Due to the cytotoxicity of NO, it is possible that other scavenging systems evolved with NOS isoforms to control NO signaling in general. We are considering the interactions of

globins and NO across organ systems in an upcoming review, but to my knowledge, there has been no discovery of globin/NOS coupling in other tissues.

This is not due to a lack of globins in other tissue or cell types. Across mammalian tissues, alpha globin (often coupled with beta globin) can be found in epithelial cells (*355*), immune cells (*356, 357*), and neurons (*358*), among others. I have shown here that alpha globin has roles other than oxygen transport and storage, could it have a unique role for nitric oxide scavenging or production from nitrite in these tissues?

Additionally, the expression of inducible and neuronal NOS isoforms match many of the expression patterns of not only hemoglobins, but closely related globin proteins myoglobin, neuroglobin, and cytoglobin. Are any of these globins coupled to a NOS isoform in these tissues to control NO availability? Further work exploring the co-expression, possible interaction, and role of the globins in the NOS system is an interesting avenue to understand the total physiology of NO.

Figure

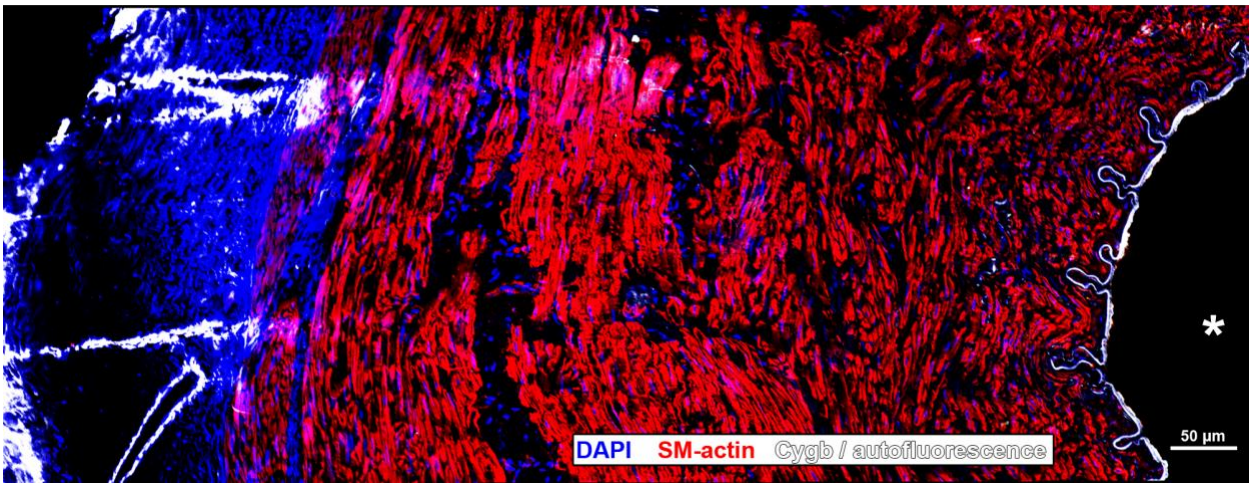

Figure 1: An artery from the knee of a giraffe, *G. camelopardalis*, stained with DAPI (blue) to visualize cell nuclei, smooth muscle actin (SM-actin, red) for the multiple, multiple, medial layers, and cytoglobin (and autofluorescence, white). The asterisk denotes the lumen of the vessel. The multiple medial layers provide stabilization against crushing forces from bending of the knee and transmural hydrostatic pressure from the vascular lumen.

Overall Appendix

eNOSox Growth and Purification Protocol

- *Media, overnights, induction, and pelleting*
    - Make and autoclave “GC Media” (20 minutes at 121 C)
        - 20 g/L casein hydrolysate*
        - 5 g/L potassium phosphate salts (pH = 7)*
        - 10% glycerol (100 mL/ 1 L)*
        - 4 mM $MgSO_4$*
        - 100 mg/L ampicillin
        - 60 µg/mL levulinic acid
        - 5 µM hemin (in DMSO)
        - * denotes autoclaved ingredients, others are added after media has cooled)
    - Start a 5 mL culture in LB-ampicillin (100 mg/L) from plates of heNOSox in *E. coli* strain UT5600. Incubate with rotation overnight at 37 C.
    - 5 mL overnight goes directly into the 1 L media, shaking at 37 C and 225 rpm.
    - Induce using 0.1 mM IPTG once OD_{600} ~ 0.8. Turn incubator temperature down to 25 C.
    - After about 14 hours, harvest cells by centrifugation (20 minutes at 5000 x g).
- *Lysis and affinity column purification*
    - Thaw pellets, and resuspend in Buffer A with DTT/BH4. I use a Dounce homogenizer to get rid of big clumps before homogenization.

- Four passes through the homogenizer at 20k psi. The lysis reaction will be a little darker red than the resuspension. Pre- and post-wash with Buffer A or B to get all of the lysate out of the instrument.
- Spin the lysate in as many tubes as necessary for 1 hour at 18,000 x g (at 4 C).
- While centrifuging, equilibrate glutathione agarose resin with Buffer B. I use about 10 mL of slurry (8 mL bed volume) for one prep. Equilibrate with at least 10 bed volumes of Buffer B.
- Incubate the soluble fraction of the lysate with the equilibrated resin, rocking at 4 C for 30 minutes.
- Collect column flow through, and save for gel fractions or re-purification. Wash the GST-eNOS bound column with ~100 mL Buffer B. Save this fraction for gel analysis. Save some volume of Buffer B in the column after wash (~35 mL works best).
- Resuspend the resin in the leftover wash buffer, and transfer to a 50 mL conical tube. Add 200 U thrombin and nutate overnight at room temperature for cleavage of the eNOSox from the GST tag.
- Elute the thrombin cleaved protein. Rinse the glutathione agarose with at least one bed volume of buffer B.
- Equilibrate 1.25 mL benzamidine agarose for every 300 units of thrombin with Buffer B. Incubate thrombin eluate with benzamidine agarose for 30 minutes at RT on the nutator. Elute the eNOSox, rinse the benzamidine agarose with one bed volume of Buffer B.
- Bring the NaCl concentration of the thrombin eluted proteins to 0.4 M (double what it is now).

- *Concentration and SEC*

- Concentrate eNOS-containing eluate to about 1.5 mL in a 30K MWCO centrifuge filter (keep centrifuge at 4 C). Protein should be reddish-brown in color when very concentrated.
- Run a size exclusion column (Superdex 200 is good column) to isolate 50 kDa eNOSox band. Concentrate fractions, repeat as needed.

- *Buffers Used*
  - Buffer A
    - 25 mM Tris-Cl pH 7.4
    - 0.2 M NaCl
    - 4 mM DTT
    - 1 mM EDTA
    - 10 uM H_4biopterin
    - add protease inhibitor, H_4biopterin/DTT just before use
  - Buffer B / SEC buffer
    - 25 mM Tris-Cl pH 7.4
    - 0.2 M NaCl
    - 4 mM DTT
    - 1 uM H_4biopterin
  - Make stock aliquots of DTT/H_4biopterin (to preserve H_4biopterin from oxidation), keep frozen and thaw before use

IF staining of PFA fixed, paraffin embedded tissues

SK 11/19/2018

Adapted from Isakson lab protocol, Missy's protocols

Solutions needed:

1. Blocking/Antibody solution
    a. 9.0 mL PBS
    b. 500 uL serum from secondary antibody animal
    c. 25 uL Triton X-100
    d. 500 uL Gelatin from cold water fish skin
2. 1x PBS (at least 200 mL)
3. PBS + FSG +Tween
    a. 500 mL PBS
    b. 3g Gelatin from cold water fish skin
    c. 500 uL Tween 20 (0.1%)

Paraffin removal

1. Take samples through Histoclear bath, 3x 10 min each
2. Rehydrate samples through EtOH gradient
    a. 100% EtOH 2x 3 min
    b. 95% EtOH 2x 3 min
    c. 70% EtOH 1 x 3 min
    d. 100% dI H_2O 1x 20 min
3. While sample is in H_2O, prepare antigen retrieval solution

Antigen Retrieval

1. Prepare solution as per bottle instructions
    a. Vector ® antigen retrieval solutions stored in general use 4C
    b. Citrate based: 2.4 mL into 250 mL dI H_2O
    c. Tris Based: ~10 mL into 250 mL (check that with instructions?)
2. Fill rest of slide rack with blank slides for weight and heat capacity, put slides into new bath with antigen retrieval solution filled
3. Microwave in small container (to catch boil over) with lid cocked on bath
    a. 2 min at medium high power
    b. wait 1 min, refill solution as needed
    c. 2 min at medium high power
    d. wait 1 min, refill solution
    e. 2 min at medium power
    f. wait 2 min
    g. 2 min at medium power
    h. Incubate hot in microwave for 20 minutes
4. Put into 4C for 30 min to cool
5. After cooling, take out of antigen retrieval and replace with room temp PBS, 5 min

Blocking and antibody incubation

1. Dry off back, front of slide (around the sections, without touching them) with the corner of a paper towel
2. Aspirate any remaining liquid with vacuum/P1000 tip
3. Draw lines around sections with Immunopen
4. Let dry for ~ 10 sec, then add blocking solution to cover sections
5. Make a nice bubble!
6. Block for 30 min
7. Mix antibodies in same solution
8. Aspirate blocking solution with vacuum/P1000, replace with primary antibody
9. Overnight at 4C (cold room is best – no shaking from fridge door)

Secondary Antibody

1. Aspirate primary antibody with vacuum/P1000
2. Wash slides in rack with PBS/FSG/Tween ~200 mL, 5 min, room temp, no shaking
3. Transfer to PBS, 5 min, room temp, no shaking
4. Secondary antibody onto sections as needed for 1 hour at room temp, in dark
5. Aspirate secondary antibody with vacuum/P1000
6. Wash slides in rack with PBS/FSG/Tween, 5 min, room temp, no shaking
7. Transfer to PBS 5 min, room temp, no shaking

Mounting slides

**helpful to cut P200 tips at first line to make pipetting viscous mounting media easier*

1. Dry off back, front of slides with corner of paper towel
2. Aspirate excess solution with vacuum/P1000
3. Pull up ~60 uL “ProLong Gold Antifade Mounting Media with DAPI” into cut P200 tip
4. Drop “ProLong Gold Antifade Mounting Media with DAPI” onto slide for each section – do not want to put this directly on section (avoid bubbles), but cut a small drop just off the section so that it spreads to cover it
5. Do not touch the tip to the slide – avoid contamination
6. Once all sections have been covered by mounting media, add cover slide, avoiding trapping bubbles
    a. Start with one side down, slowly lower other side onto slide
    b. If bubbles are trapped on section, use P10 tip to apply pressure and squeeze them away from section
7. After mounting media cures in the dark at room tempfor about 1-2 hours, outline coverslip with nail polish and store slides at 4 C until use

Crosslinking, In Gel Digestion, and MALDI-MS

Adapted from Thermo Scientific EDC Protocol, A. Shevchenko et.al "In gel digestion for mass spectrometric characterization of proteins and proteomes" Nature Protocols (2006), and Bruker Guide to MALDI Sample Preparation

T.C. Stevenson Keller IV, compiled 10/17/18

Crosslinking protocol:

1. Equilibrate EDC to room temperature from -20C storage. Fully equilibrate before opening bottle.
    a. Conjugation buffer is 0.1 M MES (2-[N-morpholino]ethane sulfonic acid], pH 6
    b. EDC will be used in small quantity
2. Use approximately 1 mg of carrier protein
    a. In this case, eNOSox purified from E. coli cell lysates
    b. Note: 1mg/mL eNOSox (48.6 kDa) is about 20nM eNOS
    c. 200 uL of this is used in the solution
3. Using about a 10 fold excess of the peptide
    a. HbαX-tat is about 2kDa
    b. 2 uL of 2uM peptide is used in the reaction
4. Reaction mixture
    a. 200uL MES conjugation buffer
    b. 200uL eNOSox protein solution
    c. 2uL tat-HbαX peptide solution
5. Dissolve 10 mg of EDC in 1 mL of ultrapure H2O, and add 100uL immediately to the reaction mixture. Let the samples react at room temperature for 2 hours with gentle nutation

6. After reaction, prepare samples for electrophoresis, and freeze other quantity (-20C)

In Gel Digestion:

1. Solutions needed
    a. 100 mM ammonium bicarbonate buffer in ultrapure water
        i. Make this solution fresh for each day
        ii. Dissolve 0.3953 g of ammonium bicarbonate in 50 mL total volume of H2O
    b. Protease
        i. Prepare a solution of 13 ng/uL protease in 10mM ammonium bicarbonate containing 10% (v/v) acetonitrile.
2. Run gel, stain, destain, and let gel rinse in distilled H2O for a few hours after electrophoresis
3. Transfer gel to laminar flow hood, onto light box, so bands are clearly visible. Excise bands
    a. For eNOSox, there will be a band at ~50 kDa, corresponding to monomer, and ~100 kDa for the dimer. The dimer band is what I think is the most relevant for these experiments.
    b. Be very careful to minimize keratin contamination of the sample. Only open bag with razor blade, tubes, etc. in the hood. Wear gloves.
    c. Cut each band into about 1 x 1 x 1mm cubes. Transfer contents of each band into a 2 mL microcentrifuge tube (shallow bottom vs 1.5 mL)
4. Destain the gel pieces

a. Add enough to cover the gel pieces (“one volume”, usually 200 uL or less) of 100 mM ammonium bicarbonate/acetonitrile (1:1, v/v), and incubate with occasional vortexing for 30 min.
b. After destain, add 5 volumes of neat acetonitrile and incubate at room temperature with occasional vortexing for another 15 or so minutes. The gel pieces will become white and shrink. After shrinkage, most of the Coomassie staining should be removed, though it is not necessary to remove all stain.
c. Remove the acetonitrile solution from the gel pieces. These can be stored for a few weeks at -20C, or used immediately.

5. Saturate the gel pieces with protease
    a. Add enough protease-containing buffer to cover the dry gel pieces (usually 100 uL or so). Leave on ice for 30 min.
    b. After that half hour, check if all solution was absorbed and add more protease buffer if necessary. Gel pieces should be completely covered.
    c. Leave the gel pieces on ice for another 90 minutes to ensure saturation with protease. Although the gel pieces may not absorb more buffer after 30 minutes, a longer time increases protease penetration in the gel matrix and increases yield.
    d. Add 10-20 uL of ammonium bicarbonate buffer to cover the gel pieces and decrease protease evaporation.
6. Digestion
    a. Leave the tubes in a 37C (or other temperature, as required) incubator overnight.
    b. After ON incubation, chill tubes to room temperature. A small sample can be used for MALDI MS experiment.

c. Otherwise, freeze digestion samples for a few months at -20C before extraction for other MS analysis.

7. Extraction
    a. Add 2x (volume of trypsin buffer) of extraction buffer (1:2 v/v 5% formic acid/acetonitrile) to each tube and incubate 15 mins at 37C in a shaker.
    b. Aspirate the solution with a gel loading tip to prevent picking up gel pieces in the extracted sample.

MALDI-MS:

Samples are in an acetonitrile-heavy buffer after digestion. This will work for MALDI analysis. Better results can be obtained with a C18 Zip Tip.

1. Aliquot the elution buffer into clean tube
    a. 4 uL of 60% acetonitrile, 0.1% formic acid in H2O
2. Equilibrate ziptip – set the pipetteman to 10 uL
    a. Pipette up and discard in waste:
        i. 3x with 100% acetonitrile
        ii. 3x with 0.1% formic acid
3. Load the sample
    a. Pipette up and down in sample
        i. 10x (discarding back into the sample tube)
4. Wash the ziptip
    a. Pipette up and discard into waste
        i. 6x with 0.1% formic acid
5. Elute the sample
    a. Pipette up and down in elution buffer
        i. 10x with elution buffer (above)

Samples are ready for MALDI. Deposit on plate 0.9 uL (**sample first**). Mix in matrix 0.9 uL (***hydroxycinnamic acid*** for peptide). Let dry, follow instructions of MALDI instrument.

Hba1Δ36-39 mouse genotyping

SK 09/24/2018

Digest tail/clean up DNA

1. Store clipped tails at -20 at least overnight
2. Add ~500 uL tail lysis buffer +5 uL Proteinase K (at 19mg/mL) to each tube containing tail.
3. Incubate at 56C overnight (water bath or incubator shaker)
4. Vortex briefly (~0.5s)
5. Spin 5 min, 14k rpm. Label new tubes with mouse #s.
6. Transfer supernatant to new, labeled tube. Add 500 uL isopropanol (equal volume).
7. Mix to precipitate.
8. Spin 5 min at 14k rpm. Precipitated DNA will pellet.
9. Pull off supernatant. Wash with 70% EtOH – inverting a few times is sufficient. Spin at 14k rpm.
10. Add 250 uL of pure H_2O – incubate at 56C for a few minutes to dissolve DNA. Flick to resuspend.
11. Nanodrop, ready for PCR.

PCR protocol

Following onetaq PCR protocol on card

1. Master mix following recipe on card
2. Nested Primers (Nest FWD and Nest REV)
3. PCR protocol – annealing step at 50C

References

1. J. E. Hall, A. C. Guyton, M. W. Brands, Pressure-volume regulation in hypertension. *Kidney International Supplement*, (1996).
2. E. D. Taco-Vasquez *et al.*, Association between Blood Viscosity and Cardiovascular Risk Factors in Patients with Arterial Hypertension in a High Altitude Setting. *Cureus* **11**, (2019).
3. G. Grassi, Assessment of sympathetic cardiovascular drive in human hypertension: achievements and perspectives. *Hypertension* **54**, 690-697 (2009).
4. M. L. Muiesan, M. Salvetti, C. A. Rosei, A. Paini, Gender differences in antihypertensive treatment: myths or legends? *High Blood Pressure & Cardiovascular Prevention* **23**, 105-113 (2016).
5. M. Barton, M. R. Meyer, Postmenopausal hypertension: mechanisms and therapy. *Hypertension* **54**, 11-18 (2009).
6. L. J. Ignarro, Nitric oxide: a unique endogenous signaling molecule in vascular biology. *Biosci Rep* **19**, 51-71 (1999).
7. L. J. Ignarro, G. Cirino, A. Casini, C. Napoli, Nitric oxide as a signaling molecule in the vascular system: an overview. *J Cardiovasc Pharmacol* **34**, 879-886 (1999).
8. L. J. Roman, P. Martásek, B. S. Masters, Intrinsic and extrinsic modulation of nitric oxide synthase activity. *Chem Rev* **102**, 1179-1190 (2002).
9. N. Volkmann *et al.*, Holoenzyme structures of endothelial nitric oxide synthase - an allosteric role for calmodulin in pivoting the FMN domain for electron transfer. *J Struct Biol* **188**, 46-54 (2014).
10. M. Piazza, V. Taiakina, S. R. Guillemette, J. G. Guillemette, T. Dieckmann, Solution structure of calmodulin bound to the target peptide of endothelial nitric oxide synthase phosphorylated at Thr495. *Biochemistry* **53**, 1241-1249 (2014).
11. M. G. Campbell, B. C. Smith, C. S. Potter, B. Carragher, M. A. Marletta, Molecular architecture of mammalian nitric oxide synthases. *Proceedings of the National Academy of Sciences* **111**, E3614-E3623 (2014).
12. B. R. Crane *et al.*, Structure of nitric oxide synthase oxygenase dimer with pterin and substrate. *Science* **279**, 2121-2126 (1998).
13. P. F. Chen, A. L. Tsai, K. K. Wu, Cysteine 184 of endothelial nitric oxide synthase is involved in heme coordination and catalytic activity. *The Journal of biological chemistry* **269**, 25062-25066 (1994).
14. P. F. Chen, A. L. Tsai, K. K. Wu, Cysteine 99 of endothelial nitric oxide synthase (NOS-III) is critical for tetrahydrobiopterin-dependent NOS-III stability and activity. *Biochem Biophys Res Commun* **215**, 1119-1129 (1995).
15. T. O. Fischmann *et al.*, Structural characterization of nitric oxide synthase isoforms reveals striking active-site conservation. *Nat Struct Biol* **6**, 233-242 (1999).
16. G. R. Hellermann, L. P. Solomonson, Calmodulin promotes dimerization of the oxygenase domain of human endothelial nitric-oxide synthase. *J Biol Chem* **272**, 12030-12034 (1997).
17. P. Lane, S. S. Gross, The autoinhibitory control element and calmodulin conspire to provide physiological modulation of endothelial and neuronal nitric oxide synthase activity. *Acta Physiol Scand* **168**, 53-63 (2000).
18. P. Lane, S. S. Gross, Disabling a C-terminal autoinhibitory control element in endothelial nitric-oxide synthase by phosphorylation provides a molecular explanation for activation of vascular NO synthesis by diverse physiological stimuli. *The Journal of biological chemistry* **277**, 19087-19094 (2002).

19. E. D. Garcin *et al.*, Structural basis for isozyme-specific regulation of electron transfer in nitric-oxide synthase. *The Journal of biological chemistry* **279**, 37918-37927 (2004).
20. P. Prabhakar, V. Cheng, T. Michel, A chimeric transmembrane domain directs endothelial nitric-oxide synthase palmitoylation and targeting to plasmalemmal caveolae. *The Journal of biological chemistry* **275**, 19416-19421 (2000).
21. C. Fernández-Hernando *et al.*, Identification of Golgi-localized acyl transferases that palmitoylate and regulate endothelial nitric oxide synthase. *J Cell Biol* **174**, 369-377 (2006).
22. S. S. Segal, S. E. Brett, W. C. Sessa, Codistribution of NOS and caveolin throughout peripheral vasculature and skeletal muscle of hamsters. *Am. J. Physiol.* **277**, 1167-1177 (1999).
23. H. Ju, R. Zou, V. J. Venema, R. C. Venema, Direct interaction of endothelial nitric-oxide synthase and caveolin-1 inhibits synthase activity. *The Journal of biological chemistry* **272**, 18522-18525 (1997).
24. H. Xu *et al.*, A heat shock protein 90 binding domain in endothelial nitric-oxide synthase influences enzyme function. *The Journal of biological chemistry* **282**, 37567-37574 (2007).
25. M. I. Lin *et al.*, Phosphorylation of threonine 497 in endothelial nitric-oxide synthase coordinates the coupling of L-arginine metabolism to efficient nitric oxide production. *The Journal of biological chemistry* **278**, 44719-44726 (2003).
26. S. Takahashi, M. E. Mendelsohn, Synergistic activation of endothelial nitric-oxide synthase (eNOS) by HSP90 and Akt: calcium-independent eNOS activation involves formation of an HSP90-Akt-CaM-bound eNOS complex. *The Journal of biological chemistry* **278**, 30821-30827 (2003).
27. J. Dedio *et al.*, NOSIP, a novel modulator of endothelial nitric oxide synthase activity. *FASEB J* **15**, 79-89 (2001).
28. K. Matsumoto *et al.*, The ECS(SPSB) E3 ubiquitin ligase is the master regulator of the lifetime of inducible nitric-oxide synthase. *Biochem Biophys Res Commun* **409**, 46-51 (2011).
29. D. Kondrikov, S. Elms, D. Fulton, Y. Su, eNOS-beta-actin interaction contributes to increased peroxynitrite formation during hyperoxia in pulmonary artery endothelial cells and mouse lungs. *The Journal of biological chemistry* **285**, 35479-35487 (2010).
30. D. Kondrikov *et al.*, Beta-actin association with endothelial nitric-oxide synthase modulates nitric oxide and superoxide generation from the enzyme. *The Journal of biological chemistry* **285**, 4319-4327 (2010).
31. N. Matsuda, Y. Hayashi, Y. Takahashi, Y. Hattori, Phosphorylation of endothelial nitric-oxide synthase is diminished in mesenteric arteries from septic rabbits depending on the altered phosphatidylinositol 3-kinase/Akt pathway: reversal effect of fluvastatin therapy. *J Pharmacol Exp Ther* **319**, 1348-1354 (2006).
32. B. C. Kone, T. Kuncewicz, W. Zhang, Z. Y. Yu, Protein interactions with nitric oxide synthases: controlling the right time, the right place, and the right amount of nitric oxide. *Am J Physiol Renal Physiol* **285**, F178-190 (2003).
33. D. Kondrikov, S. Elms, D. Fulton, Y. Su, eNOS-β-actin interaction contributes to increased peroxynitrite formation during hyperoxia in pulmonary artery endothelial cells and mouse lungs. *Journal of Biological Chemistry* **285**, 35479-35487 (2010).
34. D. Kondrikov *et al.*, β-Actin association with endothelial nitric-oxide synthase modulates nitric oxide and superoxide generation from the enzyme. *Journal of Biological Chemistry* **285**, 4319-4327 (2010).

35. A. C. Straub *et al.*, Hemoglobin alpha/eNOS coupling at myoendothelial junctions is required for nitric oxide scavenging during vasoconstriction. *Arteriosclerosis, thrombosis, and vascular biology* **34**, 2594-2600 (2014).
36. J. T. Butcher, T. Johnson, J. Beers, L. Columbus, B. E. Isakson, Hemoglobin alpha in the blood vessel wall. *Free radical biology & medicine* **73**, 136-142 (2014).
37. Y. Bian *et al.*, An enzyme assisted RP-RPLC approach for in-depth analysis of human liver phosphoproteome. *J Proteomics* **96**, 253-262 (2014).
38. B. J. Michell *et al.*, Identification of regulatory sites of phosphorylation of the bovine endothelial nitric-oxide synthase at serine 617 and serine 635. *The Journal of biological chemistry* **277**, 42344-42351 (2002).
39. M. B. Harris *et al.*, Acute activation and phosphorylation of endothelial nitric oxide synthase by HMG-CoA reductase inhibitors. *American journal of physiology. Heart and circulatory physiology* **287**, H560-566 (2004).
40. P. M. Bauer *et al.*, Compensatory phosphorylation and protein-protein interactions revealed by loss of function and gain of function mutants of multiple serine phosphorylation sites in endothelial nitric-oxide synthase. *The Journal of biological chemistry* **278**, 14841-14849 (2003).
41. Y. C. Boo *et al.*, Endothelial NO synthase phosphorylated at SER635 produces NO without requiring intracellular calcium increase. *Free radical biology & medicine* **35**, 729-741 (2003).
42. Y. C. Boo *et al.*, Shear stress stimulates phosphorylation of endothelial nitric-oxide synthase at Ser1179 by Akt-independent mechanisms: role of protein kinase A. *J Biol Chem* **277**, 3388-3396 (2002).
43. M. B. Harris *et al.*, Reciprocal phosphorylation and regulation of endothelial nitric-oxide synthase in response to bradykinin stimulation. *The Journal of biological chemistry* **276**, 16587-16591 (2001).
44. M. Montagnani, H. Chen, V. A. Barr, M. J. Quon, Insulin-stimulated activation of eNOS is independent of Ca2+ but requires phosphorylation by Akt at Ser(1179). *J Biol Chem* **276**, 30392-30398 (2001).
45. P. F. Mount, B. E. Kemp, D. A. Power, Regulation of endothelial and myocardial NO synthesis by multi-site eNOS phosphorylation. *J Mol Cell Cardiol* **42**, 271-279 (2007).
46. B. G. Drew, N. H. Fidge, G. Gallon-Beaumier, B. E. Kemp, B. A. Kingwell, High-density lipoprotein and apolipoprotein AI increase endothelial NO synthase activity by protein association and multisite phosphorylation. *Proceedings of the National Academy of Sciences of the United States of America* **101**, 6999-7004 (2004).
47. D. Fulton *et al.*, Src kinase activates endothelial nitric-oxide synthase by phosphorylating Tyr-83. *The Journal of biological chemistry* **280**, 35943-35952 (2005).
48. D. Fulton *et al.*, Agonist-stimulated endothelial nitric oxide synthase activation and vascular relaxation. Role of eNOS phosphorylation at Tyr83. *Circ Res* **102**, 497-504 (2008).
49. R. Kou, D. Greif, T. Michel, Dephosphorylation of endothelial nitric-oxide synthase by vascular endothelial growth factor. Implications for the vascular responses to cyclosporin A. *J Biol Chem* **277**, 29669-29673 (2002).
50. E. H. Heiss, V. M. Dirsch, Regulation of eNOS enzyme activity by posttranslational modification. *Curr Pharm Des* **20**, 3503-3513 (2014).
51. G. K. Kolluru, J. H. Siamwala, S. Chatterjee, eNOS phosphorylation in health and disease. *Biochimie* **92**, 1186-1198 (2010).
52. C. Li *et al.*, Role of eNOS phosphorylation at Ser-116 in regulation of eNOS activity in endothelial cells. *Vascul Pharmacol* **47**, 257-264 (2007).

53. L. Ruan *et al.*, Pin1 prolyl isomerase regulates endothelial nitric oxide synthase. *Arteriosclerosis, thrombosis, and vascular biology* **31**, 392-398 (2011).
54. B. J. Michell *et al.*, Coordinated control of endothelial nitric-oxide synthase phosphorylation by protein kinase C and the cAMP-dependent protein kinase. *The Journal of biological chemistry* **276**, 17625-17628 (2001).
55. Z. P. Chen *et al.*, AMP-activated protein kinase phosphorylation of endothelial NO synthase. *FEBS Lett* **443**, 285-289 (1999).
56. M. Matsubara, N. Hayashi, T. Jing, K. Titani, Regulation of endothelial nitric oxide synthase by protein kinase C. *J Biochem* **133**, 773-781 (2003).
57. M. Aoyagi, A. S. Arvai, J. A. Tainer, E. D. Getzoff, Structural basis for endothelial nitric oxide synthase binding to calmodulin. *EMBO J* **22**, 766-775 (2003).
58. B. Fisslthaler, A. E. Loot, A. Mohamed, R. Busse, I. Fleming, Inhibition of endothelial nitric oxide synthase activity by proline-rich tyrosine kinase 2 in response to fluid shear stress and insulin. *Circulation research* **102**, 1520-1528 (2008).
59. I. Fleming, B. Fisslthaler, S. Dimmeler, B. E. Kemp, R. Busse, Phosphorylation of Thr(495) regulates Ca(2+)/calmodulin-dependent endothelial nitric oxide synthase activity. *Circ Res* **88**, E68-75 (2001).
60. A. E. Loot, J. G. Schreiber, B. Fisslthaler, I. Fleming, Angiotensin II impairs endothelial function via tyrosine phosphorylation of the endothelial nitric oxide synthase. *The Journal of experimental medicine* **206**, 2889-2896 (2009).
61. C. Nathan, Nitric oxide as a secretory product of mammalian cells. *FASEB journal : official publication of the Federation of American Societies for Experimental Biology* **6**, 3051-3064 (1992).
62. M. Billaud *et al.*, Regulation of cellular communication by signaling microdomains in the blood vessel wall. *Pharmacol Rev* **66**, 513-569 (2014).
63. P. Prabhakar *et al.*, Receptor-regulated translocation of endothelial nitric-oxide synthase. *The Journal of biological chemistry* **273**, 27383-27388 (1998).
64. W. C. Sessa, C. M. Barber, K. R. Lynch, Mutation of N-myristoylation site converts endothelial cell nitric oxide synthase from a membrane to a cytosolic protein. *Circulation research* **72**, 921-924 (1993).
65. G. Garcia-Cardena, P. Oh, J. Liu, J. E. Schnitzer, W. C. Sessa, Targeting of nitric oxide synthase to endothelial cell caveolae via palmitoylation: implications for nitric oxide signaling. *Proceedings of the National Academy of Sciences of the United States of America* **93**, 6448-6453 (1996).
66. P. W. Shaul *et al.*, Acylation targets emdothelial nitric-oxide synthase to plasmalemmal caveolae. *The Journal of biological chemistry* **271**, 6518-6522 (1996).
67. J. Liu, G. Garcia-Cardena, W. C. Sessa, Palmitoylation of endothelial nitric oxide synthase is necessary for optimal stimulated release of nitric oxide: implications for caveolae localization. *Biochemistry* **35**, 13277-13281 (1996).
68. A. Blair, P. W. Shaul, I. S. Yuhanna, P. A. Conrad, E. J. Smart, Oxidized low density lipoprotein displaces endothelial nitric-oxide synthase (eNOS) from plasmalemmal caveolae and impairs eNOS activation. *The Journal of biological chemistry* **274**, 32512-32519 (1999).
69. J. Igarashi, H. S. Thatte, P. Prabhakar, D. E. Golan, T. Michel, Calcium-independent activation of endothelial nitric oxide synthase by ceramide. *Proceedings of the National Academy of Sciences of the United States of America* **96**, 12583-12588 (1999).

70. W. C. Sessa *et al.*, The Golgi association of endothelial nitric oxide synthase is necessary for the efficient synthesis of nitric oxide. *The Journal of biological chemistry* **270**, 17641-17644 (1995).
71. D. Fulton *et al.*, Targeting of endothelial nitric-oxide synthase to the cytoplasmic face of the Golgi complex or plasma membrane regulates Akt- versus calcium-dependent mechanisms for nitric oxide release. *The Journal of biological chemistry* **279**, 30349-30357 (2004).
72. L. J. Andries, D. L. Brutsaert, S. U. Sys, Nonuniformity of endothelial constitutive nitric oxide synthase distribution in cardiac endothelium. *Circulation research* **82**, 195-203 (1998).
73. L. Wagner, J. G. Hoey, A. Erdely, M. A. Boegehold, C. Baylis, The nitric oxide pathway is amplified in venular vs arteriolar cultured rat mesenteric endothelial cells. *Microvasc Res* **62**, 401-409 (2001).
74. M. A. Broeders, G. J. Tangelder, D. W. Slaaf, R. S. Reneman, M. G. oude Egbrink, Endogenous nitric oxide protects against thromboembolism in venules but not in arterioles. *Arterioscler Thromb Vasc Biol* **18**, 139-145 (1998).
75. E. N. Bakker, P. Sipkema, Components of acetylcholine-induced dilation in isolated rat arterioles. *The American journal of physiology* **273**, H1848-1853 (1997).
76. M. Billaud *et al.*, Characterization of the thoracodorsal artery: morphology and reactivity. *Microcirculation* **19**, 360-372 (2012).
77. A. Koller, Z. Bagi, Nitric oxide and H2O2 contribute to reactive dilation of isolated coronary arterioles. *American journal of physiology. Heart and circulatory physiology* **287**, H2461-2467 (2004).
78. A. Koller, D. Sun, E. J. Messina, G. Kaley, L-arginine analogues blunt prostaglandin-related dilation of arterioles. *The American journal of physiology* **264**, H1194-1199 (1993).
79. J. J. Hwa, L. Ghibaudi, P. Williams, M. Chatterjee, Comparison of acetylcholine-dependent relaxation in large and small arteries of rat mesenteric vascular bed. *The American journal of physiology* **266**, H952-958 (1994).
80. L. Luksha, S. Agewall, K. Kublickiene, Endothelium-derived hyperpolarizing factor in vascular physiology and cardiovascular disease. *Atherosclerosis* **202**, 330-344 (2009).
81. Y. Nishikawa, D. W. Stepp, W. M. Chilian, In vivo location and mechanism of EDHF-mediated vasodilation in canine coronary microcirculation. *The American journal of physiology* **277**, H1252-1259 (1999).
82. H. Shimokawa *et al.*, The importance of the hyperpolarizing mechanism increases as the vessel size decreases in endothelium-dependent relaxations in rat mesenteric circulation. *J Cardiovasc Pharmacol* **28**, 703-711 (1996).
83. T. Nagao, S. Illiano, P. M. Vanhoutte, Heterogeneous distribution of endothelium-dependent relaxations resistant to NG-nitro-L-arginine in rats. *The American journal of physiology* **263**, H1090-1094 (1992).
84. R. A. Cohen *et al.*, Nitric oxide is the mediator of both endothelium-dependent relaxation and hyperpolarization of the rabbit carotid artery. *Proceedings of the National Academy of Sciences of the United States of America* **94**, 4193-4198 (1997).
85. T. Chataigneau *et al.*, Acetylcholine-induced relaxation in blood vessels from endothelial nitric oxide synthase knockout mice. *British journal of pharmacology* **126**, 219-226 (1999).

86. C. J. Garland, F. Plane, B. K. Kemp, T. M. Cocks, Endothelium-dependent hyperpolarization: a role in the control of vascular tone. *Trends in pharmacological sciences* **16**, 23-30 (1995).
87. P. V. Guillot *et al.*, A vascular bed-specific pathway. *The Journal of clinical investigation* **103**, 799-805 (1999).
88. D. M. Dudzinski, T. Michel, Life history of eNOS: partners and pathways. *Cardiovascular research* **75**, 247-260 (2007).
89. J. Qian, D. Fulton, Post-translational regulation of endothelial nitric oxide synthase in vascular endothelium. *Frontiers in physiology* **4**, 347 (2013).
90. T. Michel, G. K. Li, L. Busconi, Phosphorylation and subcellular translocation of endothelial nitric oxide synthase. *Proceedings of the National Academy of Sciences of the United States of America* **90**, 6252-6256 (1993).
91. C. F. Lam *et al.*, Increased blood flow causes coordinated upregulation of arterial eNOS and biosynthesis of tetrahydrobiopterin. *American journal of physiology. Heart and circulatory physiology* **290**, H786-793 (2006).
92. Y. S. Chatzizisis *et al.*, Role of endothelial shear stress in the natural history of coronary atherosclerosis and vascular remodeling: molecular, cellular, and vascular behavior. *Journal of the American College of Cardiology* **49**, 2379-2393 (2007).
93. D. Lu, G. S. Kassab, Role of shear stress and stretch in vascular mechanobiology. *Journal of the Royal Society, Interface / the Royal Society* **8**, 1379-1385 (2011).
94. R. S. Reneman, A. P. Hoeks, Wall shear stress as measured in vivo: consequences for the design of the arterial system. *Medical & biological engineering & computing* **46**, 499-507 (2008).
95. R. S. Reneman, T. Arts, A. P. Hoeks, Wall shear stress--an important determinant of endothelial cell function and structure--in the arterial system in vivo. Discrepancies with theory. *Journal of vascular research* **43**, 251-269 (2006).
96. C. Cheng *et al.*, Shear stress affects the intracellular distribution of eNOS: direct demonstration by a novel in vivo technique. *Blood* **106**, 3691-3698 (2005).
97. M. B. Dancu, J. M. Tarbell, Coronary endothelium expresses a pathologic gene pattern compared to aortic endothelium: correlation of asynchronous hemodynamics and pathology in vivo. *Atherosclerosis* **192**, 9-14 (2007).
98. X. Guo, G. S. Kassab, Role of shear stress on nitrite and NOS protein content in different size conduit arteries of swine. *Acta physiologica* **197**, 99-106 (2009).
99. M. H. Laughlin, J. R. Turk, W. G. Schrage, C. R. Woodman, E. M. Price, Influence of coronary artery diameter on eNOS protein content. *American journal of physiology. Heart and circulatory physiology* **284**, H1307-1312 (2003).
100. F. A. Sanchez *et al.*, Functional significance of differential eNOS translocation. *American journal of physiology. Heart and circulatory physiology* **291**, H1058-1064 (2006).
101. Y. Iwakiri *et al.*, Nitric oxide synthase generates nitric oxide locally to regulate compartmentalized protein S-nitrosylation and protein trafficking. *Proceedings of the National Academy of Sciences of the United States of America* **103**, 19777-19782 (2006).
102. J. Qian *et al.*, Role of local production of endothelium-derived nitric oxide on cGMP signaling and S-nitrosylation. *American journal of physiology. Heart and circulatory physiology* **298**, H112-118 (2010).
103. A. C. Straub *et al.*, Endothelial cell expression of haemoglobin alpha regulates nitric oxide signalling. *Nature* **491**, 473-477 (2012).
104. A. C. Straub, A. C. Zeigler, B. E. Isakson, The myoendothelial junction: connections that deliver the message. *Physiology* **29**, 242-249 (2014).

105. A. C. Straub *et al.*, Compartmentalized connexin 43 s-nitrosylation/denitrosylation regulates heterocellular communication in the vessel wall. *Arteriosclerosis, thrombosis, and vascular biology* **31**, 399-407 (2011).
106. S. L. Sandow, C. E. Hill, Incidence of myoendothelial gap junctions in the proximal and distal mesenteric arteries of the rat is suggestive of a role in endothelium-derived hyperpolarizing factor-mediated responses. *Circ Res* **86**, 341-346 (2000).
107. M. H. Zou *et al.*, Modulation by peroxynitrite of Akt- and AMP-activated kinase-dependent Ser1179 phosphorylation of endothelial nitric oxide synthase. *J Biol Chem* **277**, 32552-32557 (2002).
108. M. H. Zou, C. Shi, R. A. Cohen, Oxidation of the zinc-thiolate complex and uncoupling of endothelial nitric oxide synthase by peroxynitrite. *J Clin Invest* **109**, 817-826 (2002).
109. A. A. Miller, G. R. Drummond, H. H. Schmidt, C. G. Sobey, NADPH oxidase activity and function are profoundly greater in cerebral versus systemic arteries. *Circulation research* **97**, 1055-1062 (2005).
110. J. S. Beckman, T. W. Beckman, J. Chen, P. A. Marshall, B. A. Freeman, Apparent hydroxyl radical production by peroxynitrite: implications for endothelial injury from nitric oxide and superoxide. *Proc Natl Acad Sci U S A* **87**, 1620-1624 (1990).
111. S. Dayal *et al.*, Deficiency of glutathione peroxidase-1 sensitizes hyperhomocysteinemic mice to endothelial dysfunction. *Arterioscler Thromb Vasc Biol* **22**, 1996-2002 (2002).
112. G. R. Drummond, H. Cai, M. E. Davis, S. Ramasamy, D. G. Harrison, Transcriptional and posttranscriptional regulation of endothelial nitric oxide synthase expression by hydrogen peroxide. *Circ Res* **86**, 347-354 (2000).
113. S. Wedgwood *et al.*, Increased hydrogen peroxide downregulates soluble guanylate cyclase in the lungs of lambs with persistent pulmonary hypertension of the newborn. *Am J Physiol Lung Cell Mol Physiol* **289**, L660-666 (2005).
114. J. L. Aschner *et al.*, Heat shock protein 90 modulates endothelial nitric oxide synthase activity and vascular reactivity in the newborn piglet pulmonary circulation. *Am J Physiol Lung Cell Mol Physiol* **292**, L1515-1525 (2007).
115. M. Ushio-Fukai *et al.*, Cholesterol depletion inhibits epidermal growth factor receptor transactivation by angiotensin II in vascular smooth muscle cells: role of cholesterol-rich microdomains and focal adhesions in angiotensin II signaling. *J Biol Chem* **276**, 48269-48275 (2001).
116. A. C. Straub, A. C. Zeigler, B. E. Isakson, The myoendothelial junction: connections that deliver the message. *Physiology* **29**, 242-249 (2014).
117. V. Sudhahar, S. Shaw, J. D. Imig, Epoxyeicosatrienoic acid analogs and vascular function. *Current medicinal chemistry* **17**, 1181-1190 (2010).
118. R. Breton-Romero, S. Lamas, Hydrogen peroxide signaling in vascular endothelial cells. *Redox biology* **2**, 529-534 (2014).
119. H. Shimokawa, T. Matoba, Hydrogen peroxide as an endothelium-derived hyperpolarizing factor. *Pharmacological research* **49**, 543-549 (2004).
120. U. Von Euler, On the specific vaso-dilating and plain muscle stimulating substances from accessory genital glands in man and certain animals (prostaglandin and vesiglandin). *The Journal of physiology* **88**, 213-234 (1936).
121. D. H. Evans, M. P. Gunderson, A prostaglandin, not NO, mediates endothelium-dependent dilation in ventral aorta of shark (Squalus acanthias). *American Journal of Physiology-Regulatory, Integrative and Comparative Physiology* **274**, R1050-R1057 (1998).

122. A. Huang, Y. Wu, D. Sun, A. Koller, G. Kaley, Effect of estrogen on flow-induced dilation in NO deficiency: role of prostaglandins and EDHF. *Journal of Applied Physiology* **91**, 2561-2566 (2001).
123. W. Murrell, Nitro-Glycerine in angina pectoris. *Lancet* **1**, 80-81 (1879).
124. N. H. Golwala, C. Hodenette, S. N. Murthy, B. D. Nossaman, P. J. Kadowitz, Vascular responses to nitrite are mediated by xanthine oxidoreductase and mitochondrial aldehyde dehydrogenase in the rat. *Can J Physiol Pharmacol* **87**, 1095-1101 (2009).
125. C. Napoli, L. J. Ignarro, Nitric oxide-releasing drugs. *Annual Review of Pharmacology and Toxicology* **43**, 97-123 (2003).
126. E. D. Robin, R. McCauley, Nitroprusside-related cyanide poisoning. Time (long past due) for urgent, effective interventions. *Chest* **102**, 1842-1845 (1992).
127. P. Klatt *et al.*, Characterization of heme-deficient neuronal nitric-oxide synthase reveals a role for heme in subunit dimerization and binding of the amino acid substrate and tetrahydrobiopterin. *Journal of Biological Chemistry* **271**, 7336-7342 (1996).
128. D. D. Rees, R. M. J. Palmer, R. Schulz, H. F. Hodson, S. Moncada, Characterization of 3 inhibitors of endothelial nitric oxide synthase in vitro and in vivo *British Journal of Pharmacology* **101**, 746-752 (1990).
129. I. RodriguezCrespo, N. C. Gerber, P. R. O. deMontellano, Endothelial nitric-oxide synthase - Expression in Escherichia coli, spectroscopic characterization, and role of tetrahydrobiopterin in dimer formation. *Journal of Biological Chemistry* **271**, 11462-11467 (1996).
130. K. Pant, B. R. Crane, Structure of a loose dimer: an intermediate in nitric oxide synthase assembly. *Journal of Molecular Biology* **352**, 932-940 (2005).
131. N. Sennequier, D. Wolan, D. J. Stuehr, Antifungal imidazoles block assembly of inducible NO synthase into an active dimer. *Journal of Biological Chemistry* **274**, 930-938 (1999).
132. J. S. Paige, S. R. Jaffrey, Pharmacologic Manipulation of Nitric Oxide Signaling: Targeting NOS Dimerization and Protein-Protein Interactions. *Current Topics in Medicinal Chemistry* **7**, 97-114 (2007).
133. A. Broccard *et al.*, Tissue oxygenation and hemodynamic response to NO synthase inhibition in septic shock. *Shock* **14**, 35-40 (2000).
134. J. A. Avontuur, R. P. Tutein Nolthenius, J. W. van Bodegom, H. A. Bruining, Prolonged inhibition of nitric oxide synthesis in severe septic shock: a clinical study. *Crit Care Med* **26**, 660-667 (1998).
135. P. N. Bernatchez *et al.*, Dissecting the molecular control of endothelial NO synthase by caveolin-1 using cell-permeable peptides. *Proceedings of the National Academy of Sciences of the United States of America* **102**, 761-766 (2005).
136. M. Bucci *et al.*, In vivo deliveryof the caveolin-1 scaffolding domain inhibits nitric oxide synthesis and reduces inflammation. *Nature Medicine* **6**, 1362-1367 (2000).
137. S. L. Sellers, A. E. Trane, P. N. Bernatchez, Caveolin as a potential drug target for cardiovascular protection. *Frontiers in physiology* **3**, 280 (2012).
138. A. E. Trane *et al.*, Deciphering the binding of caveolin-1 to client protein endothelial nitric-oxide synthase (eNOS): scaffolding subdomain identification, interaction modeling, and biological significance. *The Journal of biological chemistry* **289**, 13273-13283 (2014).
139. P. Bernatchez, A. Sharma, P. M. Bauer, E. Marin, W. C. Sessa, A noninhibitory mutant of the caveolin-1 scaffolding domain enhances eNOS-derived NO synthesis and vasodilation in mice. *The Journal of clinical investigation* **121**, 3747-3755 (2011).

140. X. Liu *et al.*, Diffusion-limited reaction of free nitric oxide with erythrocytes. *J Biol Chem* **273**, 18709-18713 (1998).
141. A. R. Butler, I. L. Megson, P. G. Wright, Diffusion of nitric oxide and scavenging by blood in the vasculature. *Biochimica et Biophysica Acta (BBA) - General Subjects* **1425**, 168-176 (1998).
142. J. C. Liao, T. W. Hein, M. W. Vaughn, K.-T. Huang, L. Kuo, Intravascular flow decreases erythrocyte consumption of nitric oxide. *PNAS* **96**, 8757-8761 (1999).
143. I. Azarov *et al.*, in *J Biol Chem*. (United States, 2005), vol. 280, pp. 39024-39032.
144. P. Kleinbongard *et al.*, in *Blood*. (United States, 2006), vol. 107, pp. 2943-2951.
145. M. W. Vaughn, K. T. Huang, L. Kuo, J. C. Liao, Erythrocytes possess an intrinsic barrier to nitric oxide consumption. *J Biol Chem* **275**, 2342-2348 (2000).
146. C. Helms, D. B. Kim-Shapiro, Hemoglobin-mediated nitric oxide signaling. *Free Radical Biology and Medicine* **61**, 464-472 (2013).
147. B. C. Jubelin, J. L. Gierman, in *Am J Hypertens*. (United States, 1996), vol. 9, pp. 1214-1219.
148. E. S. Kang *et al.*, in *J Lab Clin Med*. (United States, 2000), vol. 135, pp. 444-451.
149. M. M. Cortese-Krott *et al.*, in *Blood*. (United States, 2012), vol. 120, pp. 4229-4237.
150. K. C. Wood *et al.*, Circulating blood endothelial nitric oxide synthase contributes to the regulation of systemic blood pressure and nitrite homeostasis. *Arterioscler Thromb Vasc Biol* **33**, 1861-1871 (2013).
151. P. Ulker, L. Sati, C. Celik-Ozenci, H. J. Meiselman, O. K. Baskurt, Mechanical stimulation of nitric oxide synthesizing mechanisms in erythrocytes. *Biorheology* **46**, 121-132 (2009).
152. M. Bor-Kucukatay, R. B. Wenby, H. J. Meiselman, O. K. Baskurt, in *Am J Physiol Heart Circ Physiol*. (United States, 2003), vol. 284, pp. H1577-1584.
153. M. M. Cortese-Krott, M. Kelm, Endothelial nitric oxide synthase in red blood cells: Key to a new erythrocrine function? *Redox Biology* **2**, 251-258 (2014).
154. G. Garcia-Cardena, R. Fan, D. F. Stern, J. Liu, W. C. Sessa, Endothelial Nitric Oxide Synthase is Regulated by Tyrosine Phosphorylation and Interacts with Caveolin-1. *The Journal of biological chemistry* **271**, 27237-27240 (1996).
155. D. Fulton *et al.*, Regulation of endothelium-derived nitric oxide production by the protein kinase Akt. *Nature* **399**, 597-601 (1999).
156. Y. Zhao, P. M. Vanhoutte, S. W. Leung, Vascular nitric oxide: Beyond eNOS. *J Pharmacol Sci* **129**, 83-94 (2015).
157. K. Goto, T. Ohtsubo, T. Kitazono, Endothelium-Dependent Hyperpolarization (EDH) in Hypertension: The Role of Endothelial Ion Channels. *Int J Mol Sci* **19**, (2018).
158. G. Edwards, K. A. Dora, M. J. Gardener, C. J. Garland, A. H. Weston, K+ is an endothelium-derived hyperpolarizing factor in rat arteries. *Nature* **396**, 269-272 (1998).
159. C. J. Garland, K. A. Dora, EDH: endothelium-dependent hyperpolarization and microvascular signalling. *Acta Physiol (Oxf)* **219**, 152-161 (2017).
160. D. G. Welsh, S. S. Segal, Role of EDHF in conduction of vasodilation along hamster cheek pouch arterioles in vivo. *Am.J.Physiol Heart Circ.Physiol* **278**, H1832-H1839 (2000).
161. G. Edwards, K. A. Dora, M. J. Gardener, C. J. Garland, A. H. Weston, K+ is an endothelium-derived hyperpolarizing factor in rat arteries. *Nature* **396**, 269 (1998).
162. G. E. Sleek, B. R. Duling, Coordination of mural elements and myofilaments during arteriolar constriction. *Circ Res* **59**, 620-627 (1986).
163. J. A. Rhodin, The ultrastructure of mammalian arterioles and precapillary sphincters. *J Ultrastruct Res* **18**, 181-223 (1967).

164. D. H. Moore, H. Ruska, The fine structure of capillaries and small arteries. *J Biophys Biochem Cytol* **3**, 457-462 (1957).
165. P. S. Clifford *et al.*, Spatial distribution and mechanical function of elastin in resistance arteries: a role in bearing longitudinal stress. *Arterioscler Thromb Vasc Biol* **31**, 2889-2896 (2011).
166. Y. Yashiro, B. R. Duling, Participation of intracellular Ca2+ stores in arteriolar conducted responses. *Am J Physiol Heart Circ Physiol* **285**, H65-73 (2003).
167. A. T. Chaytor, P. E. Martin, D. H. Edwards, T. M. Griffith, Gap junctional communication underpins EDHF-type relaxations evoked by ACh in the rat hepatic artery. *Am J Physiol Heart Circ Physiol* **280**, H2441-2450 (2001).
168. K. A. Dora, M. P. Doyle, B. R. Duling, Elevation of intracellular calcium in smooth muscle causes endothelial cell generation of NO in arterioles. *Proc Natl Acad Sci U S A* **94**, 6529-6534 (1997).
169. S. L. Sandow, D. J. Gzik, R. M. Lee, Arterial internal elastic lamina holes: relationship to function? *J Anat* **214**, 258-266 (2009).
170. V. J. Dzau, M. E. Safar, Large conduit arteries in hypertension: role of the vascular renin-angiotensin system. *Circulation* **77**, 947-954 (1988).
171. K. R. Heberlein, A. C. Straub, B. E. Isakson, The myoendothelial junction: breaking through the matrix? *Microcirculation* **16**, 307-322 (2009).
172. R. Taugner, H. Kirchheim, W. G. Forssmann, Myoendothelial contacts in glomerular arterioles and in renal interlobular arteries of rat, mouse and Tupaia belangeri. *Cell Tissue Res* **235**, 319-325 (1984).
173. R. F. Furchgott, J. V. Zawadzki, The obligatory role of endothelial cells in the relaxation of arterial smooth muscle by acetylcholine. *Nature* **288**, 373-376 (1980).
174. P. L. Huang *et al.*, Hypertension in mice lacking the gene for endothelial nitric oxide synthase. *Nature* **377**, 239-242 (1995).
175. D. D. Rees, R. M. Palmer, H. F. Hodson, S. Moncada, A specific inhibitor of nitric oxide formation from L-arginine attenuates endothelium-dependent relaxation. *Br J Pharmacol* **96**, 418-424 (1989).
176. C. Lechauve *et al.*, Endothelial cell alpha-globin and its molecular chaperone alpha-hemoglobin-stabilizing protein regulate arteriolar contractility. *J Clin Invest* **128**, 5073-5082 (2018).
177. T. C. t. Keller *et al.*, Modulating Vascular Hemodynamics With an Alpha Globin Mimetic Peptide (HbalphaX). *Hypertension* **68**, 1494-1503 (2016).
178. S. R. Johnstone *et al.*, Oxidized phospholipid species promote in vivo differential cx43 phosphorylation and vascular smooth muscle cell proliferation. *Am J Pathol* **175**, 916-924 (2009).
179. F. Faul, E. Erdfelder, A. G. Lang, A. Buchner, G*Power 3: a flexible statistical power analysis program for the social, behavioral, and biomedical sciences. *Behav Res Methods* **39**, 175-191 (2007).
180. F. Faul, E. Erdfelder, A. Buchner, A. G. Lang, Statistical power analyses using G*Power 3.1: tests for correlation and regression analyses. *Behav Res Methods* **41**, 1149-1160 (2009).
181. M. Billaud *et al.*, in *Pharmacological Reviews*. (2014), vol. 66, pp. 513-569.
182. R. E. Haddock *et al.*, Endothelial coordination of cerebral vasomotion via myoendothelial gap junctions containing connexins 37 and 40. *American Journal of Physiology-Heart and Circulatory Physiology* **291**, H2047-H2056 (2006).
183. E. J. Behringer, M. J. Socha, L. Polo-Parada, S. S. Segal, Electrical conduction along endothelial cell tubes from mouse feed arteries: confounding actions of glycyrrhetinic acid derivatives. *British journal of pharmacology* **166**, 774-787 (2012).

184. T. S. Keller *et al.*, Modulating Vascular Hemodynamics With an Alpha Globin Mimetic Peptide (HbαX) Novelty and Significance. *Hypertension* **68**, 1494-1503 (2016).
185. K. R. Heberlein *et al.*, Plasminogen activator inhibitor-1 regulates myoendothelial junction formation. *Circ Res* **106**, 1092-1102 (2010).
186. G. G. Emerson, S. S. Segal, Electrical coupling between endothelial cells and smooth muscle cells in hamster feed arteries: role in vasomotor control. *Circ.Res.* **87**, 474-479 (2000).
187. K. R. Heberlein *et al.*, A novel mRNA binding protein complex promotes localized plasminogen activator inhibitor-1 accumulation at the myoendothelial junction. *Arteriosclerosis, Thrombosis, and Vascular Biology* **32**, 1271-1279 (2012).
188. P. Sangwung *et al.*, Regulation of endothelial hemoglobin alpha expression by Kruppel-like factors. *Vasc Med* **22**, 363-369 (2017).
189. H. Gerhardt, C. Betsholtz, Endothelial-pericyte interactions in angiogenesis. *Cell Tissue Res* **314**, 15-23 (2003).
190. M. T. Rondina, A. S. Weyrich, G. A. Zimmerman, Platelets as cellular effectors of inflammation in vascular diseases. *Circ Res* **112**, 1506-1519 (2013).
191. B. Petri, M. Phillipson, P. Kubes, The physiology of leukocyte recruitment: an in vivo perspective. *J Immunol* **180**, 6439-6446 (2008).
192. R. C. Looft-Wilson, M. Billaud, S. R. Johnstone, A. C. Straub, B. E. Isakson, Interaction between nitric oxide signaling and gap junctions: effects on vascular function. *Biochim Biophys Acta* **1818**, 1895-1902 (2012).
193. D. Fulton, G. J-P., W. C. Sessa, Post-Translational Control of Endothelial Nitric Oxide Synthase: Why Isn't Calcium/Calmodulin Enough? *The Journal of Pharmacology and Experimental Therapeutics* **299**, 818-824 (2001).
194. B. Ning *et al.*, Ultrasound-aided Multi-parametric Photoacoustic Microscopy of the Mouse Brain. *Sci Rep* **5**, 18775 (2015).
195. B. Ning *et al.*, Simultaneous photoacoustic microscopy of microvascular anatomy, oxygen saturation, and blood flow. *Opt Lett* **40**, 910-913 (2015).
196. M. Billaud *et al.*, A molecular signature in the pannexin1 intracellular loop confers channel activation by the α1 adrenoreceptor in smooth muscle cells. *Sci Signal* **8**, ra17 (2015).
197. S. Cechova *et al.*, Loss of collectrin, an angiotensin-converting enzyme 2 homolog, uncouples endothelial nitric oxide synthase and causes hypertension and vascular dysfunction. *Circulation* **128**, 1770-1780 (2013).
198. A. Doctor *et al.*, Hemoglobin conformation couples erythrocyte S-nitrosothiol content to O2 gradients. *Proceedings of the National Academy of Sciences of the United States of America* **102**, 5709-5714 (2005).
199. K. R. Rupprecht, Gordon, G., Lundrigan, M., Gayda, R. C., Markovitz, A., & Earhart, C., ompT: Escherichia coli K-12 Structural Gene for Protein a (3b). *Journal of Bacteriology* **153**, 1104-1106 (1983).
200. E. C. Hulme, M. A. Trevethick, Ligand binding assays at equilibrium: validation and interpretation. *Br J Pharmacol* **161**, 1219-1237 (2010).
201. Y. Wu, Q. Li, X.-Z. Chen, Detecting protein–protein interactions by far western blotting. *Nature protocols* **2**, 3278-3284 (2007).
202. M. Billaud *et al.*, Pannexin1 regulates α1-adrenergic receptor- mediated vasoconstriction. *Circulation research* **109**, 80-85 (2011).
203. L. Wang *et al.*, Hypoxic pulmonary vasoconstriction requires connexin 40-mediated endothelial signal conduction. *The Journal of clinical investigation* **122**, 4218-4230 (2012).

204. Y. M. Yang, A. Huang, G. Kaley, D. Sun, in *AJP: Heart and Circulatory Physiology*. (2009), vol. 297, pp. H1829-H1836.
205. R. M. Touyz, E. L. Schiffrin, Increased generation of superoxide by angiotensin II in smooth muscle cells from resistance arteries of hypertensive patients: role of phospholipase D-dependent NAD (P) H oxidase-sensitive pathways. *Journal of hypertension* **19**, 1245-1254 (2001).
206. S. Rajagopalan *et al.*, Angiotensin II-mediated hypertension in the rat increases vascular superoxide production via membrane NADH/NADPH oxidase activation. Contribution to alterations of vasomotor tone. *Journal of Clinical Investigation* **97**, 1916 (1996).
207. J. S. Beckman, W. H. Koppenol, Nitric oxide, superoxide, and peroxynitrite: the good, the bad, and ugly. *American Journal of Physiology-Cell Physiology* **271**, C1424-C1437 (1996).
208. M. M. Cortese-Krott, M. Kelm, Endothelial nitric oxide synthase in red blood cells: key to a new erythrocrine function? *Redox Biol* **2**, 251-258 (2014).
209. K. Cosby *et al.*, Nitrite reduction to nitric oxide by deoxyhemoglobin vasodilates the human circulation. *Nat Med* **9**, 1498-1505 (2003).
210. T. H. Han, D. R. Hyduke, M. W. Vaughn, J. M. Fukuto, J. C. Liao, Nitric oxide reaction with red blood cells and hemoglobin under heterogeneous conditions. *Proceedings of the National Academy of Sciences of the United States of America* **99**, 7763-7768 (2002).
211. D. B. Kim-Shapiro, A. N. Schechter, M. T. Gladwin, Unraveling the reactions of nitric oxide, nitrite, and hemoglobin in physiology and therapeutics. *Arteriosclerosis, thrombosis, and vascular biology* **26**, 697-705 (2006).
212. P. Kleinbongard *et al.*, Red blood cells express a functional endothelial nitric oxide synthase. *Blood* **107**, 2943-2951 (2006).
213. C. Liu *et al.*, Mechanisms of human erythrocytic bioactivation of nitrite. *The Journal of biological chemistry* **290**, 1281-1294 (2015).
214. V. Kuhn *et al.*, Red Blood Cell Function and Dysfunction: Redox Regulation, Nitric Oxide Metabolism, Anemia. *Antioxid Redox Signal* **26**, 718-742 (2017).
215. M. M. Cortese-Krott *et al.*, Identification of a soluble guanylate cyclase in red blood cells: preserved activity in patients with coronary artery disease. *Redox Biology* **to be publisehd soon**, (2017).
216. M. M. Cortese-Krott *et al.*, Human red blood cells at work: identification and visualization of erythrocytic eNOS activity in health and disease. *Blood* **120**, 4229-4237 (2012).
217. S. Lee *et al.*, Refractive index tomograms and dynamic membrane fluctuations of red blood cells from patients with diabetes mellitus. *Sci Rep* **7**, 1039 (2017).
218. W. Lockette, Y. Otsuka, O. Carretero, The loss of endothelium-dependent vascular relaxation in hypertension. *Hypertension* **8**, II61-66 (1986).
219. W. Durante, A. K. Sen, F. A. Sunahara, Impairment of endothelium-dependent relaxation in aortae from spontaneously diabetic rats. *Br J Pharmacol* **94**, 463-468 (1988).
220. V. M. Barodka *et al.*, New insights provided by a comparison of impaired deformability with erythrocyte oxidative stress for sickle cell disease. *Blood Cells, Molecules, and Diseases* **52**, 230-235 (2014).
221. T. M. Fischer, C. W. Haest, M. Stohr, D. Kamp, B. Deuticke, Selective alteration of erythrocyte deformabiliby by SH-reagents: evidence for an involvement of spectrin in membrane shear elasticity. *Biochim Biophys Acta* **510**, 270-282 (1978).

222. W. D. Corry, H. J. Meiselman, P. Hochstein, t-Butyl hydroperoxide-induced changes in the physicochemical properties of human erythrocytes. *Biochim Biophys Acta* **597**, 224-234 (1980).
223. A. M. McGough, R. Josephs, On the structure of erythrocyte spectrin in partially expanded membrane skeletons. *Proc Natl Acad Sci U S A* **87**, 5208-5212 (1990).
224. P. S. Becker, C. M. Cohen, S. E. Lux, The effect of mild diamide oxidation on the structure and function of human erythrocyte spectrin. *J Biol Chem* **261**, 4620-4628 (1986).
225. M. Bor-Kucukatay, R. B. Wenby, H. J. Meiselman, O. K. Baskurt, Effects of nitric oxide on red blood cell deformability. *American journal of physiology. Heart and circulatory physiology* **284**, H1577-1584 (2003).
226. D. A. Riccio *et al.*, Renitrosylation of banked human red blood cells improves deformability and reduces adhesivity. *Transfusion* **55**, 2452-2463 (2015).
227. M. Grau *et al.*, RBC-NOS-dependent S-nitrosylation of cytoskeletal proteins improves RBC deformability. *PLoS One* **8**, e56759 (2013).
228. M. Grau *et al.*, High red blood cell nitric oxide synthase activation is not associated with improved vascular function and red blood cell deformability in sickle cell anaemia. *Br J Haematol* **168**, 728-736 (2015).
229. V. Barodka *et al.*, Nitroprusside inhibits calcium-induced impairment of red blood cell deformability. *Transfusion* **54**, 434-444 (2014).
230. A. M. Belanger, C. Keggi, T. Kanias, M. T. Gladwin, D. B. Kim-Shapiro, Effects of nitric oxide and its congeners on sickle red blood cell deformability. *Transfusion* **55**, 2464-2472 (2015).
231. M. M. Cortese-Krott *et al.*, A multilevel analytical approach for detection and visualization of intracellular NO production and nitrosation events using diaminofluoresceins. *Free Radic Biol Med* **53**, 2146-2158 (2012).
232. A. Godecke *et al.*, Coronary hemodynamics in endothelial NO synthase knockout mice. *Circ Res* **82**, 186-194 (1998).
233. O. K. Baskurt, H. J. Meiselman, Data reduction methods for ektacytometry in clinical hemorheology. *Clin Hemorheol Microcirc* **54**, 99-107 (2013).
234. P. Ruef *et al.*, The new low shear viscosimeter LS300 for determination of viscosities of Newtonian and non-Newtonian fluids. *Gen Physiol Biophys* **33**, 281-284 (2014).
235. M. Martinez *et al.*, The effect of long-term treatment with hypotensive drugs on blood viscosity and erythrocyte deformability in patients with essential arterial hypertension. *Clin Hemorheol Microcirc* **17**, 193-198 (1997).
236. M. Bor-Kucukatay *et al.*, Red blood cell rheological alterations in hypertension induced by chronic inhibition of nitric oxide synthesis in rats. *Clin Hemorheol Microcirc* **22**, 267-275 (2000).
237. T. Rangasamy *et al.*, Disruption of Nrf2 enhances susceptibility to severe airway inflammation and asthma in mice. *J Exp Med* **202**, 47-59 (2005).
238. R. Erkens *et al.*, Left ventricular diastolic dysfunction in Nrf2 knock out mice is associated with cardiac hypertrophy, decreased expression of SERCA2a, and preserved endothelial function. *Free Radic Biol Med* **89**, 906-917 (2015).
239. R. Mesquita, I. Pires, C. Saldanha, J. Martins-Silva, Effects of acetylcholine and spermineNONOate on erythrocyte hemorheologic and oxygen carrying properties. *Clin Hemorheol Microcirc* **25**, 153-163 (2001).
240. S. Chien, Red cell deformability and its relevance to blood flow. *Annual review of physiology* **49**, 177-192 (1987).
241. N. Mohandas, M. R. Clark, M. S. Jacobs, S. B. Shohet, Analysis of factors regulating erythrocyte deformability. *J Clin Invest* **66**, 563-573 (1980).

242. D. Chen, D. K. Kaul, Rheologic and hemodynamic characteristics of red cells of mouse, rat and human. *Biorheology* **31**, 103-113 (1994).
243. E. M. Welbourn, M. T. Wilson, A. Yusof, M. V. Metodiev, C. E. Cooper, The mechanism of formation, structure and physiological relevance of covalent hemoglobin attachment to the erythrocyte membrane. *Free Radic Biol Med* **103**, 95-106 (2017).
244. E. Nagababu, J. G. Mohanty, S. Bhamidipaty, G. R. Ostera, J. M. Rifkind, Role of the membrane in the formation of heme degradation products in red blood cells. *Life Sci* **86**, 133-138 (2010).
245. D. Mandal, P. K. Moitra, S. Saha, J. Basu, Caspase 3 regulates phosphatidylserine externalization and phagocytosis of oxidatively stressed erythrocytes. *FEBS Lett* **513**, 184-188 (2002).
246. C. R. Kiefer, L. M. Snyder, Oxidation and erythrocyte senescence. *Curr Opin Hematol* **7**, 113-116 (2000).
247. R. J. Trotta, S. G. Sullivan, A. Stern, Lipid peroxidation and haemoglobin degradation in red blood cells exposed to t-butyl hydroperoxide. The relative roles of haem- and glutathione-dependent decomposition of t-butyl hydroperoxide and membrane lipid hydroperoxides in lipid peroxidation and haemolysis. *Biochem J* **212**, 759-772 (1983).
248. S. Chien, Red cell deformability and its relevance to blood flow. *Annu Rev Physiol* **49**, 177-192 (1987).
249. P. Horn *et al.*, Nitric oxide influences red blood cell velocity independently of changes in the vascular tone. *Free Radic Res* **45**, 653-661 (2011).
250. C. W. Haest *et al.*, Is "deformability" a parameter for the rate of elimination of erythrocytes from the circulation? *Pflugers Arch* **388**, 69-73 (1980).
251. N. V. Gorbunov *et al.*, Nitric oxide prevents oxidative damage produced by tert-butyl hydroperoxide in erythroleukemia cells via nitrosylation of heme and non-heme iron. Electron paramagnetic resonance evidence. *J Biol Chem* **272**, 12328-12341 (1997).
252. G. E. D'Alonzo *et al.*, Survival in patients with primary pulmonary hypertension. Results from a national prospective registry. *Ann Intern Med* **115**, 343-349 (1991).
253. A. Giaid, D. Saleh, Reduced expression of endothelial nitric oxide synthase in the lungs of patients with pulmonary hypertension. *New England Journal of Medicine* **333**, 214-221 (1995).
254. X. Shu *et al.*, Endothelial nitric oxide synthase in the microcirculation. *Cell Mol Life Sci* **72**, 4561-4575 (2015).
255. R. Mathew, J. Huang, J. M. Wu, J. T. Fallon, M. H. Gewitz, Hematological disorders and pulmonary hypertension. *World journal of cardiology* **8**, 703 (2016).
256. R. A. Alvarez *et al.*, Targeting pulmonary endothelial hemoglobin α improves nitric oxide signaling and reverses pulmonary artery endothelial dysfunction. *American Journal of Respiratory Cell and Molecular Biology*, (2017).
257. L. Ciuclan *et al.*, A novel murine model of severe pulmonary arterial hypertension. *American journal of respiratory and critical care medicine* **184**, 1171-1182 (2011).
258. B. E. Wade, J. Zhao, J. Ma, C. M. Hart, R. L. Sutliff, Hypoxia-induced alterations in the lung ubiquitin proteasome system during pulmonary hypertension pathogenesis. *Pulmonary circulation* **8**, 2045894018788267 (2018).
259. D. A. Schreier *et al.*, Impact of increased hematocrit on right ventricular afterload in response to chronic hypoxia. *Journal of applied physiology* **117**, 833-839 (2014).
260. M. P. Chung *et al.*, Role of repeated lung injury and genetic background in bleomycin-induced fibrosis. *American journal of respiratory cell and molecular biology* **29**, 375-380 (2003).

261. R. N. Channick, R. C. Hoch, J. W. Newhart, F. W. Johnson, C. M. Smith, Improvement in pulmonary hypertension and hypoxemia during nitric oxide inhalation in a patient with end-stage pulmonary fibrosis. *American journal of respiratory and critical care medicine* **149**, 811-814 (1994).
262. S. Yoshimura *et al.*, Overexpression of nitric oxide synthase by the endothelium attenuates bleomycin-induced lung fibrosis and impairs MMP-9/TIMP-1 balance. *Respirology* **11**, 546-556 (2006).
263. M. Ferrini *et al.*, Antifibrotic role of inducible nitric oxide synthase. *Nitric Oxide* **6**, 283-294 (2002).
264. J. D. Duarte, R. L. Hanson, R. F. Machado, Pharmacologic treatments for pulmonary hypertension: exploring pharmacogenomics. *Future cardiology* **9**, 335-349 (2013).
265. F. Ichinose, J. D. Roberts Jr, W. M. Zapol, Inhaled nitric oxide: a selective pulmonary vasodilator: current uses and therapeutic potential. *Circulation* **109**, 3106-3111 (2004).
266. M. J. Griffiths, T. W. Evans, Inhaled nitric oxide therapy in adults. *New England Journal of Medicine* **353**, 2683-2695 (2005).
267. B. R. Jacobs, R. J. Brilli, E. T. Ballard, D. J. Passerini, D. J. Smith, Aerosolized soluble nitric oxide donor improves oxygenation and pulmonary hypertension in acute lung injury. *American journal of respiratory and critical care medicine* **158**, 1536-1542 (1998).
268. J. E. Saavedra *et al.*, Localizing antithrombotic and vasodilatory activity with a novel, ultrafast nitric oxide donor. *Journal of medicinal chemistry* **39**, 4361-4365 (1996).
269. C.-F. Lam, P. V. van Heerden, J. Blott, B. Roberts, K. F. Ilett, The selective pulmonary vasodilatory effect of inhaled DETA/NO, a novel nitric oxide donor, in ARDS—a pilot human trial. *Journal of critical care* **19**, 48-53 (2004).
270. P. Failli *et al.*, Effect of N-acetyl-L-cysteine on peroxynitrite and superoxide anion production of lung alveolar macrophages in systemic sclerosis. *Nitric oxide* **7**, 277-282 (2002).
271. B. Alvarez, R. Radi, Peroxynitrite reactivity with amino acids and proteins. *Amino acids* **25**, 295-311 (2003).
272. J. Q. Liu, I. N. Zelko, E. M. Erbynn, J. S. Sham, R. J. Folz, Hypoxic pulmonary hypertension: role of superoxide and NADPH oxidase (gp91phox). *American Journal of Physiology-Lung Cellular and Molecular Physiology* **290**, L2-L10 (2006).
273. N. L. Jernigan *et al.*, Contribution of reactive oxygen species to the pathogenesis of pulmonary arterial hypertension. *PloS one* **12**, e0180455 (2017).
274. S. C. Pugliese *et al.*, A time-and compartment-specific activation of lung macrophages in hypoxic pulmonary hypertension. *The Journal of Immunology* **198**, 4802-4812 (2017).
275. Y. Xia, J. L. Zweier, Superoxide and peroxynitrite generation from inducible nitric oxide synthase in macrophages. *Proceedings of the National Academy of Sciences* **94**, 6954-6958 (1997).
276. F. Kamezaki *et al.*, Gene transfer of extracellular superoxide dismutase ameliorates pulmonary hypertension in rats. *American journal of respiratory and critical care medicine* **177**, 219-226 (2008).
277. R. H. Steinhorn *et al.*, Recombinant human superoxide dismutase enhances the effect of inhaled nitric oxide in persistent pulmonary hypertension. *American journal of respiratory and critical care medicine* **164**, 834-839 (2001).
278. N. Galiè *et al.*, Initial use of ambrisentan plus tadalafil in pulmonary arterial hypertension. *New England Journal of Medicine* **373**, 834-844 (2015).

279. C.-H. Ruan, R. A. Dixon, J. T. Willerson, K.-H. Ruan, Prostacyclin therapy for pulmonary arterial hypertension. *Texas heart institute journal* **37**, 391 (2010).
280. R. Dumitrascu *et al.*, Activation of soluble guanylate cyclase reverses experimental pulmonary hypertension and vascular remodeling. *Circulation* **113**, 286-295 (2006).
281. C. Koress, K. Swan, P. Kadowitz, Soluble guanylate cyclase stimulators and activators: novel therapies for pulmonary vascular disease or a different method of increasing cGMP? *Current hypertension reports* **18**, 42 (2016).
282. J. Mittendorf *et al.*, Discovery of riociguat (BAY 63-2521): a potent, oral stimulator of soluble guanylate cyclase for the treatment of pulmonary hypertension. *ChemMedChem: Chemistry Enabling Drug Discovery* **4**, 853-865 (2009).
283. G. F. Lasker, J. H. Maley, E. A. Pankey, P. J. Kadowitz, Targeting soluble guanylate cyclase for the treatment of pulmonary hypertension. *Expert review of respiratory medicine* **5**, 153-161 (2011).
284. A. Tovchigrechko, I. A. Vakser, GRAMM-X public web server for protein–protein docking. *Nucleic acids research* **34**, W310-W314 (2006).
285. A. Shevchenko, H. Tomas, J. Havli, J. V. Olsen, M. Mann, In-gel digestion for mass spectrometric characterization of proteins and proteomes. *Nature protocols* **1**, 2856 (2006).
286. L. Feng *et al.*, in *Cell*. (2004), vol. 119, pp. 629-640.
287. T. O. Fischmann *et al.*, Structural characterization of nitric oxide synthase isoforms reveals striking active-site conservation. *Nature Structural and Molecular Biology* **6**, 233 (1999).
288. A. Tovchigrechko, I. A. Vakser, Development and testing of an automated approach to protein docking. *Proteins: Structure, Function, and Bioinformatics* **60**, 296-301 (2005).
289. I. A. Vakser, Long-distance potentials: an approach to the multiple-minima problem in ligand-receptor interaction. *Protein Engineering, Design and Selection* **9**, 37-41 (1996).
290. D. A. Fox *et al.*, Structure of the neisserial outer membrane protein opa60: loop flexibility essential to receptor recognition and bacterial engulfment. *Journal of the American Chemical Society* **136**, 9938-9946 (2014).
291. M. G. Hinds, R. S. Norton, NMR spectroscopy of peptides and proteins. *Molecular biotechnology* **7**, 315-331 (1997).
292. C. Lechauve *et al.*, Endothelial cell α-globin and its molecular chaperone α-hemoglobin–stabilizing protein regulate arteriolar contractility. *Journal of Clinical Investigation* **128**, 5073-5082 (2018).
293. F. Poitevin, H. Orland, S. Doniach, P. Koehl, M. Delarue, AquaSAXS: a web server for computation and fitting of SAXS profiles with non-uniformally hydrated atomic models. *Nucleic acids research* **39**, W184-W189 (2011).
294. J. M. A. Bullock, N. Sen, K. Thalassinos, M. Topf, Modeling protein complexes using restraints from crosslinking mass spectrometry. *Structure* **26**, 1015-1024. e1012 (2018).
295. D. Pan, A. Brockmeyer, F. Mueller, A. Musacchio, T. Bange, Simplified Protocol for Cross-linking Mass Spectrometry Using the MS-Cleavable Cross-linker DSBU with Efficient Cross-link Identification. *Analytical chemistry* **90**, 10990-10999 (2018).
296. C. Schmidt, H. Urlaub, Combining cryo-electron microscopy (cryo-EM) and cross-linking mass spectrometry (CX-MS) for structural elucidation of large protein assemblies. *Current opinion in structural biology* **46**, 157-168 (2017).

297. J. R. Kraehling, W. C. Sessa, Contemporary Approaches to Modulating the Nitric Oxide–cGMP Pathway in Cardiovascular Disease. *Circulation research* **120**, 1174-1182 (2017).
298. S. Moncada, E. Higgs, The discovery of nitric oxide and its role in vascular biology. *British journal of pharmacology* **147**, S193-S201 (2006).
299. S. Wong, D. L. Garbers, Receptor guanylyl cyclases. *Journal of Clinical Investigation* **90**, 299 (1992).
300. T. M. Lincoln, T. Cornwell, Intracellular cyclic GMP receptor proteins. *The FASEB Journal* **7**, 328-338 (1993).
301. R. Looft-Wilson, M. Billaud, S. Johnstone, A. Straub, B. Isakson, Interaction between nitric oxide signaling and gap junctions: effects on vascular function. *Biochimica et Biophysica Acta (BBA)-Biomembranes* **1818**, 1895-1902 (2012).
302. J. B. Michel, O. Feron, K. Sase, P. Prabhakar, T. Michel, Caveolin versus calmodulin counterbalancing allosteric modulators of endothelial nitric oxide synthase. *Journal of Biological Chemistry* **272**, 25907-25912 (1997).
303. A. C. Straub *et al.*, Hemoglobin α/eNOS Coupling at Myoendothelial Junctions Is Required for Nitric Oxide Scavenging During VasoconstrictionSignificance. *Arteriosclerosis, thrombosis, and vascular biology* **34**, 2594-2600 (2014).
304. A. C. Straub *et al.*, Endothelial cell expression of haemoglobin [agr] regulates nitric oxide signalling. *Nature* **491**, 473-477 (2012).
305. J. D. Sander *et al.*, ZiFiT (Zinc Finger Targeter): an updated zinc finger engineering tool. *Nucleic acids research*, gkq319 (2010).
306. J. D. Sander, P. Zaback, J. K. Joung, D. F. Voytas, D. Dobbs, Zinc Finger Targeter (ZiFiT): an engineered zinc finger/target site design tool. *Nucleic acids research* **35**, W599-W605 (2007).
307. P. Mali *et al.*, RNA-guided human genome engineering via Cas9. *Science* **339**, 823-826 (2013).
308. W. Y. Hwang *et al.*, Efficient genome editing in zebrafish using a CRISPR-Cas system. *Nature biotechnology* **31**, 227-229 (2013).
309. E. Khandros, C. S. Thom, J. D'Souza, M. J. Weiss, Integrated protein quality-control pathways regulate free α-globin in murine β-thalassemia. *Blood* **119**, 5265-5275 (2012).
310. B. Alter, Gel electrophoretic separation of globin chains. *Progress in clinical and biological research* **60**, 157-175 (1981).
311. Y. Kong *et al.*, Loss of α-hemoglobin–stabilizing protein impairs erythropoiesis and exacerbates β-thalassemia. *The Journal of clinical investigation* **114**, 1457-1466 (2004).
312. X. Yu *et al.*, An erythroid chaperone that facilitates folding of α-globin subunits for hemoglobin synthesis. *The Journal of clinical investigation* **117**, 1856-1865 (2007).
313. S. Sorensen, E. Rubin, H. Polster, N. Mohandas, S. Schrier, The role of membrane skeletal-associated alpha-globin in the pathophysiology of beta-thalassemia. *Blood* **75**, 1333-1336 (1990).
314. N. Villalba *et al.*, Traumatic brain injury disrupts cerebrovascular tone through endothelial inducible nitric oxide synthase expression and nitric oxide gain of function. *J Am Heart Assoc* **3**, e001474 (2014).
315. L. Feng *et al.*, Structure of oxidized alpha-haemoglobin bound to AHSP reveals a protective mechanism for haem. *Nature* **435**, 697-701 (2005).
316. H. Shimokawa *et al.*, The importance of the hyperpolarizing mechanism increases as the vessel size decreases in endothelium-dependent relaxations in rat mesenteric circulation. *Journal of cardiovascular pharmacology* **28**, 703-711 (1996).

317. L. Urakami-Harasawa, H. Shimokawa, M. Nakashima, K. Egashira, A. Takeshita, Importance of endothelium-derived hyperpolarizing factor in human arteries. *The Journal of clinical investigation* **100**, 2793-2799 (1997).
318. S. K. Sonkusare *et al.*, Elementary Ca2+ signals through endothelial TRPV4 channels regulate vascular function. *Science* **336**, 597-601 (2012).
319. R. Erkens *et al.*, Left ventricular diastolic dysfunction in Nrf2 knock out mice is associated with cardiac hypertrophy, decreased expression of SERCA2a, and preserved endothelial function. *Free Radical Biology and Medicine* **89**, 906-917 (2015).
320. A. Ganau *et al.*, Patterns of left ventricular hypertrophy and geometric remodeling in essential hypertension. *Journal of the American College of Cardiology* **19**, 1550-1558 (1992).
321. F. Metivier, S. J. Marchais, A. P. Guerin, B. Pannier, G. M. London, Pathophysiology of anaemia: focus on the heart and blood vessels. *Nephrology Dialysis Transplantation* **15**, 14-18 (2000).
322. D. M. Medeiros, J. L. Beard, Dietary iron deficiency results in cardiac eccentric hypertrophy in rats. *Proceedings of the Society for Experimental Biology and Medicine* **218**, 370-375 (1998).
323. D. H. Chui, S. Fucharoen, V. Chan, Hemoglobin H disease: not necessarily a benign disorder. *Blood* **101**, 791-800 (2003).
324. D. H. Chui, J. S. Waye, Hydrops fetalis caused by α-thalassemia: an emerging health care problem. *Blood* **91**, 2213-2222 (1998).
325. V. Chan *et al.*, Hydrops fetalis due to an unusual form of Hb H disease. *Blood* **66**, 224-228 (1985).
326. V. Chan *et al.*, Molecular defects in Hb H hydrops fetalis. *British journal of haematology* **96**, 224-228 (1997).
327. O. Feron *et al.*, Modulation of the endothelial nitric-oxide synthase-caveolin interaction in cardiac myocytes Implications for the autonomic regulation of heart rate. *Journal of Biological Chemistry* **273**, 30249-30254 (1998).
328. A. Brady, J. B. Warren, P. A. Poole-Wilson, T. J. Williams, S. E. Harding, Nitric oxide attenuates cardiac myocyte contraction. *American Journal of Physiology-Heart and Circulatory Physiology* **265**, H176-H182 (1993).
329. L. A. Barouch, R. W. Harrison, M. W. Skaf, G. O. Rosas, Nitric oxide regulates the heart by spatial confinement of nitric oxide synthase isoforms. *Nature* **416**, 337 (2002).
330. R. P. Barroso, C. Osuamkpe, M. Nagamani, C. Yallampalli, Nitric oxide inhibits development of embryos and implantation in mice. *Molecular human reproduction* **4**, 503-507 (1998).
331. S. Tranguch, Y. Huet-Hudson, Decreased viability of nitric oxide synthase double knockout mice. *Molecular reproduction and development* **65**, 175-179 (2003).
332. H. Ota, S. Igarashi, N. Oyama, T. Tanaka, Y. Suzuki, Optimal levels of nitric oxide are crucial for implantation in mice. *Reproduction, Fertility and Development* **11**, 183-188 (1999).
333. L. Poston, A. McCarthy, J. Ritter, Control of vascular resistance in the maternal and feto-placental arterial beds. *Pharmacology & therapeutics* **65**, 215-239 (1995).
334. B. Krause, M. A. Hanson, P. Casanello, Role of nitric oxide in placental vascular development and function. *Placenta* **32**, 797-805 (2011).
335. E. P. Vichinsky, Clinical manifestations of α-thalassemia. *Cold Spring Harbor perspectives in medicine* **3**, a011742 (2013).

336. G. Filippov, D. B. Bloch, K. D. Bloch, Nitric oxide decreases stability of mRNAs encoding soluble guanylate cyclase subunits in rat pulmonary artery smooth muscle cells. *Journal of Clinical Investigation* **100**, 942 (1997).
337. M. Weber, N. Lauer, A. Mülsch, G. Kojda, The effect of peroxynitrite on the catalytic activity of soluble guanylyl cyclase. *Free Radical Biology and Medicine* **31**, 1360-1367 (2001).
338. R. T. Schermuly *et al.*, Expression and function of soluble guanylate cyclase in pulmonary arterial hypertension. *European Respiratory Journal* **32**, 881-891 (2008).
339. S. M. Black *et al.*, sGC and PDE5 are elevated in lambs with increased pulmonary blood flow and pulmonary hypertension. *American Journal of Physiology-Lung Cellular and Molecular Physiology* **281**, L1051-L1057 (2001).
340. A. O. Etyang *et al.*, Blood Pressure and Arterial Stiffness in Kenyan Adolescents With α+ Thalassemia. *Journal of the American Heart Association* **6**, e005613 (2017).
341. R. S. Seymour, Cardiovascular physiology of dinosaurs. *Physiology* **31**, 430-441 (2016).
342. K. Heberlein *et al.*, Plasminogen activator inhibitor-1 regulates myoendothelial junction formation. *Circulation research* **106**, 1092 (2010).
343. I. Azarov *et al.*, Nitric oxide scavenging by red blood cells as a function of hematocrit and oxygenation. *The Journal of biological chemistry* **280**, 39024-39032 (2005).
344. M. T. Gladwin, J. H. Crawford, R. P. Patel, The biochemistry of nitric oxide, nitrite, and hemoglobin: role in blood flow regulation. *Free radical biology & medicine* **36**, 707-717 (2004).
345. D.-H. Cho *et al.*, Cyclin-dependent kinase 5 phosphorylates endothelial nitric oxide synthase at serine 116. *Hypertension* **55**, 345-352 (2010).
346. Z. Chen, P. A. Cole, Synthetic approaches to protein phosphorylation. *Current opinion in chemical biology* **28**, 115-122 (2015).
347. C. D. Reiter *et al.*, Cell-free hemoglobin limits nitric oxide bioavailability in sickle-cell disease. *Nat Med* **8**, 1383-1389 (2002).
348. M. T. Gladwin, T. Kanias, D. B. Kim-Shapiro, Hemolysis and cell-free hemoglobin drive an intrinsic mechanism for human disease. *The Journal of clinical investigation* **122**, 1205-1208 (2012).
349. D. J. Schaer, P. W. Buehler, Cell-free hemoglobin and its scavenger proteins: new disease models leading the way to targeted therapies. *Cold Spring Harb Perspect Med* **3**, (2013).
350. J. H. Graversen, M. Madsen, S. K. Moestrup, CD163: a signal receptor scavenging haptoglobin-hemoglobin complexes from plasma. *Int J Biochem Cell Biol* **34**, 309-314 (2002).
351. R. O. Cannon *et al.*, Effects of inhaled nitric oxide on regional blood flow are consistent with intravascular nitric oxide delivery. *The Journal of clinical investigation* **108**, 279-287 (2001).
352. H. Grasemann, F. Ratjen, Cystic fibrosis lung disease: the role of nitric oxide. *Pediatric pulmonology* **28**, 442-448 (1999).
353. H. Grasemann, E. Michler, M. Wallot, F. Ratjen, Decreased concentration of exhaled nitric oxide (NO) in patients with cystic fibrosis. *Pediatric pulmonology* **24**, 173-177 (1997).
354. C. C. Solomons, E. K. Cotton, R. Dubois, M. Pinney, The use of buffered L-arginine in the treatment of cystic fibrosis. *Pediatrics* **47**, 384-390 (1971).

355. D. Saha, S. Koli, M. Patgaonkar, K. V. R. Reddy, Expression of hemoglobin-α and β subunits in human vaginal epithelial cells and their functional significance. *PloS one* **12**, e0171084 (2017).
356. A. Brunyanszki *et al.*, Upregulation and mitochondrial sequestration of hemoglobin occur in circulating leukocytes during critical illness, conferring a cytoprotective phenotype. *Molecular medicine* **21**, 666-675 (2015).
357. L. Liu, M. Zeng, J. S. Stamler, Hemoglobin induction in mouse macrophages. *Proceedings of the National Academy of Sciences* **96**, 6643-6647 (1999).
358. F. Richter, B. H. Meurers, C. Zhu, V. P. Medvedeva, M. F. Chesselet, Neurons express hemoglobin α-and β-chains in rat and human brains. *Journal of Comparative Neurology* **515**, 538-547 (2009).